Enhancing Prognostication

In Uveal Melanoma

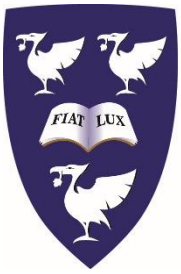

UNIVERSITY OF LIVERPOOL

Thesis submitted in accordance with the requirements of the

University of Liverpool for the degree of Doctor in Philosophy

Sophie Thornton

November 2018

For all the musicians who have provided me with the soundtrack to the last four years, without whom, writing this would have been impossible.

‘‘One good thing about music, when it hits you, you feel no pain’’ - Bob Marley

Acknowledgements

Firstly, I would like to express my sincere gratitude to my P.I. Prof. Sarah Coupland for the continuous support of my PhD study and related research, for her patience, motivation, and immense knowledge. I am also profoundly grateful to Dr. Helen Kalirai for her guidance and support which has helped me in all aspects of my research and writing of this thesis. My sincere thanks also go to Prof. Azzam Taktak for his statistical expertise and his ability to relay this to me in a way which could be clearly understood. I could not have imagined having a better team of advisors and mentors for my PhD study.

On a personal level, I would also like to thank Sarah and Helen for seeing my potential and providing me with an opportunity that has changed my life in so many ways. You are both fantastic role models and I will always treasure the compassion and kindness you've shown me. Every time I have felt like my world was ending you've taught me that it always begins again the next morning.

I would also like to express my gratitude to the CGR team; Prof. Christiane Hertz-Fowler, Dr. John Kenny, Dr. Lisa Olohan, Dr. Xuan Lui, Dr. Sam Haldenby and Julie Sibbring for all of their assistance with my next-generation sequencing and data analysis, especially when this had to be expedited due to unforeseen circumstances.

I'd also like to express my sincere appreciation for all of the uveal melanoma patients who very kindly consented to donate their tumour tissue to the Liverpool Ocular Oncology Biobank, making it possible to conduct pioneering translational research.

My heartfelt thanks to the rest of the LOORG team: Karen, Jenna, Joe, Judy, Dawn, Jo, Debbie, Jodi, Carlos, Alda, Luna, Sam, Ibrar and Dilem. Mainly for the laughs, but more so for the healthy supply of tea bags, biscuits, cakes and everything else that resides on 'temptation island'. Without your support I definitely would not be where I am today.

I thank my friends who are all so precious to me; my wife for life, Jennifer thank you for 27 years of hilarity and helping me get through the last two years that have been filled with many highs and lows. Whether it be serenading me with Jimmy Nail's 'Ain't no doubt' or sending me videos of you eating a sandwich, the laughter you bring me will never be rivalled. To Vick, my 'person', thank you for blessing me with my beautiful god daughter for and keeping my shoulders knot free whenever possible. Per la mia principessa preferita,

Jessica. Grazie mille, 'la cosa peggiore che puoi fare è lasciarmi in pace' ti amo fino alla luna e ritorno. Hillary, thank you for lighting the spark in me that changed my life so wonderfully these last three years and being a fully-fledged member of 'Team Teckers'. Thank you to my pole girls, especially Toni, Crissy and Natalie for providing me with the skills to become a great instructor who is able build women up. Danny, thank you for making me physically and mentally strong over this last year, I might even consider stopping telling all of your new clients your middle name is in fact 'Elizabeth'. Also a massive thank you to the Hawaiian contingent; Joey, Mads and Shawna, when I'd burned the candle at both ends and the middle, you looked after me and helped give me the break I sorely needed in order to refuel and get past the final finish line. And finally, Gaz, my coach and confidante, even though your 5500 miles away you've been my lighthouse these last few years. Having you as part of my trusted circle is an honour and a privilege. Your sage advice and counsel has been invaluable to me, worlds apart but close to heart, we'll always have Desiree.

Thank you Dad/Sir Dados for letting me forge my own path in life and always being there when I've needed advice and moral support. A massive thanks to my siblings Jenny, Rosie, Tom and Patrick as well as my niece and nephew Isobel and Alexander for being so wonderfully weird.

To my wonderful Oli, thank you for always believing in me and being in my corner. I'm so incredibly lucky that I found you. I love you squills partnah.

And lastly, thank you to my little mum or 'mam' (even though you hate me calling you that!). You've fought so very bravely and fiercely these last two years. I've never heard you complain once, not even when the treatment was nothing short of brutal and exhausting. If I could have taken it all from you and put it on myself, I would have in a heartbeat. I remember you saying to me at my Bachelors graduation ceremony when we saw the PhD students' graduate that would be me some day. Well I finally did it. You've raised a feisty, fierce, independent woman and even if you don't get to see me graduate with the silly hat, I know that you're already proud of me.

I dedicate this thesis to you Mum.

Enhancing Prognostication in Uveal Melanoma
Sophie Thornton

Abstract

Uveal melanoma (UM) is the most common primary intraocular malignancy occurring in adults, with a propensity for liver metastases, which occur in ~50% of patients. Despite successful treatment of the primary tumour, there is currently no effective systemic therapy to treat metastatic disease. UM patient management is dependent upon accurate stratification into high or low risk of metastatic progression. Prognostication of UM patients currently involves the integration of clinical, histological, and genetic features of the tumour obtained by multiplex ligation-dependant probe amplification (MLPA) or microsatellite analysis (MSA), in order to obtain a refined predicted metastatic risk. The aims of this thesis were to examine prognostication performed in Liverpool and improve the way patients are stratified according to metastatic risk. In chapter 2 the genetic characteristics of the rarest form of UM, iris melanoma (IM) was examined. Molecular analysis was performed on archival IM samples collected over a twenty year period and demonstrated that a low-metastatic genotype was most commonly observed; this correlates with the improved survival of this UM subtype in comparison to ciliary body and choroidal melanomas. Chromosomal aberrations often seen in posterior UM are also seen in IM, in both treatment-naïve and irradiated tumours. MSA is a common method of genotyping for small UM with low DNA yields, i.e. fine-needle aspirate biopsy samples (FNAB). In chapter 3, I demonstrated that MSA can accurately determine chromosome 3 copy number in FNAB samples. I found no demonstrable differences in the quality or clarity of the genotypes generated in both treatment-naïve and irradiated UM. By examining metastasis-free survival in these samples, I established that there was no evidence that surgical intervention causes iatrogenic dissemination. Loss of 3q was identified as an indicator of poor prognosis and allelic imbalance as an indicator of good prognosis. In chapter 4, in the largest study to date, I demonstrated that loss of nuclear BAP1 protein expression (nBAP1) was a significant independent prognostic parameter associated with metastatic risk and reduced survival, with a stronger association with poor outcome than monosomy 3 (M3). Additionally I identified two subgroups within M3 UM whereby M3 nBAP1+ cases were associated with a prolonged survival in comparison to nBAP1- UM. To address the clinical need to integrate copy number analysis of chromosomes 1, 3, 6 and 8 and gene mutation status of *GNAQ*, *GNA11*, *BAP1*, *SF3B1*, *EIF1AX*, *CYSTLR2*, *PLCB4*, *TTC28*, *KTN1*, *TP53BP1*, and *CSMD1* in chapter 5, I designed, compared and validated targeted next-generation sequencing (NGS) panels for UM. I demonstrated the superiority of hybrid capture as an enrichment method, and was able to successfully analyse copy number and single nucleotide variants in both fresh and formalin fixed tissue. Mutations in *BAP1* were found to be the most important prognostic factor in terms of survival, and gains of 1q were associated with an increased incidence of metastatic death. I identified novel mutations in *PLCB4, TTC28*, *CSMD1*, *KTN1 and TP53BP1* that require further evaluation. In chapter 6 I investigated protein expression levels of a recently identified molecule RasGRP3 in *GNAQ*/*GNA11* mutant UM cell lines and primary tumours and compared this with *BRAF* mutant conjunctival melanoma specimens. I demonstrated that RasGRP3 was significantly and selectively overexpressed in response to *GNAQ/11* mutations. This demonstrates that activation of the MAP-kinase pathway occurs through a different mechanism to that occurring in conjunctival melanoma. In conclusion, I have examined in detail ways of enhancing our current practice for prognostication in UM. There is a need for *BAP1* mutations and nBAP1 negativity to be implemented into routine prognostication. This may be achievable by replacing current MLPA and MSA testing with the targeted UM NGS panel.

Table of contents

Chapter 1

General Introduction

Chapter 2

Genetic Testing in Iris Melanoma

Chapter 3

An Audit of Choroidal Melanoma Analysed by Microsatellite Analysis

Chapter 4

An Audit of Nuclear BAP1 Expression in Choroidal Melanoma

Chapter 5

Designing and Validating Next-Generation Sequencing

Panels for Prognostic Testing in Uveal Melanoma Patients

Chapter 6

RasGRP3 Expression in Uveal Melanoma

Appendices

List of Tables

Chapter 2

Chapter 3

Chapter 4

Chapter 5

Chapter 6

List of Figures

Chapter 1

Chapter 2

Chapter 3

Chapter 4

Chapter 5

Chapter 6

List of abbreviations

AEC	3-amino-9-ethylcarbazole
AI	Allelic imbalance
AR	Allele ratio
ATL	Animal tissue lysis
ATP	Adenosine triphosphate
Bp	Base pair
BSA	Bovine serum albumin
CBI	Ciliary body involvement
CGH	Comparative genomic hybridisation
COMS	Collaborative ocular melanoma study
Cq	Quantitation cycle
Ct	Cycle threshold
D3	Disomy 3
D8	Disomy 8
DAG	Diacylglycerol
DMSO	Dimethyl sulfoxide
DNA	Deoxyribonucleic acid
dNTP's	Deoxynucleotide triphosphates
dsDNA	double-stranded DNA
DQs	Dosage quotients
DUBs	De-ubiquitylating enzymes
EDTA	Ethylenediaminotetraacetic acid
EOE	Extraocular extension
FCS	Fetal calf serum
FFPE	Formalin-fixed paraffin embedded
FISH	Fluorescent *in situ* hybridisation
FNAB	Fine-needle aspirate biopsy
gDNA	Genomic DNA
GDP	Guanosine diphosphate

GEP	Gene expression profiling
GIAB	Genome in a bottle
GTP	Guanosine-5'-triphosphate
HCL	Hydrochloric acid
H&E	Haemotoxylin and eosin staining
HPF	High power field
HR	Hazard ratio
HRP	Horseradish peroxidase
ID	Isodisomy
IHC	Immunohistochemistry
IM	Iris melanoma
LBD	Largest basal tumour diameter
LOH	Loss of heterozygosity
LOOC	Liverpool ocular oncology centre
M3	Monosomy 3
MAPK	Mitogen-activated protein kinase
Mb	Mega base
$MgCl_2$	Magnesium chloride
MLPA	Multiplex ligation-dependent Probe Amplification
mRNA	Messenger RNA
MSA	Microsatellite analysis
MUM	Metastatic uveal melanoma
nBAP1	Nuclear BAP1
NGRL	National Genetics Reference Laboratory
NGS	Next-generation sequencing
NI	Non-informative
NLOH	No loss of heterozygosity
OCT	Ocular coherence tomography
OOG	Ophthalmic Oncology Group
PAS	Periodic Acid-Schiff
PBR	Proton beam radiotherapy
PBS	Phosphate buffered saline

PCR	Polymerase chain reaction
PKC	Protein kinase C
PL	Partial loss
PL3p	Partial loss of 3p
PL3q	Partial loss of 3q
P8q	Polysomy 8q
PM	Primary management
qPCR	Quantitative polymerase chain reaction
RNA	Ribonucleic acid
RPM	Revolutions per minute
RT	Room temperature
RXT	Radiotherapy
SDS	Sodium dodecyl sulphate
TCGA	The Cancer Genome Atlas
TE	TRIS, EDTA
TEMED	Tetramethylethylenediamine
TMA	Tissue microarray
TRIS	TRIS (hydroxymethyl) aminomethane
TSCA	TruSeq Custom Amplicon
UCH	Ubiquitin carboxy-terminal hydrolase
UH	Ultrasound height
UM	Uveal melanoma
UMI	Unique molecular identifiers
YAP	Yes associated pathway

Contribution to Experimental Data

Chapter 2

- Experiment design: Retrospective database review undertaken by Dr. Yamini Krishna. All clinical, histopathological and follow up data for all 26 cases compiled by Sophie Thornton.
- Laboratory work: DNA extraction, MLPA and MSA experiments undertaken by Sophie Thornton.
- Analysis: All genetic analysis undertaken by Sophie Thornton.

Chapter 3

- Experiment design: Retrospective database review undertaken by Sophie Thornton. All clinical, histopathological and follow up data for all 285 cases compiled by Sophie Thornton.
- Laboratory work: All DNA extractions and MSA analyses experiments by Sophie Thornton.
- Analysis: All genetic analyses and all statistical analyses undertaken by Sophie Thornton.

Chapter 4

- Experiment design: Retrospective database review undertaken by Sophie Thornton and Dr. Yamini Krishna. All clinical, histopathological and follow up data for all 165 cases compiled by Sophie Thornton.
- Laboratory work: All DNA extractions, MLPA and MSA experiments undertaken by Sophie Thornton. The BAP1 IHC experiments were undertaken by the NHS immunocytochemistry department of RLBUHT and Neil Farquhar.
- Analysis: IHC scoring undertaken by Sophie Thornton, Neil Farquhar, Dr. Helen Kalirai and Prof. Sarah E. Coupland. All genetic analyses and all statistical analyses of nBAP1 protein expression and genetics in both the chapter and the subsequent publication undertaken by Sophie Thornton.

Chapter 5

- Experiment design: NGS panel design for both SureSelect and TruSeq Custom Amplicon undertaken by Sophie Thornton. All clinical, histopathological and follow up data for all 94 cases compiled by Sophie Thornton.
- Laboratory work: All DNA extractions, and all aspects of next-generation sequencing undertaken by Sophie Thornton.

- Analysis: Bioinformatics analysis undertaken by Dr. Xuan Lui, single nucleotide variant analyses and copy number analyses undertaken by Sophie Thornton, all statistical analysis undertaken by Sophie Thornton.

Chapter 6

- Experiment design: Study designed by Dr. Xu Chen and Prof. Boris Bastian at University of California, San Francisco.
- Laboratory work: All DNA extractions, Sanger sequencing, cell culture and pelleting, TMA construction, and RasGRP3 IHC undertaken by Sophie Thornton.
- Analysis: All genetic analyses and IHC analyses undertaken by Sophie Thornton.

List of Publications

PUBLISHED

1. **Thornton S**, Kalirai H, Sibbring J, Olohan L, Kenny J, Lui X, Haldenby S, Hertz-Fowler C, Coupland SE. Developing Next Generation Sequencing (NGS) Panels for Uveal Melanoma to Detect Copy Number and Single Nucleotide Variants; comparing PCR and Hybrid Capture Target Enrichment. Invest Ophthalmol Vis Sci . 59. Jul 2018 (Conference Paper)

2. Smit KN, van Poppelen NM, Vaarwater J, Verdijk R, van Marion R, Kalirai H, Coupland SE, **Thornton S**, Farquhar N, Dubbink HJ, Paridaens D, de Klein A, Kiliç E. (2018) Combined mutation and copy-number variation detection by targeted next-generation sequencing in uveal melanoma. Mod Pathol. 31(5):763-771.

3. **Thornton S***, Farquhar N*, Coupland SE, Coulson JM, Sacco JJ, Krishna Y, Heimann H, Taktak A, Cebulla CM, Abdel Rahman MH, Kalirai H. (2017) Patterns of BAP1 protein expression provide insights into prognostic significance and the biology of uveal melanoma. J Pathol Clin Res. 13;4(1):26-38.

4. Chen X, Wu Q, Depeille P, Chen P, **Thornton S**, Kalirai H, Coupland SE, Roose JP, Bastian BC. (2017) RasGRP3 Mediates MAPK Pathway Activation in GNAQ Mutant Uveal Melanoma. Cancer Cell. 8;31(5):685-696.e6.

5. Krishna Y, Kalirai H, **Thornton S**, Damato BE, Heimann H, Coupland SE. (2016) Genetic findings in treatment-naïve and proton-beam-radiated iris melanomas. Br J Ophthalmol. 100(7):1012-1016.

IN PREPARATION

1. **Thornton S**, Kalirai H, Heimann H, Taktak A, Coupland SE. A comparison of 284 non-irradiated and irradiated uveal melanomas by microsatellite analysis.

2. **Thornton S**, Kalirai H, Taktak A, Sibbring J, Olohan L, Kenny J, Lui X, Haldenby S, Hertz-Fowler C, Coupland SE. Next Generation Sequencing (NGS) in Uveal Melanoma.

* Indicates joint first authorship

List of Poster and Oral Presentations

- **10/2018**

  Poster presentation at the Society for Melanoma Research (SMR) annual meeting, Manchester, England, United Kingdom.

  Detection of Novel Mutations in TTC28 and SF3B1 using Targeted Next Generation Sequencing (NGS) Panels for Uveal Melanoma

  Poster presentation at the Society for Melanoma Research (SMR) annual meeting, Manchester, United Kingdom.

  Microsatellite Analysis of Irradiated and Non-Irradiated Uveal Melanoma; Assessing Metastasis-Free Survival and Genotype Success.

- **04/2018**

  Poster presentation at the Association for Research in Vision and Ophthalmology (ARVO) Annual Conference 2018, Honolulu, Hawaii, USA.

  Developing Next Generation Sequencing (NGS) Panels for Uveal Melanoma to Detect Copy Number and Single Nucleotide Variants; comparing PCR and Hybrid Capture Target Enrichment

  Finalist in Outstanding Poster Competition for ARVO 2018 (First author of one of the top 5 scored abstracts).

  Winner of NIHR Biomedical Research Centre at Moorfields Eye Hospital NHS Foundation Trust and UCL Institute of Ophthalmology Travel Grant.

- **04/2018**

  Poster presentation at the North West Cancer Research Centre Annual Scientific Symposium, U.K. 2018

  Next Generation Sequencing (NGS) Panels for Uveal Melanoma.

  Selected for a Rapid fire oral presentation.

- **10/2017**

Poster presentation at the World Congress of Melanoma and Society for Melanoma Research Annual Conference, Brisbane, Australia

Focal Perinuclear Cytoplasmic BAP1 Protein Expression is Associated with High Impact Mutations in Uveal Melanoma.

- **09/2017**

Oral Presentation at the Centre for Genomic Research Retreat, Liverpool, United Kingdom

Enhancing Prognostication in Uveal Melanoma.

- **02/2017**

Oral Presentation at the Ocular Oncology Group Annual Conference, Rotterdam, The Netherlands

An Audit of 285 Choroidal Melanomas by Microsatellite Analysis.

Declaration

The work presented in this thesis, unless otherwise stated was performed by myself and in no other way forms part of any other thesis or publication. Peer reviewed publications resulting from these experiments are listed in the proceeding page. Experimental work was carried out at the Institute of Translational Medicine and the Centre for Genomic Research, Institute of Integrative Biology (Faculty of Health and Life Sciences).

This project was undertaken for a period of four years under the supervision of Prof. Sarah E. Coupland, Dr. Helen Kalirai and Prof. Azzam Taktak. Funding was generously provided by the Eye Tumour Research Fund (Royal Liverpool University Hospital) and the Liverpool Health Genomics Laboratory (Centre for Genomic Research, University of Liverpool).

All uveal melanoma tumour samples were kindly provided by the Liverpool Ocular Oncology Biobank from uveal melanoma patients who gave informed consent. This study conformed to the principles of the Declaration of Helsinki and Good Clinical Practice guidelines. Approval for the study was obtained from the Health Research Authority (NRES REC ref 15/SC/0611).

Sophie Thornton

7th November 2018

Chapter 1

General Introduction

1.1 Incidence and Aetiology

Uveal melanoma (UM) is the most common primary intraocular cancer, affecting 6 individuals per million per year in the United Kingdom (1). Caucasian populations are at an increased risk of developing UM in comparison to other ethnicities, especially those individuals with fair skin and blue/grey eyes (2). The aetiology of UM is unknown however, there are known associations with UM. These include: ocular melanocytosis (increased population of melanocytes within the uvea and episclera), oculodermal melanocytosis (naevus of Ota, which also involves the periocular skin and meninges), simple and dysplastic cutaneous naevi and cutaneous melanomas, and neurofibromatosis type 1 (3) (4). Rare reports of families with an excess of UM cases have been published. UM is part of the autosomal dominantly inherited '*BAP1* (BRCA1-associated protein-1) familial cancer syndrome' (5). Affected patients, who have germline mutations in *BAP1* develop mesotheliomas and unusual benign atypical melanocytic skin tumours as well as UM.

It is assumed that UM arises from a malignant transformation of neural crest-derived melanocytes, cells that produce melanin via a process called melanogenesis, located in the uvea (6). Around 90% of UM arise in the choroid, the vascular layer responsible for limiting uncontrolled reflection in the eye, located between the retina and sclera (Figure 1.1) (7). An additional 3-4% of UM arise in the iris, the coloured part of the eye that controls dilation of the pupil, and the remainder of UM occur in the ciliary body, a ring-shaped structure consisting of ciliary muscles, ciliary processes and fibrous connective tissues (7).

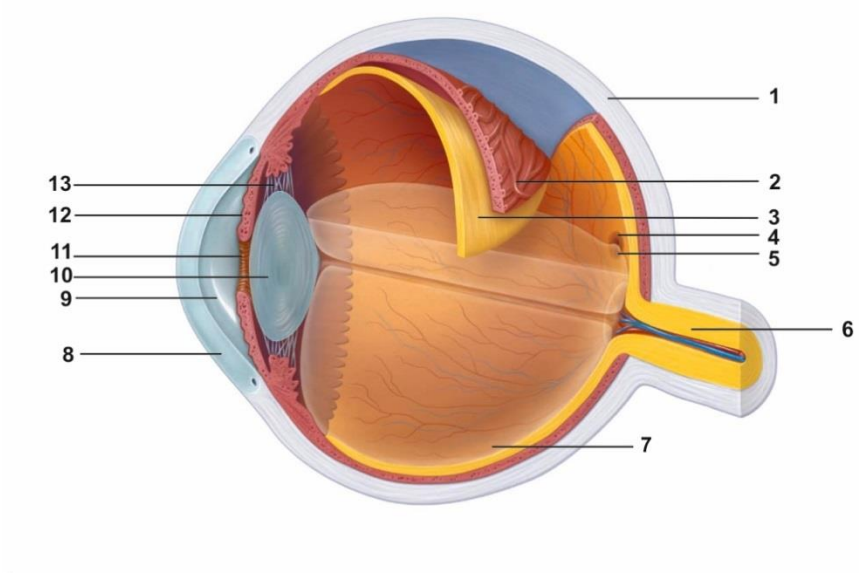

Figure 1.1 Anatomy of the human eye: **1)** sclera **2)** choroid **3)** retina **4)** macula **5)** fovea **6)** optic nerve **7)** posterior chamber **8)** cornea **9)** anterior chamber **10)** lens **11)** pupil **12)** iris **13)** ciliary body. (Image sourced from Harper Collins)

1.2 Clinical Diagnosis

UM are normally diagnosed when patients are referred to ophthalmologists in specialised ocular oncology centres by their family doctor or optometrists after presenting with symptoms or incidental findings (8). Patients who present with a variety of symptoms, such as photopsia, floaters, blurred vision, and visual field loss, are more likely to have been referred by their General Practitioner (9). However, up to 30% of patients will report no symptoms at all, and these patients are more likely to be referred by optometrists after routine eye examinations (10). In order to make a diagnosis of UM, patients undergo a clinical examination with slit-lamp microscopy and indirect ophthalmoscopy coupled with ultrasonography, optical coherence tomography, auto-fluorescence and fluorescein angiography (figure 1.2) (9). In 1995, a pneumonic with five traits were proposed as an aid to diagnose melanoma: **T**hickness >2 mm, presence of sub-retinal **F**luid, **S**ymptoms i.e. photopsia or floaters, **O**range pigment, and **M**argin near the optic disc (**TFSOM**) (11). In 2009 a multivariate analysis was performed on 2514 cases of choroidal naevi that revealed

an additional 2 risk factors associated with melanoma growth: ultrasonographic **H**ollowness, and absence of a **H**alo (**TFSOM-HH**) (12).

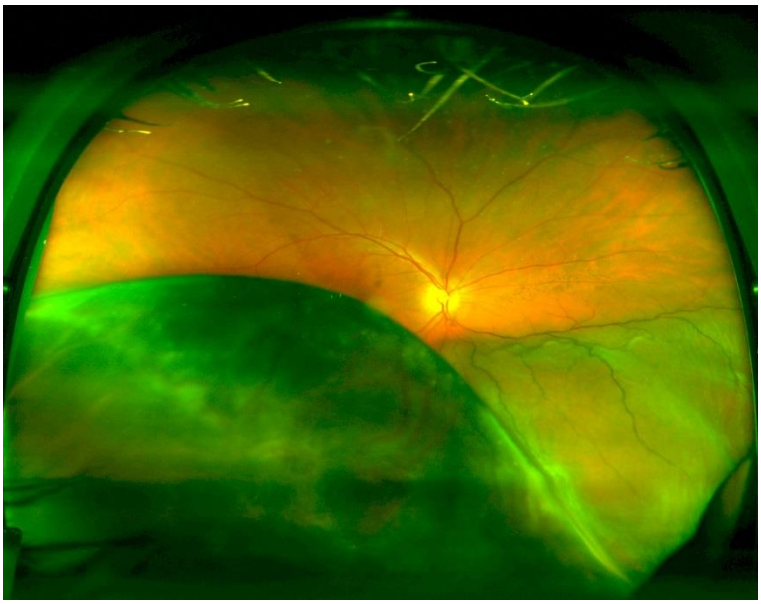

Figure 1.2 Fundoscopy (Optos) image showing an inferior choroidal and ciliary body melanoma with an extensive exudative retinal detachment (Courtesy of the Liverpool Ocular Oncology Clinic).

1.3 Clinical Management of Primary UM

Once the diagnosis has been made, the clinical management of the primary UM is highly dependent upon the size and location of the tumour. Other factors that are taken into consideration before choosing a course of treatment are patient choice/motivation, secondary illnesses (e.g. diabetes and glaucoma), and the visual acuity of the unaffected healthy eye (13).

1.3.1 Plaque Radiotherapy

Ruthenium brachytherapy for primary UM was first implemented in the 1960's by Peter Lommatzsch (14). To date, plaque radiotherapy continues to be considered a highly effective modality of treatment in institutions across the world. Although institutes vary in

their approach, iodine-125 and ruthenium-106 are the most frequently used radiation sources (15). Plaque radiotherapy is seen as an eye-sparing treatment, since the radioactive implant is sutured onto the outer sclera adjacent to the tumour, and is then removed after the appropriate amount of radiation has been emitted (figure 1.3) (16). This approach allows high doses of radiation to be delivered to the tumour without damaging the other structures in the eye enabling some visual acuity to be retained where possible. It is for these reasons that the Collaborative Ocular Melanoma Study (COMS) championed the use of plaque radiotherapy in the treatment of medium-sized choroidal melanomas (17). Plaque radiotherapy is most effective when used to treat small-to-medium sized tumours where the tumour thickness is ≤7mm (18). However, complications do arise from this treatment (particularly if larger UM are treated), such as radiation retinopathy (19), vitreous haemorrhage (20), radiation cataract (21), neovascular glaucoma (22), radiation maculopathy (23), radiation optic neuropathy and iris rubeosis due to 'toxic tumour syndrome' (24). Despite this, plaque radiotherapy remains a useful treatment in preserving the cosmetic appearance of the eye.

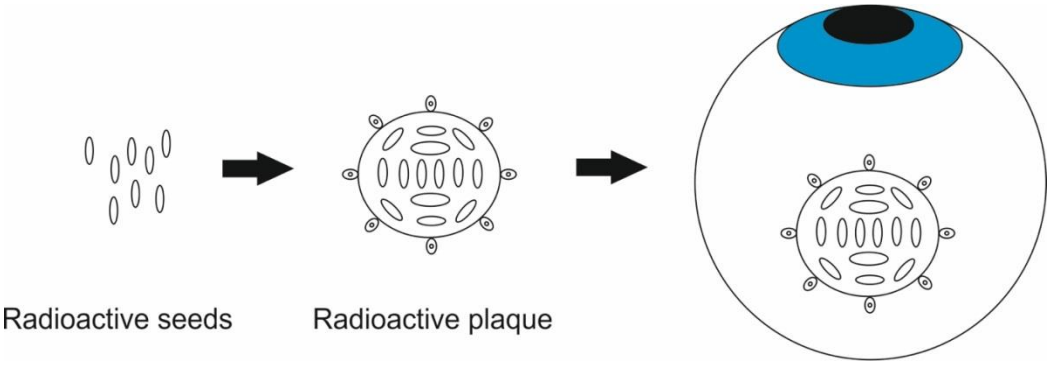

Figure 1.3 A radioactive ruthenium or iodine plaque used to treat UM (original image).

1.3.2 Proton Beam Radiotherapy

Proton beam radiotherapy (PBR) was first implemented in the treatment of UM in 1991 at the Centre de Protontherapie d'Orsay in Paris (25). It is a process that involves the surgical insertion of metallic tantalum markers around the periphery of the tumour, which are then used to direct proton radiation to the tumour (figure 1.4) (26). As with plaque radiotherapy, PBR is considered an eye-preserving treatment as the precise nature of the radiation delivery minimises damage to surrounding structures (27). However, in contrast to plaque radiotherapy, PBR can be used to treat tumours that are larger and closer to the optic disc and the fovea (28), taking advantage of the Bragg peak. The Bragg peak is a phenomenon whereby protons enter a patient's body, gradually increasing the absorbed dose of radiation as depth increases, rising to a peak when the proton ultimately stops. A dose of radiation typically between 53 to 70Gy is delivered over several visits (29). PBR is usually administered with safety margins of between 2.0 – 4.0mm of the tumour depending upon the tumour location and other considerations such as protection of the optic nerve and fovea and counteracting diffuse spread (30). The cumulative risk of local treatment failure is low (1-6%) and is correlated with tumours that have a large basal diameter and tumour height (30). Unfortunately, a proportion of eyes treated by PBR will go on to be enucleated either due to tumour recurrence or other factors i.e. painful blind-eye and neovascular glaucoma (31). However, the overall 5- year survival rate for those treated with PBR is around 80% with a 5-year metastasis free survival of 80.6% due to the typical tumour and genetic characteristics of smaller tumours. (32). As with plaque radiotherapy, PBR is also associated with some complications, such as radiation maculopathy (33), papillopathy (34), neovascular glaucoma (35), cataract (36), vitreous haemorrhage (37), intraocular inflammation (38) as well as dry eye and mydriasis. The latter can be overcome if the PBR is administered through closed eyelids (39). These complications increase the likelihood of

vision loss in the treated eye; despite this PBR remains a good treatment for conserving the cosmetic appearance of the eye.

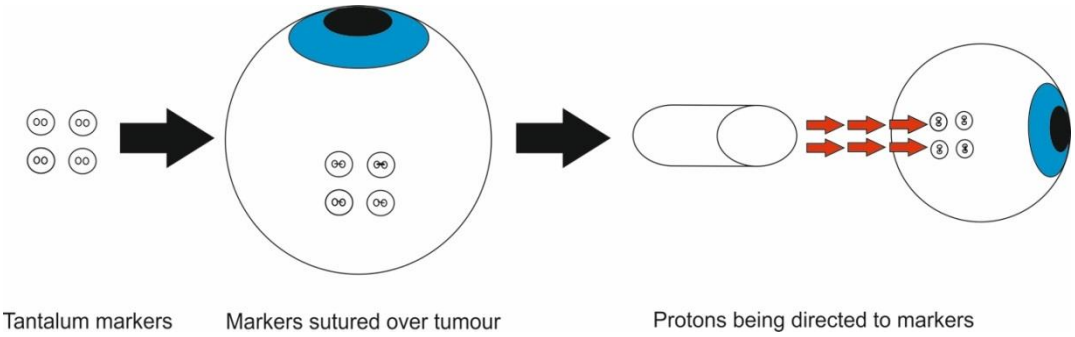

Figure 1.4 Proton beam radiotherapy in UM; tantalum markers are sutured to the tumour site and these are used to enable radiation to be delivered in this region, minimising damage to surrounding structures **(Original image).**

1.3.3 Trans-scleral Local Resection

The technique, first pioneered in Glasgow in 1973 by Wallace S Foulds, is a surgical procedure that is considered an eye and vision-preserving treatment (40). The tumour is localised preoperatively using the aforementioned clinical examination techniques. The surgery involves a lamellar scleral dissection that exposes the choroid; an incision is then made into surrounding healthy choroid and inner scleral lamella around the tumour, which is then stripped from the retina and removed (41). Following tumour removal, the outer scleral flap is closed over the surgical coloboma, and a 20mm ruthenium plaque is sutured to the outer sclera surface, and a dose of 100 – 200 Gy is administered to the resected area (42). Ideal tumours for trans-scleral local resection surgery are 5-15 mm in thickness. Local resection may be performed post-therapy: e.g. larger sized tumours associated with 'toxic tumour syndrome' (i.e. the release of cytotoxic substances causing secondary retinal detachment and neovascular glaucoma) after PBR (43) (44). In ~80% of cases, the surgery results in a cosmetically acceptable eye with approximately 66% of patients maintaining

useful vision (45). The metastatic death rate after local resection is reduced from 92% to 30% at 15 years with the presence of more than 3 risk factors, such as epithelioid cells, largest basal diameter and lack of adjunctive radiotherapy (46). Several studies have shown that in comparison with plaque radiotherapy, trans-scleral local resection preserves visual function and results in decreased incidence of optic neuropathy and secondary glaucoma (47) (48). One of the complications associated with trans-scleral local resection is incomplete tumour removal that can result in tumour recurrence months to years after treatment (49). This, in addition to retinal detachment, are the most common causes of enucleation and visual loss after trans-scleral local resection (50). Tumour recurrences can be counteracted by the addition of a plaque over the area of the local resection following completion of the surgery.

1.3.4 Endoresection

Endoresection is a surgical procedure that was initially developed to treat juxtapapillary choroidal melanomas that traditionally would have been enucleated (51). The procedure - also referred to as 'internal eye wall resection' or 'retinochoroidectomy' - involves cutting the tumour into miniscule fragments with a vitreous cutter during a pars plana vitrectomy (figure 1.5) (52) (53). Endoresection is reserved for thick, posterior UM near the macula or optic disc, where PBR would cause visual loss and are too thick for plaque radiotherapy (54). Like trans-scleral local resection, endoresection is a useful surgical technique to remove post radiotherapy toxic tumours (55). A recent study showed that only 3% of the cohort treated using endoresection over 20 years experienced local recurrence of the tumour (56). Additionally, as long as the UM have not extended into the fovea, useful vision can be retained using this procedure (57). Similar to trans-scleral local resection, endoresection also has associated risks of early and late postoperative complications. There is a belief amongst some ophthalmologists that during the surgical procedure there could

be a dissemination of tumour cells (58). However, a study by García-Arumí et al. examining the long-term outcomes of endoresection patients demonstrated a local recurrence rate at 3 and 5 years was 5.8%., with more patients experiencing retinal detachment, scleral bed bleeding, ocular hypertension, epiretinal proliferation, subretinal fibrosis, radiation retinopathy and subretinal neovascularisation (59). Therefore, endoresection remains a useful (albeit controversial) technique in preserving the cosmetic appearance of the eye and vision.

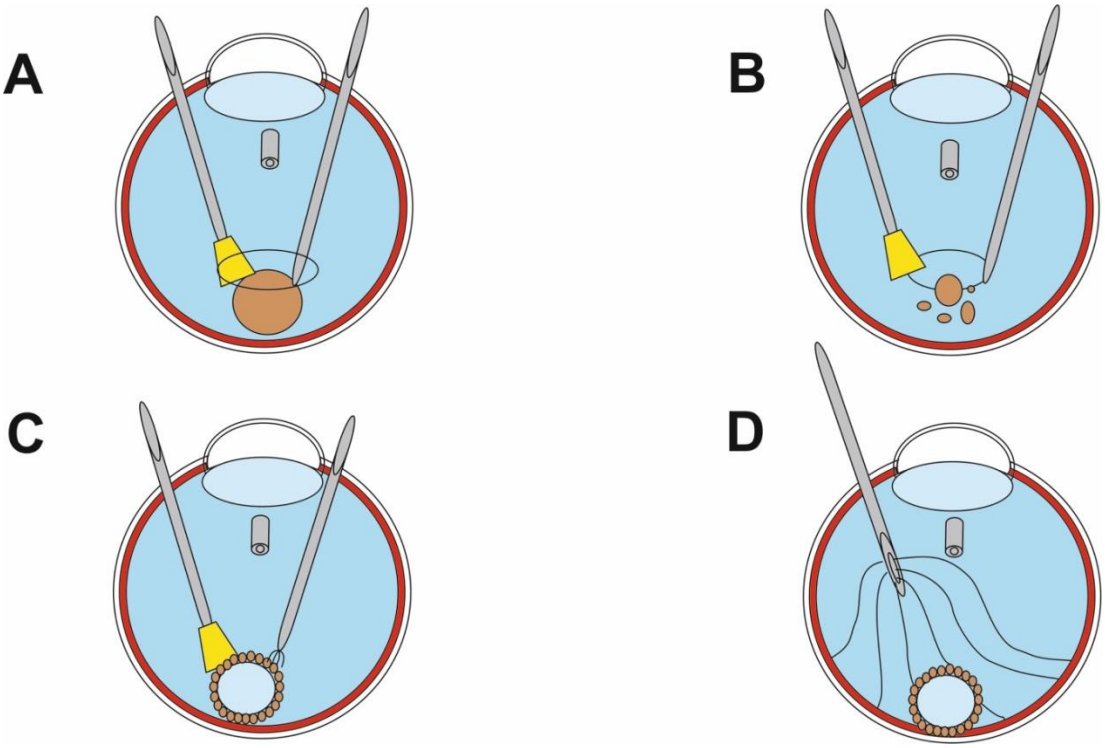

Figure 1.5 Endoresection of a choroidal melanoma; **a)** a hole is made in the retina directly above the tumour **b)** using a vitreous cutter the tumour is dissected into tiny fragments; **c)** a laser is passed into the eye to burn away any remaining tumour and edges of the retina are welded into place; **d)** silicon oil is inserted into the eye to keep the retina in place and to prevent haemorrhage (adapted from itumor.org).

1.3.5 Enucleation

Enucleation is a surgical procedure that involves removing the entire globe and replacing it with an implant or prosthesis to which the eye muscles can be sutured resulting in an acceptable cosmetic result. Patients are treated using this modality if the tumour is too

advanced at initial presentation or is located on the ciliary body (60). Similarly if the tumour has caused severe ocular complications, such as total retinal detachment or neovascular glaucoma, enucleation may be performed to remove a painful blind eye (61). Some patients opt to have the eye removed regardless of whether it can be treated using conservative therapies, such as plaque radiotherapy or PBR (62). Secondary enucleation is also sometimes performed due to complications of conservative eye-saving therapy or to tumour recurrence (63). Enucleation had previously been thought to be responsible for disseminating tumour cells and increasing the incidence of metastatic melanoma-related mortality (the Zimmerman hypothesis) (64). Additionally, enucleation was thought to be a superior treatment of UM in comparison to eye conserving radiotherapy treatments (65). However, these hypotheses were later disproved as COMS reported no statistically significant difference in survival between patients treated by enucleation alone and pre-enucleation radiotherapy (66).

1.3.6 Fine-needle Aspirate Biopsies

Diagnostic fine-needle aspirate biopsies (FNAB) for masses of indeterminate origin were first described by Jakobiec et al. in ophthalmic oncology centres (67). There are two main techniques utilised for sampling UM; tumours located anteriorly to the equator are sampled using a technique called trans-scleral biopsy whereby a scleral flap is created in order to insert the needle and biopsy, tumours located posteriorly to the equator and therefore inaccessible via the sclera, are sampled using a technique referred to as a trans-retinal biopsy, where a needle is inserted through the pars plana and used to sample the tumour. In 2002, Naus et al. of successfully examined the viability of using FNAB for prognostic testing (68). The safety of the procedure has been examined by a number of studies, confirming it is perfectly innocuous and effective at confirming chromosome 3

statuses (69) (70) (71). An assessment of the surgical technique has shown that common complications such as transient localised bleeding, vitreous haemorrhage and retinal perforation have decreased over time (72).

1.4 Management of Metastases

Due to the lack of lymphatics located in the eye, UM spreads haematogenously (73). Lymphatic spread is only possible where anterior scleral infiltration of the primary tumour occurs, allowing tumour access to the conjunctival lymphatics (74). The most common site of metastatic spread is to the liver, although UM cells can also spread to the lungs, bones and skin (75). Despite successful treatment of the primary tumour, up to 50% of UM patients will die of metastatic disease with 90% of those developing hepatic metastases (76).

The COMS study examining the development of metastatic disease discovered that metastatic spread of the primary tumour occurred in 25% of patients at 5 years and 34% of patients by 10 years (77). The development of liver metastases is associated with a particularly poor prognosis, and in the absence of treatment, life expectancy is reduced to less than 6 months (78). Currently, the most effective way to treat patients with established liver metastases is by surgical resection, which is highly dependent upon the size and location of the tumours (79). Advanced miliary disease is often missed by conventional imaging (e.g. ultrasound or magnetic resonance imaging (MRI)), and the number of liver metastases detected preoperatively is a strong prognostic indicator (80). Patient survival is strongly associated with the quality of the liver resection, with more patients being alive after two years when the tumour could be completely resected (R0) compared to incomplete resection (R1) (81). In addition, patients who are treated by liver resection have a more favourable survival in comparison to patients who are not treated (82). There are

several other treatment options available once liver metastases have been detected, such as isolated liver perfusion (83), chemoembolisation (84), immunoembolisation (85) and hepatic intra-arterial chemotherapy (86). Patients who are not suitable candidates for liver resection are limited to the treatment options they can receive. There are currently no immunotherapy or chemotherapy agents that are effective in treating metastatic UM (87). The systemic chemotherapy agents that are used to treat metastatic UM patients have little effect on overall survival in comparison to localised treatment (88). Some of the drugs used more recently to treat metastatic disease (e.g. tyrosine kinase inhibitors, angiogenesis inhibitors and mitogen-activated protein kinase (MEK) inhibitors) have demonstrated a limited effect to improve survival; however, on-going clinical trials will ultimately determine what role they will have in patient treatment (89).

1.5 Metastatic Risk Factors

Risk of metastatic spread of UM is associated with a number of factors including clinical, histological and genetic which I will describe in more detail below.

1.5.1 Chromosomal Copy Number

1.5.1.1 Monosomy 3

The most widely reported gross chromosomal abnormality in UM is complete or partial loss of chromosome 3, or monosomy 3. This was initially reported by Prescher et al. in 1990 after an examination of UM using conventional karyotyping showed 43% of the cohort had monosomy 3 (90). A subsequent study showed that chromosome 3 loss was strongly associated with UM patients who have a poor prognosis (91). Since the study in 1996, several other groups have confirmed the prognostic significance of monosomy 3, and it is now widely regarded as one of the most useful prognostic parameters when considering UM patient survival (92) (93) (94).

1.5.1.2 Chromosome 8

Abnormalities in chromosome 8 also have been established in UM, presenting as a gain of 8q or isochromosome 8q (95). Abnormalities in 8q have been reported in genetic studies of UM (96) and are often associated with monosomy 3 UM, and therefore with a poor patient prognosis (93) (92). The region of 8q, which was found to be most commonly amplified during a comparative genomic hybridisation study, was 8q24-->qter, an area that encompasses the *c-myc* oncogene (97). Gain of 8q, especially *c-myc* is thought to occur later in the genetic progression of UM, and generally follows chromosome 3 loss (98).

1.5.1.3 Chromosome 6

The development of UM is thought to be associated with oncogenes located on 6p and tumour suppressor genes on 6q of prognostic relevance, although they have not yet been identified (99) (68). Aberrations in chromosome 6, frequently found in cutaneous melanomas, have also been linked to UM (100, 101). Gains in 6p have been associated with a more favourable prognosis (93), whereas losses in 6q have been reported to worsen survival in UM (102). A study by Lake et al. 2013 examined 58 UM samples by array SNP and identified frequent amplifications of the *CNKSR3* gene located on 6q25.2, associated with increased protein expression and improved patient survival (103).

1.5.1.4 Chromosome 1

Rearrangements in chromosome 1 are a common occurrence in cutaneous melanomas and most frequently affect the p (short) arm (104) (105). Partial deletions and regions where heterozygosity is lost on 1p in cutaneous melanoma indicate the possible location(s) for tumour suppressor genes (106). Abnormalities in 1p are also routinely found in UM (107). The prognostic significance of 1p loss, particularly 1p36 has, been shown to impact disease-

free survival (102). This occurs in metastasising tumours concurrent with monosomy 3 suggesting a role in the promotion of tumourigenesis and tumour cell dissemination (108). The frequencies of 1q amplifications have been described to occur in as many as 24% of UM, however the prognostic significance is not yet fully understood (1).

1.5.2 Mutations in UM

1.5.2.1 GNAQ and GNA11

GNAQ and *GNA11* are heterotrimeric proteins, which function as G_q alpha subunits; activating phospholipase C and involved in the transduction and modulation of several cellular signalling pathways. Located on 9q21.2 and 19p13.3 respectively, studies have shown that mutations in exons 4 (R183) and 5 (Q209) of the GTPases *GNAQ* and *GNA11* are exclusive to UM and uveal nevi (figure 1.6) (109). These mutations occur in 84% of UM, and are mutually exclusive of each other (110). *GNAQ* and *GNA11* mutations are thought to be an early event in UM development (111). Mutations of R183 and Q209 inhibit the GTPase function of the gene, which results in an inability to hydrolyse GTP to GDP leaving the protein in a constitutively active state (112). There is little evidence to suggest whether *GNAQ* or *GNA11* mutations negatively influence patient survival (113). However, mutations in *GNAQ* and *GNA11* lead to downstream oncogenic signalling, due to their integral involvement in the mitogen activated protein kinase (MAPK) pathway (114). A recent study examined the effects of MAPK/ERK Kinase (MEK) and protein kinase C (PKC) inhibitors on *GNAQ* and *GNA11* mutant cell lines and found a significant reduction in proliferation and induction of apoptosis (115). Sanger sequencing of *GNAQ* and *GNA11* has proven to be an effective technique to establish the origin of metastatic melanoma (116) (117).

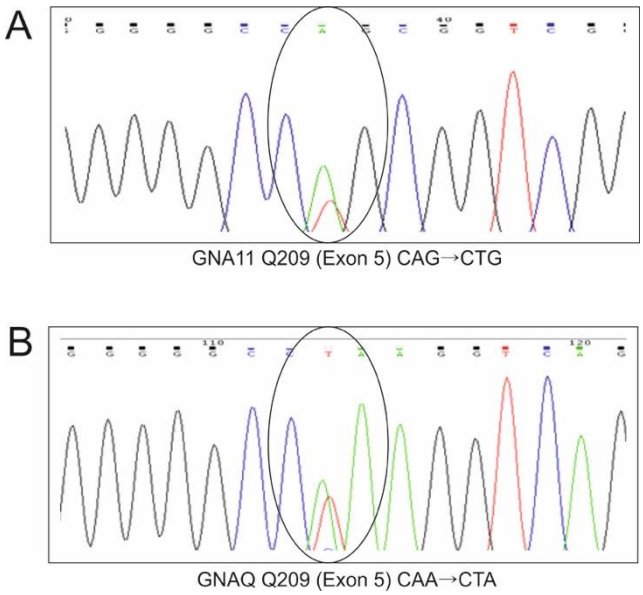

Figure 1.6 Mutations in GNAQ and GNA11 in UM; **A)** an adenosine to thymine transition resulting in a substitution to leucine (GNA11 c.626 A>T Q209L) and **B)** an adenosine to thymine transition resulting in a substitution to leucine (GNAQ c.626 A>T Q209L) (Original image).

1.5.2.2 SF3B1

SF3B1 is a protein coding gene that encodes subunit 1 of the splicing factor 3b protein complex, which contributes to the splicing of pre-mRNAs located on 2q33.1. Mutations in this gene are frequently found in breast cancer, myelodysplastic syndrome and advanced chronic lymphocytic leukaemia (118). Recently, whole exome sequencing was used to examine novel *SF3B1* mutations in UM and found these occurred frequently in UM with D3 (119). A recent study demonstrated that *SF3B1* mutations occurred in a mutually exclusive fashion to BAP1 mutations, suggesting that there are two distinct pathways of tumour progression (120). *SF3B1* mutations are thought to affect sister chromatid cohesion and mitotic segregation through compromised splicing of sororin; an essential protein involved in the stable binding of cohesion to chromatin and enabling sister chromatin cohesion in interphase pre-mRNA (121). Recurrent mutations in this gene in codon 625 have also been associated with differential alternative splicing of coding and noncoding genes (122). *SF3B1* mutations were initially thought to have a protective function as they occurred almost

exclusively in disomy 3 UM with good prognostic features (119) (120). However, recent data has shown that disomy 3 UM with *SF3B1* mutations have a 7-fold increased risk of metastatic disease occurring at a longer follow up time when compared to disomy 3 tumours without mutations in *SF3B1* (123).

1.5.2.3 EIF1AX

EIF1AX encodes an essential eukaryotic translation initiation factor found on Xp22.12, which is required for ribosome dissociation and stabilising the binding of Met-tRNA to 40S ribosomal subunits. *EIF1AX* mutations in UM are a relatively recent finding, occurring across hotspots on exons 1 and 2 (119). Mutations in *EIF1AX* are associated with a more favourable prognosis as they have only been shown to occur in disomy 3 cases, and are mutually exclusive of *BAP1* and *SF3B1* mutations (110). Several studies have shown that mutations in EIF1AX play a protective role to prevent metastasis even when taking into consideration other risk factors (119, 124). Moreover, a recent study was able to establish that mutations in *EIF1AX* are also associated with clinical and histopathological features typically associated with a good prognosis (125).

1.5.2.4 BAP1

BAP1, or "BRCA associated protein 1", is a deubiquitinating enzyme found on the short arm of chromosome 3. Somatic *BAP1* mutations are associated with cancers, such as clear cell renal carcinoma, mesothelioma and non-small cell lung cancer, in addition to being strongly associated with metastasis in UM and other cancers (126). *BAP1* is involved in numerous cellular processes, such as DNA damage response, regulation of transcription, cell cycle and cell growth (127) (128). There is also evidence that germline mutations in *BAP1* increase susceptibility to UM, cutaneous melanoma, mesothelioma and other cancers (5) (3). Recent studies have shown that *BAP1* mutations are found more frequently in monosomy 3 UM

and are associated with metastatic progression (129) (130). Mutations in *BAP1* frequently lead to a loss of nuclear BAP1 protein expression which is associated with reduced survival time irrespective of chromosome 3 status (131). Both are factors which make *BAP1* mutations extremely important indicators of prognosis.

1.5.2.5 Other mutations

In addition to the aforementioned mutations, other less frequently occurring mutations have also been documented that may contribute to metastatic progression of UM. A recurrent mutation of the G-Coupled protein receptor *CYSLTR2* (13q14.2) was identified in 4/9 UM samples where *GNAQ/GNA11* mutations were absent (132). Similarly, a gain-of-function mutation was detected in *PLCB4* (20p12.3) in 1/54 UM, a downstream target of *GNAQ/GNA11* in a mutually exclusive fashion (133). A recent study by Royer-Bertrand et al. identified an additional five mutations in more than one of the 33 UM sampled examined in their study; *KTN1*, *DLK2*, *CSMD1*, *TTC28* and *TP53BP1*, however the impact of these mutations has yet to be established (134). Additionally, mutations in the splicing factor *SRSF2* resulting in a change-of-function have also been identified in two separate studies in the same region that has been reported to disrupt splicing in myelodysplastic syndrome (135) (136) (137). A mutation in FBXW7 in metastases was identified by Luscan et al. and this was also observed by Martin et al. however its involvement in tumourigenesis remains unknown (138) (119).

1.5.3 Clinical Risk Factors

1.5.3.1 Tumour Size

Tumour size is an important prognostic parameter, which is typically associated with a poor clinical outcome in UM patients. Widely used as a predictor of metastatic disease, tumour size is made up of the largest basal tumour diameter and tumour height, which is

established during the initial examination by the ophthalmologist using ultrasonography. Patients who have tumours larger than 16mm at initial presentation usually undergo liver function tests and liver ultrasonography as these features are associated with an increased risk of metastatic disease (139). It is hypothesised that large UM have existed longer, and hence may be composed of aggressive cells that grow rapidly, which are both factors that predispose to metastatic disease (140). Multivariate analysis has shown that the frequency of monosomy 3 and disease specific mortality increases about two-fold when the largest tumour diameter >18mm (141). An American Joint Committee on Cancer (AJCC) commissioned study to develop a tumour, node, metastasis (TNM) staging for UM utilising baseline and survival data of 7369 patients which demonstrated a strong correlation between reduced survival and tumour size (PMID: 23258307).

1.5.3.2 Ciliary body involvement

Ciliary body involvement occurs in approximately 10% of all UM. Due to their location and delayed onset of visual changes, ciliary body melanomas tend to grow to a larger size before they are detected, remaining hidden behind the iris diaphragm (142). Various studies have shown an association with ciliary body involvement and increased mortality, making ciliary body involvement an important prognostic parameter to consider when predicting metastases (143).

1.5.3.3 Extraocular extension

Extraocular extension from a primary UM occurs in ~13% of patients (144). Up to two thirds of patients with extraocular extension will eventually die of metastatic disease (145). There are different routes by which UM can spread extraocularly; vortex veins, optic nerve, ciliary arteries, scleral perforation and aqueous drainage channels (Figure 1.7). The route of extraocular spread is highly dependent on the intraocular tumour location, (139).

Extraocular spread has been shown to be significantly associated with large basal diameter, presence of closed loops, epithelioid cell morphology and monosomy 3 UM, which are all features of aggressive tumours (146).

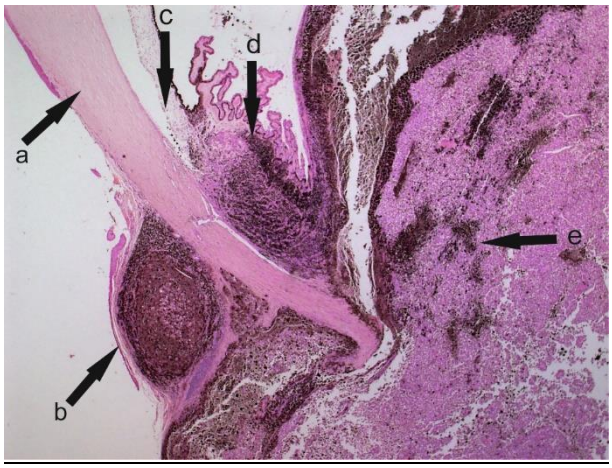

Figure 1.7 Haematoxylin and Eosin stained sections depicting extraocular growth of UM cells; a) the cornea, b) an area of extraocular growth of melanoma cells outside of the sclera c) the iris, d) the ciliary body and e) a choroidal melanoma.

1.5.3.4 Age and gender

Studies have shown that there is no gender difference in the incidence of UM, with males and females affected equally. An in-depth analysis of UM revealed that men had a tendency to have posteriorly located tumours that were larger than the tumours in females (147) and which had a higher disease-specific mortality (148). UM diagnosed in females were more likely to be in the ciliary body or iris (147). Age at diagnosis is also another important factor to consider when determining a patient's long term prognosis. Studies have shown that older patients have significantly worse survival rates compared to their younger counterparts (149). Univariate analysis has shown that patients <60 years old have a better survival rate (150).

1.5.4 Histopathological Risk Factors

1.5.4.1 Cytomorphology

Cytological classification of UM is a significant predictor of disease-free survival. Cell types were first categorised by Callendar in 1931 (151) into 6 histologic types; spindle A, spindle B, epithelioid, mixed, fascicular and necrotic. Spindle A cells are cigar-shaped with finely dispersed chromatin whereas spindle B cells have plumper nuclei with more distinct nucleoli and are generally more oval in shape. Epithelioid cells are named as such because they are epithelial-like, with an abundant cytoplasm, round nuclei and prominent nucleoli. This then formed the basis for subsequent modifications made by McLean et al. who simplified the classification by subdividing mixed-cell types into percentage and size of epithelioid content, and classifying spindle-cell types as mixed-cell if they containing small or rare epithelioid cells (Figure 1.8) (152). The fascicular and necrotic cell types were also removed from the classification system, and most spindle A cell specimens are now classified as spindle cell naevi (153).

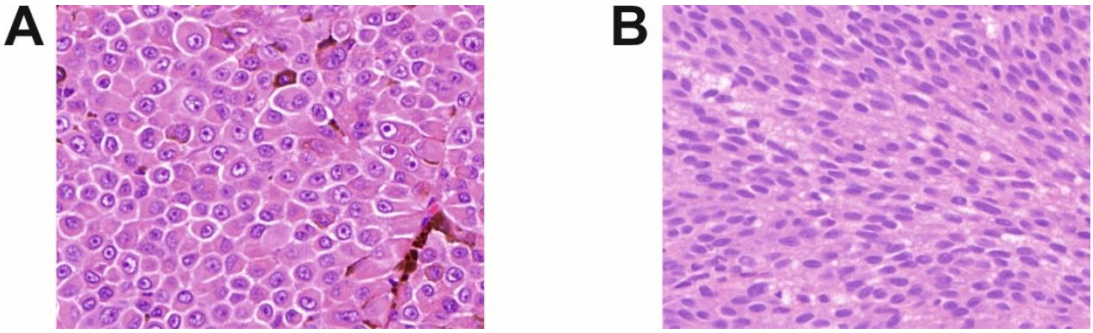

Figure 1.8 Cytomorphology of UM: **A)** Epithelioid cells distinguishable by their round nuclei and abundant cytoplasm **B)** Spindle cells with a long cigar-like shape nucleus. (Courtesy of Prof. S.E. Coupland)

1.5.4.2 Mitotic count

Mitotic count is defined as the number of tumour cells undergoing mitosis and is a useful prognostic tool in numerous cancer types. The mitotic count is determined by examining haematoxylin and eosin (H&E) stained sections of UM and counting the number of mitoses per 40 high-power field (40x objective) (154). Observable mitotic figures are classified using

the criteria established by Van Diest et al. in 1992; absence of nuclear membrane, presence of condensed chromosomes which are either clotted, arranged in planes or in separate clots (Figure 1.9) (155). Another approach to measuring mitotic activity has involved immunohistochemical analysis using an antibody that detects the mitotic marker, phospho-histone H3 (Figure 1.9) (156). A method commonly used to assess the mitotic count is examining tumour sections following immunohistochemical detection of Ki67 positive cells, a well-known marker of cellular proliferation (157). A study examining mitosis in 918 UM patients by examining H&E stained sections established that a high mitotic count (>4/40) was an independent predictive factor for metastatic death regardless of chromosome 3 status (158). A high mitotic count is symptomatic of aggressive, fast-growing tumours and is a useful predictor of metastatic disease

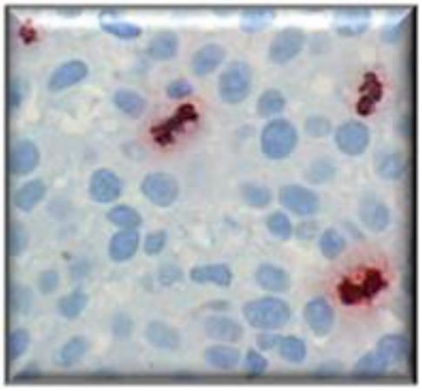

Figure 1.9 A phospho-histone H3-stained UM tumour section showing proliferating tumour cells (Courtesy of Prof. S.E. Coupland).

1.5.4.3 Closed connective tissue loops

In 1992 it was suggested that metastatic potential and tumour progression were linked to the arrangement of the microvasculature or connective tissue patterns within UM (159). Several vascular patterns were identified using Periodic acid-Schiff (PAS) positive staining; straight channels, parallel straight channels, cross-linked channels, incomplete closed loops, and complete closed loops (Figure 1.10) (160). These patterns were later organised into two distinct hierarchical groups: tumours with parallel and straight channels, and tumours with

networks of complete and incomplete loops branched or unbranched, with the latter being associated with a more aggressive tumour phenotype (161). Statistical analysis has shown that the incidence of closed connective tissue loops are associated with ciliary body tumours, epithelioid cell types, and large tumour size (162). It is not clear whether these 'loops' represent blood vessels or only connective tissue; however, formation of microvascular channels in UM has been described in vitro, and has been termed 'vasculogenic mimicry', which is a *de novo* event lacking the presence of endothelial cells (163) (164).

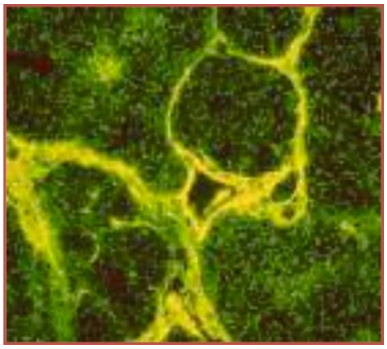

Figure 1.10 A Periodic acid-Schiff stained UM section under green light, showing the PAS+ closed connective tissue loops. (Courtesy of Prof. S.E. Coupland)

1.5.4.4 Lymphocytes

Cancer-related inflammation has recently been defined as the seventh hallmark of cancer, which includes the presence of inflammatory mediators such as chemokines and cytokines in addition to inflammatory cells such as macrophages and lymphocytes (165). Tumour-infiltrating lymphocytes (TILs) can be found in around 5–12% of all UM (166). Studies have shown that the immune response in UM is enhanced by the high levels of HLA (Human Leukocyte Antigen)-DR on the surface of T-helper cells (167). In tumours such as cutaneous melanoma, the increased presence of TILs is associated with a good prognosis (168). However, in UM the presence of TILs has been shown to be associated with an adverse prognostic outcome (169) (170). A recent study demonstrated a clear association between monosomy 3 and the presence of CD8+ and CD4+ lymphocytes (171).

1.5.4.5 Macrophages

Macrophages originate from a specific type of white blood cells called monocytes that are responsible for destroying intra-cellular material such as microbes, foreign substances and cancer cells in a process known as phagocytosis. However, tumour-associated macrophages (TAMs) contribute directly to growth and progression of tumour cells in a number of ways. TAMs are a source of growth factors, promote angiogenic factors, matrix proteases and suppress the adaptive immunity as well as inhibiting apoptosis resulting in increased cell proliferation (172). A study examining 139 macrophage-infiltrated enucleated eyes showed a positive correlation between the numbers of CD68+ TAMs and the presence of epithelioid cells, heavy pigmentation and high microvascular density, as well as an association with increased melanoma-specific mortality (173). The presence of macrophages in UM has been also proposed to correlate to monosomy 3 (174).

1.6 Prognostication Methods

1.6.1 Fluorescence in situ Hybridisation

Fluorescence in situ Hybridisation (FISH) is a molecular cytogenetic technique that employs the use of fluorescently-labelled probes that bind to sequences of DNA for the detection and localisation of specific genes on chromosomes (175). FISH is considered a useful tool in establishing copy number changes and chromosomal rearrangements in cancers, and developmental disorders (176, 177), and is still widely used today to determine chromosome 3 status of UM (178) (Figure 1.11). However, many ocular oncology treatment centres are no longer using FISH in routine analysis of UMs. This is partly due to the fact that the centromeric probes used to identify loss of chromosome 3 are unable to identify partial losses of either 3p or 3q, (179). Furthermore, FISH is unable to detect isodisomy 3, which is associated with an unfavourable prognosis (180). There are numerous issues performing FISH for FFPE tissues such as lengthy pre-treatment regimens and labour

intensive procedures. Other techniques are now available that provide more detailed analysis of copy number changes and yield more accurate results with FFPE material (181) (182).

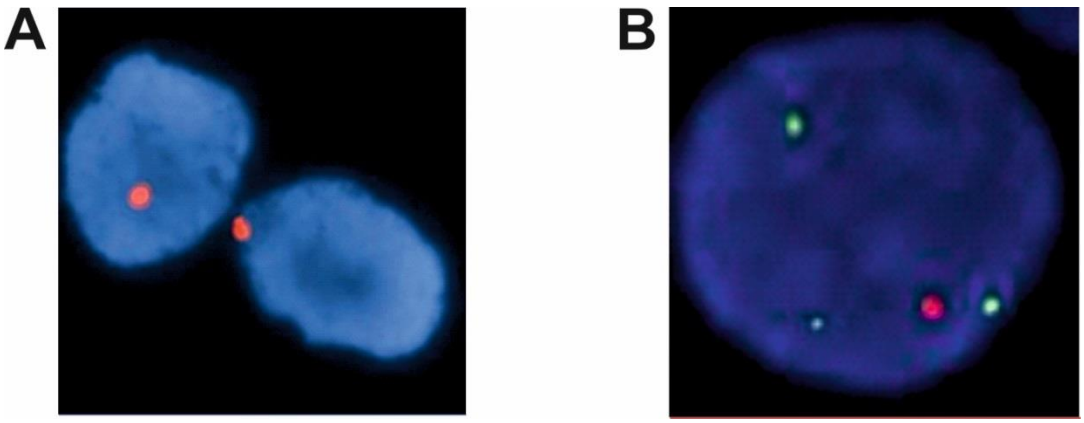

Figure 1.11 A fluorescence in situ hybridisation (FISH) image of UM cells: **A)** a monosomy 3 UM cell; the red dots are centromeric chromosome 3 probes only one centromere is present in each cell **B)** a monosomy 3 UM cell with amplification of the *c-myc* region; the red probe corresponds to the centromeric region of chromosome 8 and the green probe corresponds to the c-myc gene of which there are three copies. (Courtesy of Prof. B. Damato)

1.6.2 Multiplex Ligation-dependent Probe Amplification

Multiplex Ligation-dependent Probe Amplification (MLPA) is a commercially-available and widely used assay to detect ploidy, mutations, single nucleotide polymorphisms (SNPs) and DNA methylation. It is a unique technique whereby multiple targets are amplified using a single primer pair, hybridised and ligated into a complete probe resulting in uniquely sized amplicons, which facilitate separation via capillary electrophoresis (182). The use of MLPA for copy number analysis in UM is undertaken using a specific kit, SALSA P027, designed by the manufacturers MRC Holland (MRC Holland, The Netherlands). The kit contains 50 probes that hybridise to gene loci on chromosomes 1p, 3, 6 and 8 (183). MLPA was

established as a useful tool for predicting metastatic death in UM by Damato et al. 2009 (184). A study of 452 choroidal melanomas supported the use of MLPA for routine clinical prognostication with combined chromosome 3 loss and 8q gain having a worse prognosis that monosomy 3 alone, especially when considered together with the clinical and histologic risk factors (76). A recent larger study encompassing a cluster analysis of 602 MLPA results and clinical outcome, identified three prognostic groups: group 1 (normal chromosomes 3 and 8q), group 2 (either 3 or 8q abnormal), and group 3 (3 and 8q abnormal).(185). Although suitable for both fresh and FFPE material, MLPA has been shown to perform better on fresh/snap-frozen tumour material (186). In addition, tumour heterogeneity has also been demonstrated to be a limitation of MLPA, as not all sampling methods are representative of the whole tumour which can yield equivocal results (187). Heterogeneous populations of tumour cells can contribute to differences in molecular profiling; this has led to concerns that a single tumour biopsy may not be representative of the whole tumour.

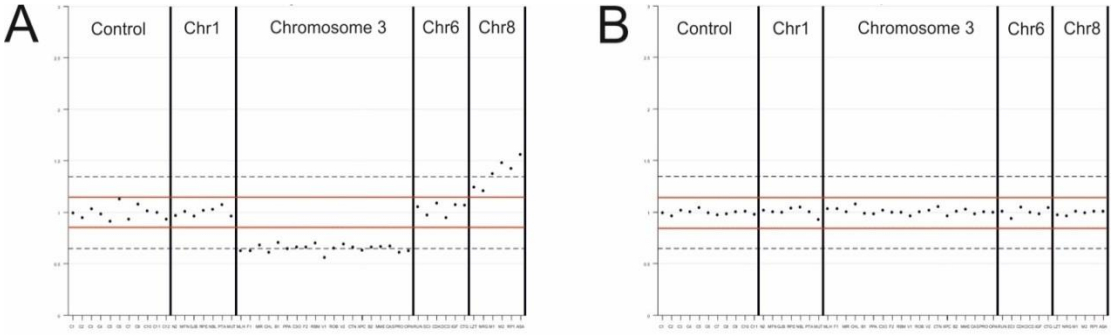

Figure 1.12 MLPA 'Piano' scores highlighting the different results seen in UM patients: all probes that fall in between the red lines are considered within the 'normal range. **A**) MLPA results showing losses across the loci chr3 (monosomy 3) and polysomy 8q; **B**) MLPA results showing normal copy numbers for chromosomes 3 and 8.

1.6.3 Microsatellite Analysis

Microsatellite analysis (MSA) is a valuable diagnostic tool used routinely in clinical practice to determine aneuploidy in pre-natal tissues (188). MSA is also used as a prognostic tool to

establish chromosome 3 status in UM (189). Microsatellites are generally found in the non-coding regions of the genome and are small repeating regions of 1-6 base pairs. MSA is a relatively easy and rapid test to perform whereby the region containing the microsatellite is amplified by multiplex-PCR. Fragment analysis of the fluorescently tagged probes is then employed to establish an allelic ratio; a comparison of tumour material and matched blood sample from each patient. The genotype of a locus is determined from the value of the allelic ratio, where loss of heterozygosity (LOH) is >2.5, no loss of heterozygosity (NLOH) <1.4 and allelic imbalance between 1.4 and 2.5 (190). MSA only requires tiny amounts of DNA >5ng/µl making this a suitable technique to employ on smaller samples such as fine-needle aspiration biopsies (70). A large study of 374 UM samples by Thomas et al. 2012 demonstrated the prognostic value of establishing chromosome 3 status using MSA, with LOH and allelic imbalance being associated with metastatic death (190). MSA is also a useful technique in establishing tumours with acquired homozygosity, or isodisomy, where conventional methods of testing such as karyotyping have shown a normal disomy 3 result (180).

1.6.4 Gene Expression Profiling

Gene expression profiling (GEP) is a technique that simultaneously measures mRNA expression of multiple genes. GEP was employed by Tschentscher et al. 2003, who established an association between different levels of gene expression and chromosome 3 status in UM (191). The relationship between gene expression and survival was later also explored by Onken et al. 2004 leading to a classification of UM as low-grade/class 1 or high-grade/class 2. The data identified 12 signature genes that could distinguish between low and high metastatic risk UM and has led to the development of a commercial test in which the 12 signature genes and 3 housekeeping genes form the Decision DxUM panel marketed by Castle Biosciences in the USA for prognostication of UM patients (192). The GEP

classification system for UM was later revised to take into account low-risk/class 1 patients who developed metastases. This led to the creation of class 1a and 1b tumours, with the latter indicating an intermediate risk of metastasis (193). Recent studies have shown 'Preferentially Expressed Antigen In Melanoma' or PRAME to be an independent prognostic biomarker in UM, which is hypomethylated and activated in both class 1 and 2 tumours and associated with an increased metastatic risk (194, 195). Although an effective method of classifying tumours as high or low risk, these results are not used in conjunction with other well published clinical and histopathological prognostic features, reducing the accuracy of the prognostication. Moreover, recent data suggests that GEP cannot distinguish between primary UM and secondary metastases from other primary tumours (196).

1.6.5 The Liverpool Uveal Melanoma Prognostication Online (LUMPO) Tool

'Liverpool Uveal Melanoma Prognostication Online' or LUMPO is a freely available multivariate analysis tool used to create a personalised prognostic curve for UM patients (www.ocularmelanomaonline.org) (Figure 1.13). The patient's own clinical, histopathological and genetic results are compared with a healthy age- and gender-matched individual using a clinically validated mathematical algorithm (197). This is particularly important because the survival prognosis of choroidal melanoma correlates with clinical stage in addition to histologic grade, genetic type, and other competing causes of death. LUMPO allows each patient prognostication to be personalised, sparing them from unnecessary screening tests that cause anxiety. This allows screening to be focused to high-risk UM patients allowing any metastatic spread to be detected earlier. The Liverpool Ocular Oncology Centre (LOOC) was the first centre to provide this personalised service to patients and a recent google analysis of the tool showing 3836 hits from 2204 users in 717 cities around the world. An updated version of this software is currently online which also

incorporates chromosome 8q status. This is in the process of being externally validated by the ocular oncology group (OOG).

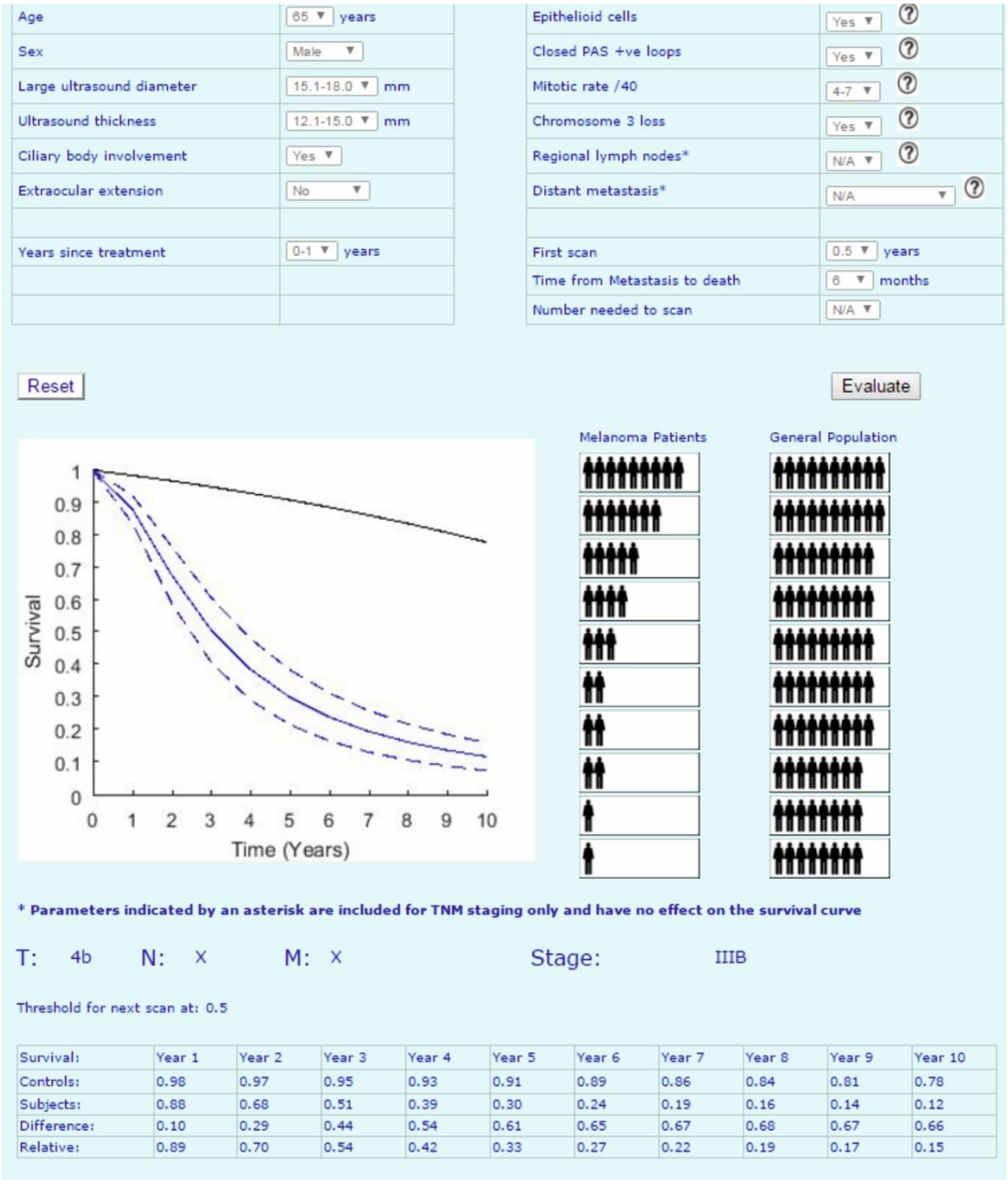

Survival:	Year 1	Year 2	Year 3	Year 4	Year 5	Year 6	Year 7	Year 8	Year 9	Year 10
Controls:	0.98	0.97	0.95	0.93	0.91	0.89	0.86	0.84	0.81	0.78
Subjects:	0.88	0.68	0.51	0.39	0.30	0.24	0.19	0.16	0.14	0.12
Difference:	0.10	0.29	0.44	0.54	0.61	0.65	0.67	0.68	0.67	0.66
Relative:	0.89	0.70	0.54	0.42	0.33	0.27	0.22	0.19	0.17	0.15

Figure 1.13 LUMPO – Version I: A personalised survival curve that is indicative of a high risk of developing metastatic UM. This patient is a 65 year old man with an epithelioid celled, monosomy 3 ciliochoroidal melanoma. They have an 80% greater chance to have died of metastatic disease when compared to age and gender matched population. The normal population is depicted using the black line at the top of the graph where the patients are depicted using the blue line with each dashed line representing the confidence interval.

1.7 Advances in Prognostication

Next-generations (NGS) studies of UM have contributed to the identification of recurrent mutations in UM in *BAP1*, *SF3B1*, *EIF1AX*, *CYSLTR2* and *PLCB4* (129) (119) (132) (133). Larger whole exome studies like those carried out by Royer-Bertrand et al. and Robertson et al. that integrated copy number and mutation data enabled the identification of four distinct molecular subgroups in terms of survival (134) (135). This has facilitated the development of targeted NGS panels that have the potential to be used to aid prognostication in the clinic (198).

1.8 Scope of Thesis

This review of the published literature makes it abundantly clear that there are numerous prognostic factors to consider when determining the metastatic risk of patients with UM. Most recently, mutations identified in *BAP1, SF3B1* and *EIF1AX* have been shown to contribute to the metastatic risk stratification of patients with this disease. In an era of 'personalised medicine' it is becoming increasingly important to look at the specific genes and proteins that contribute to cancer growth, survival and spread in order to provide more accurate diagnoses and targeted therapies. The clinical use of next generation sequencing (NGS) has increased over the last 5 years enabling medical professionals to create large targeted sequencing panels for hereditary cancers, neurodegenerative disorders and other diseases. NGS has many advantages over traditional Sanger sequencing, primarily the ability to fully sequence a range of mutations on a multitude of genes, at a comparatively low cost. This thesis examines our current methods of prognostication for UM patients and aims to investigate how these can be improved/enhanced. In **Chapter 2** the similarities and differences between the rare subtype of uveal melanoma; iris melanoma and the more commonly diagnosed choroidal melanoma by analysing genetic data alongside clinical and histopathological features of the tumours. The efficacy of MSA in correctly predicting

patient outcome based on their chromosome 3 status and the effect that radiotherapy has on obtaining a clear genetic result was investigated in **Chapter 3.** We also examined the relationship between nBAP1 protein expression and survival in **Chapter 4** by undertaking a statistical analysis to establish the relationships between nBAP1 expression, chromosome 3 data and survival. In **Chapter 5**, I describe a bespoke NGS panel that we designed on the basis of TCGA data, which mapped out in detail the most common mutations in UM. This new NGS panel for UM includes both the most common mutations in UM as well as the significant copy number variations. This panel was tested on both fresh and formalin-fixed paraffin embedded (FFPE) tumour material, with the view of ultimately introducing into medical care. **Chapter 6** focussed on understanding the role of a protein recently identified in uveal melanoma, RasGRP3, by examining protein expression in primary UM samples by IHC and in well characterised UM and conjunctival cell lines using western blotting.

Chapter 2

Genetic Testing in Iris Melanoma

2.1 Introduction

The iris is a thin, circular, multi-layered structure consisting of the iris pigment epithelium and the pigmented outer stroma. There are two muscles within the iris: the sphincter that constricts the iris pupil, and the dilator that dilates it. The iris is responsible for controlling the amount of light that reaches the retina by controlling the diameter and size of the pupil. The pigmented outer stroma, with its scattered melanocytes, is the structure within the iris responsible for defining the range of eye colours present in humans: blue, hazel, green or brown.

Iris melanomas (IM) are the rarest of all UMs, consisting of only 5% of all cases, and are thought to arise from neoplastically-transformed iris melanocytes (199) (Figure 2.1). Primary treatment of IM varies depending on the behaviour and size of the tumour: small lesions where there is not any documented growth can be observed and treatment delayed. Different treatment options are available when the lesion is more aggressive, and include PBR, brachytherapy, local resection or iridocyclectomy and enucleation, if there is involvement of the angle or diffuse iris involvement. IM are considered less aggressive than choroidal and ciliary body melanomas, primarily because they are detected earlier as they are externally visible due to their physical location. In addition, IM are thought to be privy to host immune responses within the aqueous that suppress the metastatic potential of the tumours in comparison to other UM (200). Moreover, IM are more likely to be comprised of spindle cells, which are associated with a more favourable prognosis (201). Metastatic spread in IM is reported in 0.5% of cases at 3 years and 7% at 10 years with an overall 5-year mortality of 2-3% (202). There are several risk factors for the metastatic spread of IM: increased patient age, ciliary body involvement, angle involvement, raised intraocular pressure, extrascleral extension, size (>3mm diameter, 1mm thickness), diffuse growth pattern, rapid growth, indistinct edges, hyphaema, pigment dispersion, ectropion uveae, prominent vascularity and pupillary ‘peaking’ or ‘splinting’ (203). The chromosomal

alterations in posterior UM are well-documented in the literature, and there is a clear correlation between genetics and metastatic death; however, due to the rarity of IM there have been limited studies on their genetic alterations.

The aim of **chapter 2** was to determine whether the genetic changes associated with posterior UM are also detected in IM. This was achieved by: 1) undertaking MLPA/MSA analysis of IM; and 2) analysing the genetic data together with the clinical and histopathological features of the tumours.

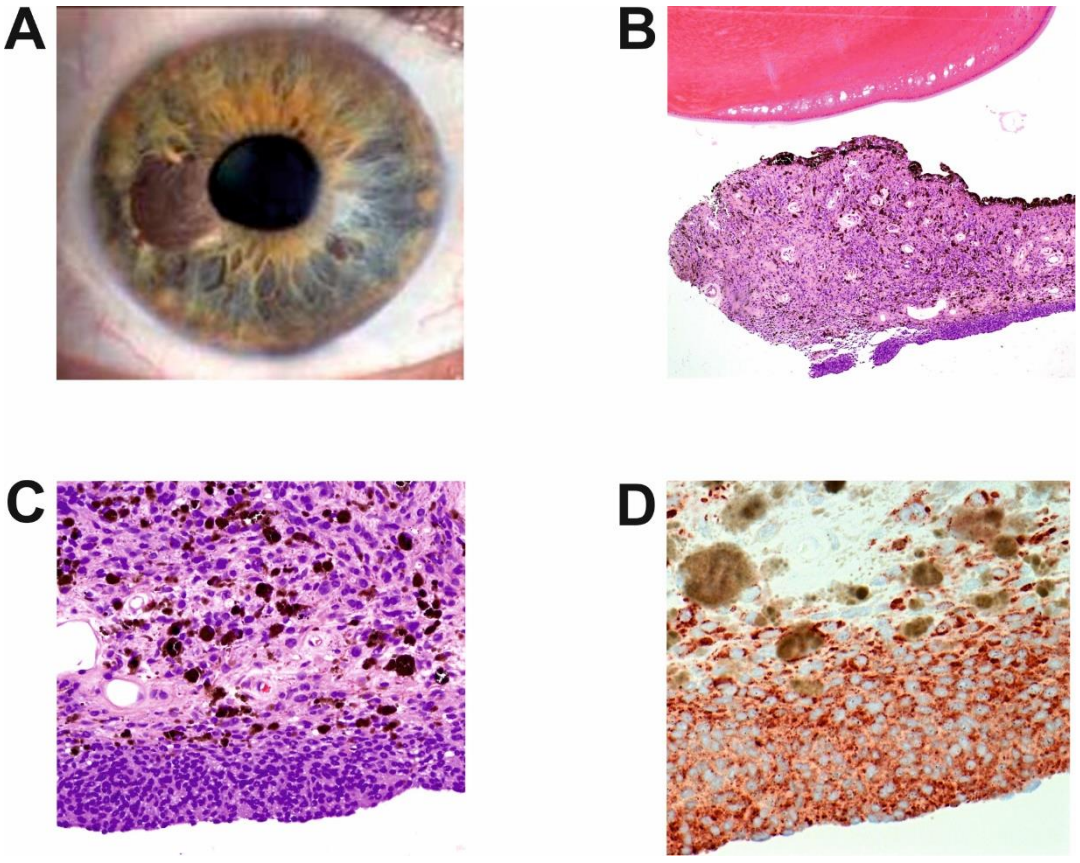

Figure 2.1 Clinical and histological examples of IM. A) An iris melanoma that extends from 8-9 o'clock (courtesy of Prof. B Damato); B) An IM section at x10 magnification; the iris pigment epithelium is on the posterior surface, the anterior stroma and iris leaf show atypical melanocytes C) An IM section of the lesion in B at x40 magnification showing the atypical melanocytes in greater detail; D) Melan-A immunohistochemical staining of the same IM in B and C (courtesy of Prof. S. E. Coupland).

2.2 Materials and Methods

A retrospective database review of all IM patients attending the LOOC between January 1993 and March 2015 was performed. Clinical, histopathological, genetic and follow-up information for the identified IM cases was recorded. All samples had been examined and classified by an Ophthalmic Pathologist according to the modified Callender's classification of UM. Cases were excluded in which iris involvement was judged to be secondary to invasion from a posterior UM based on the clinical history of the patients. All patients had undergone full pre-operative ophthalmic and systemic examinations including slit-lamp examination, gonioscopy, ocular coherence tomography (OCT) and echographic measurements of the tumour using a water-bath filled ultrasound probe with 2% hypromellose (EyeCubed Ultrasound, Ellex Ltd.).

2.2.1 DNA extraction from fresh UM

FNAB were centrifuged at 1500RPM for 2 mins. Tissue lysis and protein digestion was carried out using 180µl Buffer ATL (Qiagen GmbH, Hilden) and 40µl of Proteinase K (20mg/µl) (Qiagen GmbH, Hilden). Samples were incubated at 56°C 350RPM on a Thermomixer comfort (Eppendorf). An additional 20µl of Proteinase K was added after 4 hours and the samples were incubated overnight. Genomic DNA was isolated using DNeasy Blood and Tissue spin columns (Qiagen GmbH, Hilden), purifying the DNA with two AW1 buffer washes to remove contaminants and enzyme inhibitors followed by a further wash in AW2 buffer. DNA was re-suspended in 35µl TE buffer (10mM Tris-HCl pH 8.0, 0.1mM EDTA) (Life Technologies ltd. Carlsbad).

2.2.2 DNA extraction from FFPE tumour samples

After H&E-stained sections were examined and the tumour area identified, 5-10 20µm thick sections were microdissected from 6 iridocyclectomy and 6 enucleation samples using a

scalpel and each placed in a sterile 1.5ml Eppendorf tube. Tissue lysis and protein digestion was carried out using 180µl Buffer ATL (Qiagen GmbH, Hilden) and 40µl of Proteinase K (20mg/µl) (Qiagen GmbH, Hilden). Samples were incubated at 56°C 350RPM on a Thermomixer comfort (Eppendorf) overnight. On day 2, an additional 10µl of Proteinase K was added at three separate intervals and the samples were incubated overnight. On day 3, FFPE lysis underwent an additional incubation at 70°C to destroy crosslinks with histones. Genomic DNA was isolated using DNeasy Blood and Tissue spin columns (Qiagen GmbH, Hilden), purifying the DNA with two AW1 buffer washes to remove contaminants and enzyme inhibitors and one AW2 wash. DNA was re-suspended in 35µl TE buffer (10mM Tris-HCl pH 8.0, 0.1mM EDTA) (Life Technologies ltd. Carlsbad).

2.2.3 DNA extraction from patient matched whole blood

200µl of matched whole blood was digested in 20µl of proteinase K (20mg/µl) (Qiagen GmbH, Hilden) and 200µl AL buffer (Qiagen GmbH, Hilden). Samples were incubated at 56°C 350RPM on a Thermomixer comfort (Eppendorf) for 10 minutes. Genomic DNA was isolated using DNeasy Blood and Tissue spin columns (Qiagen GmbH, Hilden). The DNA was then purified by washing with AW1 and AW2 buffers. DNA was re-suspended in 35µl TE buffer (10mM Tris-HCl pH 8.0, 0.1mM EDTA) (Life Technologies ltd. Carlsbad).

2.2.4 DNA Quantification

DNA concentration was quantified by fluorometry (Invitrogen Qubit fluorometer and broad-range DNA quantification assay; Life Technologies, Carlsbad, CA; Glasgow, UK). The fluorometer was calibrated using two DNA standards; standard 1 which has a concentration of 0ng/µl and standard 2 which has a concentration of 100ng/µl. The Qubit working solution was prepared by diluting the dsDNA BR Reagent 1:200 in Qubit dsDNA BR Buffer.

1µl of sample DNA was then mixed with 199µl of the Qubit working solution and incubated at RT for 2 minutes. DNA concentration was subsequently measured.

2.2.5 Multiplex Ligation-Dependant Probe Amplification (MLPA)

Copy number variations in chromosomes 1, 3, 6 and 8 were identified using the SALSA MLPA UM P027 kit (MRC-Holland, Amsterdam, The Netherlands). 100ng of tumour DNA extracted from IM samples in addition to DNA from 6 normal choroid samples for FFPE tumour material and 6 fresh blood samples for fresh tumour material, was diluted in 5µl (20ng/µl) of TE buffer (10 mM Tris-HCl (pH 8.0) 0.1 mM EDTA, Life Technologies, Scotland) and transferred into 0.2ml thin walled 8-strip tubes (Thermo Scientific). Negative and positive controls were included in each run; negative control used was TE buffer and positive controls consisted of previously tested samples of known outcome. All PCR steps were carried out using a G-Storm GS1 Thermal Cycler (GRI- Genetic Research Instrumentation Ltd, Essex). Samples were denatured at 98°C for 5 minutes and allowed to cool to 25°C. A hybridisation mixture, consisting of 1.5µl of SALSA Probemix and 1.5µl of MLPA buffer, was added to the denatured DNA. The samples were then heated at 95°C for 1 min and the probes were hybridised overnight at 60°C for 16-18 hours. 32µl of a ligation mixture consisting of 3µl of Ligase-65 Buffer A, 3µl Ligase-65 Buffer B, 1µl of Ligase-65 enzyme and 25µl nuclease free water was added to the samples and incubated at 54°C for 15 mins (for ligation of adjacent probes), 98°C for 5 mins (for heat inactivation of Ligase-65 enzyme) and allowed to cool to 20°C. 10µl of PCR mix consisting of 6.5 µl nuclease free water, 2 µl SALSA PCR primer mix, 1µl of 22% BSA (Sigma) and 0.5 µl SALSA Polymerase was added to samples. The samples were then subjected to 35 cycles of 30 seconds 95°C; 30 seconds 60°C; 60 seconds 72°C, ending with 20 min incubation at 72°C.

2.2.6 MLPA fragment analysis using capillary electrophoresis

1µl of MLPA PCR products was mixed with 0.5µl GeneScan 500 LIZ size standard (Applied Biosystems, Foster City, California) and 8.5µl HiDi Formamide (Applied Biosystems, Foster City, California) in a semi-skirted 96-well plate (Starlabs Ltd, United Kingdom). Samples were denatured at 95°C for 3 minutes and placed on ice to cool for 5 minutes. The IM samples were separated and analysed on a 3500 Genetic Analyser (Applied Biosystems) 8 capillary sequencer and GeneMapper software (Applied Biosystems) in the molecular pathology department of the Royal Liverpool University Hospital, Liverpool. Fluorescence intensity was depicted by varying peak heights for each of the 50 probes included in the SALSA MLPA UM PO27 kit (Figure 3.1). Analysis of MLPA data was performed using a MatLab adapted version of a spreadsheet (Excel; Microsoft, Redmond, WA) designed by the National Genetics Reference Laboratory (NGRL), Manchester, UK (http:/www.ngrl.org.uk/Manchester/). MLPA data was considered reliable if 6 or more control probes were within the normal range. As previously described by Lake et al. (2012) dosage quotients were categorised as; ≤0.65 deletion, 0.65 – 0.84 borderline loss, 0.85 – 1.14 normal, 1.15 – 1.35 borderline amplification and ≥1.35 amplification. 75% of the probes needed to be in agreement in order to definitively classify chromosomal 'loss' or 'gain' and anything under 75% is considered an unclassified result (186).

2.2.7 Microsatellite analysis

IM samples yielding <100 ng DNA were analysed for chromosome 3 aberrations by MSA. 5ng of IM tumour DNA with matched blood DNA from the same patient was transferred into 0.2ml thin walled 8-strip tubes (Thermo Scientific). Two separate multiplex PCR reactions containing primer pairs that flank 8 microsatellites on chromosome 3 (4 on 3p and 4 on 3q) have previously been optimised for MSA testing (Table 2.1) (190). 24µl of master mix consisting of; 8.9µl nuclease free water (Qiagen, GmbH, Hilden Germany), 12µl

2x Qiagen Multiplex PCR mix (Qiagen, GmbH, Hilden Germany), 0.5µl 22% BSA (Sigma) and 2.1µl primers (Eurofins, Germany) was added to the samples. The samples were transferred to a G-Storm GS1 Thermal Cycler (GRI- Genetic Research Instrumentation Ltd, Essex) and after an initial activation step at 95°C for 15 minutes they are subjected to 35 cycles of; 94°C for 30 seconds, 56°C for 90 seconds and 72°C for 60 seconds with a final extension for 30 minutes at 60°C, allowing the samples to cool at 10°C. PCR products were then analysed using the ABI 3500 Genetic Analyser (Applied Biosystems) and the fragment analysis completed using GeneMapper (Applied Biosystems). The electropherograms generated show the peaks of the marker and the "peak area" obtained from the test (tumour) and reference (whole blood) samples of the same patient. A marker is classed as "informative" when the two allelic peaks are present in the reference sample (i.e. blood) and can be compared to the corresponding test sample (i.e. tumour). If two allelic peaks are not present in the reference blood sample, the marker is classified as "non-informative" (NI) and an allelic ratio (AR) cannot be calculated for that particular microsatellite. From the data generated by the informative markers, the following classifications are given: Loss of heterozygosity (LOH) - Data shows LOH for a particular marker when AR > 2.5. No Loss of heterozygosity (NLOH) - Data shows NLOH for a particular marker when the AR = 1 – 1.3. Allelic Imbalance (AI) Data shows AI when the AR = 1.4 - 2.5.

Based on the MSA data generated the IM were classified as follows: M3 when two or more microsatellites on chromosome arm 3p and two or more microsatellites on chromosome arm 3q show LOH the case is classified as being at high risk of developing metastatic disease; D3 when two or more microsatellites on chromosome arm 3p and two or more microsatellites on chromosome arm 3q show NLOH; and the remaining markers do not display LOH the case is classified as being at low risk of developing metastatic disease or AI. The significance of AI is unclear but was investigated in Chapter 3.

Table 2.1 Primer Sequences for microsatellites covering chromosome 3

Marker				Marker position in Chr 3		Amplicon size	Repeat	Primer label/ colour
Name	**Primer sequence**	**Multiplex primer group**	**Tm**	**cM**	**Arm**			
D3S3050	For_TGGTGGTATGCATTTGTCAG Rev_ATTCCCTGACTTCAAGTGCA	2	55.3 °C	10.31	p (26-24.2)	230-250bp	Tetranucleotide	HEX/ green
D3S1263	For_CTAAGTAGGCAGTTGGTATTATTTC Rev_ATCACAGCAGGGGTTCATTTTTTC	1	58.1 °C	29.62	p (25.3)	200-230bp	Dinucleotide	FAM/ blue
D3S1300	For_ GAATAAACCTGAGAATCATCCCT Rev_ CATGACGTTCCTTTGTAGTGTTT	3	57.1 °C	82.22	p (14.2)	110-158 bp	Dinucleotide	FAM/ blue
D352406	For_GGCTGGATGATCCACTTTAA Rev_CCAGTTCCTGCTTCTTGAAA	2	55.3 °C	102.64	p (13)	306-350bp	Tetranucleotide	TET/ blue
D3S3045	For_ACCAAATGAGACAGTGGCAT Rev_ATGAGGACGGTTGACATCTG	2	55.3 °C	117.29	q (13.12)	180-200bp	Tetranucleotide	FAM/ blue
D3S1744	For_TTTAAGCGGAAGGAAGTGTG Rev_CTGGCCCCATCTCTCTCTAT	1	55.3 °C	153.36	q (24-25)	131-167bp	Tetranucleotide	TET/ blue
D3S2421	For_AGCCATGATCACACCACTCT Rev_GGTCTTCATCATGCATCCTC	1	57.3 °C	180.68	q (26.31)	297-310bp	Tetranucleotide	FAM/ blue
D3S1311	For_GGAAGTTTCAGCCAACG Rev_TTAGTCCCACTGATGTTACATTT	2	52.8 °C	198.5	q (29)	134-152bp	Dinucleotide	HEX/ green

2.3 Results

2.3.1 Patients

A retrospective database review was carried out by Mrs. Yamini Krishna of all IM patients attending LOOC between January 1993 and March 2015. Of these I identified 26 cases where DNA could be obtained to perform molecular analysis.

2.3.2 Molecular Genetic Analysis

DNA was available from 26 patients: 22 samples were obtained after primary treatment of the tumour (12 were biopsies taken on the last day of PBR) and 4 samples were secondary procedures due to tumour recurrence (enucleations or iridocyclectomies). Eight of the IM had secondary ciliary body involvement where the primary tumour had been iridal in origin. Genetic analysis of IM was performed by MLPA in 20 cases and MSA in 6 cases. D3 was reported in 15/26 (58%) of the cases and M3 in 4/26 (15% cases). 3/26 (12%) cases yielded an unclassifiable chromosome 3p result but both cases had a normal 3q. 4/26 (15%) cases showed loss of chromosome 3p only. MLPA was performed on 18/26 (69%) cases; polysomy 8q was present in only 1 case and gain of 6p was found in 4 cases (Table 2.2). Of the patients who died from metastatic IM one patient was M3 with a loss of 6p, the other had D3 with a gain of 6p, loss of 6q, loss of 8p and gain of 8q.

2.3.3 Histopathological Analysis

14/26 (54%) of the IM examined genetically had spindle cell morphology; 10/26 (38%) were of mixed cell type; and 2/26 (8%) were of epithelioid morphology. The mean follow-up time of the IM patients from our cohort was 99.9 months (median 88.5 months; range 6 - 247). At the end of the study 19/26 (73%) patients were alive with no evidence of metastatic spread and 6/26 (23%) patients had died; 2 from metastatic IM and 4 from other causes

including sepsis, metastatic rectal carcinoma and an upper gastrointestinal haemorrhage. One patient was lost to follow up overseas.

Table 2.2 Clinical, genetic and histopathological data for the 26 iris melanoma cases examined. *Sample on which genetic testing was performed; †Biopsy taken prior to PBR; ‡Chromosome 3 data determined by MSA; –, Not performed/not applicable; AI, angle involvement; CBI, ciliary body involvement; F, female; G, gain; IM, iris melanomas; L, loss; LBD, largest basal diameter; M, male; MSA, microsatellite analysis; N, normal; NMD, no mutation detected; PBR, proton beam radiotherapy; U, unclassifiable; UH, ultrasound height

Patient	Gender	Age at Diagnosis (years)	Diagnosis	Primary Management	Secondary Treatment	Follow-up time (months)	LBD (mm)	UH (mm)	Cell Type	Chromosome Data							Death; Cause
										Chr1p	Chr3p	Chr3q	Chr6p	Chr6q	Chr8p	Chr8q	
1	F	32	IM	Iris excisional biopsy*	–	217	2.3	2.2	Spindle	N	U	N	N	N	N	N	No
2	M	33	IM; CBI	Iridocyclectomy*	–	205	1.5	1.1	Mixed	N	L	N	N	N	N	N	No
3	M	55	IM	Iridocyclectomy*	–	142	7.5	1.1	Mixed	N	N	N	N	N	N	N	Yes: Other
4	M	58	IM	PBR+biopsy*	–	88	6.5	2.9	Spindle	N	L	L	G	N	N	N	No
5	M	48	IM	PBR	Iridocyclectomy*	176	3.3	1.8	Mixed	N	N	N	N	N	N	N	No
6	M	51	IM; CBI	PBR	Enucleation*	111	2.9	1.3	Mixed	N	L	L	N	N	L	N	No
7	M	57	IM	PBR+biopsy*†	–	90	4.2	1.3	Spindle	N	N	N	N	N	N	N	No
8	M	53	IM	PBR+biopsy*	–	6	5.4	3.1	Mixed	N	N	N	N	N	N	N	No
9	M	79	IM; CBI	Enucleation*	–	79	7.2	3.3	Mixed	N	L	L	L	N	N	N	Yes; MM
10	M	57	IM; CBI; AI	PBR	Enucleation*	66	6.7	5.0	Mixed	N	N	N	G	L	L	G	Yes; MM
11	F	52	IM	Iridocyclectomy*	–	247	1.2	1.1	Spindle	N	U	N	G	N	N	N	Yes; Other
12	F	84	IM; CBI; AI	Enucleation*	–	94	12.3	3.6	Mixed	N	L	L	N	N	N	N	Yes; Other
13	M	25	IM; CBI	Iridocyclectomy*	–	72	1.9	1.6	Spindle	–	N‡	N‡	–	–	–	–	No
14	M	64	IM; AI	PBR	Enucleation*	89	4.5	0.7	Epithelioid	N	L	N	N	N	N	N	No
15	M	35	IM	PBR+biopsy*	–	57	2.3	0.5	Spindle	–	N‡	N‡	–	–	–	–	No
16	M	61	IM	PBR+biopsy*	–	56	4.3	1.8	Spindle	–	N‡	N‡	–	–	–	–	No
17	F	44	IM	PBR+biopsy*	–	55	2.4	1.0	Spindle	–	N‡	N‡	–	–	–	–	No
18	M	73	IM	PBR+biopsy*	–	8	8.7	1.2	Spindle	N	N	N	N	N	N	N	Yes; Other
19	M	60	IM	PBR+biopsy*	–	109	8.6	3.3	Spindle	N	N	N	G	N	N	N	No
20	F	61	IM; CBI	Iridocyclectomy*	–	94	4.6	2.0	Spindle	N	N	N	N	N	N	N	No
21	M	47	IM; CBI; EOE	Enucleation*	–	90	2.6	1.1	Mixed	N	N	N	N	N	N	N	No
22	M	54	IM	PBR+biopsy*	–	178	4.4	1.1	Epithelioid	–	N‡	N‡	–	–	–	–	No
23	F	62	IM	PBR+biopsy*	–	88	6.5	1.2	Mixed	N	L	N	N	N	N	N	No
24	M	22	IM	PBR+biopsy*	–	64	3.3	2.0	Spindle	–	N‡	N‡	–	–	–	–	No
25	F	64	IM	PBR+biopsy*	–	62	4.7	1.6	Spindle	N	U	N	N	N	N	N	No
26	M	43	IM	PBR+biopsy*	–	53	3.7	1.1	Spindle	N	L	N	N	N	N	N	No

2.4 Discussion

At the close of study in February 2018 this was the largest study carried out on IM (204). The genetics of IM has been investigated in other studies by different methodologies: e.g. karyotyping, MSA and FISH. This study was the first of its kind to examine the molecular genetics using MLPA. The incidence of chromosome 3 loss and polysomy 8q in IM in this study was not consistent with the previously reported cases in the literature, possibly reflecting the varying genetic techniques used to examine these tumours. This is discussed below.

The first reported case of cytogenetic analysis of IM was by White et al. (1995) where they utilised conventional karyotyping to examine a single case of IM (205). They reported aneuploidies on chromosomes; X, 2 7, 15 and 18 in addition to rearrangements of 4q, 8q, 12p and several marker chromosomes. This is in contrast to the well-documented copy number changes in chromosomes 1, 3, 6 and 8 expected in posterior UM. An analysis of 20 IM cases using the molecular cytogenetic technique FISH (206) reported 6/20 (30%) cases with complete loss of chromosome 3, 3/20 (15%) showed partial loss of chromosome 3 and 9/18 (50%) cases had polysomy 8q. This differed to our present study where polysomy 8q was present in only one sample. In this study by Mensink et al. 4/20 patients developed metastatic disease and 3 of these patients had died at the close of study. All of these patients had complete loss of chromosome 3 and polysomy 8q with presence of epithelioid cells.

Shields et al. (2011) analysed 17 treatment naïve IM using MSA, reporting D3 in 5/17 (29%) cases, M3 in 5/17 (29%) cases, and partial loss of chromosome 3 in 7/17 (41%) cases, again different to the 15% cases with partial loss of chromosome 3 found in this study (207). None of the cases that were found to have a normal chromosome 3 copy number had a mixed/epithelioid cytomorphology, whereas in my study 6/17 (35%) of disomy 3 tumours contained epithelioid cells. Furthermore, in contrast to the data from Mensink et al. and the data obtained in my study, Shields et al. did not report any patients developing a local

recurrence or metastatic disease. This may be due to the relatively short follow up for the cases included in the Shields study; 16 months as compared with 247 months in my study.

In the present study, two patients died from metastatic IM. One of the patients who died from metastatic UM had a normal chromosome 3 with gain of 6p and polysomy 8q. One explanation for this is that the normal chromosome 3 result could be due to a rare phenomenon known as acquired homozygosity or isodisomy (180). Isodisomy occurs when one copy of chromosome 3 is lost and subsequently duplicated. This may then result in chromosome 3 with two copies of the mutated tumour suppressor gene *BAP1*. However, this case also had other hallmarks of a 'high risk' UM, in particular it had a large tumour diameter (LBD), both ciliary body and angle involvement, in addition to the presence of epithelioid cells. Taken together, these factors can also contribute to the development of metastatic disease. The other patient's tumour showed loss of chromosome 3 and loss of 6p in addition to other high risk features such as ciliary body involvement and presence of epithelioid cells.

In the present study the follow-up time available for patients who had monosomy 3 ranged from 79 – 111 months, a longer follow up period would have perhaps seen more deaths from metastatic disease. Nevertheless the frequency of monosomy 3 (15%) and polysomy 8q (6%) detected in this study is inconsistent with that reported for posterior UM (216). Two recent next generation sequencing studies of IM have shed further light on the mutations present in melanomas arising at this location. Scholz et al. 2017 identified frequent mutations in *EIF1AX* which fits with the prevalence of D3 that occurs in IM (208). In contrast, the study by Van Poppelen et al. 2018 identified *BAP1* mutations in 43% of their cohort, in addition to 2 mutations in *SF3B1*. A possible explanation for this could be the IM selected for their study had not originated from the iris (209).

In this chapter, I have demonstrated that the same chromosomal aberrations observed in posterior UM are also seen in IM, in both treatment naïve and irradiated IM, with a low-

metastatic risk genotype most commonly observed. Further follow-up and assessment of more cases are necessary to determine the prognostic significance of these alterations.

Chapter 3

An Audit of Choroidal Melanoma Analysed by Microsatellite Analysis

3.1 Introduction

Non-coding regions of the genome contain small tandem nucleotide repeats known as microsatellites. Microsatellites or 'Short Tandem Repeats' are small repeating regions of between 1 to 6 base pairs and the numbers of these repeats can be highly variable. As the majority of microsatellites occur in non-coding regions of the genome they do not produce proteins, enabling the unimpeded accumulation of mutations, facilitating variation. This variability enables microsatellites to be utilised as markers for a range of genetic tests such as aneuploidy screening, paternity testing and DNA fingerprinting. Individuals typically have two alleles for all microsatellites as they are inherited from each parent and these maternal and paternal alleles are often different lengths. As microsatellites are inherited they are heterozygous, and when one pair of alleles is mutated or deleted, this is defined as loss of heterozygosity (LOH). LOH occurs frequently in tumour cells, arising from multiple genetic events, such as faulty repair of DNA breaks and errors during mitosis i.e. non-disjunction. LOH can impact the genome in numerous ways, e.g. loss of gene expression, haploinsufficiency and unmasking recessive tumour suppressor genes. Microsatellite analysis (MSA) is a polymerase chain reaction (PCR)-based technique that amplifies microsatellites of interest using unique fluorescently-tagged sequences flanking these regions as primers. These loci are amplified on nuclear DNA extracted from a tissue sample and a matched whole blood DNA sample. This can then be easily analysed using fragment analysis by capillary electrophoresis. Human chromosome 3 consists of 210 Mb of DNA (~7% of the human genome), with one study identifying at least one hundred and six microsatellite repeat-containing loci on this chromosome (210). MSA of UM was first performed by Tschentscher et al. to examine the feasibility of identifying tumours with M3 in comparison to other methods such as karyotyping and array CGH (211). In this study, fluorescently-tagged primers pairs were obtained from Research Genetics (Research Genetics, Huntsville, USA) corresponding to 7 sites on chromosome 2; 3 on 3p and 4 on 3q, preferring loci with a tetra-repeat structure to enable

quantitative evaluation of the signals. In a similar study, Shields et al., evaluated 10 polymorphic microsatellite markers on chromosome 3 selected from the Applied Biosystems Inc. (ABI; http://www.appliedbiosystems.com/) human genome mapping kit, v2.5 (212). In their 2012 study, Thomas et al. assessed 8 loci using primers purchased from Eurogentec (Seraing, Belgium). Each study utilised forward primers linked to distinct fluorescent labels in order to enable single-lane analysis of markers from one chromosome. To correct for the difference in amplification efficiency of different marker alleles, the ratio of allele peak areas (allele ratio (AR)) in the tumour was normalised against the peak ratio obtained in the corresponding DNA from blood (190). Once determined the genotype of the loci can be classified depending on the AR calculated. At Liverpool AR are classified as follows: AR≥2.5, loss of heterozygosity (LOH); AR 2.49 - 1.4, allelic imbalance (AI) or AR≤1.39, no loss of heterozygosity (NLOH). At the Liverpool Ocular Oncology Centre (LOOC), MSA is used to detect LOH of chromosome 3. Due to the relatively low amount of input DNA required for the PCR-based test, this is usually reserved for smaller UM samples, especially those obtained from fine-needle aspirate biopsies (FNAB) often after radiotherapy has been administered, where there is <100ng of DNA available for genetic analysis. Additionally, MSA of chromosome 3 can be used when other techniques for example, MLPA, fail to provide a result for chromosome 3 or 'acquired homozygosity' or isodisomy is suspected (180). The use of FNAB for prognostication is controversial. Those reluctant to use the procedure argue that it increases the risk of disseminating tumour cells, precipitating metastasis (213-215). There are some cases in the literature that show local recurrence and extraocular extension can occur following intraocular biopsy (215-217). An ex vivo study performed by Glasgow et al (1988) demonstrated iatrogenic dissemination of tumour cells following transvitreal biopsy, however, in general this is a rare complication (218). At the LOOC, FNAB are routinely used in clinical practice to aid diagnosis of indeterminate lesions in addition to genetic characterisation of the tumour.

The aim of **chapter 3** was to: (1) examine survival of patients with UM where the chromosome 3 status was determined by MSA (2) assess the effect, if any, that radiotherapy has on obtaining chromosome 3 classification (3) establish whether taking a FNAB before the administration of radiotherapy (RXT) affects survival.

3.2 Methods

3.2.1 DNA extraction from fresh UM

DNA extracted from 284 fresh UM samples were performed using the methods described in chapter 2.2.1.

3.2.2 DNA extraction from patient matched whole blood

DNA extracted from 284 blood samples were performed using the methods described in chapter 2.2.3.

3.2.3 DNA Quantification

DNA quantification performed using the methods described in chapter 2.2.4.

3.2.4 Microsatellite Analysis

Microsatellite Analysis was performed using the methods described in chapter 2.2.7.

Based on the MSA data generated the UM were classified as follows: M3 when two or more microsatellites on chromosome arm 3p and two or more microsatellites on chromosome arm 3q show LOH the case is classified as being at high risk of developing metastatic disease; D3 when two or more microsatellites on chromosome arm 3p and two or more microsatellites on chromosome arm 3q show NLOH; and the remaining markers do not display LOH the case is classified as being at low risk of developing metastatic disease or AI.

3.2.5 Statistical Analysis

Metastasis-free survival (months) was calculated from the date of first diagnosis until death, or study closure on 15th May 2018. Kaplain Meier survival and Fisher's exact statistical analysis carried out using SPSS Statistics v.24

3.3 Results

3.3.1 Clinical and Histopathological features of the examined UM

Chromosome 3 status as determined by MSA was examined in 284 patients treated at the LOOC between January 2011 and December 2015 (Table 3.2). The study consisted of 134 males and 150 females with a mean age of 58.6 years at primary management (median age 61; range 14 – 92 years). The mean follow-up period was 37.6 months (median follow-up 37 months; range 0– 133 months). At study closure, 240/284 (85%) patients were alive, 34/284 (12%) patients had developed or died from metastatic disease and 12/284 (4%) patients died from other causes. The 284 samples consisted of: 249 biopsies, 27 enucleations, 3 local resections, 2 endoresections and 3 iridocyclectomies. The primary treatment for the 284 samples was: 85 PBR, 158 ruthenium plaque, 26 enucleations, 6 diagnostic biopsies and subsequent genetic analysis, 4 local resections, 3 iridocyclectomies, 1 endoresection and 1 photodynamic therapy. The tumours had a median LBD of 11.05mm (range, 1.82 – 20.80mm) and a median UH of 3.1mm (range, 0.9 – 18.5mm). 93/259 (36%) tumour samples contained epithelioid cells and 171/264 (65%) were spindle cell tumours, cytomorphology was not available for 20 cases due to low cellularity. 38/284 (13%) of tumours involved the ciliary body and 5/284 (2%) of tumours had extraocular extension. 21/38 (55%) surgical resection samples contained PAS+ loops and 6/40 (15%) had necrosis. Of the 240 UM that received radiotherapy, 131 (55%) were biopsied before and 109 (45%) after administration of radiotherapy (Table 3.1).

Table 3.1 Patients receiving biopsy pre and post RXT

Primary Treatment	Biopsy taken		Total
	Before RXT	After RXT	
Proton Beam RXT	22	61	83
Ruthenium Plaque RXT	109	48	157
Total	131	109	240

Table 3.2 Tumour demographics

	All Tumours (n=284)	M3 (n=78)	D3 (n=174)	Partial loss of 3q (n=8)	AI (n=17)	Unclassifiable (n=7)
Median age at PM (years)	61 (14 – 92)	62 (14 -90)	57 (16 – 92)	62 (45 – 81)	59 (44 – 82)	61 (46-71)
Female	150 (53%)	44 (57%)	89 (51%)	6 (75%)	11 (65%)	3 (43%)
Male	134 (47%)	34 (43%)	85 (49%)	2 (25%)	6 (35%)	4 (57%)
Median LBD (mm)	11.05 (1.82 – 20.80)	13.2 (4.4 – 20.80)	10.45 (1.82 – 19.4)	8.65 (5.5 – 13.7)	9.8 (5.8 – 17.4)	10.5 (7.7 – 14.8)
Median UH (mm)	3.1 (0.90 – 18.50)	4.1 (0.9 - 18.5)	2.65 (0.9 – 11.7)	2.2 (1.1 – 10.1)	2.4 (0.9 – 9.8)	3.3 (1 – 5.4)
AJCC Stage	(n=284)	(n=78)	(n=174)	(n=8)	(n=17)	(n=7)
1	133 (47%)	21 (27%)	92 (53%)	7 (88%)	9 (53%)	4 (57%)
2	99 (35%)	34 (44%)	56 (32%)	-	6 (35%)	3 (43%)
3	41 (14%)	16 (20%)	22 (13%)	1 (12%)	2 (12%)	-
4	11 (4%)	7 (9%)	3 (2%)	-	-	-
Cell Type	(n=259)	(n=78)	(n=156)	(n=6)	(n=13)	(n=7)
Epithelioid	93 (36%)	52 (67%)	34 (22%)	1 (2%)	3 (23%)	3 (43%)
Spindle	166 (64%)	26 (33%)	122 (78%)	5 (8%)	10 (77%)	4 (57%)
Ciliary Body Involvement	(n=284)	(n=78)	(n=174)	(n=8)	(n=17)	(n=7)
Yes	38 (13%)	18 (23%)	16 (10%)	3 (4%)	1 (6%)	-
No	246 (87%)	60 (77%)	158 (90%)	5 (6%)	16 (94%)	7 (100%)
Extraocular Extension	(n=283)	(n=77)	(n=174)	(n=8)	(n=17)	(n=7)
Yes	5 (2%)	3 (4%)	2 (1%)	-	-	-
No	278 (98%)	74 (96%)	172 (99%)	8 (100%)	17 (100%)	7 (100%)
Biopsy taken Pre/Post RXT	(n=240)	(n=65)	(n=147)	(n=6)	(n=15)	(n=7)
Pre	131 (56%)	39 (60%)	79 (54%)	3 (50%)	7 (47%)	-
Post	109 (45%)	26 (40%)	68 (46%)	3 (50%)	8 (53%)	7 (100%)
Survival	(n=284)	(n=78)	(n=174)	(n=8)	(n=17)	(n=7)
Months	56.9 (5.7 – 111.7)	46.35 (6.1 – 86.9)	58.85 (11.1 – 111.7)	47.6 (5.7 – 80.6)	62.1 (30.8 – 82.6)	50.0 (48.3 – 73.3)
Status	(n=284)	(n=78)	(n=174)	(n=8)	(n=17)	(n=7)
Alive	240 (85%)	46 (59%)	163 (94%)	6 (75%)	17 (100%)	7 (100%)
Metastatic	33 (12%)	27 (35%)	5 (3%)	2 (25%)	-	-
Death other causes	11 (3%)	5 (6%)	6 (3%)	-	-	-

3.3.2 Genetic features of examined UM

As described in the materials and methods, MSA results were classified into 5 groups; 78/284 (28%) tumours were M3, 174/284 (61%) tumours were D3, 8/284 (3%) tumours had a partial loss of chromosome 3 (all loss of 3q), 17/284 (6%) tumours were AI and 7/284 (3%) tumours were unclassifiable. Of the 34 patients who developed metastatic disease 27 had M3 UM, 2 had loss of 3q and 5 were D3 (Table 3.3).

Table 3.3 Chromosome 3 status and outcome for 284 cases of UM analysed by MSA

Status	Chromosome 3					
	Unclassifiable	Loss	Disomy	Loss 3q	Allelic Imbalance	Total
Alive	7	46	163	6	16	238
Metastasis	0	27	5	2	0	34
Other	0	5	6	0	1	12
Total	7	78	174	8	17	284

Of the 17 UM patients classified as AI, 5 were treated with PBR and had biopsies taken after radiotherapy was administered, 10 were treated with ruthenium plaque, 5 of whom had biopsies taken after radiotherapy, 1 patient was treated by enucleation and the remaining by local resection. The AI cohort consisted of 6 males and 11 females with a median age at primary management of 50 years (rang 44 – 82 years). The tumours had a median LBD of 9.8mm (range, 5.8 – 17.4mm) and a median UH of 2.4mm (range, 0.9 – 9.8mm). 16/17 (94%) had no ciliary body involvement and no cases demonstrated extraocular growth. 10/17 (59%) cases had a spindle cell morphology, 3/17 (18%) contained epithelioid cells and for 4/17 (23%) cytomorphology could not be assessed. At the close of the study in May 2018, all AI patients were all alive and well with no evidence of metastatic disease.

The 240 cases treated by radiotherapy revealed little difference in the frequency of M3/D3 results (Table 3.4). When comparing the success rate of the genetic testing in these samples we classified successful samples as those where a discernible chromosome 3 status could

be obtained, and those as unsuccessful if chromosome 3 status was unclassifiable or showed AI. A comparison of the genetic results obtained from biopsies taken pre- and post-radiotherapy did not show any significant difference in the success rate for chromosome 3 classification (Fisher's Exact p=0.799). This was then compared to the time lapsed from administration of radiotherapy to date of biopsy. Of the 109 post-RXT samples, 12 (11%) were considered unclassifiable and 97 (89%) yielded a chromosome 3 classification. The time to biopsy had a median of 52 days (range, 1 -102 days) and wasn't significantly associated with unsuccessful genotyping by MSA (Mann-Whitney U p=0.307). Successful samples had a median biopsy sampling at 52 days (range, 1 – 102 days) and unsuccessful 47 days (range, 11 – 82 days) (Table 3.5). Any samples >270 post radiation were excluded from analysis as they were more likely associated with tumour regression or regrowth.

Table 3.4 A comparison of chromosome 3 status in samples taken pre- and post-radiotherapy

Chromosome 3	Biopsy taken Pre-RXT	Biopsy taken Post-RXT	P-value
Loss	39	26	0.799§
Normal	79	68	
Partial Loss	3	3	
Allelic Imbalance	7	8	
Unclassifiable	3	4	

§ = Fisher exact test.

Table 3.5 A comparison of genotype success and sampling times in irradiated vs. non-irradiated tumours.

Primary Treatment	Biopsy taken		Total
	Before RXT	After RXT	
Total	131 Median 33 days; Range 0 – 66 days	109 Median 52 days; Range 1 – 102*	240
Genotype unsuccessful	10 Median 16 days; Range 0 – 35 days	12 Median 47 days; Range 11 – 82*	22
Genotype successful	121 Median 33; Range 0 – 66 days	97 Median 52 days; Range 1 – 102*	218

*Post-radiotherapy tumour samples retrieved >270 days post-radiation were removed from statistical analysis to exclude regrowth or tumour regression.

3.3.3 Survival

Kaplan–Meier survival curves and tables were examined for all primary UM stratified according to chromosome 3 status as determined by MSA. Both M3 UM (Log rank, p=<0.001) and loss of 3q (Log rank, p=<0.001) were significantly associated with a reduced metastasis-free survival time (Figure 3.3 and Figure 3.4). UM classified as having AI of chromosome 3 were the most similar to patients with D3 in terms of metastasis-free survival (Log rank, p=0.480) (Figure 3.5). Survival was also compared for patients who had samples taken either before or after administration of radiotherapy and was found to be similar between both groups (p=0.413).

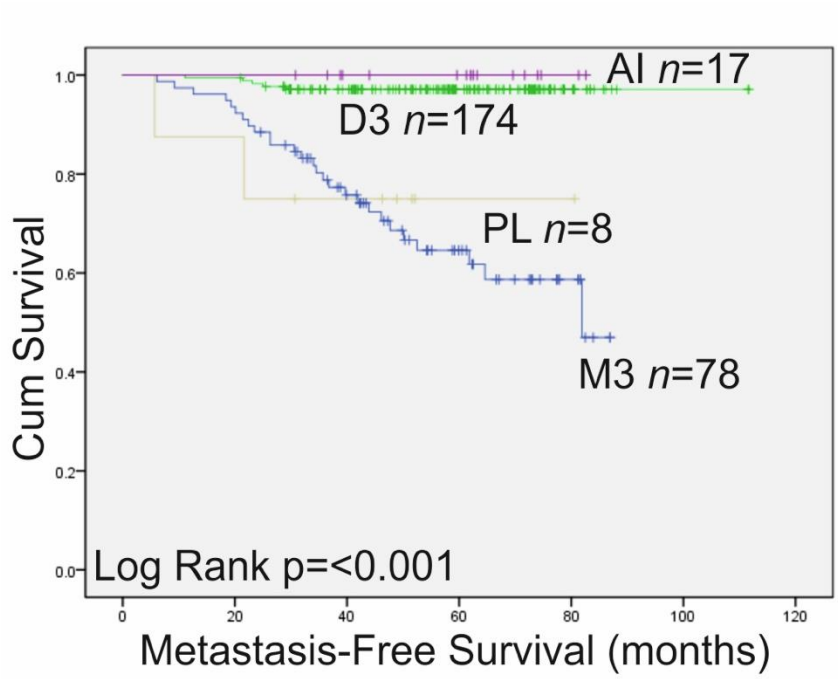

Figure 3.1 Kaplan Meier plots of patient survival where the chromosome 3 status was determined by MSA n=285; disomy 3 n=174, monosomy 3 n=78, partial loss of 3 (loss of 3q) n=8 and allelic imbalance n=17 (log rank p=<0.001).

3.4 Discussion

The efficacy of MSA in chromosome 3 classifications in UM has been explored in other studies, however, this study was the first to examine this technique in samples taken pre- and post PBR and ruthenium plaque radiotherapy (212) (70) (190). The incidence of chromosome 3 loss in this study was not consistent with some of the previously reported MSA studies in the literature, which is possibly a reflection of the varying classification systems used to categorise the tumours as M3 or D3. Although the percentage of M3 cases differed between MSA studies (e.g. between 28 - 56%) (see Table 3.6), it was consistently associated with a poor outcome. In an audit of 500 cases of UM tested using MSA, Shields et al. reported M3 in 25% of cases, a figure consistent with 28% of cases identified as M3 in this study (70). However, in the same study, a large percentage of UM were classified as partial loss of chromosome 3 (27%), which is much greater than that reported in the present study (3%). Partial loss of chromosome 3 was found in 8/286 cases in this study, and was exclusively loss of 3q. This alteration was found to be significantly associated with a poor prognosis (p=0.001) (figure 3.3). The classification system used by Shields et al. (2011) required 9/10 markers to be LOH to be considered complete M3, and 8/10 for partial loss (70). The system adopted in the current study classified cases as partial loss if 2 or more markers were LOH on one chromosome arm. This made Shields et al partial loss cases more similar to our M3. In contrast, Thomas et al. assigned cases as partial loss if at least one chromosome 3 marker showed LOH in a tumour with others showing retention of heterozygosity; these cases were more like the present studies' D3 UM (190). Despite this, the amount of partial loss identified in the Thomas cohort was similar to that seen in this study with a detection rate of 3% and 4%, respectively. The incidence of partial loss of chromosome 3 differs significantly in the literature with some studies reporting between 0% and others as much as 48% (219). This is most likely due to the different ways each individual research group classifies their cases. Some studies suggest that partial loss is

likely caused by tumour heterogeneity (219). Cytomorphological heterogeneity is well documented in posterior melanomas and has fuelled fears that extracting a biopsy from a single site may reflect in the accuracy of chromosome 3 genotyping (220). Previous studies examining this have shown heterogeneity of gene loci dosage quotients in studies utilising MLPA, but it did not alter the overall chromosome 3 statuses observed (187). Similarly Coupland et al. showed that Chromosome 3 data showed prognostic concordance for patient-matched samples in 28 cases that were initially biopsied and subsequently resected (221).

AI were first reported by Tschentscher et al. who consistently observed allele ratios that fell just below the cut-off thresholds for gain or loss (211). They reasoned that this may be the result of clonal heterogeneity or more focal dosage changes. Zeschnigk and Lohmann described MSA as largely successful in evaluating allelic ratios in UM, but named AI as an issue that only affects chromosome 8 (189). Thomas et al. found 19/374 UM had AI of chromosome 3, suggesting heterogeneity of cells consisting of both M3 and D3 as a conceivable explanation for the phenomenon (190). They believe that AI UM defined by MSA should be given a poor prognosis. In contrast, all cases in this study defined as 'AI' were associated with good survival showing no significant correlation with a poor outcome ($p=0.754$) (figure 3.4) Another reason for the marked difference in survival could be the type of sample analysed by Thomas et al.; their study comprised mainly enucleation samples, whilst the vast majority of the cases analysed in the present study were intraocular biopsies (190). Enucleations tend to contain larger tumours, which are associated with a poor prognosis (139). In the study by Thomas et al, the AI cohort had a mean LBD 16.9mm and mean UH 11.3mm whereas in the present study AI tumours have a mean LBD 11.04mm and mean UH 3.8mm.

Table 3.6 A comparison of chromosome 3 status between studies that analysed UM samples by MSA

Study	Disomy 3	Monosomy 3	Partial Loss of 3	Allelic Imbalance
Tschentscher et al. 2000	15/30 (50%)	13/30 (43%)	-	-
Shields et al. 2007	44/140 (32%)	76/140 (54%)	-	-
Shields et al. 2011	241/500 (48%)	126/500 (25%)	133/500 (27%)	-
Thomas et al. 2012	128/374 (34%)	211/374 (56%)	16/374 (4%)	19/374 (5%)
Present study 2017	175/286 (62%)	79/286 (28%)	8/286 (3%)	17/286 (6%)

This present study examined the largest cohort to date of biopsies taken before and after radiotherapy; 131 pre and 109 post. There was no significant difference in the ability to determine chromosome 3 status in samples taken after radiotherapy (Fisher's exact p=0.799) (Table 3.5). Other studies have reported similar results: Hussain et al (2016) analysed 102 cases of UM that had been treated by PBR wherein all patients had a biopsy by 20 days post treatment (222). Genetic analysis by MLPA and MSA was able to successfully differentiate between M3 and D3 tumours, and therefore predict metastasis-free survival. Coupland et al. (2015) examined 28 UMs where an initial biopsy specimen was tested and a subsequent resection sample was available and the genetic results compared (221): for 4 cases in this cohort pre-radiotherapy and post-radiotherapy samples were assessed and were found to have concordant genetic results. Another study by Wackernagel et al. utilised array CGH to test samples pre- and post-radiotherapy; 5 patients had genetic analysis performed before and after radiotherapy and their results were also completely concordant (223). In contrast, Dogrusöz et al (2015) examined 36 eyes that had previously received radiotherapy prior to enucleation by karyotyping and FISH (224). The studies were performed on samples that were taken in some instances many months after administration of radiotherapy (range, 5-146 months). Analysis of these samples was largely unsuccessful by karyotyping, mainly due to tumour shrinkage and necrosis

associated with irradiation. This study contradicts the finding of the present study and other studies of its kind, and may be due to the lack of robustness of the genetic techniques employed in radiotherapy treated UM. In this study I also examined whether taking a biopsy before treatment with radiotherapy disseminates tumour cells, triggering metastases. An ex vivo study performed by Glasgow et al demonstrated iatrogenic dissemination of tumour cells following transvitreal biopsy (218). There have also been other case reports and series of suspected dissemination, which contribute to the reluctance of some ophthalmologists to take diagnostic and prognostic biopsies (225) (225) (217) (216). When metastasis-free survival between the two sampling groups was compared, no significance difference in survival was demonstrated. This is consistent with the findings of a recent study by Bagger et al. where a retrospective nationwide audit conducted demonstrated no association between tumour biopsy and increased mortality (226).

In summary, this study has shown that MSA is a molecular technique that can accurately determine chromosome 3 status in small UM biopsy samples with low DNA concentrations. Moreover, it has shown that MSA can be used to reliably establish chromosome 3 status in post radiotherapy samples including both proton beam and ruthenium plaque. Unlike other studies this study has identified partial loss of chromosome 3 as an indicator of poor prognosis, making these cases more like M3 cases. Similarly this study has shown that AI cases are most similar to D3 in terms of patient survival. Our findings indicate that there is no increased metastatic risk when biopsies are taken before administration of radiotherapy.

Chapter 4

An Audit of Nuclear BAP1 Expression in Choroidal Melanoma

4.1 Introduction

As mentioned previously in Chapter 1.5.5.4, *BAP1* is a prognostically important gene located at 3p21.1 consisting of 17 exons that produces 4Kb transcript and encodes a 759 amino acid protein. *BAP1* is a 90kDa member of the deubiquitylating enzyme family, which functions as an ubiquitin C-terminal hydrolase. Ubiquitylation is an important biological process whereby the small protein, ubiquitin, attaches to another targeted protein via isopeptide bonding to lysine residues. Ubiquitin is a highly conserved 76-amino acid regulatory protein found in most tissues in eukaryotic organisms. Ubiquitylation regulates several processes including: protein degradation, protein-protein interactions, protein localisation, differentiation, cell cycle progress, DNA repair and apoptosis. This post-translational modification is an ATP-dependent process carried out by 3 classes of enzymes: E1, E2 and E3. The E1 enzymes are classed as activating enzymes; they initiate the ubiquitylation process by forming thioester bonds with ubiquitin. The active ubiquitin is then transferred to active cysteine sites on the E2 enzymes; also known as 'ubiquitin conjugating enzymes'. E3 molecules or 'ubiquitin ligases' bind the target protein substrates by forming an isopeptide body between the carboxy-terminus of ubiquitin and the lysine residue on the protein substrate. The ubiquitylation process results in protein monoubiquitylation, multi- monoubiquitylation or polyubiquitylation of which there are numerous topologies: homogeneous, mixed, branched and unanchored ubiquitin chains (227). Monoubiquitin is mostly involved in the following processes: DNA damage response and repair, gene transcription and protein trafficking. Whereas polyubiquitylation is most associated with protein degradation, mainly due to the 7 lysine residues (K6, K11, K27, K29, K33, K48 and K63) allowing 7 linkages of ubiquitin to occur in a heterogeneous or homogenous manner, marking the protein for degradation. The ubiquitylation process is a reversible process mediated by de-ubiquitylating enzymes (DUBs) such as *BAP1*. DUBs serve three major roles: removing ubiquitin chains that can result in either the safeguarding

of proteins from degradation or the reversal of ubiquitin signalling; trimming ubiquitin chains changing the form of ubiquitin modification; and generating free ubiquitin molecules (228). *BAP1* is part of the ubiquitin carboxy-terminal hydrolase (UCH) family of DUBs, which are classified as cysteine proteases. *BAP1* contains the following: an N-terminal conserved catalytic domain (UCH), an additional C-terminal domain (CTD) region consisting of ~500 amino acids, which contains a coiled-coil motif responsible for interacting with Putative Polycomb group proteins ASXL1/2; a nuclear localisation signal (NLS) in the C terminal; and various other binding sites (229) (**Figure 4.1**). Due to its involvement in controlling various cellular processes - such as cell cycle, differentiation, transcription and DNA damage response through deubiquitylating activity -, *BAP1* is considered an important tumour suppressor. *BAP1* complexes with host cell factor-1 (HCF1) by ubiquitylating lysine residues on the transcriptional regulator. HCF1 is involved in cell cycle progression as it is responsible for controlling transition from G1 to S phase (230). When BAP1 is lost either through gene deletion or loss of function mutations HCF1 is no longer ubiquitylated, resulting in an accumulation of HCF1 and promotion of S phase (231). Also *BAP1* is essential for the formation of a ternary protein complex between HCF1 and forkhead transcription factors FoxK1/K2 which control cell cycle progression and cell proliferation. (230, 231). *BAP1* is also an integral part of the polycomb repressive deubiquitinase complex (PR-DUB), which is fundamental in maintaining transcriptional balance. The complex is formed via an interaction between *BAP1* and additional sex comb like 1/2 (ASXL1/2) genes. Within this group of proteins there are polycomb-repressive complexes (PRC), which function as histone ubiquitylators. Therefore, transcriptional balance is achieved by the ubiquitylation of histones by the PRCs and subsequent deubiquitylation by PR-DUB. Since polycomb proteins regulate cellular processes involved in differentiation, embryonic development and self-renewal, somatic mutations of *BAP1* can significantly alter these processes by inhibiting the DUB activity of BAP1, leading to

tumour development via increased ubiquitylation of histone 2A, which disrupts the cell cycle (126). BAP1 also interacts with the BRCA1/BARD1 heterodimer, a complex with dual E3 ubiquitin ligase activity that is involved in the regulation of DNA damage response (232). BAP1 binds to the RING finger domain of BARD1 and deubiquitylates ubiquitin chains. This coordinated activity of BAP1 and the BRCA1/BARD1 complex regulates ubiquitylation during DNA damage signalling and cell cycle progression (233). Due to BAP1's involvement in numerous cellular processes, mutations or deletions of this gene have disastrous consequences that result in the formation of tumours. In addition to UM, inactivating germline and somatic mutations of *BAP1* are also reported in other cancers including: breast, mesothelioma, clear cell renal carcinoma, cutaneous melanoma, and lung adenocarcinoma (5, 128, 234-238).

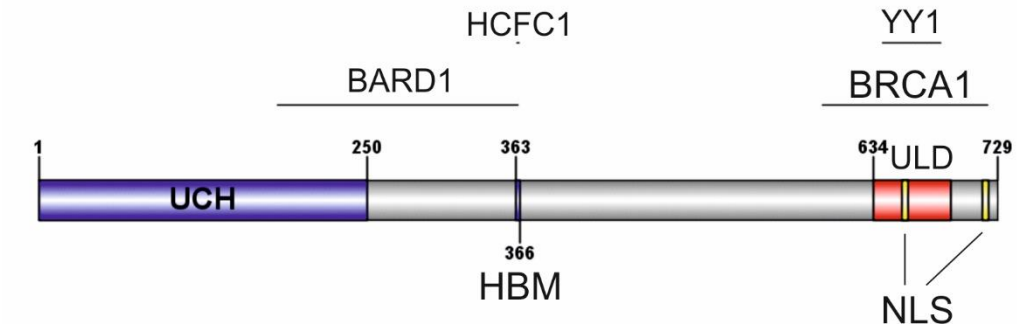

Figure 4.1. The *BAP1* gene and its functional domains; N-Terminal ubiquitin C-terminal hydrolase domain (blue amino acid (aa) 1-250), HCF1-binding domain (HBM) like motif (aa 363-366), UCH37-like domain (ULD) (red; aa 634-693) and a nuclear localisation signal (NLS) (yellow; aa 656-661 and 717-722). Sites are also shown for interactions with BARD1 (aa 182-365), HCF1 (aa 365-385), BRCA1 (aa 596-721) and YY1 (aa 642-686). Modified from Koopmans et al.

BAP1 is located on chromosome 3p21.1, which is frequently lost in UM. There are two schools of thought on the events leading to mutations in *BAP1*. Robertson et al. suggest that *BAP1* alterations occur after loss of one copy of chromosome 3. Others believe that the event occurs prior to the loss of chromosome 3, with the loss of chromosome 3 exposing a mutation on the remaining copy (239). *BAP1* mutations in UM were first described by Harbour et al. where they identified a range of different mutations in 84% of metastasising

tumours (128). Since this study, numerous other reports have shown *BAP1* to be mutated in 25% to 100% of M3 UM (108, 117, 122). Mutations in *BAP1* are strongly associated with loss of BAP1 protein expression (Koopmans et al. 2014). There are a number of studies that have examined BAP1 protein expression by immunohistochemistry (IHC); this chapter is an expansion of these studies, examining the largest cohort to date (240).

The aim of **chapter 4** was examine the relationship between nBAP1 protein expression and survival. This was achieved by: 1) undertaking MLPA/MSA analysis of enucleation samples; 2) analysing BAP1 protein expression by IHC; and 3) undertaking statistical analysis to look at the relationship between nBAP1 expression, chromosome 3 status and survival.

4.2 Materials and Methods

4.2.1 BAP1 Immunohistochemistry

165 patients treated by enucleation or local resection underwent IHC for BAP1 either as part of routine prognostication or undertaken by PhD student NF.

4.2.2 IHC on Whole Tissue Sections

Sections (4 µm thick) were cut from FFPE enucleated eyes, and mounted on X-tra™ adhesive tissue slides (Leica, United Kingdom). Antigen retrieval was performed at 96°C for 20 minutes using a PT Link (Dako, Carpinteria, CA; Ely, UK) pretreatment module and high-pH (pH 9.0) retrieval solution. The following steps were performed at room temperature (RT) using a Dako FLEX Envision kit and Autostainer Plus: 5 mins endogenous peroxidase blocking, 30 mins incubation with primary antibody, 15 min incubation with mouse linker, 20 min incubation with horseradish peroxidase, and positive staining was visualized by use of 3,3'-Diaminobenzidine (DAB) (DAKO, UK). Slides were washed with FLEX wash buffer between each step. Primary mouse anti human BAP1 antibody (Santa Cruz) was used at a concentration of 0.5µg/ml (1:400 dilution). An IgG1 isotype control was run at the same concentration as the primary antibody (1:200 dilution). Human pancreas tissue served as a positive control for the antibody. The slides were counterstained with Mayer's haematoxylin (VWR, Leicestershire, UK) dehydrated and cover-slipped using a solvent based mountant (DPX™, Sigma).

4.2.3 Scoring

The stained slides were scored by four independent investigators within the Liverpool Ocular Oncology Research Group using a light microscope (Nikon Eclipse E600). A binary score was used for nBAP1 expression, with cases being defined as positive when staining

was present in the nucleus of the tumour cell, and negative in its absence. There was 100% concordance between all scorers.

4.2.4 Chromosomal copy number analysis

DNA was extracted from FFPE and frozen UM samples and quantified using methods described previously in chapter 2.

The MLPA and MSA procedures for the assessment of chromosome 3 copy number alterations were performed using methods described in chapter 2. MLPA was performed in all cases yielding >100ng DNA whilst MSA was undertaken for samples with lower DNA yield.

4.2.5 Statistical Analysis

Multivariate analysis of risk factors associated with development of metastatic UM was undertaken using the Cox proportional hazards model for all covariates with $p \leq 0.10$ by univariate analysis. Survival time (months) was calculated from the date of first diagnosis until death, or study closure on 28th February 2018. All analyses were carried out using SPSS Statistics v.24 (IBM).

4.3 Results

4.3.1 Clinical and histological features of examined UM

BAP1 protein expression was examined in 165 patients treated by surgical excision at the LOOC between January 2013 and December 2015. For 29/165 (17.5%) cases surgical excision was performed subsequent to tumour recurrence or treatment complications. The median time from initial presentation to surgical excision for these cases was 33.5 months (range 1 – 570). The study consisted of 96 males and 69 females with a median age of 63 years at primary management (range, 20 – 88 years) with a median follow-up of 31.3 months (range, 5.7 – 348.5 months). At the time of the study closure on 28/02/2018, 133/165 (81%) patients were alive, 25/165 (15%) patients had died from metastatic disease, and 8/169 (5%) patients died from other causes. The UM had a median LBD of 14.4mm (range, 3.3 – 23.6mm) and a median ultrasound height of 8.3mm (range, 0.1 – 18.5mm). 104/165 (63%) of UMs contained epithelioid cells; 61/165 (37%) of tumours involved the ciliary body and 20/165 (12%) of tumours had extraocular extension. 99/165 (60%) tumours contained PAS+ loops and 31/165 (19%) tumours had necrosis. The samples had a median mitotic count of 3 mitoses per 40 high powered fields (range, 0 – 72).

4.3.2 Genetics

Genetic analysis was performed by either MLPA (153 cases) or MSA (12 cases). 103/165 (62%) UM were M3, 48/165 (29%) cases were D3, and one case was isodisomy 3 (1%). 13/165 (8%) were unclassifiable for chromosome 3 status due to the poor quality of the DNA. For the remaining chromosomes classified by MLPA, the following numbers of cases were unclassifiable for each chromosome arm and thus excluded from analyses: 1p, n=7; 6p, n=15; 6q, n=8; 8p, n=17; 8q, n=7.

Chromosome 8p was lost in 25/136 (19%) of cases, normal in 98/136 (72%) of cases, gained in 13/136 (9%). Chromosome 8q was lost in 2/146 (1%) of cases, normal in 54/146 (37%) of

cases and gained in 90/146 (62%). 8q gain was seen in 71/106 (67%) of monosomy 3 cases, 17/51 disomy cases (33%), and 2/12 (17%) unclassifiable. Chromosome 6p was lost in 7/138 (5%), normal in 77/138 (56%) cases and gained in 54/138 (39%) of cases. Chromosome 6q was lost in 20/145 (14%) of cases, normal in 105/145 (72%) of cases, and gained in 20/145 (14%) of cases. Chromosome 1p was lost in 43/146 (30%) of cases, normal in 101/146 (69%) of cases and gained in 2/146 (1%) of cases.

4.3.3 Immunohistochemistry

Nuclear BAP1 protein expression was observed in 77/166 (45.5%) of cases and was absent in 88/165 (54.5%) cases. Of the M3 UM, 84/104 (81%) were nBAP1 negative, and interestingly 20/104 (19%) were nBAP1 positive (these are discussed in more detail below). Of the 48 D3 UM, 46/48 (96%) were nBAP1 positive, and 2/48 (4%) were nBAP1 negative. Of the 91 UM with gains on chromosome 8q, 63 (68%) were also nBAP1 negative. Of the 25 UM patients who died from metastatic disease during the study, 22/25 (83%) had nBAP1 negative UM, and 3/25 (17%) had nBAP1 positive UM.

With regard to the M3/nBAP1+ve group there were 12 males and 8 females with a mean age of 59.4 with a median age of 61.5 (22 – 80 years) and only one patient died by at the close of this study. The median follow up for these cases was 2.1 months with a mean follow up period of 8.2 months (0.10 – 39.40 months). The UM had a mean LBD of 13.69mm with a median of 12.2mm (7.10 – 22.7mm), and a mean UH of 7.07mm, median of 8.25mm (1.7 – 11.6mm).

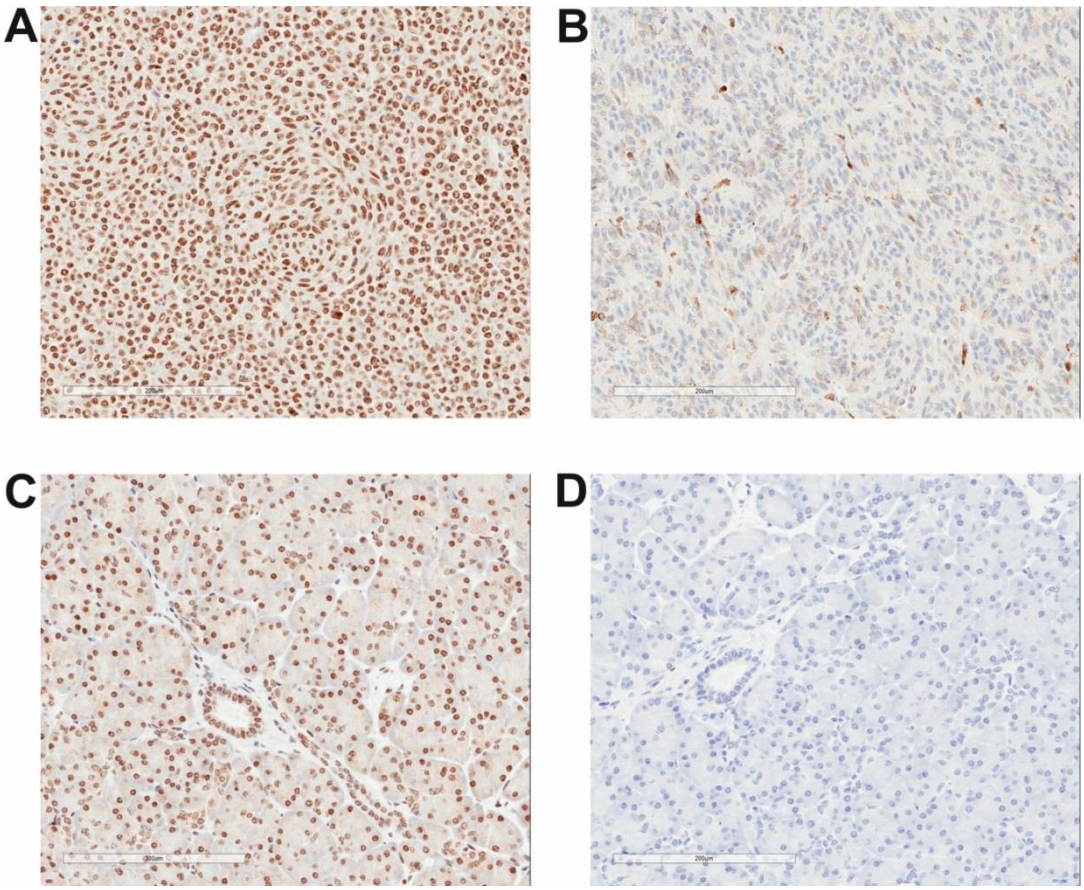

Figure 4.2. Immunohistochemistry of BAP1 using the Santa Cruz BAP1 Antibody at a dilution of 1:400. **A**) A nuclear BAP1 positive UM section showing clear brown staining in the cell nucleus. **B)** A nuclear BAP1 negative UM section showing a distinct lack of protein expression, no brown pigment is seen in the cell nucleus. **C)** Positive BAP1 staining on the positive control pancreas control section. **D)** Negative BAP1 staining of the negative control pancreas control section.

Table 4.1: Association between nBAP1 status and clinical and pathological risk factors.

Variable	Total (n=165)	nBAP1 Present (n=77)	nBAP1 Absent (n=88)	p-value
Age at PM (years)				
Median	63 (20 – 88)	59 (20 – 83)	65 (33 – 88)	**0.003***
Gender				
Female	69 (42%)	28 (36%)	41 (47%)	0.184†
Male	96 (58%)	49 (64%)	47 (53%)	
Survival				
Alive	133 (81%)	72 (94%)	61 (69%)	**<0.001†**
Death from MUM	25 (15%)	3 (4%)	22 (25%)	
Death other causes	7 (4%)	2 (2%)	5 (6%)	
Median (months)	31.3 (5.7 – 348.5)	35.0 (5.7 – 348.5)	28.6 (7.9 – 249.7)	**0.023***
Largest Basal Diameter (mm)				
Median	14.4 (3.3 – 23.6)	13.5 (4.98 – 22.7)	16.1 (3.3 – 23.6)	**0.001***
Ultrasound Height (mm)				
Median	8.3 (0.1 – 18.5)	7.8 (0.1 – 14.6)	9.2 (1.4 – 18.5)	**0.005***
Ciliary Body Involvement				
Yes	61 (37%)	14 (18%)	47 (53%)	**<0.001†**
No	104 (63%)	63 (82%)	41 (47%)	
Extraocular Extension				
Yes	20 (12%)	6 (8%)	14 (16%)	0.111†
No	145 (88%)	71 (92%)	74 (84%)	
Epithelioid Cells				
Yes	104 (63%)	35 (45%)	69 (78%)	**<0.001†**
No	61 (37%)	42 (55%)	19 (22%)	
Closed connective tissue Loops Present				
Yes	99 (60%)	38 (49%)	61 (70%)	**0.007†**
No	66 (40%)	39 (51%)	26 (30%)	
Necrosis				
Yes	31 (19%)	11 (14%)	20 (23%)	0.166†
No	134 (81%)	66 (86%)	68 (77%)	
Mitotic Count per 40 High Power Field				
Median	3 (0 – 72)	3 (0 - 72)	3 (0 – 21)	0.197*

PM = Primary management; MUM = metastatic melanoma.
Boldface values indicate statistical significance ($p \leq 0.05$).

*= Mann–Whitney *U* test.
† = Chi-square test.

Table 4.2: Association between nBAP1 status and genetic factors

Variable	Total	nBAP1 Present	nBAP1 Absent	p-value
Chromosome 3	**(n=152)**	**(n=66)**	**(n=86)**	
Loss	104 (68%)	20 (30%)	84 (98%)	**<0.001**§
Normal	48 (32%)	46 (70%)	2 (2%)	
Chromosome 8p	**(n=136)**	**(n=58)**	**(n=78)**	
Normal	98 (72%)	54 (93%)	44 (56%)	**<0.001**§
Loss	25 (19%)	1 (2%)	24 (31%)	
Gain	13 (9%)	3 (5%)	10 (13%)	
Chromosome 8q	**(n=146)**	**(n=64)**	**(n=82)**	
Normal	54 (37%)	34 (53%)	20 (24%)	**0.001**§
Loss	2 (1%)	1 (2%)	1 (1%)	
Gain	90 (62%)	29 (45%)	61 (75%)	
Chromosome 6p	**(n=138)**	**(n=61)**	**(n=77)**	
Normal	77 (56%)	26 (43%)	51 (66%)	**0.001**§
Loss	7 (5%)	1 (1%)	6 (8%)	
Gain	54 (39%)	34 (56%)	20 (26%)	
Chromosome 6q	**(n=145)**	**(n=66)**	**(n=79)**	
Normal	105 (72%)	45 (68%)	60 (76%)	0.424†
Loss	20 (14%)	9 (14%)	11 (14%)	
Gain	20 (14%)	12 (18%)	8 (10%)	
Chromosome 1p	**(n=146)**	**(n=66)**	**(n=80)**	
Normal	101 (69%)	51 (77%)	50 (63%)	0.083§
Loss	43 (30%)	15 (23%)	28 (35%)	
Gain	2 (1%)	0 (0%)	2 (2%)	

Boldface values indicate statistical significance ($p \leq 0.05$).

§ = Fisher exact test.
† = Chi-square test.

4.3.4 Survival

Kaplan–Meier survival curves and tables were examined for all primary UM stratified according to chromosome 3 status and nBAP1 protein expression. Both M3 UM (Log rank, p=0.001) and UM negative for nBAP1 (Log Rank, p<0.001) were significantly associated with a reduced survival time (Figure 4.3). The cases were further subdivided according to their chromosome 3 status. M3/nBAP1 positive UM had a significantly better prognosis than M3/nBAP1 negative tumours (Log rank, p=0.014) and were most similar to the patients with D3/nBAP1 positive UM in terms of survival (Figure 4.4).

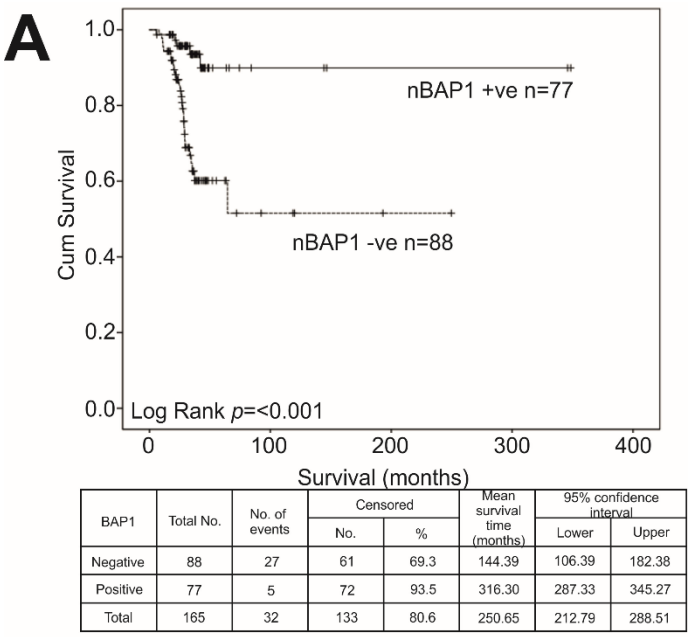

BAP1	Total No.	No. of events	Censored		Mean survival time (months)	95% confidence interval	
			No.	%		Lower	Upper
Negative	88	27	61	69.3	144.39	106.39	182.38
Positive	77	5	72	93.5	316.30	287.33	345.27
Total	165	32	133	80.6	250.65	212.79	288.51

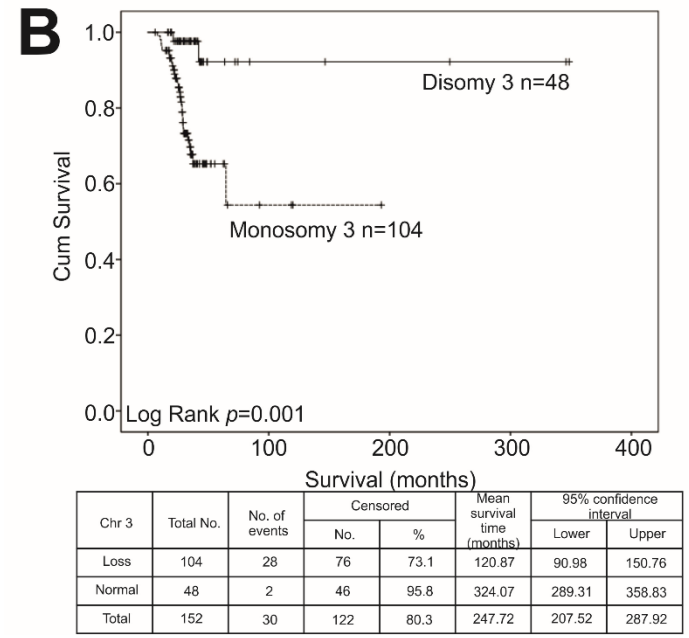

Chr 3	Total No.	No. of events	Censored		Mean survival time (months)	95% confidence interval	
			No.	%		Lower	Upper
Loss	104	28	76	73.1	120.87	90.98	150.76
Normal	48	2	46	95.8	324.07	289.31	358.83
Total	152	30	122	80.3	247.72	207.52	287.92

Figure 4.3 Kaplan–Meier survival curves and tables for all primary UM stratified according to: A) nBAP1 protein expression (p=<0.001) in 165 patients (nBAP1 protein expression was scored as positive or negative); and **B) chromosome 3 status (p=0.001) in 152 patients.** Only cases with a discernible normal or loss of chromosome 3 were included. No. of events indicates the number of deaths. Log-rank tests utilised to compare survival across groups (Farquhar and Thornton et al. 2017; PMID: 29416875).

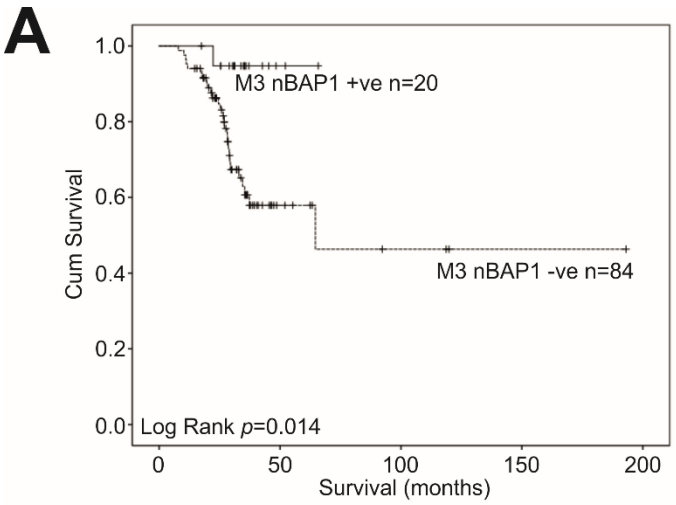

Chr3 Loss BAP1	Total No.	No. of events	Censored		Mean survival time (months)	95% confidence interval	
			No.	%		Upper	Lower
Negative	84	27	57	67.9	107.65	75.70	139.60
Positive	20	1	19	95.0	63.51	59.14	67.88
Total	104	28	76	73.1	120.81	90.97	150.76

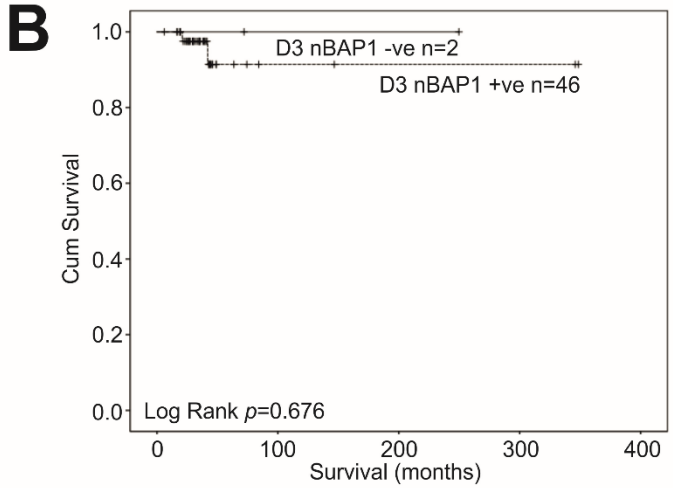

Chr3 Normal BAP1	Total No.	No. of events	Censored		Mean survival time (months)	95% confidence interval	
			No.	%		Upper	Lower
Negative	2	0	2	100.0	-	-	-
Positive	46	2	44	95.7	-	-	-
Total	48	2	46	95.8	-	-	-

Figure 4.4. Kaplan–Meier survival curves estimate disease free survival in UM patients with: A) nBAP1+ve/-ve in monosomy 3 UM, n=104 (p=0.014); and B) nBAP1+ve/-ve in disomy 3 UM, n=48 (p=0.676), no survival statistics because all cases are censored. No. of events indicates the number of deaths. Log-rank tests utilised to compare survival across groups (Farquhar and Thornton et al. 2017; PMID: 29416875).

4.3.5 Univariate and Multivariate Analysis

Univariate analysis using the Cox proportional hazards model identified the following factors as significantly associated with survival time (Table 4.3): nBAP1 protein expression, p=<0.001 (HR 0.173; 95% CI 0.067 – 0.450); age at primary management p=0.005 (HR 1.046; 95% CI 1.014 – 1.080); presence of closed connective loops p=0.003 (HR 3.596; 95% CI 1.541 – 8.389); mitotic count per 40 hpf, p=0.016 (HR 1.029; 95% CI 1.005 – 1.054); epithelioid cell morphology p=0.014 (HR 3.059; 95% CI 1.257 – 7.443); tumour height p=0.002 (HR 1.169; 95% CI 1.058 – 1.292); LBD p=0.006 (HR 1.142; 95% CI 1.039 – 1.255); and chromosome 3 loss, p=0.036 (HR 0.482; 95% CI 0.243 – 0.955). Multivariate analysis using the Cox proportional hazards model, demonstrated only nBAP1 protein expression as an independent factor significantly associated with survival, p=0.002 (HR 0.211; 95% CI 0.079 – 0.562) in this cohort (Table 4.4).

Table 4.3 Univariate Analysis of risk factors associated with metastatic disease

Variable	Sig.	Hazard Ratio (HR)	95.0% CI for HR	
			Lower	Upper
nBAP1	**0.000**	0.173	0.067	0.450
AgePM	**0.005**	1.046	1.014	1.080
Loops	**0.003**	3.596	1.541	8.389
Mitotic	**0.016**	1.029	1.005	1.054
Epithelioid	**0.014**	3.059	1.257	7.443
UH	**0.002**	1.169	1.058	1.292
LBD	**0.006**	1.142	1.039	1.255
CBI	**0.078**	1.872	0.933	3.756
EOE	0.287	1.622	0.666	3.948
Chr3	**0.036**	0.482	0.243	0.955
Gender	0.740	0.886	0.433	1.813
Necrosis	0.138	1.794	0.829	3.880

UH = Ultrasound height
LBD = Largest basal diameter
CBI = Ciliary body involvement
EOE = Extraocular extension
Chr3 = Chromosome 3

Table 4.4. Multivariate Analysis of risk factors associated with metastasis in UM

Variable	Sig.	Hazard Ratio (HR)	95.0% CI for HR	
			Lower	Upper
nBAP1	**0.006**	0.212	0.070	0.645
AgePM	0.071	1.030	0.997	1.064
Chr3	0.974	1.011	0.540	1.892

4.4 Discussion

To date, this is the largest study of BAP1 protein expression by IHC of primary UM. The incidence of nBAP1 negativity was consistent with other reports in the literature. BAP1 protein expression in UM by IHC was first analysed by Shah et al (2013) who found lack of nBAP1 expression in 58% of primary UM (239). Kalirai et al (2014) found nBAP1 negativity in 51% of primary UM and 77% of metastatic UM (131). Koopmans et al. (2014) reported a lack of BAP1 protein expression in 43% and Van de nes et al. (2016) in 54% of primary UM; both studies showing a strong correlation between the presence of *BAP1* mutations as examined by Sanger sequencing and an absence of nBAP1 protein expression by IHC (130, 241).

The current study found nBAP1 protein expression to be absent in 54%, similar to our previous data on a different cohort of primary UM. Furthermore, our study showed similarities to other BAP1 studies where there was a correlation between loss of nBAP1 protein expression and factors associated with high metastatic risk such as chromosome 3 status, epithelioid cytomorphology, PAS+ loops, and ciliary body involvement. There was no correlation between nBAP1 expression and necrosis or extraocular growth.

Other studies of primary UM where the *BAP1* mutational rate were examined show a variety of results. Harbour et al. identified *BAP1* mutations in 84% of the 'class 2' or high risk UM, consistent with the 81% of M3 cases in this study that were nBAP1 negative (129). Whereas Dono et al found a *BAP1* mutation rate of 100% in their M3 cohort, with no *BAP1*

mutations in their D3 cases, with an overall study mutation rate of 31.5%. Interestingly, we observed that 4 D3 UM were nBAP1 negative. In contrast only 33% of M3 UM examined by Martin et al. had mutations in *BAP1* and 1 D3 case that later metastasised, with an overall study *BAP1* mutation rate of 11% (119). Interestingly, Koopmans et al. identified 3/74 (4%) cases of UM without BAP1 mutations but also had loss of nBAP1 protein (130).

In a small number of cases in our series, loss of nBAP1 protein expression did not appear to be the metastatic driver. That is, 3/26 (11.5%) patients that developed metastatic disease were found to have nBAP1 positive tumours. Two of these patients had unfavourable clinical and histological characteristics, which would have placed them at high risk of developing metastases irrespective of nBAP1 status.

The first case was a 39 year-old male who was initially treated by local resection who later underwent enucleation after recurrence disease. Clinically, the tumour had an LBD 15.5mm and an UH of 7.8mm with involvement of the ciliary body and extraocular growth. Histologically, the pUM contained epithelioid cells, PAS+ loops and had an extremely high mitotic count of 72/40 high power field. Interestingly, the patient was categorised as unclassifiable for chromosome 3, despite having a loss of 1p which is significantly associated with chromosome 3 loss (McNemar p=0.000) and gain of 8q (McNemar p=0.000). However his tumour had other poor prognostic characteristics, which would have placed him in the 'high risk' category for developing metastatic disease, irrespective of the Chr3 and nBAP1 status.

Case 2 was a 70 year-old male whose primary treatment was enucleation. Clinically, the tumour was large, with an LBD 19.1mm and UH 2.8mm, in addition to having an epithelioid cell cytomorphology, a mitotic count of 5/40HPF and PAS+ loops. Moreover, the patient's

tumour also showed M3 with a gain of 8q: both features associated with a poorer survival outcome.

The third case was that of a 71 year-old male whose primary treatment was enucleation. The tumour had an LBD of 13.9mm and a UH of 1.8mm, with no ciliary body involvement or evidence of extraocular growth. The tumour consisted predominantly of spindle cells, no PAS+ loops with a low mitotic count of 1/40 hpf, and was cytogenetically normal for chromosome's 1, 3, 6 and 8. However, previous studies have shown that disomy 3 UM do infrequently metastasise, due to mutations in *SF3B1* and this could be why the patient developed metastatic disease.

In this study chromosome 3 loss has been shown to be significantly associated with nBAP1 negativity (Fisher's Exact p=<0.001); however, interestingly, there were 3 disomy cases in the examined cohort that were nBAP1 negative. Chromosome 3 status for all of these cases was retested using MSA to rule out the possibility of isodisomy or 'acquired homozygosity', which cannot be detected by MLPA. Only one of these 3 cases showed isodisomy by MSA. The isodisomy case was that of a 75 year-old female who was initially treated by plaque radiotherapy but later underwent enucleation; she unfortunately subsequently died of metastatic UM. The tumour had an LBD of 5.8mm, an UH of 4.9mm with no involvement of the ciliary body or evidence of extraocular extension. The UM had an epithelioid cytomorphology, a mitotic count of 3/40hpf and did not contain any PAS+ loops. MLPA results showed a normal chromosome 3 with polysomy 8q and gain of 6p; MSA testing subsequently confirmed loss of heterozygosity of chromosome 3.

The remaining two cases were tested for BAP1 mutations but were found to be wild type, indicative of an alternative non-genetic mechanism of nBAP1 loss.

A particularly interesting finding of this study was the identification of a subset of 20 cases (19%) of M3 UM where nBAP1 protein expression was counterintuitively positive.

Histologically, the samples shared several characteristics that would place them in a lower risk group with respect to metastasis but the vast majority of samples contained epithelioid cells, a risk factor associated with increased metastatic potential. This indicates there two distinct subgroups are present with monosomy 3 tumours: M3 UM with a loss of *BAP1* function and M3 UM with a retained functional copy of *BAP1*. This was evident in the multivariate analysis whereby nBAP1 was found to be the only independent variable significantly associated with an increased risk of developing metastatic disease. This suggests that bi-allelic inactivation of *BAP1* is required to influence metastases and therefore prognosis. This was consistent with the findings of Robertson et al. who found *BAP1* mutations in 83.3% of M3 UM, identifying 16.7% M3 UM that were BAP1 wild-type, although they didn't explore this in terms of survival..

In summary, I have demonstrated the importance of nBAP1 protein expression as an independent marker of prognosis in patients with UM that identifies a subpopulation of M3 primary tumours with favourable survival times compared to their nBAP1-negative counterparts. Moreover, assessment of nBAP1 protein expression using IHC is an efficient and cost-effective way of stratifying UM patients, in order to ensure they are followed up with the appropriate surveillance program. In the meantime, BAP IHC is part of the routine work-up of all UM histological specimens sent to the Pathology Dept. in Liverpool, and in other major eye pathology centres.

Chapter 5

Designing and Validating a Targeted Next Generation Sequencing Panel for Prognostic Testing in Uveal Melanoma Patients

5.1 Introduction

Whole exome studies of UM have vastly improved our understanding of the molecular drivers of metastatic progression, which has laid the groundwork for improving the detection, prevention and treatment of the disease. The first study to examine UM by exome sequencing was Harbour et al. (2010) where they discovered recurrent mutations of *BAP1* in two tumour samples. After re-sequencing by Sanger sequencing, they found this was a common molecular characteristic of high metastatic risk or 'class 2' uveal melanoma (129). Later a larger exome sequencing study of 22 UM undertaken by Martin et al. (2013) revealed recurrent somatic mutations in *EIF1AX* and *SF3B1.* This was the first study to associate mutations in *SF3B1* to unusual D3 tumours where patients developed metastasis after a long period of time (119). These findings were confirmed by Yavuzyigitoglu et al. (2016) who examined *SF3B1* and *EIF1AX* mutations in 151 UM patients and demonstrated that D3 *SF3B1* mutants had an increased metastatic risk in comparison to D3 *SF3B1* wild-type tumours (242). In 2016, Royer-Bertrand et al. examined 33 UM by deep-coverage whole-genome sequencing where four major subgroups associated with mutational and metastatic status were identified as a result of unsupervised hierarchical clustering of copy number variation (134). These findings were echoed by the TCGA study of 80 UM where four molecular subsets of UM were identified based on copy number, mutation, methylation and mRNA profiles (135). Based on these findings there have been several efforts to design targeted NGS panels specifically for UM. In 2017, Reiman et al. designed a custom panel used to examine mutations in cutaneous and uveal melanoma simultaneously; however, this only examined mutations in *GNAQ* and *GNA11,* which are not associated with patient prognosis (243). More recently, Smit et al. developed a panel, which combines copy number and mutation analysis, the first of its kind (198). Using the Ion Torrent (Thermofisher Scientific) sequencing platform they developed a custom design integrating chromosomal aberrations in chromosomes 1, 3 and 8 and mutations in *GNAQ*,

GNA11, *BAP1*, *SF3B1* and *EIF1AX* and successfully validated this on a cohort of 70 samples (198).

However this panel did not include *CYSLTR2*, a cysteinyl leukotriene receptor that functions as a G-coupled protein receptor on 13q14.2 that activates the Gα subunits and has been shown to be mutated in some UM that lack mutations in *GNAQ* or *GNA11* (132). Chromosome 6 was also not included on this panel despite loss of 6q being identified by Royer-Bertrand et al. as a somatic event defining tumour classes (134). Moreover, although previous studies have suggested that gains in 6p contribute to a better prognosis, this was also not included. Additionally, the panel does not detect mutations in *PLCB4*, which has been shown previously to be a downstream target of *GNAQ/GNA11*, suggesting that this is an alternative way of activating this signalling pathway (133).

In Chapter 3, I established that mutations in *BAP1* that result in loss of protein expression drastically impact disease-free survival in UM with monosomy of chromosome 3 creating two subsets in terms of metastatic progression. This, in addition to recent studies implicating *SF3B1* as a driver of late onset of metastases, highlights the need for a test that encompasses all of the major alterations. In an era of personalised medicine or 'theranostics' NGS is an emerging and exciting technology that can allow the examination of both copy number changes and mutations simultaneously, eliminating the need for two separate, time-consuming molecular tests. Clinicians and scientists alike now recognise that a one size fits all approach is no longer appropriate for the effective management and treatment of patients with chronic diseases such as cancer. Technologies like NGS allow for a tailored approach in terms of patient surveillance in addition to arming the patient with knowledge of the mutational makeup of their tumours, allowing targeted therapies to be administered where available.

No two tumours are alike; they come in all shapes and sizes which affects the yield and quality of the DNA from commonplace extractions. As UM is a relatively rare cancer, centres such as the Liverpool Ocular Oncology centre receive a large number of referrals from other sites in the U.K. but also worldwide, most of which are FFPE. It is widely known that formalin fixation of tissues at room temperature results in poor preservation of high molecular weight DNA. In addition, low DNA yield is not just a problem affecting FFPE tissues. As established in chapter 3 prognostic and diagnostic biopsies often result in tiny amounts of tumour material being utilised for DNA extraction, which then results in a very low DNA yield. Therefore the development of a test that will allow testing of all sample types with a low DNA input is of paramount importance.

In this chapter I examined the feasibility of designing and developing targeted NGS panels for UM utilising different sequencing chemistries that allow copy number changes in chromosomes 1, 3, 6 and 8 and mutations in *GNAQ*, *GNA11*, *CYSLTR2*, *BAP1*, *SF3B1* and *EIF1AX* to be examined in tandem. I first validated the accuracy of these panels by testing samples that had already been fully profiled by the TCGA and others that had copy number information available from MLPA testing. When this was been achieved I took a cohort of samples with previous NGS data available and retested DNA extracted from matched FFPE material to ensure there was concordance and ergo was suitable for this sample type. Once a final design and sequencing chemistry was determined I tested a cohort of 80 samples. These samples had known copy number data but unknown mutational status. I then utilised these results to examine survival, which will help inform the way patients are managed clinically in the future.

5.2 Materials and Methods

5.2.1 SureSelect QXT

5.2.1.1 Panel Design

The panel was designed to cover mutations in *SF3B1* exons 12 & 14, *GNAQ* exons 4 & 5, *GNA11 exons* 4 & 5, *EIF1AX* exons 1 & 2 and all exons of: *BAP1*, *FBXW7*, *DLK2*, *BRAF* (as a negative control), *CSMD1*, *CYSLTR2*, *KTN1*, *TP53BP1*, *SRSF2*, *PLCB4*, *TTC28*. Additional probes were included to examine copy number changes in chromosome 1: 1541 probes; chromosome 3: 1287 probes; chromosome 6: 1094 probes; chromosome 8: 933.

5.2.1.2 Fragment and Adaptor-Tag

14 fresh UM samples plus an additional two reference samples (Genome In A Bottle HDx) were diluted and measured to 25ng/µl using 2 serial fluorometric assays (Qubit, Invitrogen). All reagents and enzymes were prepared as per manufacturer's instructions (Agilent). The gDNA was fragmented enzymatically and adaptors were adhered to ends of DNA fragments following the manufacturer's instructions (Agilent). In brief, 17µl SureSelect QXT buffer added to strip tubes with 2µl DNA samples and 2µl SureSelect QXT Enzyme Mix. Samples were vortexed and centrifuged briefly and placed on a thermal cycler (SureCycler 8800, Agilent) for DNA fragmentation; 45°C 10 minutes, 4°C 1 minute and 4°C Hold. Upon completion of the fragmentation samples were placed on ice and 32µl 1X SureSelect QXT Stop Solution was added (containing 25% ethanol) to each reaction. These were then vortexed, centrifuged and allowed to incubate at room temperature for 1 minute.

5.2.1.3 Purifying the adaptor tagged library using AMPure XP beads

Using pre-incubated and homogenous AMPure XP beads (Agencourt AMPure XP Kit, Beckman Coulter Genomics) 52µl of bead suspension was added to each reaction, vortexed

and spun briefly. Reactions were then incubated at room temperature for 5 mins before placing on a magnetic stand (Thermo Fisher Scientific) until solution was cleared. The cleared solution was removed and discarded and subjected to 2 washes with 200µl of fresh 70% ethanol, waiting for 1 min before removing 70% ethanol. Samples were dried on a thermal cycler at 37°C for between 1 – 3 mins or until dry. Once dry, samples were re-suspended in 11µl nuclease free water (Ambion), mixed well and centrifuged. Reactions were incubated at room temperature for 2 mins and cleared on magnetic stand. The cleared supernatant was removed and placed in fresh strip tubes.

5.2.1.4 Amplify the adaptor-tagged DNA library

All reagents and enzymes were prepared as per manufacturer's instructions (Agilent). 40µl of Precapture PCR mix (nuclease free water, Herculase II 5x Reaction buffer, 100mM dNTP Mix (25nM), DMSO, SureSelect QXT Primer Mix, Herculase II Fusion DNA Polymerase) was added to 10µl purified DNA library samples. The strip tubes were placed in the thermal cycler and the pre-capture PCR was performed: 68°C 2 mins, 98°C mins and 8 cycles of; 98°C 30 seconds, 57°C 30 seconds and 72°C for 1 min followed by 72°C 5 mins, 4°C hold.

5.2.1.5 Purifying the amplified library with AMPure XP beads

The amplified library was purified by adding 50µl of AMPure XP bead suspension to amplified DNA samples, vortexing and briefly spinning the library. Samples were incubated for 5 mins at room temperature and the reactions cleared on a magnetic stand for between 3-5 mins. The supernatant was removed and discarded and subjected to 2 washes with 200µl of fresh 70% ethanol, waiting for 1 min before removing 70% ethanol. Samples were dried on a thermal cycler at 37°C for between 1 – 3 mins or until dry. Once dry, samples were re-suspended in 13µl nuclease free water (Ambion) mixed well and centrifuged.

Reactions were incubated at room temperature for 2 mins and cleared on magnetic stand. The cleared supernatant was removed and placed in fresh strip tubes.

5.2.1.6 Assessing library DNA quantity and quality

Library quality and quantity assessed using Agilent DNA 1000 kit (Agilent) using the manufacturer's instructions. In brief, 9µl of gel was pipetted into the corresponding well and the remaining 9µl loaded into remaining wells marked 'G'. 5µl of marker was loaded into all 12 samples wells and ladder well. 1µl of ladder loaded into ladder well and 1µl of sample added to corresponding wells. The chip was vortexed for 1min and loaded onto the Agilent 2100 Bioanalyzer (Agilent). Samples were deemed successful if the peak of the DNA fragment size was between 245-325bp.

5.2.1.7 Hybridising DNA samples to the capture library

The DNA libraries were diluted to 750ng in 12µl and 5µl of SureSelect QXT Fast Blocker Mix was added, pipette mixing between 8 – 10 times. Reactions were transferred to a thermal cycler for the hybridisation PCR program; 95°C 5 mins, 65°C 10 mins, 65°C 1 min and 60 cycles of; 65°C 1 min, 37°C seconds, 65° hold. The cycler was paused on the 3rd step and 13µl room temperature capture library hybridisation mix was added to each sample well, pipette mixing 8-10 times before continuing the PCR program.

5.2.1.8 Capture hybridised DNA using streptavidin-coated beads

Dynabeads MyOne Streptavidin T1 magnetic beads (Thermo Fisher Scientific) were prepared as per manufacturer's instructions. Samples were transferred to room temperature and 50µl re-suspended beads were added to fresh strips tubes. The beads were washed 3 times by adding 200µl SureSelect Binding Buffer and pipette mixing up and down 10 times, then transferring to the magnetic stand for 5 mins until cleared and discarding supernatant. The beads were then re-suspended in 200µl SureSelect Binding

Buffer. The hybridisation mixture was then transferred to wells containing 200ul washed streptavidin beads and incubated on a 96-well plate mixer (Eppendorf) at 1800RPM for 30mins at room temperature. During this time 200µl aliquots of Wash Buffer 2 were prewarmed at 65°C in fresh strips, aliquoting 3 wells of buffer for each reaction. The hybridisation and bead mixture was then centrifuged briefly and placed on a magnetic stand to clear before removing and discarding the supernatant. The beads were then re-suspended in 200ul SureSelect Wash Buffer 1, pipette mixing up and down 8-10 times. The mixture was then placed on a magnetic stand to clear for 1 min before removing and discarding the supernatant. The beads were then washed 3 times in 200µl prewarmed Wash Buffer 2 incubated at 65°C on a thermal cycler then placed on a magnetic stand waiting 1 min until cleared then removing and discarding the supernatant. Samples were centrifuged briefly after the last wash step to remove any remaining droplets. 23µl of nuclease free water (Ambion) was then added to each sample well.

5.2.1.9 Amplify the captured libraries to add index tags

The post-capture PCR reaction mix was prepared as per manufacturer's instructions; nuclease fee water 13.5µl, Herculase II 5x Reaction Buffer 10µl, 100mM dNTP mix (25mM each dNTP) 0.5µl and Herculase II Fusion DNA Polymerase 1µl. 25µl of PCR reaction mix was added to the bead bound DNA samples in addition to 1ul of both P7 and P5 dual indexing primers (Table 6.1). The samples were mixed well, ensuring beads were fully re-suspended and transferred to thermal cycler to complete Post-capture PCR cycling; 98°C 2 mins, 10 cycles of: 98°C 30s, 58°C 30s, 72°C 1 min. 72°C 5 mins and 4°C hold. Once completed, the strip tubes were centrifuged briefly and place on magnetic stand to clear at room temperature for 2 mins. Once cleared the supernatant was removed and aliquoted into fresh strip tubes.

5.2.1.10 Purify the amplified captured libraries using AMPure XP beads

60µl of homogeneous AMPure XP bead suspension were added to each 50ul amplified DNA sample, vortexed and incubated at room temperature for 5 mins. The solution was then cleared on a magnetic stand for between 3-5mns, once cleared the supernatant was removed and discarded. 2 washes were carried on the magnetic stand by dispensing 200µl fresh 70% ethanol each sample well, waiting for 1 minute before removing the ethanol. Samples were then dried on a thermal cycler at °37C for 1-3 mins. Once dried, 25µl of nuclease free water (Ambion) was added to each sample well and incubated at room temperature for 2 mins. The reactions were then cleared on a magnetic stand for 2 mins and the cleared supernatant transferred into fresh 1.5ml DNA LoBind tubes (Eppendorf).

Table 5.1 Index assignments for Agilent validation cohort.

Sample ID	Index 1	Index 2
S154.11	P7i1	P5i4
S191.11	P7i2	P5i4
S173.13	P7i3	P5i4
S162.12	P7i4	P5i4
S183.13	P7i5	P5i4
S031.13	P7i6	P5i4
S107.12	P7i7	P5i4
S032.13	P7i8	P5i4
S080.09	P7i1	P5i3
S095.08	P7i2	P5i3
S001.09	P7i3	P5i3
S102.09	P7i4	P5i3
S129.09	P7i5	P5i3
S083.08	P7i6	P5i3
GIAB	P7i7	P5i3
GIAB	P7i8	P5i3

5.2.1.11 Assess indexed library DNA quantity and quality

Quantity and quality of the indexed library DNA was assessed using the High Sensitivity DNA Assay (Agilent) as per manufacturer's instructions. In brief, 9µl of gel was pipetted into

the corresponding well of the High Sensitivity Chip (Agilent) and the remaining 9µl loaded into remaining wells marked 'G'. 5µl of marker was loaded into all 12 samples wells and ladder well. 1µl of ladder loaded into ladder well and 1µl of sample added to corresponding wells. The chip was vortexed for 1min and loaded onto the Agilent 2100 Bioanalyzer (Agilent). DNA quantity and quality was deemed successful if the electropheragram showed the peak of DNA fragment size positioned between 325 and 450bp.

5.2.1.12 Pooling

Libraries (16 in total) were then pooled in equimolar amounts based on the aforementioned Qubit and Bioanalyser data. The pool was further purified using Agencourt AMPure XP beads (Beckman Coulter). The size of the final pool was assessed on a Bioanalyser high sensitivity DNA chip and the DNA concentration was determined initially by Qubit double-stranded DNA high sensitivity assay, and then by qPCR, using an Illumina library quantification kit (KAPA) on a Roche LightCycler 480 II system. The pool of 16 target enriched libraries was sequenced on one MiSeq run, using custom sequencing primers (as per the Agilent protocol) and version 3 chemistry, generating 2 x 250bp paired end reads.

5.2.2 TruSeq Customer Amplicon Low Input Kit

5.2.2.1 Panel Design

The panel was designed to cover mutations in *SF3B1* exons 12 & 14, *GNAQ* exons 4 & 5, *GNA11 exons* 4 & 5, *EIF1AX* exons 1 & 2 and all exons of: *BAP1*, *FBXW7*, *DLK2*, *BRAF*, *CSMD1*, *CYSLTR2*, *KTN1*, *TP53BP1*, *SRSF2*, *PLCB4*, *and TTC28*. Additional probes were included to examine copy number changes in chromosome 3: 83 amplicons consisting of 39 on 3p and 44 on 3q; chromosome 6: 76 amplicons consisting of 34 on 6p and 42 on 6q; chromosome 8: 67 amplicons consisting of 23 on 8p and 44 on 8q.

5.2.2.2 Quantify and Dilute DNA

14 fresh UM samples plus an additional two reference samples were quantified using fluorometric assay (Qubit, Thermo Fisher). gDNA was diluted to 25ng/µl in Resuspension Solution 1 (RS1) (Illumina) and re-quantified to check final amount. gDNA was then further diluted to 2.5ng/µl in RS1 in a LoBind tube (Eppendorf) and 1µl of Sample Stablization Solution (SS1) (Illumina) was added.

5.2.2.3 Hybridise Oligo Pool

All reagents and enzymes prepared as per manufacturer's instructions. The following reagents were added to the HYB plate; 5µl of diluted 2800M, 5µl of diluted ACP3 was added to well containing diluted 2800M as a control, 5µl of RS1 added to one well as a no template control, 5µl of gDNA added to remaining wells, 5µl of CAT added to each well containing gDNA and no template control and 15µl of OHS2 added to each well, pipetting slowly to mix. The samples placed on a Veriti thermal cycler (Applied Biosystems) and the HYB program was run (Table 5.2)

Table 5.2 HYB PCR program for Applied Biosystems 96-Well Thermal Cycler

Step	Ramp Speed	Increment (°C)	Temperature (°C)	Hold
1			95	3 minutes
2	2.1%	-0.5	90	30 seconds
3			Step 2 for 59x	
4	2%	-0.5	60	1 minute
5			Step 4 for 19x	
6	2.1%	-1.0	50	2 minutes
7			Step 6 for 9x	
8	2%		40	10 minutes

5.2.2.4 Remove Unbound Oligos

All reagents and enzymes prepared as per manufacturer's instructions.25µl of Sample Purification Beads (SPB) (Illumina) were added to each well of the HYB plate, pipetting

slowly to mix. The plate was incubated at room temperature for 5 mins and the plate was placed on magnetic stand (DynaMag-96 Side Skirted Magnet) to clear for 2 mins. The supernatant was removed and discarded and the beads were washed three times as follows; 80µl of Stringent Wash 1 (SW1) (Illumina) was added to each well and incubated at room temperature for 30 secs before removing and discarding the supernatant. Any residual SW1 was removed from each well and 80µl of 60% ethanol was added to each well, incubated at room temperature for 30 secs and then removed and discarded. Any residual ethanol was removed before air drying for 5 mins.

5.2.2.5 Extend-Ligate Bound Oligos

The plate was removed from the magnetic stand and 22µl of ELB/ELE mix was added to each well and mixed using a pipette. The plate was then placed on the thermocycler and the EXT_LIG program was run; 37°C 45 mins, 70°C 20 mins and 4°C hold.

5.2.2.6 Amplify Libraries

The HYP plate containing beads was placed on a TruSeq Index Plate Fixture (Illumina) and 4µl of each Index 1 and Index 2 adapter was added. Index 1 and Index 2 adapters were arranged as follows (Table 6.3). The plate was then placed on ice and 20µl of EDP/EMM mixture was added to each well, pipetting well to mix. The plate was then centrifuged at 280 x g for 1 minute then placed on ice. The custom design included 751 amplicons; therefore, 27 PCR cycles were used for the library amplification step. The plate was placed on the thermal cycler and the library amplification PCR was run; 95°C for 3 minutes, 27 cycles of; 98°C for 20 secs, 67°C for 20 secs and 72°C for 40 secs.

Table 5.3 Index assignments for Illumina validation cohort.

	1	2	3	4	5	6	7	8
A				501-701	501-709	501-705		
B				502-702	502-710			
C				503-703	503-711			
D				504-704	504-712			
E				505-705	505-701			
F				506-706	506-702			
G				507-707	507-703			
H				508-708	508-704			

5.2.2.7 Clean-Up Libraries

All reagents prepared as per manufacturer's instructions. The HYP plate was centrifuged at 280 x g for 1 min and 45µl of supernatant from each well of the HYP plate was transferred to the corresponding wells of the CLP plate. 36µl of SPB was added to each well of the CLP plate and the plate was shaken at 1800RPM for 2 mins. The plate was then incubated at room temperature for 5 mins before centrifuging at 280 x g for 1 minute. The plate was then transferred to a magnetic stand for 2 mins until the samples were cleared before removing and discarding the supernatant. Two washes were carried out by adding 200µl freshly prepared 80% ethanol to each sample well, incubating on the stand for 30 secs and removing and discarding all supernatant from each well. The plate was then removed from the magnetic stand and air dried for 5 mins. Once dry 25µl RSB was added to each well and the plate was placed on the shaker at 1800 RPM for 2 minutes. The plate was then incubated at room temperature for 2 mins before centrifuging at 280 x g for 1 minute. The plate was transferred to the magnetic stand for 2 mins until the liquid was cleared and 20µl of purified library was transferred into a new LNP plate. The remaining liquid in the CLP plate was used to assess quality and quantity of DNA libraries. The final purified libraries were quantified by Qubit dsDNA HS assay (Qubit) and ran on a Bioanalyser DNA 1000 chip (Agilent).

5.2.2.8 Troubleshooting

The Bioanalyser DNA 1000 chip results (Agilent) showed primer dimer in some of the libraries and lower than expected amplicon concentrations, suggesting the possible presence of a contaminant which interfered with the Qubit assay. Therefore, each of the libraries was further purified using 0.8× Agencourt AMPure XP beads (Beckman Coulter). After this, the libraries were again quantified by Qubit ds DNA HS assay and the size distribution assessed on a Fragment Analyser (Advanced Analytical Technologies) using a HS NGS kit. The concentration of library 14 (sample S083.08) was similar to some of the other libraries; however, the amount of amplicon visible on the Fragment Analyser electropheragram was negligible. Also, some of the libraries still contained primer dimer: in order to remove these, firstly the libraries (including sample 14) were pooled in equimolar amounts based on the Qubit and Fragment Analyser data, then the pool was size-selected on a 1.5% agarose Pippin gel cassette (Sage Science). For this, 1.5% DF Marker K settings were used, with collection of fragments between 240 and 500bp. The size-selected pool was purified using 1.8× Agencourt AMPure XP beads and then ran on a Bioanalyser HS DNA chip, which showed that primer dimer had been removed. The DNA concentration of the pool was determined initially by Qubit ds DNA HS assay, and then by qPCR, using an Illumina library quantification kit (KAPA) on a Roche LightCycler 480 II system.

5.2.2.9 Pooling

The pool of 15 TruSeq custom amplicons was sequenced on one MiSeq run, using version 3 chemistry generating 2 x 300bp paired end reads.

5.2.3 SureSelect XT HS

5.2.3.1 Panel Design

The original SureSelect XT design (see **5.2.2.1**) was modified for the 96 cohort to include FFPE samples. The 14 validation cohort samples were aligned using SureCall (Agilent) and the average and median read depths were 200-300x. The percentage of target bases covered at 50x and 100x were very high with ~99% and ~97% respectively. Regions that were consistently lower than 50x across more than 6 samples were identified. These comprised of 13 regions corresponding to exons in the following genes *KTN1* (6 exons), *TP53BP1*, *PLBC4*, *TTC28*, *FBXW7* and *CSMD1* (3 exons). These had a tendency to at the edges of the regions, so we duplicated the probes in these regions to boost the coverage.

5.2.3.2 Sample Preparation

Fresh samples were quantified using the Qubit BR dsDNA Assay Kit (Qubit, Invitrogen) and 75ng of gDNA was diluted with 1X Low TE Buffer to a final volume of 50µl. DNA integrity of FFPE samples DNA integrity was qualified performing a qPCR using the Agilent NGS FFPE QC Kit (Agilent) resulting in an $\Delta\Delta$Cq DNA integrity score and the precise quantity of amplifiable DNA in the sample. Samples with $\Delta\Delta$Cq DNA integrity score $\leq$1, were deemed as good quality amplifiable gDNA and the Qubit- based gDNA concentration was used to determine input. Samples with $\Delta\Delta$Cq DNA integrity score $>$1, the qPCR- based concentration of amplifiable gDNA, was utilised to determine amounts of input DNA.

5.2.3.3 DNA Shearing

High quality gDNA was sheared using the Covaris S-series instrument (SonoLab software) using a two-round shearing protocol: shearing for 2 minutes, centrifuging for 10s, vortexing for 5 seconds and centrifuging for 10 seconds then repeating this process. FFPE samples

were sheared for 6 minutes and centrifuged briefly. The settings for both sample types had: a 10% duty factor, 175 Peak Incident Power (PIP) and 200 cycles per burst.

5.2.3.4 Repairing and dA-Tailing the DNA ends

All reagents were prepared as per the manufacturer's instructions. The ligation master mix was prepared by adding the 23µl ligase buffer and 2µl T4 DNA Ligase per reaction into a 1.5ml Eppendorf tube. This was kept at room temperature for 30–45 minutes before use to allow equilibration to room temperature. The End Repair/dA-Tailing master mix was prepared by combining 16µl End Repair-A Tailing Buffer and 4µl End Repair-A Tailing Enzyme Mix per reaction. 20 µl of the End Repair/dA- Tailing master mix was added to each sample well containing approximately 50 µl sheared DNA and placed on a thermal cycler for 15mins at 20°C and 15 minutes at 72°C for End Repair/dA-Tailing.

5.2.3.5 Ligating the molecular-barcoded adaptor

Once the thermal cycler reached the 4°C hold step, samples were transferred to ice. 25 µl of the Ligation master mix that was prepared previously was added to each end-repaired/dA- tailed DNA sample (approximately 70 µl) and mixed by pipetting up and down at least 10 times using a pipette set to 85 µl, then briefly spun. 5 µl of Adaptor Oligo Mix was added to each sample and mixed by pipetting up and down 15–20 times using a pipette set to 85 µl. Samples were spun and transferred to a thermal cycler for 30 minutes at 20°C. A unique molecular barcode sequence is incorporated into each library DNA fragment at this step.

5.2.3.6 Purify the sample using AMPure XP beads

Performed as described in **6.2.2.3** with 80µl AMPure XP beads (Agencourt AMPure XP Kit, Beckman Coulter Genomics) eluted in 35µl nuclease free water (Ambion).

5.2.3.7 Amplify the adaptor-ligated library

Pre- capture PCR reaction mix was prepared by adding 10µl 5× Herculase II Reaction Buffer, 0.5µl 100 mM dNTP Mix, 2µl Forward Primer and 1µl Herculase II Fusion DNA Polymerase per reaction. 13.5 µl of the PCR reaction mixture was added to each purified DNA library sample in the PCR strip tubes. 2 µl of the corresponding SureSelect XT HS Index Primer was added to each reaction. Samples were transferred to a thermal cycler for: 2 minutes at 98°C, 9 cycles for intact fresh DNA or 12 cycles for FFPE DNA of 30 s at 98°C, 30 s 60°C 1min at 72°C and 5 minutes at 72°C.

5.2.3.8 Purifying the sample using AMPure XP beads

Performed as described in **6.2.2.3** with 50µl AMPure XP beads (Agencourt AMPure XP Kit, Beckman Coulter Genomics) eluted in 15µl nuclease free water (Ambion).

5.2.3.9 Assessing Precapture library DNA quantity and quality

Performed as described in **6.2.2.6**. DNA quantity and quality was deemed successful if the electropheragram showed the peak of DNA fragment size positioned between 300 to 400bp for high- quality DNA and approximately 200 to 400bp for FFPE DNA.

5.2.3.10 Hybridising DNA samples to the Capture Library

The hybridization reaction required 500–1000 ng of prepared DNA in a volume of 12 µl. The maximum amount of prepared DNA available within this range was used. 5 µl of SureSelect XT HS and XT Low Input Blocker Mix was added to each DNA library sample well, vortexed at high speed for 5s and spun briefly. Sealed sample strips were transferred to the thermal cycler for 5mins at 95°C and 10 mins at 65°C. The thermal cycler was paused at 65°C. Whilst the cycler was running the hyb solution was prepared by combining: 0.5µl SureSelect RNase Block, 4.5µl Nuclease-free water, 2 µl Capture Library, 6µl SureSelect Fast Hybridization Buffer per reaction. Keeping the DNA and Blocker samples in the cycler, 13 µl of the room-

temperature Capture Library Hybridization Mix was added to each sample well and mixed by pipetting up and down slowly 8 to 10 times. The thermal cycler was then resumed for 60 cycles of: 1 min at 65°C and 3 seconds at 37°C with a final hold at 65°C.

5.2.3.11 Preparing streptavidin-coated magnetic beads

Dynabeads MyOne Streptavidin T1 magnetic beads (Invitogen) were vigorously re-suspended on a vortex mixer. 50µl per hybridisation sample of the re-suspended beads were added to wells of a fresh strip tube. The beads underwent three washes by: adding 200µl of SureSelect Binding Buffer, mixing by pipetting up and down 20 times, clearing the strip tube on a magnetic separator device and waiting at least 5 minutes until the solution was clear and removing and discard the supernatant. The beads were re-suspended in 200 µl of SureSelect Binding Buffer.

5.2.3.12 Capturing the hybridized DNA using streptavidin-coated beads

After the hybridization step was completed and the thermal cycler reached the 65°C hold step), the samples were transferred to room temperature. The entire volume (approximately 30 µl) of each hybridization mixture was transferred to wells containing 200 µl of washed streptavidin beads using a multichannel pipette. These were mixed by pipetting up and down 5–8 times to mix then sealed with fresh caps. The samples were incubated on a 96-well plate mixer, mixing vigorously at 1500rpm, for 30 minutes at room temperature. During the 30 minute incubation for capture, SureSelect Wash Buffer 2 was prewarmed at 70°C. 200µl aliquots of Wash Buffer 2 were transferred to in wells of a fresh 96- well plate, aliquoting 6 wells of buffer for each DNA sample in the run. The wells were capped and incubated in the thermal cycler, with heated lid on, held at 70°C until used later. When the 30 minute incubation period initiated was completed, the sampled were spun briefly to collect the liquid. The strip tubes were then placed on a magnetic separator to collect the beads, when the solution was cleared the supernatant was removes and

discarded. The beads were re-suspended in 200 µl of SureSelect Wash Buffer 1 and mixed by pipetting up and down 15–20 times, until beads were fully re-suspended. The strip tubes were then placed in a magnetic separator for 1 minute until the solution was cleared. The supernatant was then removed and discarded. The strip tubes were removed from the magnetic separator and transferred to a rack at room temperature. The beads were then with the prewarmed Wash Buffer 2 a total of 6 times using the following steps. The beads were re-suspended in 200 µl of 70°C Wash Buffer 2, and pipetted up and down 15–20 times, until the beads were fully re-suspended. The wells were sealed with fresh caps and vortexed at high speed for 8 seconds. The strip tubes were spun briefly to collect the liquid without pelleting the beads. The samples were incubated for 5 minutes at 70°C on the thermal cycler with the heated lid on. The strip tubes were placed on the magnetic separator at room temperature for 1 minute until the solution was clear, then the supernatant was removed and discarded. After the last wash and after verifying that all wash buffer had been removed, 25 µl of nuclease-free water was added to each sample well, and pipetted up and down 8 times to re-suspend the beads.

5.2.3.13 Amplifying the captured libraries

The PCR reaction mix was prepared by combining 12.5µl Nuclease-free water, 10µl 5× Herculase II Reaction Buffer, 1µl Herculase II Fusion DNA Polymerase, 0.5µl 100 mM dNTP Mix and 1µl SureSelect Post-Capture Primer Mix per reaction. 25 µl of the PCR reaction mix was added to each sample well containing 25 µl of bead- bound target- enriched DNA. PCR reactions were mixed well by pipetting up and down until the bead suspension was homogeneous. The samples were transferred to a thermal cycler 98°C for 2 minutes then 12 cycles of 98°C 30s, 60°C 30s and 72°C 1 minute with a final elongation 72°C for 5 mins. When the PCR amplification program was complete, the strip tubes were briefly spun. The streptavidin-coated beads were removed by placing the plate or strip tube on the magnetic

stand at room temperature for 2 minutes until the solution was clear. The supernatant was removed and transferred (approximately 50 µl) into wells of fresh strip tubes.

5.2.3.14 Purifying the amplified captured libraries using AMPure XP beads

Performed as described in **5.2.2.3** with 50µl AMPure XP beads (Agencourt AMPure XP Kit, Beckman Coulter Genomics) eluted in 25µl nuclease free water (Ambion).

5.2.3.15 Assessing sequencing library DNA quantity and quality

AS performed in **5.2.2.11**. DNA quantity and quality was deemed successful if the electropheragram showed the peak of DNA fragment size positioned between 200 and 400 bp.

5.2.3.16 Sample Pooling

Libraries (96 in total) were pooled in equimolar amounts based on the aforementioned Qubit and Bioanalyser data. Two pools were created; one pool of 14 FFPE samples and one pool of 82 fresh samples. The pool was further purified using Agencourt AMPure XP beads (Beckman Coulter). The size of the final pool was assessed on a Bioanalyser high sensitivity DNA chip and the DNA concentration was determined initially by Qubit double-stranded DNA high sensitivity assay, then by qPCR, using an Illumina library quantification kit (KAPA) on a Roche LightCycler 480 II system. The pool of 96 target enriched libraries was sequenced on two MiSeq runs, using custom sequencing primers (as per Agilent protocol) and version 2 chemistry, generating 2 x 250bp paired end read.

5.2.4 Bioinformatics Analysis

Samples were sequenced on the Illumina MiSeq platform (2x 250 bp paired-end) (Illumina, Inc., San Diego, CA) by the Center for Genomic Research (www.cgr.liv.ac.uk), University of Liverpool, UK. Base-calling and de-multiplexing of indexed reads were performed by CASAVA version 1.8.2 (Illumina, Inc., San Diego, CA) to produce the raw sequence data in FASTQ format. The raw FASTQ reads were trimmed to remove Illumina adapter sequences using Cutadapt version 1.2, and low quality bases using Sickle version 1.200.

Trimmed reads were aligned to the human GRCh37 reference genome (ftp://ftp-trace.ncbi.nih.gov/1000genomes/ftp/technical/reference/phase2_reference_assembly_sequence/hs37d5.fa.gz) with the short read alignment tool, BWA-MEM (version 0.7.5a-r405). Following alignment, PCR and optical duplicate reads were identified and removed with UMI-tools (https://github.com/CGATOxford/UMI-tools). Subsequently, the Genome Analysis Toolkit (GATK) (version 3.7) Indel Re-aligner module was used to locally re-align reads around putative insertion and deletion sites. GATK BaseRecalibrator module was used for recalibrating the base calls. The aligned data was then analysed using tCoNut (https://github.com/tgen/tCoNuT) to detect CNVs. The variants were called by GATK and annotated by SNPeff. The allelic frequency threshold to call a mutation was 10%.

5.2.5 Statistical Analysis

Survival time (months) was calculated from the date of first diagnosis until death, or study closure on 28th February 2018. Analyses were carried out using SPSS Statistics v.24 (IBM), Microsoft R 3.5.1 and the packages rms, cmprsk and mstate. A Cox model was used to estimate the hazard rates of the two causes of death. Each of the causes of death is accounted for in the model by a stratum, so that the baseline hazards are different as it's wasn't realistic to assume proportionality of hazards to hold across different causes of death.

5.3 Results

5.3.1 Comparison of validation panels

5.3.1.1 Copy-Number Variation

Of the 14 samples analysed, 1/14 (7%) and 3/14 (21%) failed to produce discernible copy number variation data with the SureSelect and TSCA panels respectively (Table 5.5). 13/14 (93%) samples had available copy number data from previous MLPA analysis for chromosomes 1, 3, 6 and 8; the remaining sample was tested via MSA and only examined chromosome 3. Chromosome 1p was not included on the TSCA NGS panel due to tiling limitations. 12/13 (92%) samples analysed using SureSelect were concordant with previous MLPA data; the non-concordant sample was reported as unclassifiable by MLPA and loss by SureSelect. Chromosome 3 data for MLPA, SureSelect and TSCA were concordant across all analysable samples; 13/13 and 11/11 respectively. Chromosome 6p showed less concordance with only 4/13 (31%) SureSelect and 5/11 (45%) TSCA in agreement with the previous MLPA results, however there was 100% concordance between SureSelect and TSCA results. Similarly, there was 100% concordance for chromosome 6q copy number between SureSelect and TSCA but only 8/13 (62%) SureSelect and 6/11 (55%) TSCA data matched the MLPA classification. Chromosome 8p was concordant with previous MLPA data in 8/13 (62%) SureSelect and 7/11 (64%) TSCA; SureSelect and TSCA were in agreement in 8/10 (80%) of samples. Chromosome 8q was 100% concordant between previous MLPA data and the SureSelect and TSCA samples. The SureSelect and TSCA were able to produce a clear result for 2 cases where 8q was unclassifiable by MLPA.

Table 5.4 Concordance data from 14 sample validation run

Enrichment Method	Copy Number detection	Copy Number Concordance with MLPA data
PCR	11/14 (79%)	11/11 (100%)
Hybrid Capture	13/13 (93%)	13/13 (100%)

Table 5.5 A comparison of copy number variations as detected by MLPA, SureSelect and TSCA target enrichment

TEST	MLPA	SS	TSCA	MLPA	SS	TSCA	MLPA	SS	TSCA	MLPA	SS	TSCA	MLPA	SS	TSCA	MLPA	SS	TSCA
CHR	1p			3			6p			6q			8p			8q		
ID																		
S154.11	N	N	-	N	N	N	U	G	G	N	L	L	G	L	L	U	G	G
S191.11	N	N	-	L	L	L	N	N	N	N	N	N	L	L	L	G	G	G
S177.13	-	L	-	L	L	L	-	N	N	-	N	N	-	G	G	-	G	G
S162.12	L	L	-	L	L	L	L	N	N	U	N	N	N	N	N	U	G	G
S183.13	L	L	-	L	L	L	L	N	N	N	N	N	N	G	N	G	G	G
S031.13	U	N	-	L	L	L	U	G	G	U	L	L	N	N	N	G	G	G
S107.12	N	N	-	L	L	L	N	G	G	N	L	L	L	L	L	G	G	G
S032.13	U	L	-	L	L	*	G	N	*	N	N	*	G	N	*	G	G	*
S080.09	N	N	-	L	L	*	N	G	*	N	N	*	N	N	*	G	G	*
S095.08	N	N	-	N	N	N	G	G	G	N	N	N	N	N	N	N	N	N
S001.09	N	N	-	N	N	N	N	N	N	N	N	N	N	N	N	G	G	G
S102.09	N	N	-	L	L	L	N	N	N	N	N	N	N	L	N	G	G	G
S129.09	N	*	-	L	*	L	G	*	G	N	*	N	N	*	N	N	*	N
S083.08	N	N	-	N	N	*	G	N	*	N	N	*	N	L	*	G	G	*

- = Not included on NGS panel

*= Sample fail

5.3.1.2 Single Nucleotide Variation

Of the 14 samples analysed, 8/14 (57%) had previous mutation data from TCGA analyses and 6/14 (43%) had an unknown mutation status (Table 2.6). TCGA analysis yielded: 1 *GNAQ*, 5 *GNA11*, 1 *SF3B1* and 1 *CYSLTR2* mutation, which were also detected by both the SureSelect and TSCA. The *BAP1* mutations were detected by both SureSelect and TSCA were 100% concordant in the TCGA cohort of samples; however, they weren't completely in agreement with those detected by the TCGA. The TCGA did not detect the W196* mutation in sample S107.12 and both SureSelect and TSCA panels did not find the homozygous deletion in sample S177.13, which was visible on the SNP array data (Figure 5.1). For the samples for which TCGA mutation data were not available, there was 100% (6/6) concordance between mutations detected in *GNAQ, GNA11, BAP1, SF3B1* and *EIF1AX* by both the SureSelect and TSCA panels. The discovery genes on each panel produced varying results. A novel missense mutation of unknown significance was detected on *TTC28* I1296V on both SureSelect and TSCA panels (Table 5.7).

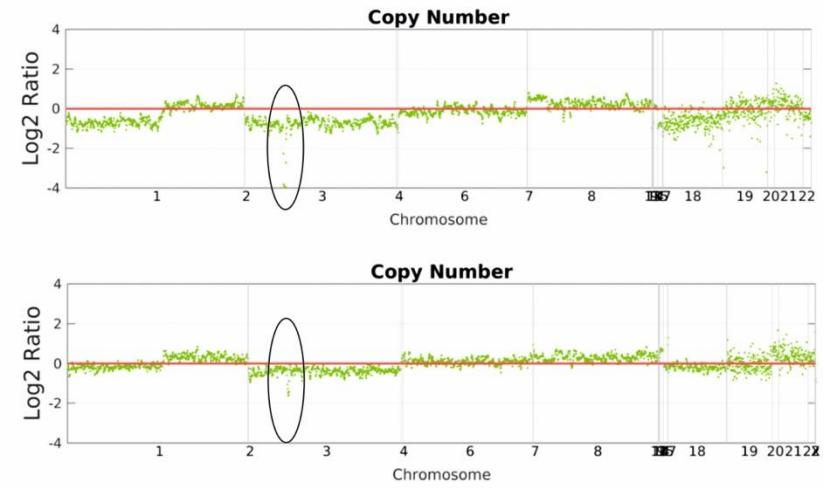

Figure 5.1 A homozygous deletion of the *BAP1* loci.

Table 5.6 A comparison of single nucleotide variations in *GNAQ, GNA11, BAP1, SF3B1* and *EIF1AX* as detected by MLPA, SureSelect and TSCA target enrichment

TEST	TCGA	SS	TSCA	TCGA	SS	TSCA	TCGA	SS	TSCA	TCGA	SS	TSCA	TCGA	SS	TSCA
CHR	GNAQ			GNA11			BAP1			SF3B1			EIF1AX		
ID															
S154.11	N/A	N/A	N/A	N/A	N/A	N/A	NA	N/A	N/A	N/A	N/A	N/A	N/A	N/A	N/A
S191.11	N/A	N/A	N/A	Q209L	Q209L	Q209L	Frameshift	V62fs, inframe del K61del	V62fs, inframe del K61del	N/A	N/A	N/A	N/A	N/A	N/A
S177.13	N/A	N/A	N/A	N/A	N/A	N/A	Homozygous deletion	N/A	N/A	N/A	N/A	N/A	N/A	N/A	N/A
S162.12	N/A	N/A	N/A	Q209L	Q209L	Q209L	N/A	N/A	N/A	R625H	R625H	R625H	N/A	N/A	N/A
S183.13	N/A	N/A	N/A	Q209L	Q209L	Q209L	Splicing variant	V27fs	V27fs	N/A	N/A	N/A	N/A	N/A	N/A
S031.13	Q209P	Q209P	Q209P	N/A	N/A	N/A	Frameshift	P124fs	P124fs	N/A	N/A	N/A	N/A	N/A	N/A
S107.12	N/A	N/A	N/A	Q209L	Q209L	Q209L	N/A	W196*	W196*	N/A	N/A	N/A	N/A	N/A	N/A
S032.13	N/A	N/A	N/A	Q209L	Q209L	Q209L	Frameshift	R213fs	R213fs	N/A	N/A	N/A	N/A	N/A	N/A
S080.09	-	N/A	N/A	-	R183C	R183C	-	N/A	N/A	-	R625C	R625C	-	N/A	N/A
S095.08	-	Q209L	Q209L	-	N/A	N/A	-	N/A	N/A	-	N/A	N/A	-	P2R	P2R
S001.09	-	Q209P	Q209P	-	N/A	N/A	-	N/A	N/A	-	N626I	N626I	-	N/A	N/A
S102.09	-	Q209P	Q209P	-	N/A	N/A	-	T69fs	T69fs	-	N/A	N/A	-	N/A	N/A
S129.09	-	*	NA	-	*	N/A	-	*	Q642 A648del	-	*	N/A	-	*	N/A
S083.08	-	N/A	*	-	Q209L	*	-	S58fs	*	-	N/A	*	-	N/A	*

- = Not included in TCGA analyses

* = Sample fail

Table 5.7 A comparison of single nucleotide variations *CYSLTR2, TP53BP1, CSMD1, TTC28, DLK2* and *KTN1* as detected by MLPA, SureSelect and TSCA target enrichment

TEST	TCGA	SS	TSCA	TCGA	SS	TSCA	TCGA	SS	TSCA	TCGA	SS	TSCA	TCGA	SS	TSCA	TCGA	SS	TSCA
CHR	CYSLTR2			TP53BP1			CSMD1			TTC28			DLK2			KTN1		
ID																		
S154.11	N/A	N/A	N/A	N/A	N/A	N/A	N/A	N/A	N/A	N/A	I1296V	I1296V	N/A	N/A	N/A	N/A	N/A	N/A
S191.11	N/A	N/A	N/A	N/A	N/A	N/A	N/A	N/A	N/A	N/A	N/A	N/A	N/A	N/A	N/A	N/A	N/A	N/A
S177.13	L129Q	L129Q	L129Q	N/A	N/A	N/A	N/A	N/A	N/A	N/A	N/A	N/A	N/A	N/A	N/A	N/A	N/A	N/A
S162.12	N/A	N/A	N/A	N/A	N/A	N/A	N/A	N/A	N/A	N/A	N/A	N/A	N/A	N/A	N/A	N/A	N/A	N/A
S183.13	N/A	N/A	N/A	N/A	N/A	N/A	N/A	N/A	N/A	N/A	N/A	N/A	N/A	N/A	N/A	N/A	N/A	N/A
S031.13	N/A	N/A	N/A	N/A	N/A	N/A	N/A	N/A	N/A	N/A	N/A	N/A	N/A	N/A	N/A	N/A	N/A	N/A
S107.12	N/A	N/A	N/A	N/A	N/A	N/A	N/A	N/A	N/A	N/A	N/A	N/A	N/A	N/A	N/A	N/A	N/A	N/A
S032.13	N/A	N/A	N/A	N/A	N/A	N/A	N/A	N/A	N/A	N/A	N/A	N/A	N/A	N/A	N/A	N/A	N/A	N/A
S080.09	-	N/A	N/A	-	N/A	N/A	-	N/A	N/A	-	N/A	N/A	-	N/A	N/A	-	N/A	N/A
S095.08	-	N/A	N/A	-	N/A	N/A	-	N/A	N/A	-	N/A	N/A	-	N/A	N/A	-	N/A	N/A
S001.09	-	N/A	NA	-	N/A	N/A	-	N/A	N/A	-	N/A	N/A	-	N/A	N/A	-	N/A	N/A
S102.09	-	N/A	NA	-	N/A	N/A	-	N/A	N/A	-	N/A	N/A	-	N/A	N/A	-	N/A	N/A
S129.09	-	*	NA	-	*	N/A	-	*	N/A	-	*	N/A	-	*	N/A	-	*	N/A
S083.08	-	N/A	*	-	N/A	*	-	N/A	*	-	N/A	*	-	N/A	*	-	N/A	*

5.3.1.3 Quality of Sequencing

Table 5.8 A comparison of sequencing quality in hybrid capture vs. PCR-based enrichment

Enrichment Method	Reads mapped %	Reads mapped % after UMI removed	Number of bases with coverage more than 0 (%)	Mean Depth of Coverage for the bases with coverage more than 0
PCR	92.06	16.33	92.99	302x
Hybrid Capture	97.68	74.37	99.99	497.25x

Table 5.9 Sequencing quality in 94 sample cohort.

Reads mapped %	Reads mapped % after UMI removed	Number of bases with coverage more than 0 (%)	Mean Depth of Coverage for the bases with coverage more than 0
97.95	89.65	99.27	94.46x

5.3.2 94 sample cohort

5.3.2.1 Clinical and Histopathological features of the examined UM

The study consisted of 54 males and 40 females with a mean age of 63 years at primary management (median age 64; range 16 – 87 years). The mean follow-up period was 129 months (median follow-up 142 months; range 0 – 287 months). Primary management was enucleation 69/94 (73%), local resection 11/94 (12%), endoresection 1/94 (1%), fine-needle aspirate biopsy 3/94 (3%), PBR 3/94 (3%) and ruthenium plaque RXT 7/94 (7%). Secondary treatment was necessary for 4/94 (4%) patients; one local resection patient required a subsequent enucleation 32 months after treatment, one patient treated by PBR required an endoresection 36 months after administration of RXT, another patient treated by PBR required enucleation 29 months after treatment and one patient treated by plaque RXT required an enucleation 24 months after treatment. At study closure (28/02/2018), 50/94 (53%) patients were alive, 30/94 (32%) patients had died from metastatic disease, 10/94 (11%) patients died from other causes and 4/94 (4%) patients were lost to follow-up. Epithelioid cells were present in 54/94 (57%) of cases with the remaining 40/94 (43%) having a spindle cell morphology. Closed PAS+ loops were identified in 40/94 (44%) cases, absent in 41/94 (43%) cases and not assessed in 13/94 cases (14%). Necrosis was seen in 19/94 (65%) cases, absent in 19/94 (20%) cases and not assessed in 14/94 (15%) cases. There was ciliary body involvement in 29/94 (31%) cases and extraocular extension was present in 6/94 (6%) of cases. The mean LBD was 14.8mm (median LBD 15.3; range 4 – 21mm) with a mean UH of 7.89mm (median UH 8.2; range 1 – 16mm). The tumours had a mean mitotic count of 7/40hpf (median 5; range 1 – 72/hpf).

5.3.2.2 Mutation Frequency

The following frequencies of mutations were detected; *GNAQ* 51/94 (54%), *GNA11* 36/94 (38%), *BAP1* 39/94 (41%), *SF3B1* 19/94 (20%), *EIF1AX* 20/94 (21%), *CYSLTR2* 2/94 (2%),

PLCB4 1/94 (1%), *KTN1* 1/94 (1%), *TTC28* 3/94 (3%), *CSMD1* 2/94 (2%), *TP53BP1* 2/94 (2%) (Table 5.10). No mutations were detected in *BRAF*, *DLK2*, *FBXW7* or *SRSF2*.

Table 5.10 Mutations identified according to copy number status of chromosome 3

	All Tumours (n=94)	**M3 (n=44)**	**D3 (n=46)**	**L3p (n=1)**	**ID (n=2)**
GNAQ	51/94 (54%)	19/44 (43%)	29/46 (63%)	1/1 (100%)	2/2 (100%)
GNA11	36/94 (38%)	21/44 (48%)	14/46 (30%)	-	-
BAP1	39/94 (41%)	35/44 (80%)	1/46 (4%)	-	2/2 (100%)
SF3B1	19/94 (20%)	4/44 (9%)	14/46 (30%)	1/1 (100%)	-
EIF1AX	20/94 (21%)	2/44 (5%)	17/46 (37%)	-	-
CYSLTR2	2/94 (2%)	1/44 (2%)	1/46 (2%)	-	-
PLCB4	1/94 (1%)	1/44 (2%)	-	-	-
SRSF2	-	-	-	-	-
KTN1	1/94 (1%)	-	1/46 (2%)	-	-
TTC28	3/94 (3%)	5/44 (2%)	1/46 (2%)	-	-
CSMD1	2/94 (2%)	1/44 (2%)	1/46 (2%)	-	-
TP53BP1	2/94 (2%)	1/44 (2%)	-	-	-
BRAF	-	-	-	-	-
DLK2	-	-	-	-	-
FBXW7	-	-	-	-	-

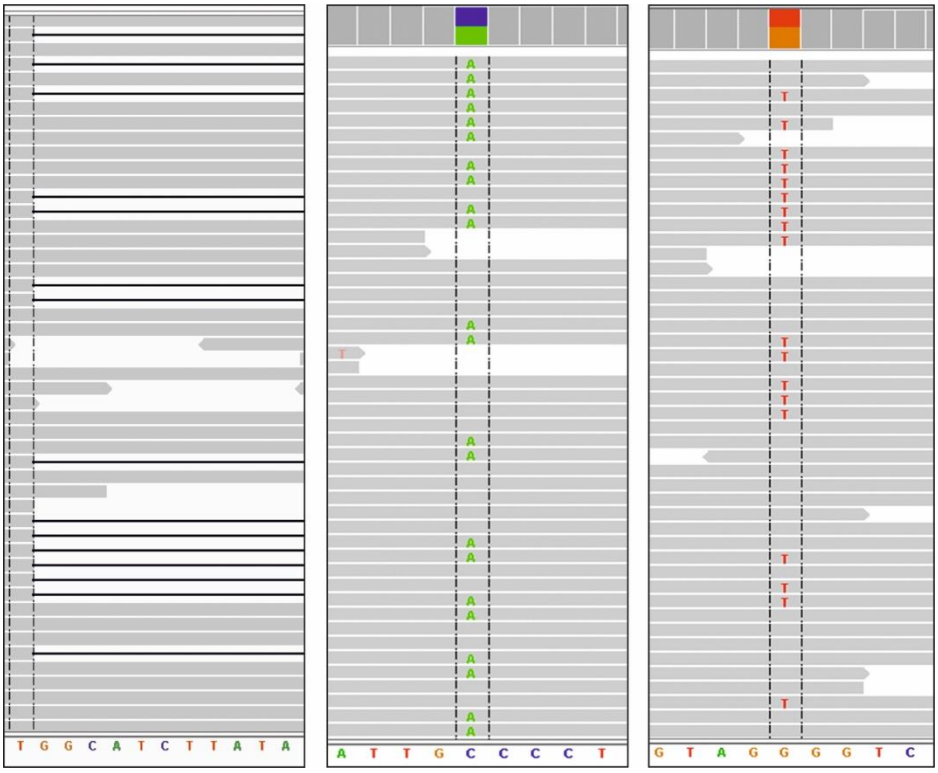

Figure 5.2 IGV Ver 2.3.94 images of novel mutations in *PLCB4*, *KTN1* and *TTC28*. From left to right: a disruptive in-frame deletion p.M549_G556delinsI in *PLCB4*, a missense mutation in p.P195Thr *KTN1* and a missense mutation in p.P1216H in *TTC28*.

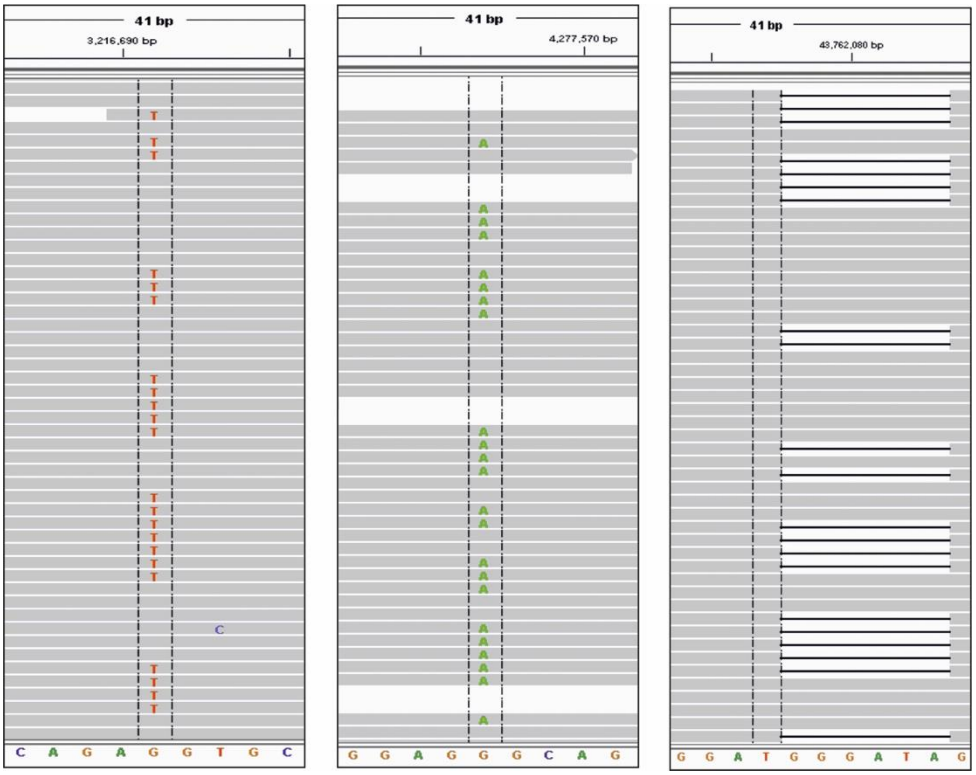

Figure 5.3 IGV Ver 2.3.94 images of novel mutations in *CSMD1* and *TP53BP1.* From left to right: missense mutations in p.P1097H and p.P108L in *CSMD1* and a disruptive in-frame deletion of p.I455_P456del in *TP53BP1*.

5.3.2.3 Copy Number Variation

The cut off values set for the log2 ratio to classify losses and gains were set at 0.65 and 1.35 respectively based on the dosage quotients set for the current MLPA testing performed at Liverpool (186). One case failed to produce a clear genotype. Chromosome 1p was lost in 26/94 (28%), normal in 66/94 (70%) and gained in 1/94 (1%) of cases. The q arm of chromosome 1 was normal in 80/94 (85%), gained in 12/94 (13%) and showed regions of loss and gains in 1/94 (1%) of cases. Monosomy 3 was seen in 44/94 (47%), normal in 46/94 (49%), isodisomy in 2/94 (2%), gained in 1/94 (1%) and loss of 3p in 1/94 cases (1%). Chromosome 6p was normal in 58/94 (62%) and gained 35/94 (37%); 6q was normal in 71/94 (71%), lost in 19/94 (20%) and gained in 3/94 (3%) of cases. The p arm of chromosome 8 was lost in 17/94 (18%), normal in 67/94 (71%) and gained in 9/94 (10%) of

cases. Chromosome 8q was normal in 41/94 (44%) and gained in 52/94 (55%) of cases. One 1/94 (1%) case displayed polyploidy (Figure 5.4).

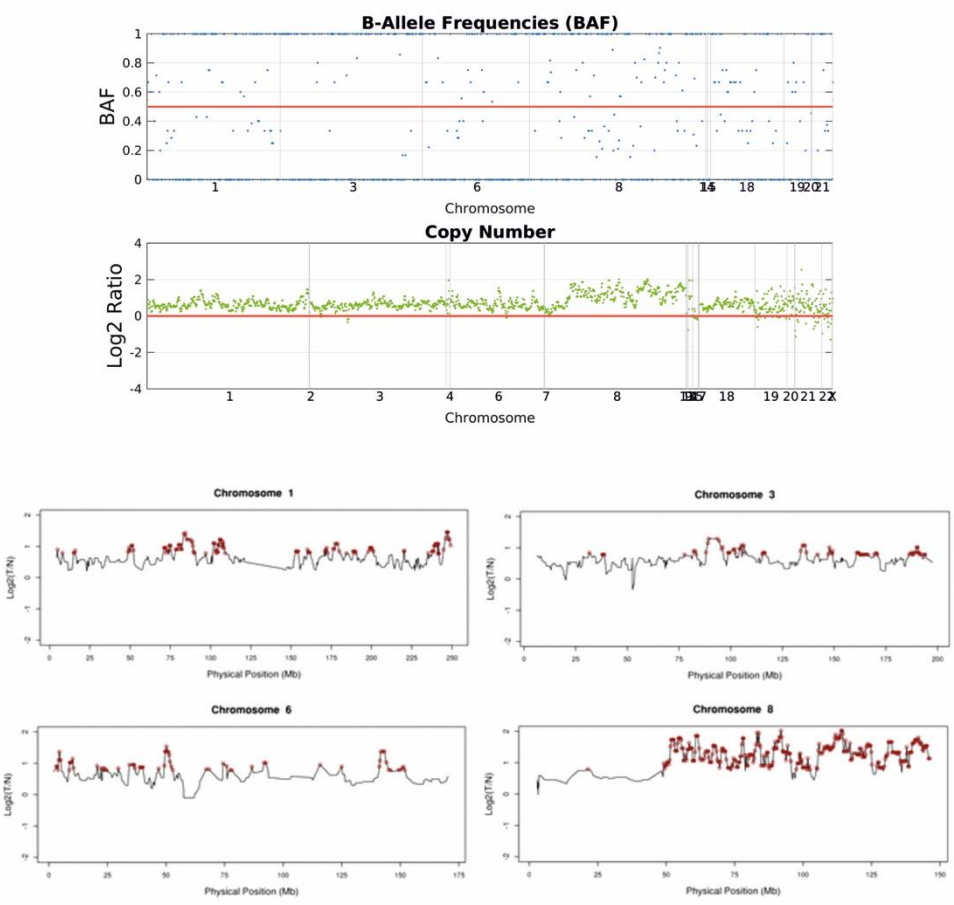

Figure 5.4 Copy number analysis of sample 56 (S027.08) displaying polyploidy

5.3.2.4 Concordance

When compared with previous genotypes conducted by MLPA, concordance was observed in: 80/93 (86%) chromosome 1p, 90/93 (97%) chromosome 3, 75/93 (81%), chromosome 6p 75/93 (81%) chromosome 6q, 70/93 (75%) chromosome 8p and 75/93 chromosome 8q (Table 5.11).

Table 5.11 Concordance between chromosome copy number detected by NGS vs. MLPA

	Chr1p	**Chr3**	**Chr6p**	**Chr6q**	**Chr8p**	**Chr8q**
Concordant	80/93 (86%)	90/93 (97%)	75/93 (81%)	75/93 (81%)	70/93 (75%)	75/93 (81%)
Discordant	13/93 (14%)	3/93 (3%)	18/93 (19%)	18/93 (19%)	20/93 (25%)	18/93 (19%)

5.3.2.5 FFPE concordance

When compared with mutation and genotype data obtained from previous MLPA testing, NGS conducted at Rotterdam and NGS conducted during part of the panel validation the following levels of concordance were found: *GNAQ* (100%); *GNA11* (100%); *BAP1* (86%), *SF3B1* (86%), *EIF1AX* (86%) and *CYSLTR2* (100%) (Table 5.12). An additional missense mutation in p.P108L was also detected in *CSMD1* in sample 3. Copy number was found to be concordant with previous MLPA analyses: chromosome 1p, 10/13 (77%); chromosome 3, 12/13 (92%); chromosome 6p, 7/12 (58%); chromosome 6q, 10/12 (83%); chromosome 8p, 8/12 (67%) and chromosome 8q, 8/12 (67%) (Table 5.13).

Table 5.12 Mutation concordance Fresh vs FFPE validation

	Fresh	FFPE	Fresh	FFPE	Fresh	FFPE	Fresh	FFPE	Fresh	FFPE	Fresh	FFPE
Sample	**GNAQ**		**GNA11**		**BAP1**		**SF3B1**		**EIF1AX**		**CYSLTR2**	
1	Q209R	Gln209Leu	Na	Na	V478fs	Val460fs	Na	Na	Na	Na	Na	Na
2	Na	Na	Q209L	Gln209Leu	L334fs	Na	Na	Na	Na	Na	Na	Na
3	N/A	Na	N/A	Na	N/A	Na	N/A	Na	N/A	Na	L129Q	L129Q
4	Q209L	Gln209Leu	Na	Na	Na	Na	E622D	Glu622Asp	Na	Na	Na	Na
5	Na	Na	Q209L	Gln209Leu	T111fs	Thr111fs	V634I	Na	Na	Na	Na	Na
6	Q209P	Gln209Pro	Na	Na	Na	Na	R625H	Arg625His	N4H	Asn4His	Na	Na
7	Na	Na	Q209L	Gln209Leu	Na	Arg213fs, Ile214_Gly220del	Na	Na	Na	Na	Na	Na
8	Q209L	Gln209Leu	Na	Na	Na	Na	Na	Na	N4S	Asn4Ser	Na	Na
9	Q209L	Gln209Leu	Na	Na	S489fs	Ser489fs	Na	Na	Na	Na	Na	Na
10	Na	Na	Na	Na	L633fs	Leu633fs	Na	Na	Na	Na	Na	Na
11	Q209P	Gln209Pro	Na	Na	Q260*	Gln260*	Na	Na	Na	Na	Na	Na
12	Q209P	Gln209Pro	NA	Na	NA	Na	N626I	Na	NA	Na	Na	Na
13	Na	Na	Q209L	Gln209Leu	Q593*	Gln593*	Na	Na	Na	Na	Na	Na
14	Na	Na	Q209L	Gln209Leu	Na	Na	Na	Na	G6D	Na	Na	Na
Concordance	14/14 (100%)		14/14 (100%)		12/14 (86%)		12/14 (86%)		13/14 (93%)		14/14 (100%)	

Table 5.13 Copy number concordance Fresh vs FFPE validation

	Fresh	FFPE	Fresh	FFPE	Fresh	FFPE	Fresh	FFPE	Fresh	FFPE	Fresh	FFPE
Sample	**Chr1p**		**Chr3**		**Chr6p**		**Chr6q**		**Chr8p**		**Chr8q**	
1	Loss	Normal	Loss	Loss	Gain	Normal	Normal	Normal	Loss	Gain	Gain	Gain
2	Loss	Loss	Loss	Loss	Normal	Normal	Normal	Normal	Normal	Normal	Normal	Gain
3	Loss	Normal	Loss	Loss	Gain	Normal	Normal	Normal	Normal	Normal	Gain	Normal
4	Normal	Loss	Normal	Normal	Gain	Gain	Normal	Normal	Normal	Normal	Gain	Gain
5	Loss	Normal	Loss	Loss	Unclassifiable	Normal	Gain	Normal	Unclassifiable	Normal	Unclassifiable	Gain
6	Loss	Normal	Unclassifiable	Normal	Gain	Normal	Gain	Normal	Gain	Normal	Gain	Normal
7	Loss	Loss	Loss	Loss	Loss	Normal	Normal	Normal	Normal	Gain	Gain	Gain
8	*	Normal	Loss	Normal	*	Normal	*	Normal	*	Normal	*	Normal
9	Normal	Normal	Loss	Loss	Loss	Gain	Unclassifiable	Loss	Loss	Loss	Gain	Gain
10	Normal	Normal	Loss	Loss	Normal	Normal	Normal	Normal	Loss	Loss	Gain	Gain
11	Normal	Normal	Loss	Loss	Normal	Normal	Loss	Loss	Loss	Loss	Gain	Gain
12	Normal	Normal	Normal	Normal	Normal	Normal	Normal	Normal	Normal	Normal	Gain	Gain
13	Normal	Normal	Loss	Loss	Normal	Normal	Normal	Normal	Normal	Normal	Gain	Normal
14	Normal	Normal	Normal	Normal	Normal	Normal	Normal	Normal	Gain	Normal	Normal	Normal
Concordance	10/13 (77%)		12/13 (92%)		7/12 (58%)		10/12 (83%)		8/12 (67%)		8/12 (67%)	

5.3.2.6 Survival

5.3.2.6.1 Mutations

Kaplan–Meier survival curves and tables were examined for all UM examined according to mutation status as determined by NGS. Mutations in *BAP1* (Log rank, p=≤0.001) were significantly associated with a reduced survival time (figure 5.5). Mutations in *EIF1AX* (Log rank, p=0.040) were associated with improved survival overall but not within the disomy 3 cohort alone (Log rank, p=0.254) (figure 5.6). Mutations in *SF3B1* were not significantly associated with a worse clinical outcome in terms of survival (Log rank, p=0.378). This was also true when only disomy 3 cases were analysed for the effect of *SF3B1* mutations on survival (Log rank, p=0.140) (figure 5.7). There was no difference in survival between *GNAQ*, *GNA11*, *CYSLTR2* mutants and wild type UM (Log rank, p=0.533) (figure 5.8). When survival was compared based on the combined chromosome 3 and chromosome 8q status M3 P8q had the highest metastatic risk (Log rank, p=≤0.001), M3 D8 had an intermediate risk whereas D3 D8 and D3 P8q shared a similar low risk (figure 5.9).

5.3.2.6.2 Copy Number

Kaplan–Meier survival curves and tables were examined for all UM according to copy number status as determined by NGS. Gain of chromosome 1q was associated with a worse outcome (Log rank, p=0.027) whereas changes in chromosome 1p were not (Log rank, p=0.568) (Figure 5.10). Loss of chromosome 3 and isodisomy of chromosome 3 were significantly associated with reduced disease-free survival (Log rank, p= ≤0.001) (Figure 5.11). Loss of 6p was associated with improved disease-free survival (Log rank, p=0.006) whereas changes in copy number of 6q was not (Log rank, p=0.462) (Figure 5.12). Loss of 8p was significantly associated with a poor survival outcome (Log rank, p=0.008), as was gain

of 8q (Log rank, p=0.006) (Figure 5.13). Due to multiple testing, only *BAP1* qualifies as a significant factor; EIF1AX will dropout after multiple testing correction.

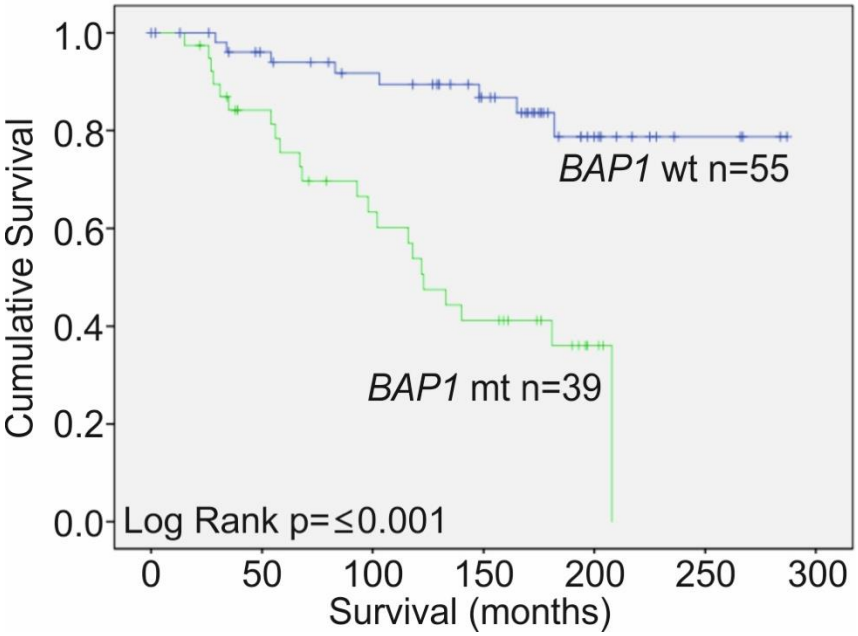

BAP1	Total No.	No. of Events	Censored		Mean Survival (months)	95% Confidence Interval	
			No. %	%		Lower	Upper
Mutant	39	22	17	43.6	130.418	106.752	154.084
Wild-type	55	8	47	85.5	250.614	227.570	273.658
Overall	94	30	64	68.1	206.549	183.333	229.764

Figure 5.5 Kaplan Meier curves and tables where patient survival was stratified according to *BAP1* mutation status determined by NGS; *BAP1* wild-type (n=55) vs. *BAP1* mutants (n=39) (p≤0.001).

A)

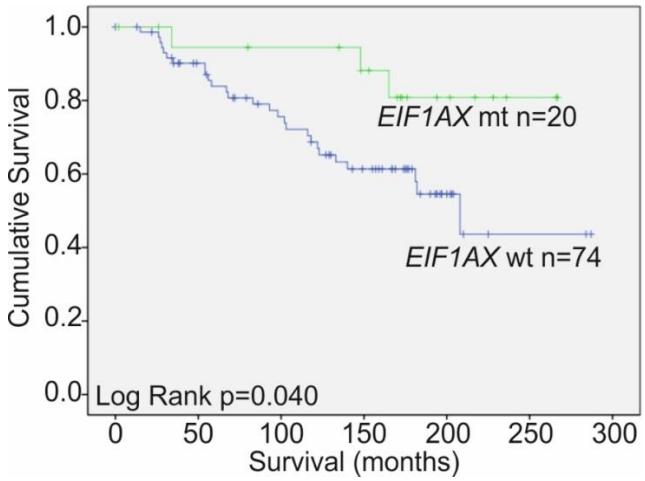

EIF1AX	Total No.	No. of Events	Censored		Mean Survival (months)	95% Confidence Interval	
			No. %	%		Lower	Upper
Mutant	20	3	17	85.0	239.070	209.084	269.057
Wild-type	74	27	47	63.5	190.357	161.831	218.882
Overall	94	30	64	68.1	206.549	183.333	229.764

B)

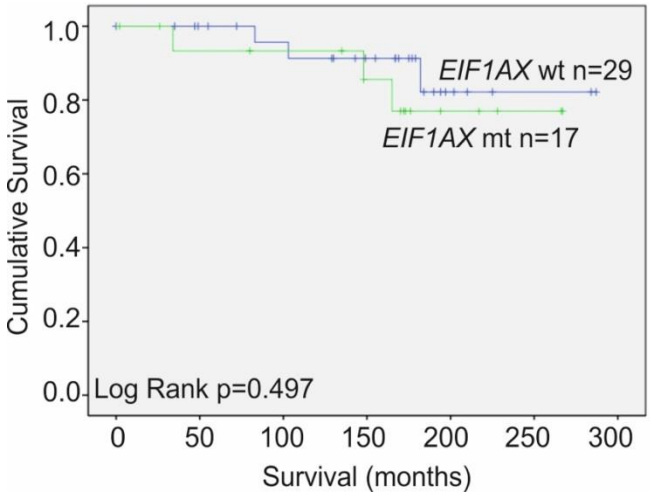

Disomy 3 *EIF1AX*	Total No.	No. of Events	Censored		Mean Survival (months)	95% Confidence Interval	
			No. %	%		Lower	Upper
Mutant	17	3	14	82.4	233.484	198.222	268.747
Wild-type	29	3	26	89.7	260.543	232.871	288.216
Overall	47	6	440	87.0	261.364	233.344	278.914

Figure 5.6. Kaplan Meier curves and tables where patient survival was stratified according to *EIF1AX* mutation status determined by NGS; **A)** Overall *EIF1AX* wild-type (n=74) vs. *EIF1AX* mutants (n=20) (p=0.040) and **B)** Disomy 3 *EIF1AX* wild-type (n=29) vs. *EIF1AX* mutants (n=17) (p=0.497).

A)

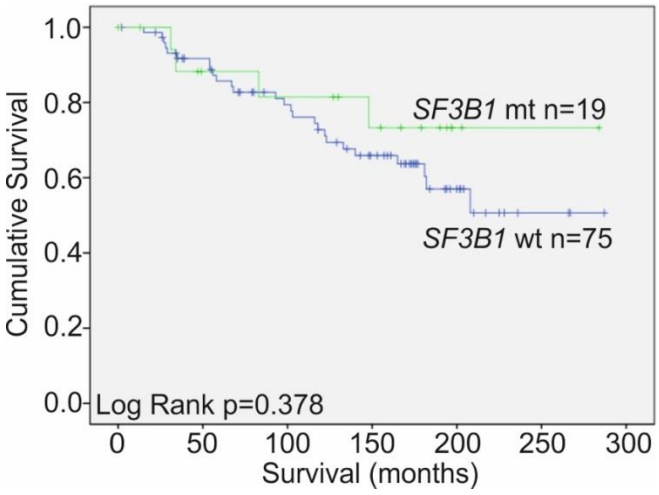

SF3B1	Total No.	No. of Events	Censored		Mean Survival (months)	95% Confidence Interval	
			No. %	%		Lower	Upper
Mutant	19	4	5	78.9	229.692	183.113	276.271
Wild-type	75	26	49	65.3	201.298	175.579	227.016
Overall	94	30	64	68.1	206.549	183.333	229.764

B)

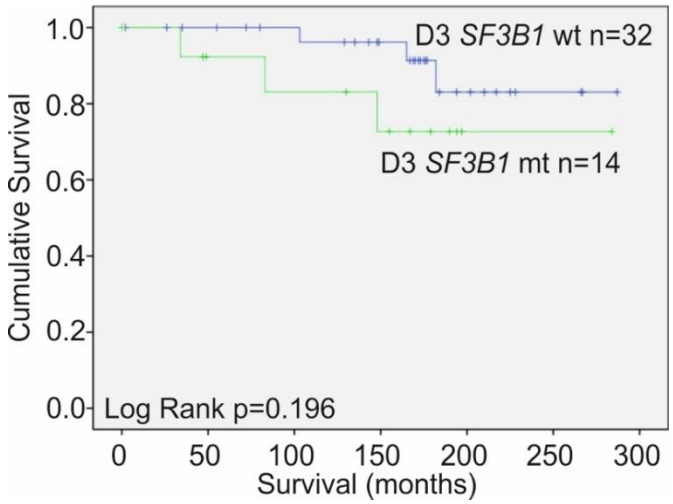

Disomy 3 *SF3B1*	Total No.	No. of Events	Censored		Mean Survival (months)	95% Confidence Interval	
			No. %	%		Lower	Upper
Mutant	14	3	11	78.6	232.092	180.768	283.417
Wild-type	32	29	29	90.6	265.338	242.361	288.417
Overall	47	40	40	87.0	261.364	233.344	278.914

Figure 5.7 Kaplan Meier curves and tables where patient survival was stratified according to *SF3B1* mutation status determined by NGS; A) Overall *SF3B1* wild-type (n=75) vs. *SF3B1* mutants (n=19) (p=0.378) and **B)** Disomy 3 *SF3B1* wild-type (n=32) vs. Disomy 3 *SF3B1* mutants (n=14) (p=0.140).

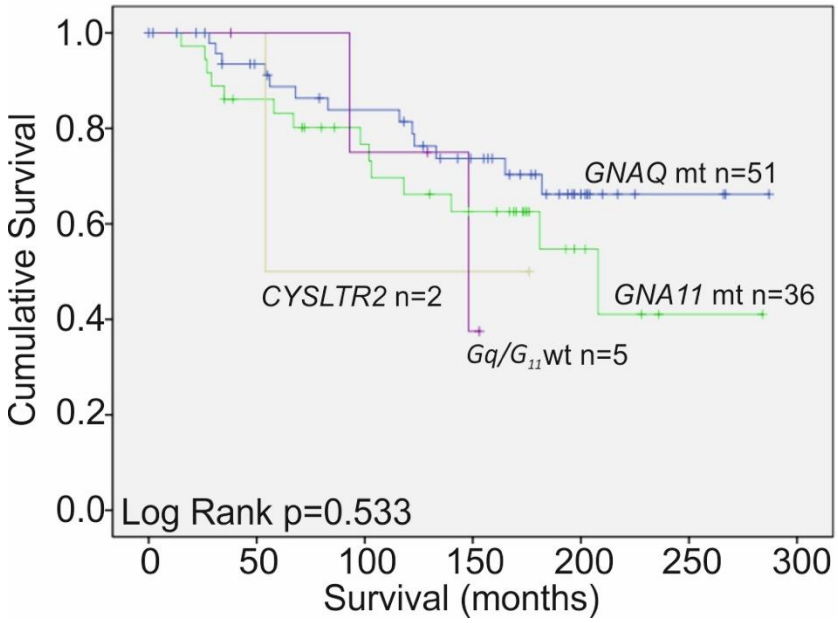

Mutation	Total No.	No. of Events	Censored		Mean Survival (months)	95% Confidence Interval	
			No. %	%		Lower	Upper
GNAQ	51	13	38	74.5	223.961	195.053	252.869
GNA11	36	14	22	61.1	186.394	148.429	224.359
CYSLTR2	2	1	1	50.0	115.000	30.458	199.542
Wild-type	5	2	3	60.0	136.125	111.587	160.663
Overall	94	30	64	68.1	206.549	183.333	229.764

Figure 5.8 Kaplan Meier curves and tables where patient survival was stratified according to *GNAQ, GNA11 and CYSTLTR2* mutation status determined by NGS; *GNAQ* mutants (n=51), *GNA11* mutants (n=36)*, CYSLTR2* mutants (n=2) and *GNAQ, GNA11, CYSLTR2* and *PLCB4* wild-type (n=5) (p=0.533).

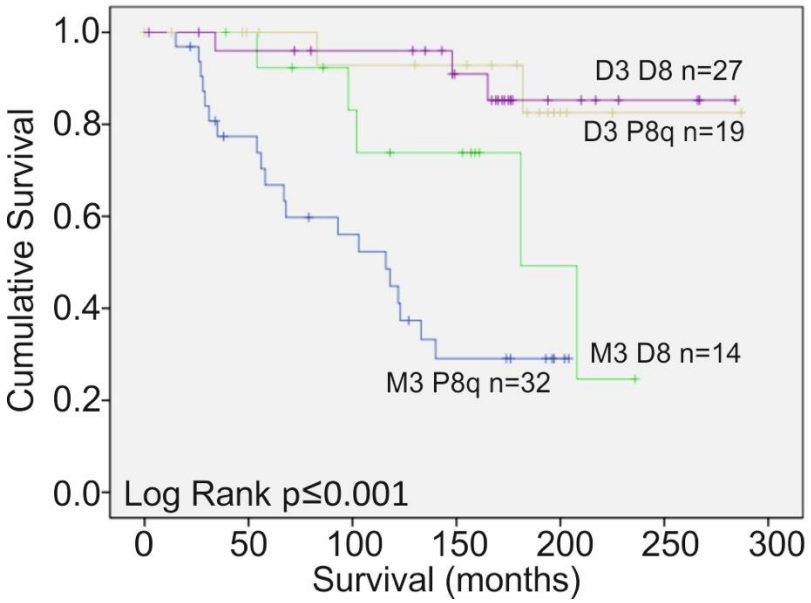

Survival Group	Total No.	No. of Events	Censored		Mean Survival (months)	95% Confidence Interval	
			No. %	%		Lower	Upper
M3 P8q	32	20	12	37.5	112.693	87.845	137.542
M3 D8	14	5	9	64.3	176.462	139.906	213.017
D8 P8q	19	2	17	89.5	261.595	228.823	294.367
D8 D8	27	3	24	88.9	260.364	234.939	285.789
Overall	92	30	62	67.4	205.290	181.856	228.724

Figure 5.9 Kaplan Meier curves and tables where patient survival was stratified according to chromosome 3 and chromosome 8q status determined by NGS; M3 P8q (n=32), M3 D8 (n=14), D3 P8q(n=19) and D3 D8 (n=27) (p=≤0.001). Cases of isodisomy and partial loss were included in the monosomy cohort.

A)

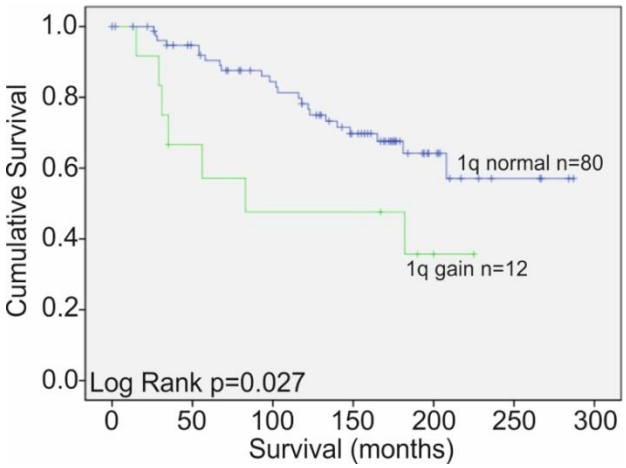

Chromosome 1q	Total No.	No. of Events	Censored		Mean Survival (months)	95% Confidence Interval	
			No. %	%		Lower	Upper
Normal	80	23	57	71.3	215.228	190.959	239.497
Gain	12	7	5	41.7	124.429	73.037	175.820
Overall	92	30	62	67.4	205.290	181.856	228.724

B)

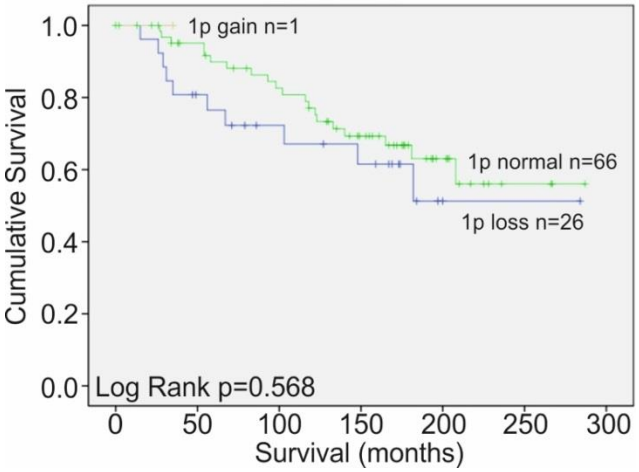

Chromosome1p	Total No.	No. of Events	Censored		Mean Survival (months)	95% Confidence Interval	
			No. %	%		Lower	Upper
Loss	26	10	16	61.5	-	-	-
Normal	66	20	46	69.7	-	-	-
Gain	1	0	1	100.0	-	-	-
Overall	93	30	63	67.7	-	-	-

Figure 5.10 Kaplan Meier curves and tables where patient survival was stratified according copy number of **A)** chromosome 1q normal (n=80) and gain (n=12) (p=0.027) and **B)** chromosome 1p gain (n=1), normal (n=66) and loss (n=26) (p=0.568). *No survival statistics because all cases are censored.

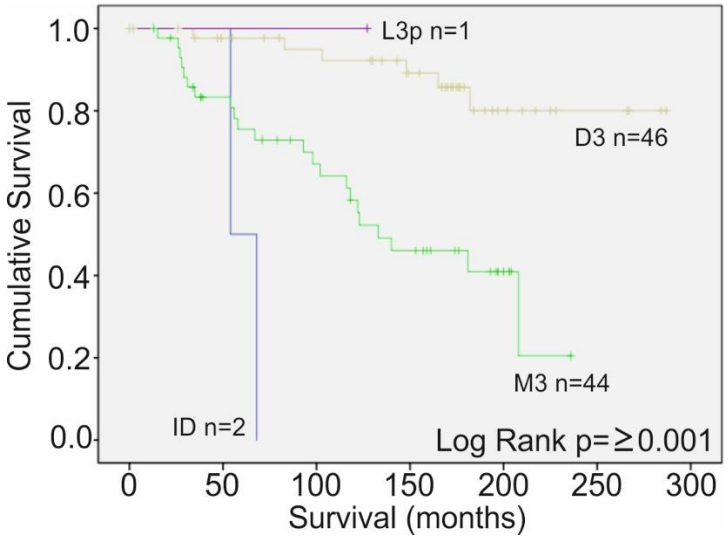

Chromosome 3	Total No.	No. of Events	Censored		Mean Survival (months)	95% Confidence Interval	
			No. %	%		Lower	Upper
Isodisomy	2	2	0	0.0	-	-	-
Monosomy	44	22	20	50.0	-	-	-
Disomy	46	6	40	87.0	-	-	-
Loss of 3p	1	0	1	100.0	-	-	-
Overall	93	30	63	67.7	-	-	-

Figure 5.11. Kaplan Meier curves and tables where patient survival was stratified according copy number of chromosome 3; isodisomy (n=2), monosomy 3 (n=44), disomy 3 (n=46) and loss of 3p (n=1) (p=≤0.001). *No survival statistics because all cases are censored.

A)

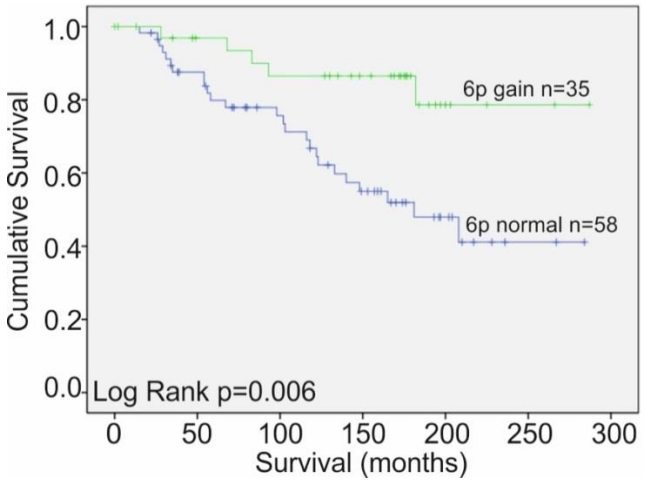

Chromosome 6p	Total No.	No. of Events	Censored		Mean Survival (months)	95% Confidence Interval	
			No. %	%		Lower	Upper
Normal	58	25	33	56.9	179.978	150.912	209.044
Gain	35	5	30	85.7	249.303	219.254	279.352
Overall	93	30	63	67.7	205.493	182.103	228.883

B)

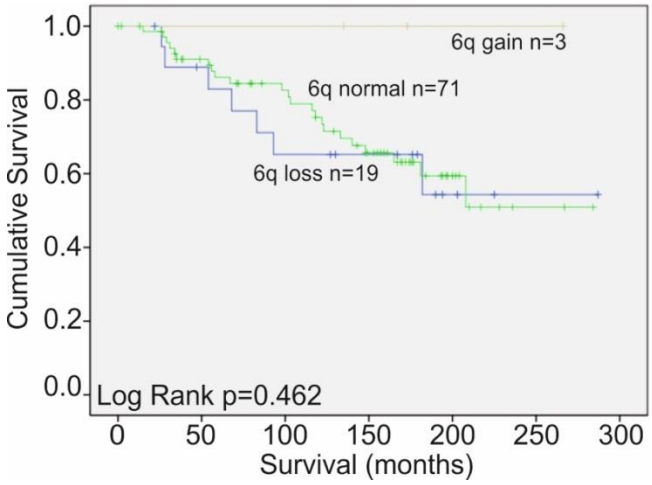

Chromosome 6q	Total No.	No. of Events	Censored		Mean Survival (months)	95% Confidence Interval	
			No. %	%		Lower	Upper
Loss	19	7	12	63.2	-	-	-
Normal	71	23	48	67.6	-	-	-
Gain	3	0	3	100.0	-	-	-
Overall	93	30	63	67.7	-	-	-

Figure 5.12. Kaplan Meier curves and tables where patient survival was stratified according copy number of **A)** chromosome 6p normal (n=58) and gain (n=35) (p=0.006) and **B)** chromosome 6q gain (n=3), normal (n=71) and loss (n=19) (p=0.462). *No survival statistics because all cases are censored.

A)

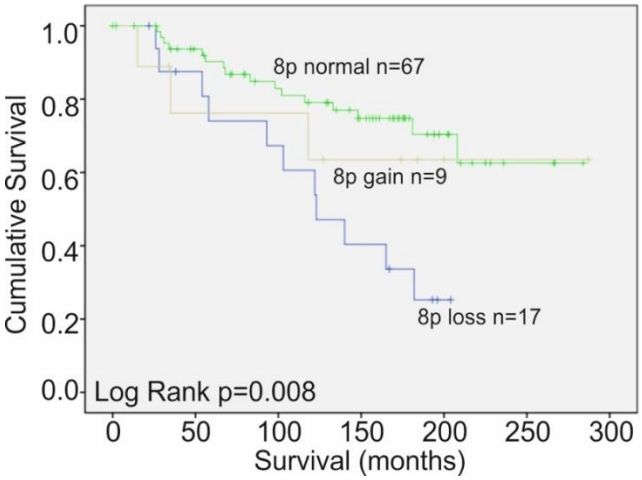

Chromosome 8p	Total No.	No. of Events	Censored		Mean Survival (months)	95% Confidence Interval	
			No. %	%		Lower	Upper
Loss	17	11	6	35.3	127.928	96.537	159.319
Normal	67	16	51	76.1	221.768	195.740	247.797
Gain	9	3	6	66.7	203.317	125.685	280.949
Overall	93	30	63	67.7	205.493	182.103	228.883

B)

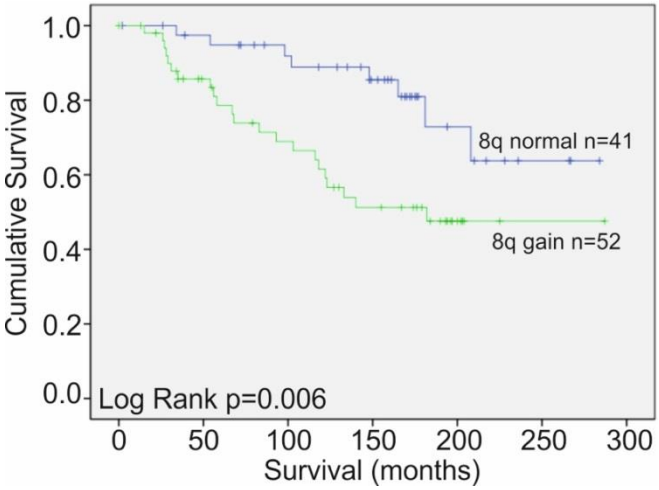

Chromosome 8q	Total No.	No. of Events	Censored		Mean Survival (months)	95% Confidence Interval	
			No. %	%		Lower	Upper
Normal	41	8	33	80.5	235.368	206.375	264.362
Gain	52	22	30	57.7	180.303	148.043	212.562
Overall	93	30	63	67.7	205.493	182.103	228.883

Figure 5.13. Kaplan Meier curves and tables where patient survival was stratified according copy number of **A)** chromosome 8p loss (n=17), normal (n=67) and gain (n=9) (p=0.008) and **B)** chromosome 8q gain (n=52) and normal (n=41) (p=0.006).

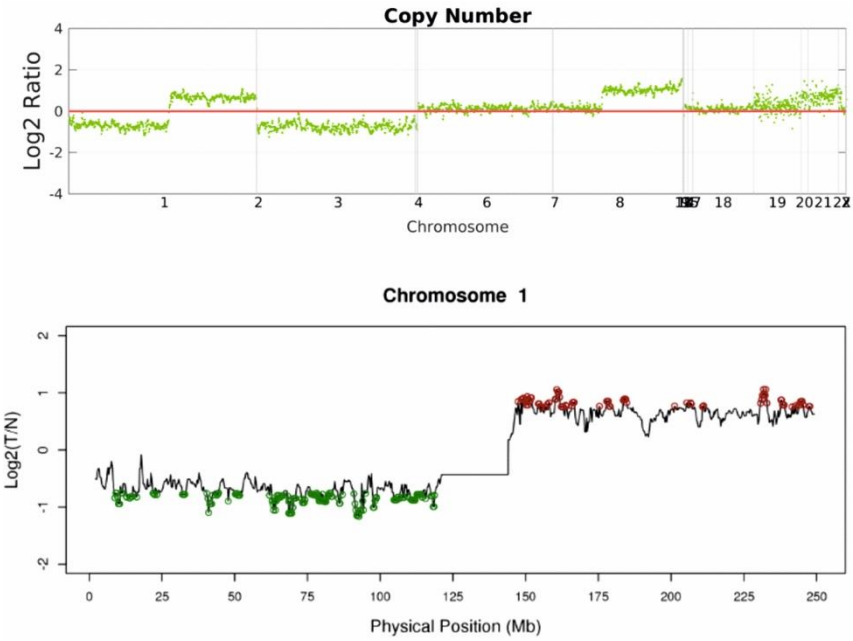

Figure 5.14. Concomitant loss of 1p and gain of 1q in a M3 P8q UM associated with a poor survival outcome.

5.3.2.7 Cox Regression

Multivariate analysis of: age; gender; *BAP1, SF3B1, EIF1AX* and chromosome 1q was carried using the cox proportional hazards model (table 5.14). *BAP1* was selected as I have previously shown it can be used as a surrogate marker for chromosome 3. Chromosome 1q was selected as it was shown to be significant by Kaplan-Meier. *SF3B1* and *EIF1AX* were chosen due to the suggested influence on survival in the literature. Age and gender were included to adjust for the impact on survival. The model identified the following factors as significantly associated with survival: *BAP1* mutation status p=0.00058 (HR 5.88: 95% CI 2.14 – 16.11) and copy number of chromosome 1q p=0.015 (HR 3.22 CI 1.25 – 8.26). The hazard ratios are shown in Table 5.13 for each prognostic factor with 95% confidence intervals, z test p-values and Schoenfeld's χ^2 test of proportionality of hazards (PH) p-values. The model's likelihood ratio statistic is 35.64 on 6 degrees of freedom (p-value 0.000003). The global Schoenfeld's χ2 test of proportionality of hazards is 2.71 (p-value 0.85.). No strong deviation from the hypothesis of proportionality of hazards was observed.

Table 5.14 Hazard ratios for prognostic factors in UM

Factor	Hazard ratio [95% CI]	z test p-value	PH χ^2 test p-value	Cause of Death
Age	1.12 [1.03,1.21]	0.0047	0.24	Other
Gender	0.51 [0.12, 2.09]	0.35	0.99	Other
BAP1	5.88 [2.14, 16.11]	0.00058	0.83	Metastasis
SF3B1	0.63 [0.20, 1.98]	0.43	0.59	Metastasis
EIF1AX	1.13 [0.25, 5.02]	0.87	0.63	Metastasis
Chr1q	3.22 [1.25, 8.26]	0.015	0.62	Metastasis

5.4 Discussion

5.4.1 14 sample cohort

This is the first study of its kind to compare hybrid capture and PCR-based enrichment methods in UM. Both methods vary in exactly how the targeted regions are amplified and hybridised. Hybrid capture methodologies involve shearing gDNA into smaller fragments and hybridising the sample with targeted biotinylated RNA baits. Using magnetic streptavidin beads these baits can be separated and amplified. Whereas PCR-based methods hybridise a custom oligo pool flanking targeted regions on unfragmented gDNA. These are then extended and ligated and PCR is performed to integrate indexes and sequencing primers. There are advantages to using a PCR-based method such as reduced DNA input and a relatively short sample preparation time. However, in this study, I have demonstrated that hybrid capture outperformed the PCR-based enrichment as it provided a deeper coverage, had a larger percentage of reads mapped before and after unique molecular barcode removal, and had a greater mean depth of coverage (Table 5.8). Although there were no differences in the ability to call variants, the failure rate for copy number variant analysis for the PCR-based method was higher than the hybrid capture method. This echoes the finding of several comparison studies examining the differences between each methodology. In a similar study Hung et al. compared the enrichment chemistries used in the present study to personalise the management of lymphoma and found limited sensitivity of PCR-based sequencing, with several variants being missed due to regions of high GC content and suboptimal PCR conditions yielding a minimal coverage, limitations that were not seen using hybrid capture (244). Similarly, Samorodnitsky et al. demonstrated an increased incidence of false positives and missed variants in PCR-based enrichment when evaluating hybrid capture versus PCR-based methods for whole-exome

sequencing (245). Though neither study found differences between the success rates of copy number analysis unlike the present study. A reason for this could be common trouble shooting issues typically experienced during PCR ranging from suboptimal PCR conditions such as: presence of inhibitors such as melanin; a high GC content or insufficient coverage (246) (247). Due to the higher failure rate of PCR-based amplification I chose to move forward with the larger subset of samples using the hybrid capture methodology.

There was a high degree of copy number concordance between SureSelect and TSCA classifications for chromosomes 6 and 8. The concordance for these chromosomes was however lower when the NGS data from each panel was compared with MLPA classifications. This was, however not the case for chromosome 3, where there was 100% agreement between all genetic tests. This is likely due to the low probe coverage on chromosomes 6 and 8 in the MLPA panel; 6q and 8p 2 probes and 6p and 8q 4 probes respectively. The increased coverage of these on the NGS panel will increase accuracy of copy number variant detection moving forward.

Both hybrid capture and PCR-based enrichment panels were effective in detecting mutations in both samples molecularly profiled by TCGA analyses and in those samples with unknown mutation status. There was 100% concordance for *GNAQ*, *GNA11*, *SF3B1* and *EIF1AX* between all samples. There was some discordance between the detection of *BAP1*. Sample 3 (S177.13), a sample submitted to the TCGA by the Liverpool Ocular Oncology Research Group, contained a homozygous deletion not detected by the NGS panel. Homozygous deletions are a rare in phenomenon occurring in cancers and often target tumour suppressor genes such as *BAP1*. However, after carefully analysing the copy number data it is apparent there is a homozygous deletion (Figure 5.1).

An additional W196* nonsense mutation was detected in *BAP1* for sample 12 (S107.12), detected by both enrichment methods but was not described in the recent TCGA analyses. However, a recent study by Field et al. analysed the same TCGA sample (A8KF) and surmised that it had been missed due to low exome coverage by the mutation could be detected when compared with matched RNA-Seq (136). This is an obvious advantage to adopting a targeted approach to NGS as it enables for an increase in gene coverage. This was also true of sample 1 (S154.11) where a p.I1296V missense mutation in *TTC28* was detected by both enrichment methods but not by the TCGA analyses.

5.4.2 94 sample cohort

Three samples were not concordant with the original MLPA analyses results for chromosome 3. Sample 54 (S245.13) was shown to have region of deletion in chromosome 3p not identified in previous analyses. This is potentially due to an increased number of probes covering chromosome 3p not included in the MLPA assay. The other two samples both had a M3 genotype in the original analyses but were shown to have a D3 profile by NGS. Neither sample contained a mutation in *BAP1,* which is strongly associated with loss of chromosome 3 (Chi-squared p=≤0.001), and one sample contained a mutation in *SF3B1,* which has also been associated with a D3 profile (Chi-squared p=0.015). Two cases of isodisomy of chromosome 3 were also detected that had been classified as disomy by MLPA due to the limitations of the assay in detecting acquired homozygosity.

There was discordance between the original MLPA analyses and the NGS copy number for chromosomes 1, 6 and 8 in several of the cases, however, this is likely due to the low probe coverage of these genes on the MLPA panel as mentioned previously.

In the larger 94 sample cohort, sample 46 (S151.11) failed to produce a clear genotype, however this was expected as the sample had a low yield post-capture. This was reflected in the quality results whereby the sample only had 3.36x depth of coverage.

Some of the samples used in the FFPE validation cohort were the FFPE counterpart to fresh tissue sequenced in Rotterdam for a different study. Although there was complete concordance between *GNAQ* and *GNA11* there was a disparity between mutations identified in *BAP1, SF3B1,* and *EIF1AX*. Sample 2 (S056.14) did not harbour a p.L334fs mutation in *BAP1* that was called by the Ion Torrent analysis. When the coordinates were checked using IGV to authenticate its presence, the mutation could not be found in the sequencing reads. In contrast, two *BAP1* mutations (p.R213fs and p.I214_G220del) were observed in the present study in sample 7 (S183.13) that were not called by the initial analysis in Rotterdam. Additionally, two *SF3B1* mutations were called in the initial analyses in samples 5 (S106.13) and 12 (S001.09) in p.V634I and N626I respectively that were not identified in the present study. Similarly, a mutation in *EIF1AX* p.G6D not detected in this study, was observed in the Ion Torrent data. When the sequencing reads were checked using IGV no mutation could be detected even at low levels. The most logical explanation for these differences is the variance in chemistry used in both the enrichment and sequencing during the initial analyses. The group that sequenced the samples initially utilise a PCR-based enrichment (AmpliSeq) and the sequencing is run on the Ion Torrent Personal Genome Machine (PGM) (Thermofisher). Several studies have demonstrated that false-positives can arise from multiplex PCR-based enrichment methodologies such as AmpliSeq (248) (245). Similarly, the Ion torrent PGM is well known for sequencing errors caused by homopolymers; repeats of the same nucleotide present on the template strand. The semi-conductor detects nucleotides based on the hydrogen ions released during polymerisation

of DNA, measuring the pH change. Homopolymers cause more hydrogen ions to be released in a single cycle due to the repeats of the same nucleotide, resulting in a greater pH change and a proportionally greater electronic signal.

Mutations in *GNAQ* and *GNA11* occurred in a mutually exclusive fashion in 92% of cases (54% and 38%, respectively). This is consistent with the reported cases in the literature (134) (135) (198). Mutations predominantly occurred in exon 5, although interestingly sample 46 (S151.11) contained two unusual mutations in exon 4 p.R214K and p.R214S. These regions do not lie within any of the known functional domains of *GNA11* and have not been characterised in the scientific literature and therefore, their effect on *GNA11* protein function are unknown. Only one mutation occurred in exon 4 in *GNAQ* and *GNA11*, p.R183Q and p.R183C respectively. Mutations in *CYSLTR2* were found in 2 cases in the hot spot region p.L129Q in exon 1, previously reported by other studies and occurred in a mutually exclusive manner to mutations in *GNAQ* and *GNA11* (132). Consistent with our general understanding of the function of these mutations, there were no differences in survival outcome based on the mutational status of the driver mutations *GNAQ*, *GNA11* and *CYSLTR2* (p=0.533) (Figure 5.8). This is in agreement with the study by Koopmans et al. where univariate analysis showed no correlation between disease-free survival and mutation status in *GNAQ* or *GNA11* (249). Similarly, Staby et al. demonstrated no significant differences in the prevalence of mutations in UM patients with or without metastatic disease (250). Mutations in *GNAQ* or *GNA11* have been shown to consistently activate the protein kinase C (PKC) pathway and the map kinase pathway (MAPK) (115). However, a recent review of the efficacy and safety of MEK inhibitors in metastatic or unresectable UM low radiologic response rates in UM (251). Though there is no prognostic significance of these mutations, the therapeutic potential of them remains hopeful.

The mutation rate for *BAP1* in the literature ranges from 18% to 60% in all UM (129) (133) (134, 135) (198). The frequency of *BAP1* mutations in the present study was 41%, a figure consistent with the findings of Robertson et al, Royer-Bertrand et al and Smit et al (134, 135, 198). Mutations in *BAP1* occurred in 80% of monosomy 3 cases in this study, concordant with the findings of Harbour et al. (129). Only one missense *BAP1* p.A142P mutation was detected in a D3 tumour similar with the rate reported by Koopmans et al. (252). The majority of mutations observed were frameshift mutations (54%) although some nonsense (15%), missense (10%), INDELS (10%) and splice site mutations (15%) were also identified. In chapter 4, I demonstrated the prognostic impact of loss of nuclear BAP1 (nBAP1) protein expression on patient survival, with multivariate analysis identifying this as a worse prognostic factor than loss of chromosome 3 (240). Loss of nBAP1 has been strongly associated with loss of function mutations in other studies (130). In the present study, I was unable to correlate mutations and protein expression due to the unavailability of some of the pathology samples and the lack of time. In the present study *BAP1* mutation was also the strongest predictor of metastatic death during cox analysis, despite a wide confidence interval (Table 5.14). Unlike the previous study, M3 *BAP1* wild-type UM samples did not have a significantly better survival (p=0.062). However, this may be due to the small numbers. In the present study, mutation in *BAP1* was strongly associated with a reduced disease-free survival (p=≤0.001) (Figure 5.5). Of the patients with UM that harboured a mutation in *BAP1*, 22/39 (56%) died from metastatic disease. Mutations in *BAP1* were significantly associated with loss of one copy of chromosome 3 and isodisomy of chromosome 3 (Fisher's Exact p=≤0.001).

The frequency of *EIF1AX* mutations detected in the present NGS UM study is consistent with the mutation rates of Smit et al. and Royer-Bertrand et al. (134). The frequency of

EIF1AX mutations in studies conducted by others was higher and lower than the present study at 34% and 14% respectively (119) (133) (135). Interestingly, two samples contained mutations in both *EIF1AX* and *SF3B1* despite previously reports that these occur in a mutually exclusive fashion (134) (198). One sample that contained a p.N4H mutation in *EIF1AX* also contained a mutation in p.R625H of *SF3B1* and the other contained a mutation in p.G9D in *EIF1AX* and p.K666N in *SF3B1*. Both samples had a normal chromosome 3, 6 and 8, with one sample containing a loss of 1p. Also of interest, both patients died from metastatic disease 34 months and 148 months, respectively, after primary treatment. There is only one other reported case of this phenomenon in the literature by Robertson et al. (135), however, in contrast to the present study, this patient was still alive and well at study closure with a follow up of 62 months. *EIF1AX* mutations are typically associated with D3 tumours; however in the present study we identified two cases of M3 tumours that harboured mutations. Both cases lacked mutations in *BAP1* and one patient had died from other causes leaving the other patient alive and well at the end of the study. Only one other case of an *EIF1AX* mutation has been reported in the literature in a M3 tumour, however this also harboured a splicing mutation in *BAP1* whereas the M3 *EIF1AX* mutants in the present study were *BAP1* wild type (134). In our cohort mutations in EIF1AX were associated with an overall improved survival (p=0.040), however within the D3 subset of samples there was no discernible difference (p=0.254 (Figure 5.6). This was most likely because 3/5 (60%) of the patients with D3 who died from metastatic disease harboured mutations in *EIF1AX*. When examined In the Cox proportional hazards model, *EIF1AX* was associated with an increase of the hazard; however, the confidence interval included the value 1, so no conclusions can be drawn from this. However, mutations in *EIF1AX* were significantly associated with D3 tumours (Fisher's exact p=≤0.001).

The incidence of *SF3B1* mutations in the literature ranges from 11% - 34%. In this study *SF3B1* mutations occurred in 20% of UM, which was consistent with the findings of Smit et al and Royer-Bertrand et al (134) (198). *SF3B1* mutations were identified in 5% of M3 cases and 34% of D3 cases. *SF3B1* mutations are thought to occur primarily in D3 tumours, however, in this study, two were found in M3 UM and one in a UM case with loss of 3p. Four cases of M3 UM with *SF3B1* mutations were identified by Robertson et al; two of which did not have mutations in *BAP1,* neither of which died from metastatic disease and two with BAP1 mutations, one of which died from metastatic disease (135). In this study three *SF3B1* mutations were found to occur alongside *BAP1* mutations. Two cases contained the p.R625H mutations in *SF3B1* alongside p.L14fs and p.A142P. The third case has a missense mutation in p.N626H with a p.F118fs in *BAP1*. One patient died from metastatic disease 31 months following a local resection. The other two patients are alive and well with no evidence of metastatic disease with a follow up of 190 and 197 months respectively. This has been described in the literature once before by Robertson et al. who identified two cases with mutations in both *SF3B1* and *BAP1* (135). In their study, only one of the patients had died from metastatic disease also. Unlike other studies, the present study did not find mutations in *SF3B1* to be associated with an increased metastatic risk in comparison to those without when all UM cases were considered (p=0.378) (Figure 5.7). Similarly, when only D3 cases were analysed there was no difference in survival between those with or without *SF3B1* mutations (p=0.140) (Figure 5.7). This is in contrast to the study by Yavuzyigitoglu et al. who found an association between *SF3B1* and late onset metastases for D3 UM (242). This could be due to the relatively short-follow up (5 years minimum) in comparison to other studies, which may have contributed to the lack of deaths in this cohort of samples, despite a similar rate of mutations detected. However, my

data are consistent with that of TGCA, whereby an association between *SF3B1* and an increased late onset risk of metastasis could not be made (135). Longer follow-up of this patient cohort may shed further light on the role of *SF3B1* mutations and metastatic risk.

Disruptive in-frame deletions in p.M549_G556delinsI and M561_G568delinsI mutations were observed in *PLCB4* in a single sample of the 94 sample cohort (Figure 5.2). Interestingly, this sample also contained a p.R183Q mutation in *GNAQ*. Previous studies identified recurrent mutations in *PLCB4* in a hotspot region p.D630Y and p.D630N on exon 20 (133). The mutation identified in the present study occurred in exon 18 and is the first mutation in this region to be described in UM. Though it was initially thought that *PLCB4* mutations occurred in a mutually exclusive manner to *GNAQ*, *GNA11* and *CYSLTR2*, this study and Robertson et al. have demonstrated the occurrence of *PLCB4* mutations alongside *GNAQ* and *GNA11* mutations (135). The mutation observed in this is located in highly conserved catalytic domain of *PLCB4*, the Y-Box, which has been shown to control signal transduction in the retina. (133). As a downstream target of the GNAQ and GNA11 alpha subunits of G-protein coupled receptors, PLCB4 interacts with the alpha subunit to catalyse the conversion of phosphatidylinositol 4,5-bisphosphate (PIP2) into inositol 1,4,5-trisphosphate (IP3) and diacylglycerol (DAG) (253).

Three mutations in *TTC28* were identified in this study; two missense mutations in p.P1216H and A18G and one nonsense mutation in p.R21*, occurring in both M3 and D3 tumours (Figure 5.2). Other studies have also detected mutations in *TTC28* in UM at a similar low frequency (119) (134). *TTC28* is a ubiquitous protein thought to have a role in regulating mitosis and cytokinesis during mammalian cell cycle processes (254). Dysfunction of *TTC28* has been shown to contribute to tumour progression (255). Inactivating mutations

in TTC28 have been demonstrated to increase microtubule turnover and induce mitotic defects; cell cycle aberrations are a hallmark of cancer (256).

Two mutations in *CSMD1* were discovered in this study; two missense mutations in p.P1097H and p.P108L (Figure 5.3). Other studies have also detected mutations in *CSMD1* at similar low levels (134). *CSMD1* is located on chromosome 8p23, a region that is commonly deleted in many cancers including UM. As a candidate tumour suppressor gene, loss of *CSMD1* has been shown to be associated with a number of cancers including breast, head and neck, lung and skin tumours (257) (258), and is specifically associated with a poor prognosis in breast cancer.

A single missense mutation in p.P195T of *KTN1* was identified in sample 19 (S231.11) (Figure 5.2). *KTN1* encodes Kinectin 1, a protein primarily localised to the endoplasmic reticulum (259). *KTN1* has various functions including kinesin binding which plays a role is mitosis, particularly in microtubule movement and spindle formation (260). This protein also binds with translation elongation factor-1 delta by acting as membrane anchor for kinesin on intracellular organelles (261). In cancer, *KTN1* has been observed to form a fusion with *RET*, creating a novel rearranged form of a proto-oncogene observed in radiation-induced childhood papillary thyroid carcinoma (262) (263). The functional impact of the mutation observed in the present study is unknown; however missense mutations can render the affected protein non-functional, which in this case could result in dysregulation of mitosis or unregulated cytoskeletal activities (264).

Two mutations in *TP53BP1* were observed in the present study; one nonsense mutation in Glu1529* and a disruptive in-frame deletion in p.I455_P456del (Figure 5.3). The only other study to identify mutations in *TP53BP1* in UM found a splice site mutation and a missense

in p.V1496D, suggesting mutations in this gene do not occur in hotspots (134). *TP53BP1* interacts with the tumour suppressor protein p53, a critical protein for cells in multicellular organisms to suppress cancer formation. *TP53BP1* is heavily involved in the DNA double-strand break repair pathway, promoting non-homologous end joining pathways. *TP53BP1* promotes checkpoint signalling following DNA damage and acts as a molecular scaffold, recruiting proteins that assist in the repair of damaged chromatin (265). Mutations in *TP53BP1* have been observed in aggressive inflammatory breast cancer and have been shown to increase cell proliferation in colon cancer (266) (267).

This panel was custom designed to have full coverage of the *TTC28, CSMD1, KTN1 and TP53BP1* genes and due to its targeted nature had fuller coverage in comparison to whole-exome sequencing methodologies. This could be a possible explanation to the low frequency of mutations in the literature. However, due to the low frequency of mutations identified in *TTC28, CSMD1, KTN1* or *TP53BP1* in this study no association could be made with a particular genotype or survival group. More functional work needs to be undertaken in the future to understand the implications of these.

This is the largest NGS study to date; however, previously described mutations in *SRSF2*, *DLK2* or *FBXW7*, which have been detected in low frequency in other studies, were not detected (135) (138) (134). The prognostic significance of these genes remains unknown.

Table 5.15 Frequency of mutations in original whole-exome and targeted NGS UM studies

	Mutation Frequency					
Gene	Martin et al. (n=22)	Johansson et al. (n=28)	Smit et al. (n=70)	Royer-Bertrand et al. (n=33)	Robertson et al. (n=80)	Present Study (n=94)
GNAQ	9/22 (41%)	8/28 (29%)	31/70 (44%)	19/33 (58%)	40/80 (50%)	51/94 (54%)
GNA11	9/22 (41%)	14/28 (50%)	30/70 (42%)	14/33 (42%)	36/80 (45%)	36/94 (38%)
BAP1	4/22 (18%)	11/28 (39%)	29/70 (41%)	16/33 (48%)	35/80 (44%)	39/94 (41%)
SF3B1	3/22 (14%)	3/28 (11%)	11/70 (16%)	6/33 (18%)	27/80 (34%)	19/94 (20%)
EIF1AX	3/22 (14%)	4/28 (14%)	14/70 (20%)	7/33 (21%)	27/80 (34%)	20/94 (21%)
CYSLTR2	1/22 (5%)	-	-	-	3/80 (4%)	2/94 (2%)
PLCB4	-	2/28 (7%)	-	-	2/80 (3%)	1/94 (1%)
TTC28	1/22 (5%)	-	-	2/33 (6%)	-	3/94 (3%)
CSMD1	1/22 (5%)	-	-	2/33 (6%)	-	2/94 (2%)
TP53BP1	-	-	-	2/33 (6%)	-	2/94 (2%)
SRSF2	-	-	-	-	3/80 (4%)	-
KTN1	-	-	-	2/33 (6%)	-	1/94 (1%)
DLK2	-	-	-	2/33 (6%)	-	-
FBXW7	2/22 (10%)	-	-	-	-	-

As expected, both M3 and isodisomy of chromosome 3 were associated with a poor survival (p=≤0.001) consistent with numerous published studies (Figure 5.11) (268) (91) (95). Both cases of isodisomy of chromosome 3 harboured nonsense *BAP1* mutations, the tumour would therefore have two non-functional alleles of the tumour suppressor gene. This is evident in the median survival of the isodisomy group, which was 61 months (range, 54 – 64 months) in comparison to the M3 cohort who had a median survival of 126 months (range, 15 – 236).

In the present study loss of 6q did not appear to be associated with overall poor survival (p=0.462) or impact the survival of those with M3 (p=0.157) in this study, contradicting the findings of other studies that demonstrated loss of 6q to be predictive of poor prognosis (Figure 5.12) (269) (270) (102). In contrast, gain of 6p was significantly associated with an improved disease-free survival (p=0.006), consistent with the findings of a plethora of studies (93) (271). There are suggestions in the literature that the presence of oncogenes

and tumour suppressor genes on 6p and 6q respectively are involved in the development of UM though the importance is not yet fully understood (99).

In agreement with previous studies, both loss of chromosome 8p and gain of 8q were associated with a poor overall survival outcome (p=0.008 and p=0.006, respectively) (Figure 5.13) (268) (270) (76). Concomitant loss of 8p and gain of 8q were observed in 16/52 (31%), of these 14/16 (88%) were M3 or isodisomy of chromosome 3 and 10/16 (63%) of patients died from metastatic disease. In the D3 cohort, loss of 8p was associated with a worse survival (p=0.004). Gain of 8q in the same cohort had a neglible effect on survival in disomy 3 tumours (p=0.654) or *SF3B1* or *EIF1AX* mutant tumours (p=0.986) in contrast to the findings of other studies (134) (135).

In a study of interest, Caines et al. performed cluster analysis on 602 cases of UM genotyped by MLPA and found four distinct subgroups in terms of survival based on a combination of chromosome 3 and 8q data, whereby D3 with polysomy 8q (P8q) was associated with an intermediate metastatic risk (185). This was consistent with the study by Cassoux et al. who also found D3 with P8q to be associated with an intermediate metastatic risk (272). When grouped in a similar fashion, the data in the present study found three distinct subgroups in terms of survival, however there was no difference in survival for samples with disomy 3 plus or minus polysomy 8q (Figure 5.5). Increased copy number burden of 8q has been described in the literature and is associated with a worse survival outcome, with an association between a ploidy of five copies or more and metastatic potential (135) (134). In the present study, I did not assess ploidy of 8q, which could have potentially aided our analysis. Moving forward with the panel, this will be something that would be useful to develop.

Loss of 1p has been well documented in the literature in UM. It is said to be one of the few abnormalities that provide prognostic information regarding disease-free survival, independent of chromosome 3 copy number status (94). It has been demonstrated that a concurrent loss of 1p and monosomy 3 contribute to poor survival in UM patients (108). Other studies have pinpointed specific loci that are believed to harbour genes directly involved with the progression of UM specifically with M3 (273). The p-arm of chromosome 1 contains *p73*, a homolog of *P53* and loss of the p73 locus was associated with the upregulation of p73Deltaex2 and TAp73 transcripts, suggesting a potential function of p73 deletion transcripts in UM progression (274). In the present study 1p loss was not associated with a reduced disease-free survival overall (p=0.568) or in M3 tumours (p=0.505). An interesting observation of this study was the significance of 1q gain and its association with a worse outcome in terms of patient survival (p=0.027) (Figure 5.10). In the cox model, 1q gains were associated with an increase in the hazard of metastatic death, although not as strongly as *BAP1* (Table 5.13). Early studies suggest there is an association between M3 and an isochromosome formation of 1q (102). The frequency of 1q amplifications have been described to occur in as many as 24% of UM (1). However, little has been published regarding the prognostic significance of these gains. In the present study, 62% of 1q amplifications were accompanied with loss of 1p (figure 5.14). Field et al., found gains of 1q were associated with Class 1 PRAME positive UM who in GEP profiling studies, identifying an increased metastatic risk for patients with 'Class 1' or disomy 3 UM (194). This juxtaposes the findings of the current study where 1q loss was observed in both M3 (46%) and D3 (54%) tumours with the vast majority having P8q (92%).

In summary, I have demonstrated it is possible to analyse both copy number and single nucleotide variants using an NGS assay in both fresh and formalin-fixed tissues. A

comparison of hybrid capture and PCR-based library preparation identified hybrid capture as the superior methodology in terms of quality. Mutations in *GNAQ*, *GNA11* and *CYSLTR2* occurred in a mutually exclusive fashion and were not associated with increased metastatic risk, supporting the evidence in the literature these are initiating mutations. A previously undescribed mutation in *PLCB4* was identified in this study that did not fall within the hotspot on exon 20. Mutations in *BAP1* were the biggest indicator of metastatic risk in both Kaplan-Meier and cox analysis, consistent with the findings of **Chapter 4**. In contrast to suggestions in the literature, *SF3B1* was associated with a reduction of metastatic risk and *EIF1AX* with an increase in metastatic risk. However, mutations in *EIF1AX* were still associated with improved disease-free survival. No mutations in *SRSF2*, *DLK2* or *FBXW7* were detected in this study; however novel mutations in *TTC28*, *CSMD1*, *KTN1 and TP53BP1* were detected at a low frequency. The prognostic significance of these genes remains unknown. Copy number analysis showed monosomy 3, 6p gain, loss of 8p and 8q gains to be associated with a worse outcome. Novel concomitant losses of 1p and gains of 1q were observed in this study, with gain of 1q being identified as a significant hazard in the increased incidence of metastatic death. A larger cohort of samples with a longer follow-up is needed to further validate the panel for clinical use.

Chapter 6

RasGRP3 Expression in Uveal Melanoma

6.1 Introduction

As mentioned in chapter 1, UM possess inactivating mutations in *GNAQ* and *GNA11,* which have been shown to inhibit the GTPase function of the gene. The inability to hydrolyse GTP to GDP leaves the alpha subunit in a constitutively active state leading to prolonged signalling. Ras guanyl-releasing protein 3 or RasGRP3 is a guanine nucleotide exchange factor that activates small GTPases. RasGRP3 acts as a *RAS* activator by maintaining an active GTP bound state and promoting acquisition of GTP. This conversion of Ras-GDP to Ras-GTP stimulates the activation of numerous downstream pathways, such as the Raf-Mek-Erk kinase cascade (275). Activation of the RAS pathway is abundant in many human cancers and several of the RasGRP family members are involved in cancer development. RasGRP molecules contain C1 domains that bind to diacylglycerol (DAG) and diacylglycerol analogs such as phorbol esters, which are tumour-promoting molecules through the activation of protein kinase C (PKC). RasGRP3 in particular has a high affinity for binding phorbol esters. Therefore, RasGRP3 serves as a PKC-independent pathway due to its affinity for phorbol ester binding (276). RasGRP3 has been shown in the literature to be expressed in B-cells (277), in addition to regulating B cell proliferation by facilitating B cell receptor-Ras signaling (275). High expression of RasGRP3 has been linked to Burkitt's lymphoma, precursor–B-cell leukaemia and natural killer (NK)/T-cell leukaemia (278). Additionally, RasGRP3 transcripts were found to be elevated in a subset of prostate carcinomas, which contributed to increased proliferation, anchorage independent growth, and tumour growth (279). Moreover, increased expression of RasGRP3 has been shown play a role in the malignant progression and increased prostate specific antigen (PSA) levels in recurrent prostate cancer (226). RasGRP3 overexpression has also been linked to increased cell proliferation in cutaneous melanoma cells, with suppression inhibiting cell proliferation in

numerous melanoma cell lines (280). A recent study has shown a link between RasGRP3 expression and oncogenic signalling downstream of *GNAQ/11* mutant UMs to the Ras/Raf/MEK/ERK pathway through a number of mechanisms; DAG binding, phosphorylation by PKC and consequential upregulation at the protein level by PKC activation (281). This, therefore, makes RasGRP3 a molecule of interest as it has the potential to be used as a promising therapeutic target.

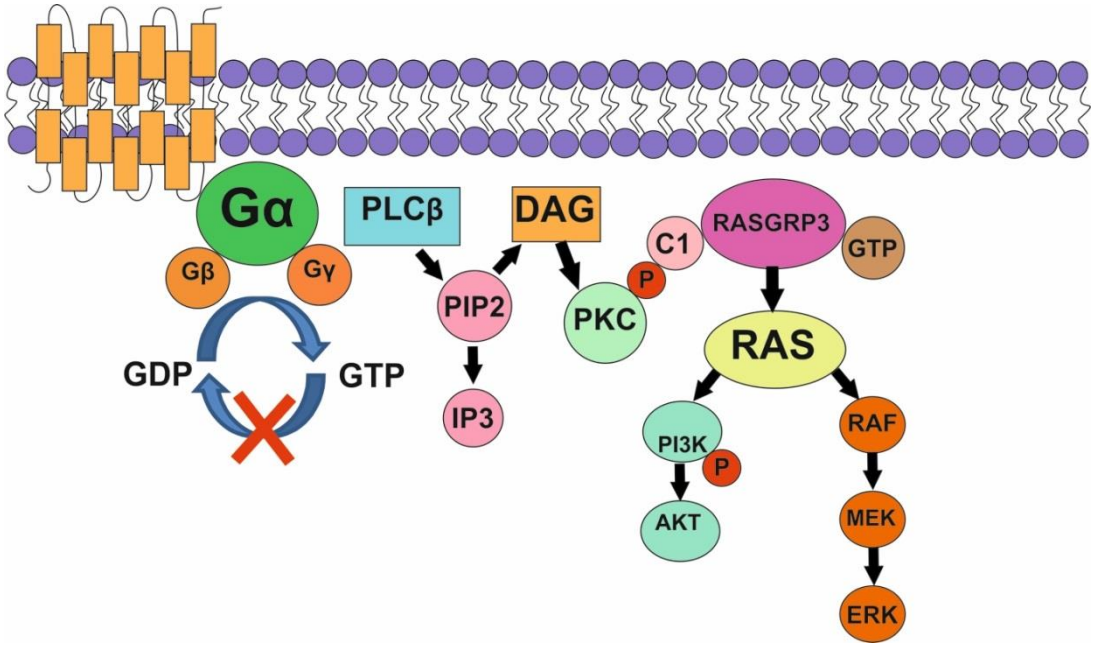

Figure 6.1 Involvement of RasGRP3 in the GNAQ/11 pathway; phospholipase C beta (PLCβ) cleaves phosphatidylinositol (4,5)-bisphosphate (PIP2) to yield diacylglycerol (DAG) and inositol triphosphate (IP3) promoting stimulation of protein kinase C (PKC), which leads to activation of the mitogen-activated protein kinase (MAPK or MEK) pathway and cell proliferation. Original image.

The aim of Chapter 6 was to further understand the role of RasGRP3 protein in UM by: (1) examining its expression by IHC in a tissue microarray (TMA) consisting of primary UM samples with known *GNAQ/11* mutation status; and (2) using Western blotting to determine RasGrp3 protein expression in well-characterised UM cell lines.

6.2 Materials and Methods

6.2.1 Preparation of cell lysates and protein determination

Cell lysates were prepared from the GNAQ/11 mutant UM cell lines, 92.1, MEL270, OMM1 and the conjunctival melanoma cell lines CRMM1 and CRMM2 (BRAF V600E positive and GNAQ/GNA11 wild-type). The 92.1, Omm1 and Mel270 UM cell lines were grown in RPMI (Life Technologies, Paisley, UK) supplemented with 10% fetal calf serum (FCS) (Biosera, France) 2mM L-glutamine (Sigma-Aldrich Ltd, United Kingdom), 200µg/ml Penicillin–Streptomycin (Sigma-Aldrich Ltd, United Kingdom). All cell lines used in the study were kindly provided by Professor Martine Jager (Leiden University Medical Centre, Leiden). The CRMM1 and CRMM2 conjunctival melanoma cell lines (used as additional controls) were grown in Ham's F-12K (Kaighn's) Medium (Life Technologies) plus 10% FCS (Biosera, France) 2mM L-glutamine (Sigma-Aldrich Ltd, United Kingdom), at 37°C in a humidified atmosphere containing 5% CO2. The cell lines had previously been shown to be mycoplasma free and had concordant short tandem repeat (STR) profiles with those published in the literature/ATCC website (Table 6.2) (282) (283) (284) (285). At ~70% confluency, media was removed from the 75cm2 tissue culture flasks and a wash was performed using cold phosphate buffered saline (PBS). 500µl of lysis buffer (1% SDS, 5mM EDTA, 50mM Tris-HCl (pH.6.8) and 1% Glycerol) and 5µl of protease cocktail inhibitor at 1:100 (EMD Biosciences, San Diego, USA) were added to the flask. Cells were scraped off and transferred to an Eppendorf tube and incubated on ice for 30mins. Cells were sonicated using a water bath sonicator (look for make and model) for 10 mins; 30secs at high level sonication and 30secs rest. The Eppendorf tube was then placed on a Thermomixer (Eppendorf) and heated at 90°C for 10mins. The cells were then spun at 14,000 RPM in a cold centrifuge (4°C) for 10mins. The supernatant was then carefully transferred into a fresh Eppendorf tube. A

protein determination assay was performed using the colourimetric Bio-Rad DC protein assay (Bio-Rad, Hemel Hempstead, UK). Bovine Serum Antigen (BSA) standards were prepared at the following decreasing concentrations; 1000µg/ml, 500µg/ml, 250µg/ml, 125µg/ml, 62.5µg/ml, 31.25µg/ml, 15.625µg/ml and 0µg/ml. 5µl of standard and 5µl of sample lysate were added to the corresponding wells and were run in triplicate. A working mix of Protein Assay Reagent A + S was prepared at a dilution of 1:50 (1ml of reagent A and 20µl Reagent S) and 25µl of Reagent A + S was added into each well. 200µl of Reagent B was added into each well and the plate was incubated in the dark for 15 mins. The absorbance was subsequently read using a plate reader at 750nm.

Table 6.1 STR profiles of cell lines cultured for RasGRP3 experiments. All cell lines correspond to the profiles as published by De Waard-Siebinga et al., White et al., Chen et al. and Nareyeck et al.

		Cell Lines				
		92.1	Mel270	OMM1	CRMM1	CRMM2
Marker	AMEL	X	X, Y	X	X	X, Y
	vWA	16	17, 18	19	15	16, 17
	TPOX	8,9	10	8, 9	8, 11	8
	TH01	9, 9.3	6, 9	7	7	7, 9.3
	D21S11	30	28, 29	30, 30.2	29, 32.2	28, 31.2
	D5S818	9, 11	12	11	12, 13	11
	D13S317	11, 12	12	12	12	8, 11
	D7S820	10, 11	8, 9	13	8, 11	8, 11
	D16S539	12	12	9	5, 11	9, 13
	CSF1PO	10, 11	11	10, 12	10, 13	12

6.2.2 Western Blotting

The 12.5% running gel was prepared using 5.95mL water, 4.25mL, ProtoGel resolving buffer (Geneflow, Staffordshire, UK) and 6.8mL ProtoGel 30% 37.5:1 acrylamide (Geneflow, Staffordshire, UK). The 5% stacking gel was prepared using 4.36mL water, 1.9mL ProtoGel stacking buffer (Geneflow, Staffordshire, UK) and 1.24mL 30% 37.5:1 acrylamide (Geneflow,

Staffordshire, UK). Ammonium persulphate (APS) (0.2g in 2mls water) and TEMED were added to the resolving gel mixture, poured between the glass plates and overlaid with water until set. This step was repeated with the stacking gel mix, which was then pipetted on top of the resolving gel and a 10-well comb was inserted prior to allowing the gel to set. Samples were loaded onto the gel with a molecular weight ladder and the gel was run at 30mA for an hour using 1x running buffer (3.03g Tris base, 14.4g Glycine and 1.0g SDS). The gels were removed from the cassettes and the stacking gel discarded. Sponges soaked in cold 1x transfer buffer (3.03g Tris base and 14.4g Glycine) were placed on the back of the cassette followed by blotting paper dipped in transfer buffer and the gel. The (PVDF) poly vinyl difluoride, 0.2µm membrane was submerged in methanol and placed directly onto the gel. A final sponge soaked in transfer buffer was placed on top. The cassette was then closed and placed inside the electrode assembly and the proteins were allowed to transfer at 400mA for 1 hour. The membrane was removed from cassette and a small cut made in the top left hand corner to mark the orientation. The membrane was blocked in 5% non-fat milk (NFM) for 1 hour at RT on a shaker. The RasGRP3 antibody at a dilution of 1:1000 (ProteinTech, Manchester, UK) was prepared in 5% NFM and incubated overnight at 4°C on a shaker. The membrane underwent the following wash steps: 2 x 30 seconds, 2 x 5 min and 1 x 15 min with wash buffer (1X TBS, 0.1% Tween 20). The secondary antibody, horseradish peroxidase conjugated (HRP) goat anti-rabbit (DAKO) was prepared at a dilution of 1:5000 in 2.5% milk and incubated for 1 hour at RT. The previous wash steps were then repeated. The blot was developed via chemiluminescence using the Immobilon Western Chemiluminescent HRP Substrate kit (Merck-Millipore, United Kingdom). A working HRP substrate mixture was prepared by mixing 1mL Luminol Reagent and 1mL Peroxide Solution. The mixture was allowed to reach room temperature for 10 minutes.

The membrane was blotted dry and the HRP substrate mixture was pipetted on ensuring even coverage and left for 1 minute. Excess mixture was removed by blotting the edge of the membrane. The membrane was then sealed in plastic wrap and imaged on the GeneGnome XRQ Image Capture machine (Syngene).

6.2.3 DNA extraction from fresh UM tissue

Seventeen frozen UM samples collected between 2014 and 2015 were sampled in microfuge tubes, snap frozen in liquid nitrogen and stored at -80°C. Samples were thawed at RT and the tissue minced using a sterile scalpel blade in a petri dish. DNA extraction was carried out using methods previously described in Chapter 2.2.1

6.2.4 DNA quantity assessment

DNA quantitation was carried out using the methods previously described in Chapter 2.2.4

6.2.5 Sanger Sequencing for *GNAQ* and *GNA11* mutations

Exons 4 and 5 of *GNAQ* and *GNA11* were amplified using end-point PCR in a G-Storm GS1 Thermal Cycler (GRI – Genetic Research Instrumentation Ltd, Essex) using; 0.5% BSA (Sigma, St. Louis) Thermo-Start *Taq* DNA Polymerase, 10x HP Buffer, 25mM $MgCl_2$, 10mM dNTPs (Thermofisher, Massachusetts) and PCR Primers (Table 6.2). DNA was initially denatured for 15 min at 95°C followed by 35 cycles of 15 sec 95°C, 30 sec 60°C and 1 min 72°C. The reaction was then completed by 10 min elongation at 72°C. 25ng DNA was used in each reaction. PCR products were purified using the Qiagen QIAquick PCR purification kit (Qiagen GmbH, Hilden). The purified PCR products were then quality assessed on a 2% agarose gel run at 100V for 30 mins. PCR products were sent to GATC Biotech, (Konstanz, Germany) for

chain termination reaction and subsequent analysis of electropherograms was performed using Chromas Lite (Technelysium Pty Ltd, Australia).

Table 6.2 Primer Sequences for Exons 4 & 5 of *GNAQ* and *GNA11*

Gene	Primer Sequence
GNAQ Q209 Forward	TTTTCCCTAAGTTTGTAAGTAGTGC
GNAQ Q209 Reverse	CCCACACCCTACTTTCTATCATTTAC
GNAQ R183 Forward	TGGTGTGATGGTGTCACTGACATTCTCAT
GNAQ R183 Reverse	AGCTGGGAAATAGGTTTCATGGACTCAGT
GNA11 Q209 Forward	CGCTGTGTCCTTTCAGGATG
GNA11 Q209 Reverse	CCACCTCGTTGTCCGACT
GNA11 R183 Forward	GTGCTGTGTCCCTGTCCTG
GNA11 R183 Reverse	GGCAAATGAGCCTCTCAGTG

6.2.6 Preparation of FFPE cell pellets of UM and conjunctival melanoma cell lines

At ~75% confluence the cells were removed from the bottom of 75cm^2 tissue culture flasks using a cell scraper. The cells were then pelleted at 1500rpm for 2 minutes and fixed in 10% neutral buffered formalin for 10 minutes. Following fixation, the cells were washed in PBS (Sigma-Aldrich Ltd, United Kingdom) before transferring the cell pellet to a microfuge tube for a final wash with PBS and centrifugation at 8000rpm for 1 minute. The supernatant was removed and 100µl of 4% molten agar was added and mixed quickly into the cell pellet prior to centrifugation at 14,000rpm for 30 seconds. The agar cell pellet was then removed from the microfuge tube and placed into a tissue cassette for processing through a series of alcohols and xylenes. After dehydration, the pellet was paraffin wax embedded, such that the agar tip containing cells was at the surface of the block.

6.2.7 Tissue Microarray (TMA) construction

A TMA was constructed using a Beecher tissue microarrayer (Beecher Instruments, Sun Prairie, WI). Arrays contained triplicate 0.6-mm cores taken at random from the tumour areas of FFPE tissues for each of the UM samples.

6.2.8 Immunohistochemistry

6.2.8.1 Optimising the Antibody

The Protein Tech RasGRP3 antibody (Protein Tech, Manchester, UK) was tested at 1:50-, 1:100- and 1:200 dilutions using human pancreas and duodenum control tissue. A 1:200 dilution was selected as the optimum concentration for IHC. Duodenum was selected as the positive control tissue for all subsequent experiments.

6.2.8.2 IHC on whole tissue sections, TMA and cell pellets

Sections (4 µm thick) were cut from the cell pellet blocks of UM and conjunctival melanoma specimens, TMA and whole tissue sections and mounted on X-tra^{TM} adhesive tissue slides (Leica, United Kingdom). Antigen retrieval was performed at 96°C for 20 minutes using a PT Link (Dako, Carpinteria, CA; Ely, UK) pretreatment module and high- pH (pH 9.0) retrieval solution. The following steps were performed at room temperature (RT) using a Dako FLEX Envision kit and Autostainer Plus: 5 mins endogenous peroxidase blocking, 30 mins incubation with primary antibody, 15 min incubation with mouse or rabbit linker, 20 min incubation with horseradish peroxidase, and positive staining was visualized by use of 3-amino-9-ethylcarbazole (AEC, Vector Laboratories Ltd., Peterborough, UK, 30 min). Slides were washed with FLEX wash buffer between each step. The following RasGRP3 primary antibodies were used: rabbit polyclonal, 13162-1-AP (ProteinTech, Manchester, UK) at

1:200, and mouse monoclonal, ab156937 (Abcam, Cambridge, UK) at 1:200. An IgG1 isotype control was run at the same concentration as the mouse monoclonal, and omission of the primary antibody served as the negative control for the rabbit polyclonal. Human duodenal tissue served as a positive control for both antibodies. The slides were counterstained with Mayer's haematoxylin (VWR, Leicestershire, UK) and cover-slipped using an aqueous mountant (Aquatex™, VWR).

6.3 Results

6.3.1 Patient Demographics

DNA was extracted from 17 frozen UM from eyes enucleated between 2014 and 2015. The cases included 12 males and 5 females with a median age of 62 years (range, 22 – 78 years). The median LBD was 17.35mm (range, 8.9 – 22.7mm) and the median UH was 9.9mm (range, 2.8 – 16.3mm). 11/17 (65%) of the examined UM contained epithelioid cells and 3/17 (35%) cases had extraocular extension. 5/17 (29%) UM contained necrotic cells. At the time of the study 14 patients were alive, 1 patient was alive with liver metastases and 2 patients had died from metastatic disease. The mean DNA concentration was 334.94ng/µl with a median of 183ng/µl (range, 40.2 – 1600ng/µl), DNA extracted from 17 (100%) of the primary UM samples yielded a concentration >25ng/µl.

6.3.2 Sanger Sequencing for *GNAQ* and *GNA11*

2% agarose gels run to assess the quality of the PCR and subsequent PCR purification confirmed the tests had yielded good quality products (Figure 6.2 and Figure 6.3). Of the 20 sequenced cases, there were 8 *GNA11* Q209 mutant UM, 8 *GNAQ* Q209 mutant UM, and 2 samples were wild type (Figure 6.4). One of the GNAQ/11 wild type samples was a *BRAF* V600E positive conjunctival melanoma. No mutations were detected in exon 4 at codon R186 for either *GNAQ* or *GNA11*, but this was expected as the literature has shown these alterations account for 4.8% of UM (109).

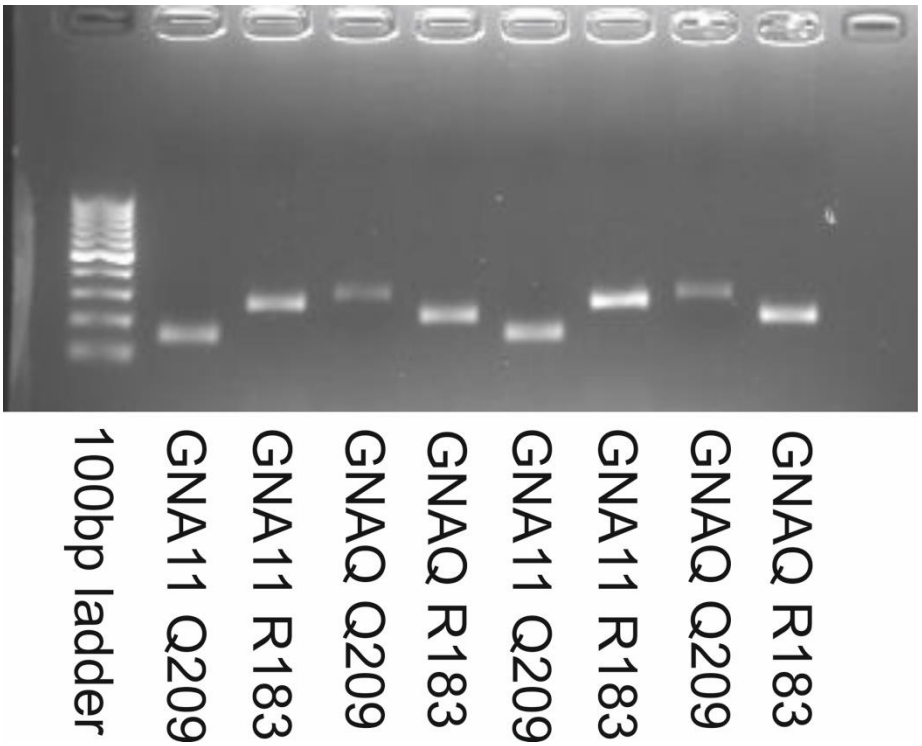

Figure 6.2 Electropherograms from quality assessment of *GNAQ* and *GNA11* PCR products for primers flanking exons 4 (R183) & 5 (Q209)

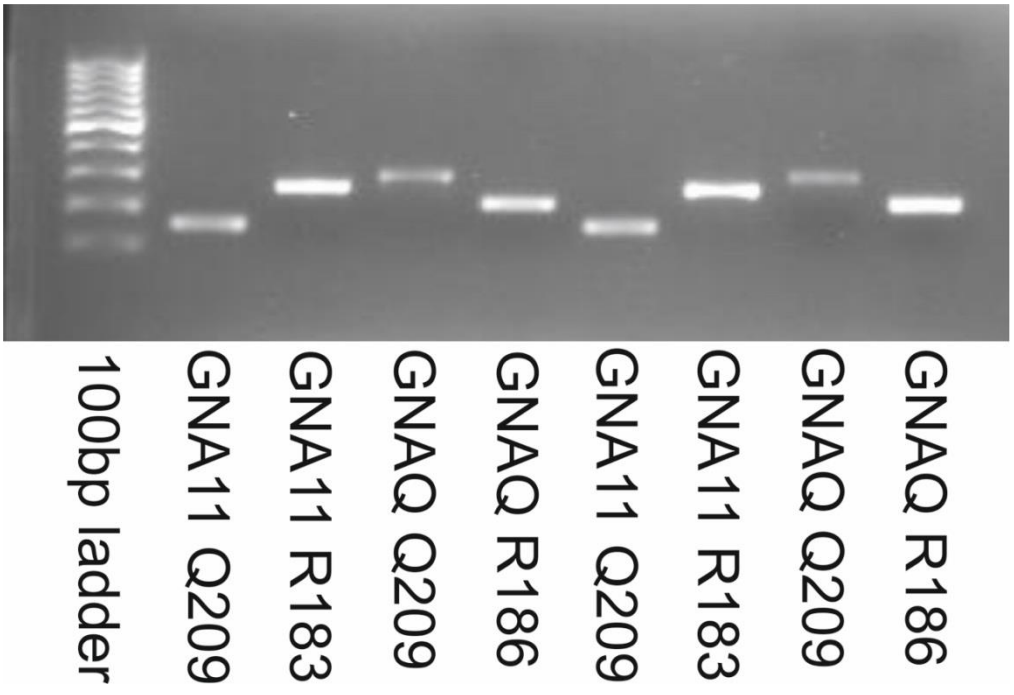

Figure 6.3 Electropherograms assessing the quality of PCR purification for Sanger sequencing.

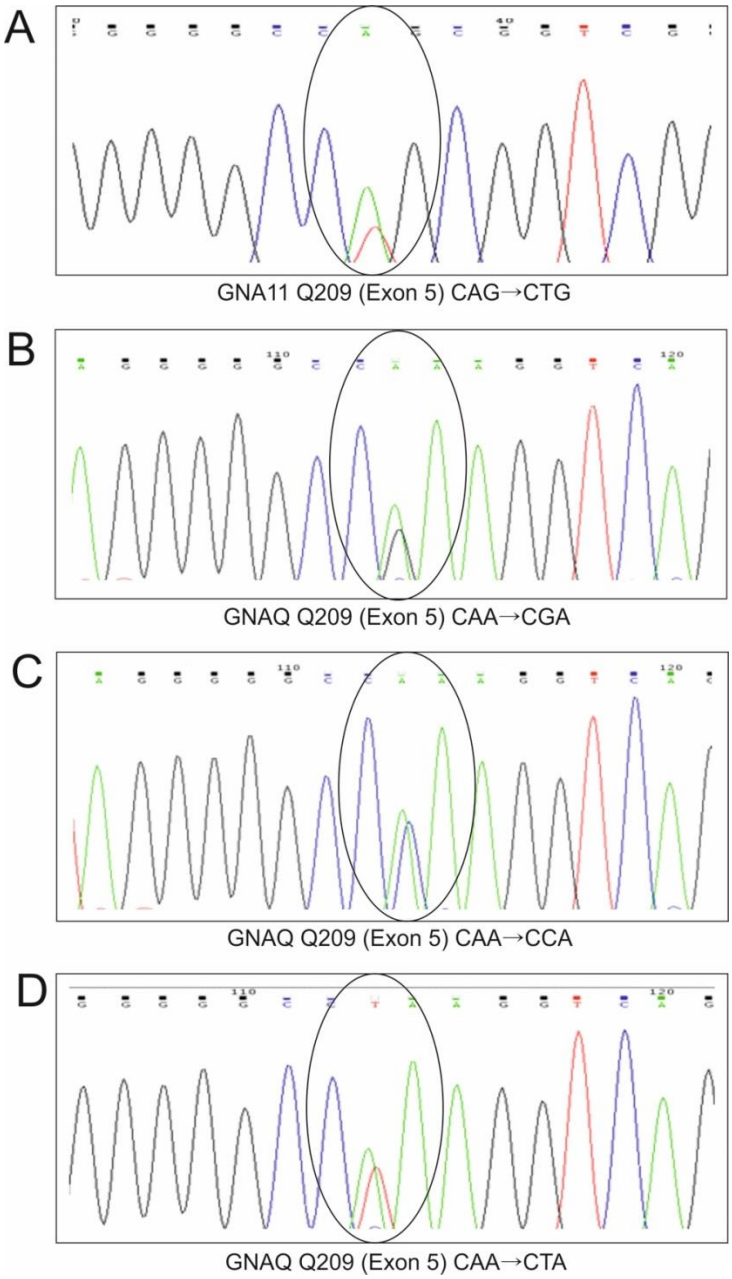

Figure 6.4 Mutation spectra of *GNAQ* and *GNA11* at codon Q209. **A)** The only mutation observed in GNA11 was an adenosine to thymine transition resulting in a substitution to leucine (GNA11 c.626 A>T Q209L) **B)** An adenosine to guanine transition resulting in a substitution to arginine (GNAQ c.626 A>G Q209R) **C)** An adenosine to cytosine transition resulting in a substitution to proline (GNAQ c.626 A>C Q209P) and **D)** An adenosine to thymine transition resulting in a substitution to leucine (GNAQ c.626 A>T Q209L).

6.3.3 Protein Determination Assay

A

	T1	T2	T3	Av	Av - blk	STDEV	SEM
1000	0.284	0.262	0.297	0.281	0.206	0.018	0.010
500	0.176	0.175	0.182	0.178	0.103	0.004	0.002
250	0.134	0.141	0.135	0.137	0.062	0.004	0.002
125	0.104	0.114	0.095	0.104	0.029	0.010	0.005
62.5	0.086	0.085	0.087	0.086	0.011	0.001	0.001
31.25	0.077	0.086	0.081	0.081	0.006	0.005	0.003
15.625	0.075	0.084	0.078	0.079	0.004	0.005	0.003
0	0.073	0.077	0.075	0.075	0.000	0.002	0.001

B

	T1	T2	T3	Av	Av - blk	STDEV	SEM	CONC ug/mL
92.1	0.138	0.141	0.143	0.141	0.066	0.003	0.001	320.33
Mel270	0.152	0.164	0.169	0.162	0.087	0.009	0.005	425.33
OMM1	0.148	0.15	0.149	0.149	0.074	0.001	0.001	362.00
CRMM1	0.226	0.239	0.235	0.233	0.158	0.007	0.004	783.67
CRMM2	0.241	0.239	0.249	0.243	0.168	0.005	0.003	832.00
OMM2.3	0.131	0.136	0.14	0.136	0.061	0.005	0.003	295.33
OMM2.5	0.169	0.174	0.183	0.175	0.100	0.007	0.004	493.67

C

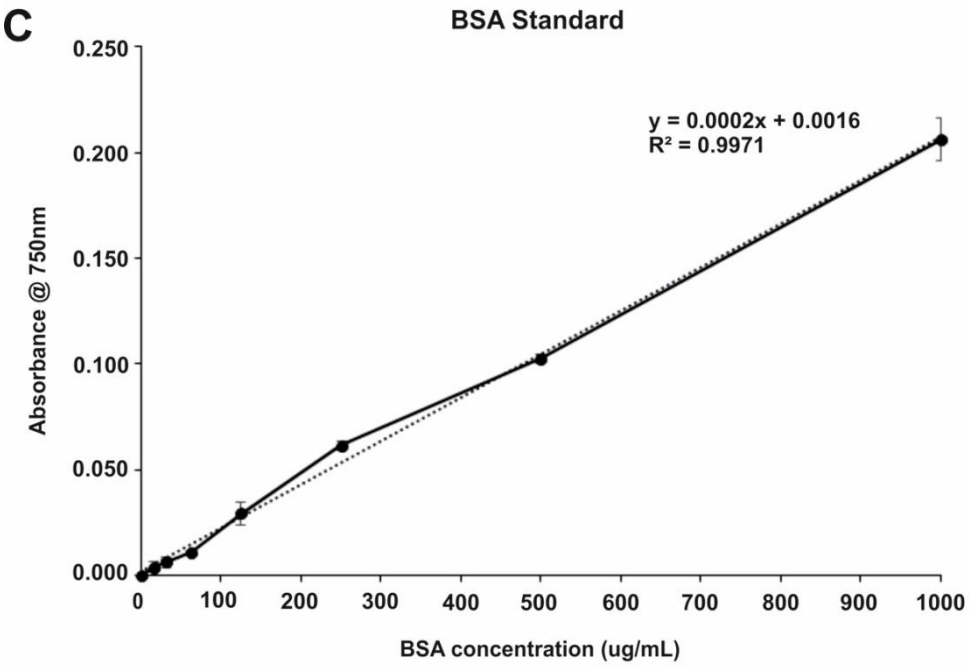

Figure 6.5 A standard curve showing the absorbance of BSA standards at 750nm. **A)** Absorbance of BSA standards at 750nm; **B)** Absorbance of 92.1, MEL270, OMM1, CRMM1 and CRMM2 cell lines at 750nm; **C)** BSA Standard curve.

6.3.4 Western Blot

Western blot examination of RasGRP3 protein expression was carried out in 5 UM cell lines and the 2 conjunctival melanoma cell lines (Figure 6.6). Of these, all UM cell lines demonstrated protein expression of RasGRP3 at the expected molecular weight 78kDa. No additional bands were present on the western blot demonstrating specificity of the antibody for RasGRP3. Neither conjunctival melanoma cell line, regardless of BRAF mutation status, expressed RasGRP3.

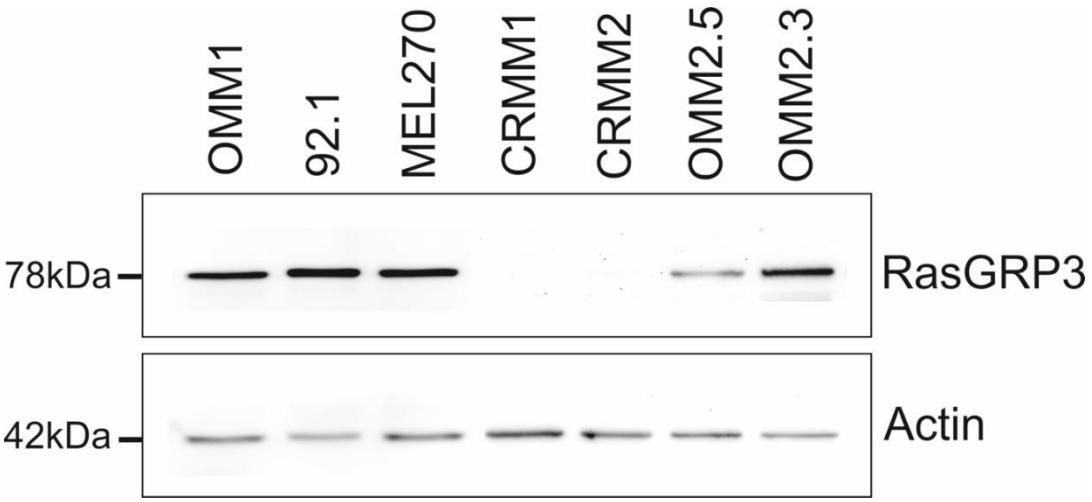

Figure 6.6 Expression of RasGRP3 in *GNAQ* mutant (92.1, Mel270, OMM2.3 and OMM2.5) and *GNA11* mutant (OMM1) UM cell lines and *BRAF* V600E mutant (CRMM1) and *BRAF* wild type (CRMM2) conjunctival melanoma cell lines.

6.3.5 Immunohistochemistry

6.3.5.1 Tissue Microarray Immunohistochemistry

18 samples were run in triplicate totalling 54 cores plus 8 normal tissue controls; 2 pancreas, 2 testis, 2 gallbladder and 2 colon. Of the 54 cores; 17/54 (31%) scored weakly, 23/54 (43%) moderate, 2/54 (4%) strong, 9/54 (17%) couldn't be scored and 3/54 (5%) cores were missing. Both nuclear and cytoplasmic protein expression was observed for RasGRP3 in the primary UM tissue microarray. The pattern of cytoplasmic and nuclear staining showed no significant association with *GNAQ/GNA11* mutation status, as no difference between the mutant and wild type primary UMs was noted (Figure 6.7 A, B and D). However, the *GNAQ/11* wild type *BRAF* V600E mutant conjunctival melanoma sample exhibited strong cytoplasmic staining (Figure 6.7 C).

A

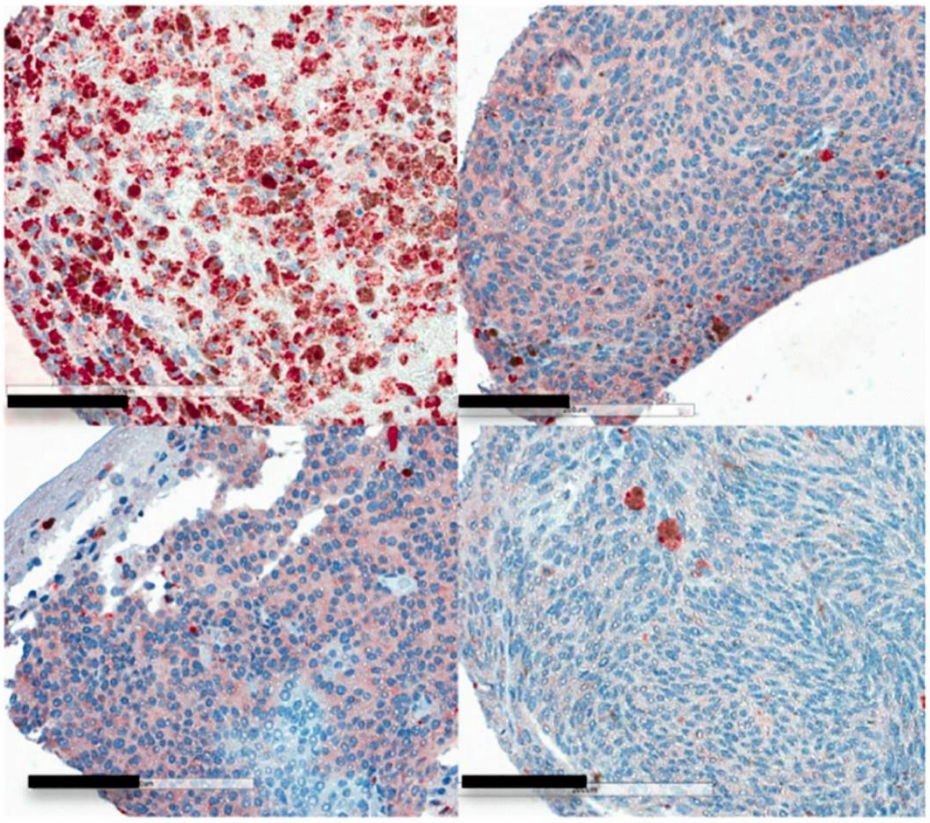

B

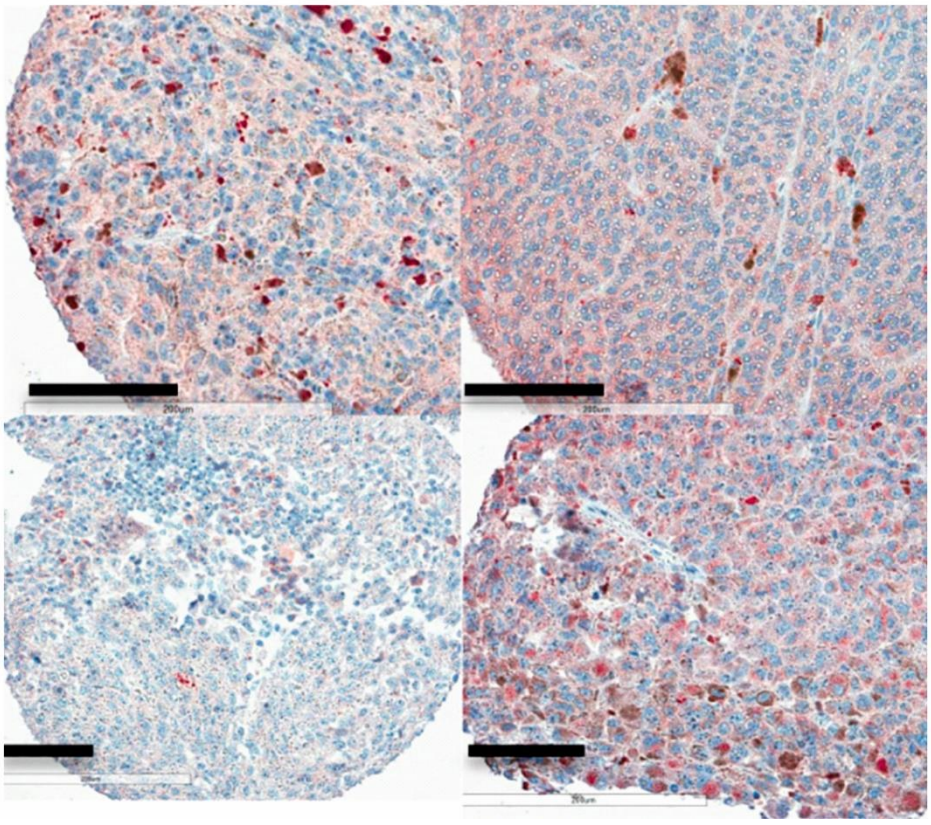

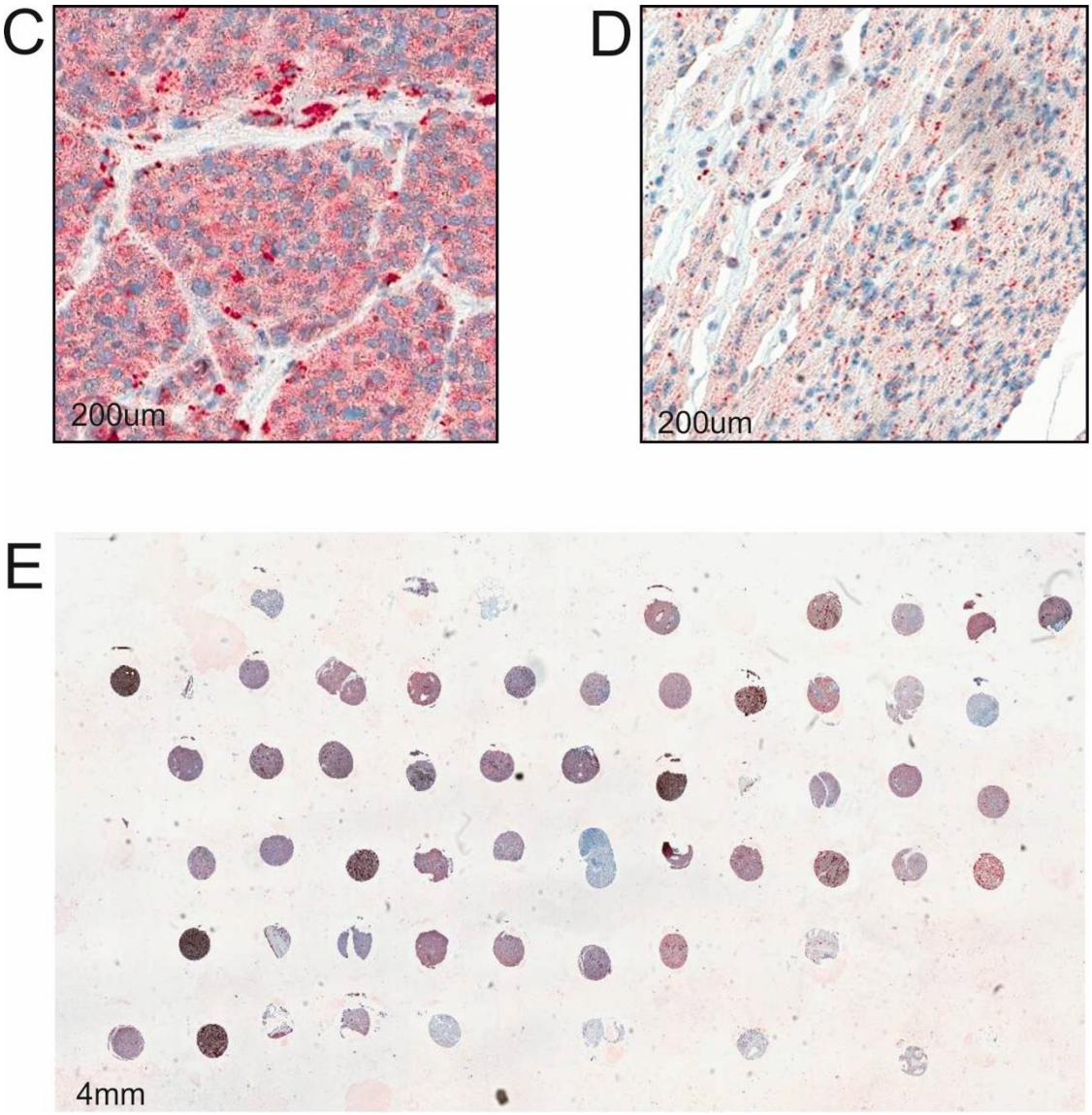

Figure 6.7 RasGRP3 Immunohistochemistry of primary UM samples using Protein Tech antibody at 1:200 A) *GNAQ* mutant primary UM samples, **B)** *GNA11* mutant primary UM samples, **C)** *BRAF* V600E mutant primary conjunctival melanoma sample (used as control), **D)** *GNAQ* and *GNA11* wild type primary UM sample and **E)** Tissue microarray consisting of 8 *GNAQ*, 8 *GNA11* and 2 wild type primary Ums**.**

6.3.5.2 Cell Pellet Immunohistochemistry

Positive cytoplasmic staining was observed in the majority of the UM cell lines, Mel270, 92.1 and OMM1. Staining was not present in either of the two conjunctival cell lines CRMM1 and CRMM2. Speckled cytoplasmic staining was observed in the duodenum positive control and nuclear staining was not observed in any of the samples (Figure 6.8 and 6.9).

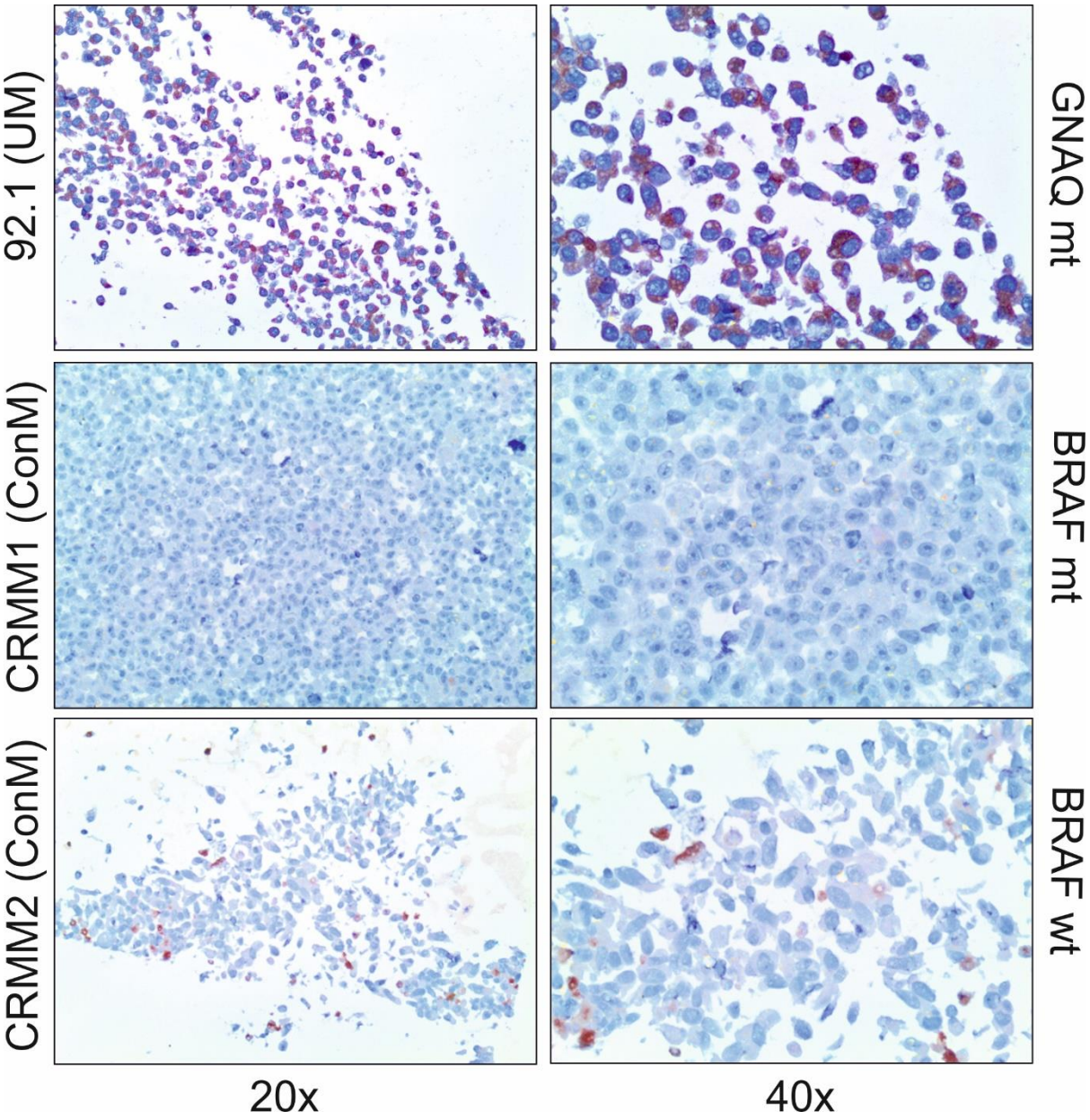

Figure 6.8 Immunohistochemistry of cell pellets using the Protein Tech RasGRP3 antibody at a dilution of 1:200.

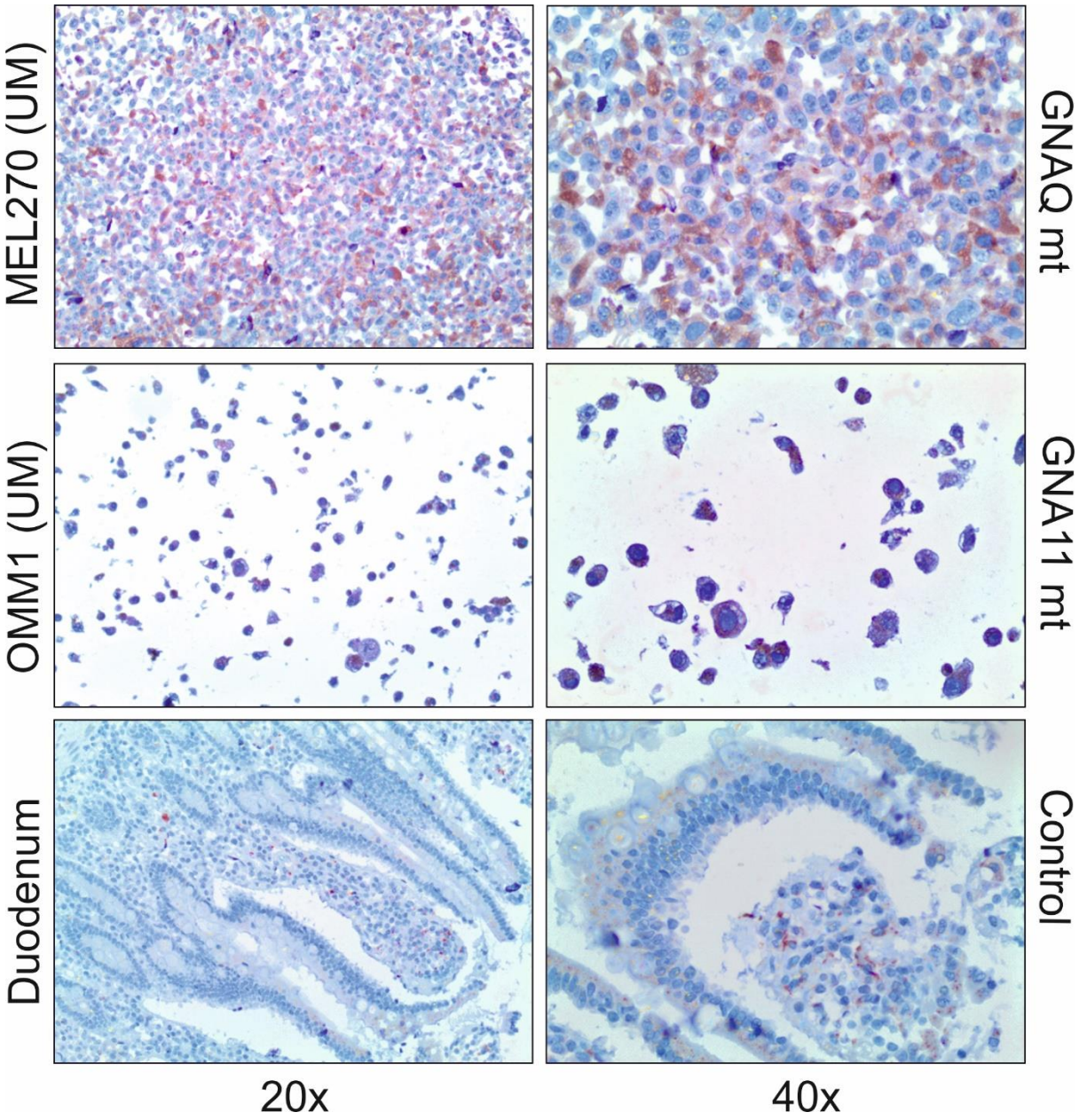

Figure 6.9 Immunohistochemistry of cell pellets using the Protein Tech RasGRP3 antibody at a dilution of 1:200.

6.4 Discussion

Examination of RasGRP3 in both primary UM tumour samples and well-characterised UM cell lines by IHC and western blotting revealed several key differences in protein expression. In the primary UM samples, there was no clear association between *GNAQ* and *GNA11* mutation status and the pattern of RasGRP3 protein expression. However, there was a distinct absence of RasGRP3 protein expression for the *GNAQ/11* wild type conjunctival melanoma cell lines and strong protein expression in the UM cell lines in both the IHC and western blotting experiments. An observation of this work was the lack of consistency between the protein expressions of RasGRP3 in UM cell lines and primary UM samples. A reason for this could be the less heterogeneous nature of cell lines in comparison to primary UM which are more likely to contain clonal populations of both GNAQ/11 mutant and wild-type cells. Intra-tumour heterogeneity is a well-documented phenomenon in UM and this is likely the reason the cell line strand of this study generated more consistent results (179, 229-231). Another limitation of the primary UM component of this study was the degree of pigmentation present in a proportion of the UM samples. This made scoring some of the TMA cores problematic and several of the cores had to be excluded from analysis. Despite these limitations, in this study RasGRP3 has been shown to be markedly upregulated in *GNAQ/11* mutant UM cells and is an essential effector linking oncogenic *GNAQ/11* signalling. Activation of the MAPK pathway typically occurs through mutations or amplifications in genes such as *BRAF* or *NRAS*, in cancers such as cutaneous melanoma. As UM lacks mutations in these genes, it is thought that mutations in *GNAQ/11* activate the MAPK pathway by stimulation of PKC. The work presented in this study was part of a larger study that was able to demonstrate that MAPK activation is dependent on activation of Ras by RasGRP3 (286). They were able to show that activation of RasGRP3 was PKC independent as well via PKC δ- and ε-dependent phosphorylation. However, mutations in

GNAQ and *GNA11* have also been shown activate other oncogenic pathways, such as the Yes-associated pathway (YAP)-Hippo pathway tumour suppressor pathway (287). YAP is translocation into the cell nucleus is triggered by mutations in *GNAQ/11* that stimulate YAP-dependent activation of the guanine exchange factor Trio, activating small GTPases RhoA and Rac1 (Figure 2.10) (288). This signalling cascade contributes to YAP-dependent growth of UM cells, which means YAP inhibitors such as verteporfin are potential therapies for UM patients with *GNAQ/11* mutations (289). Therefore, activation of a different pathway such as the Hippo-YAP may also be another possible explanation for the inconsistent staining patterns observed in the primary UM samples, as it is likely not all GNAQ/11 mutants have the same activated pathways.

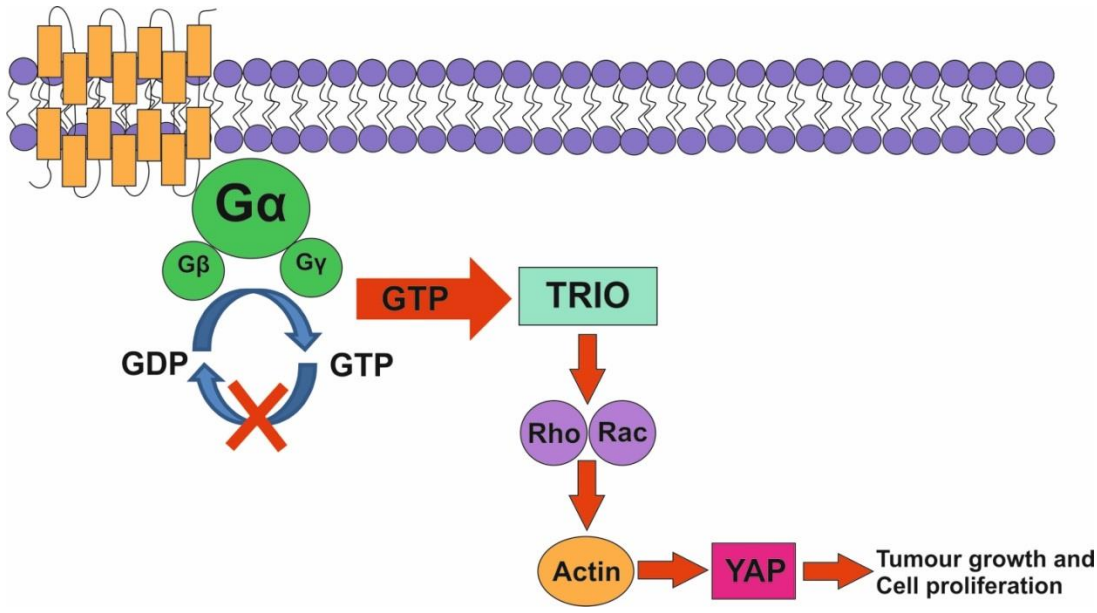

Figure 6.10 The Hippo-YAP signalling pathway in UM. Constitutively active GTP stimulate YAP-dependent activation of the guanine exchange factor Trio, activating small GTPases RhoA and Rac1which leads to activation of the YAP pathway leading to tumour growth and cell proliferation. Original image.

In this chapter I have shown a lack of RasGRP3 protein expression in BRAF V600E mutant and wild-type conjunctival melanoma. In contrast, RasGRP3 is expressed in primary UM tumour tissues and GNAQ and GNA11 mutant UM cell lines. This demonstrates that activation of the MAP-kinase pathway occurs through a different mechanism to conjunctival melanoma. These findings change the way oncogenic signalling in UM is perceived and identify RasGRP3 as a potential therapeutic target for cancers driven by oncogenic GNAQ/11.

Summary and Future Directions

The purpose of this thesis was to examine different aspects of the methodologies used to stratify UM patients into high or low-risk with respect to developing metastatic disease, in order to refine prognostication for UM patients.

In **Chapter 2,** I examined the rarest subtype of UM, namely iris melanomas (IM). Little was known about the genetic characteristics of these tumours at the time of my examinations. By performing a retrospective database review and identifying 24 archival tissue specimens over a twenty year period, I was able to perform molecular analysis. Previous data suggested monosomy 3 (M3) leads to a poor outcome in posterior UM; therefore, I sought to establish whether this was the same for IM. This was the largest at the time that examined tumours that originated in the iris. Interestingly, I was able to demonstrate that the same chromosomal aberrations observed in posterior UM are also seen in IM, in both treatment naïve and irradiated IM, with a low-metastatic risk genotype most commonly observed in these tumours. During the course of this research there have been subsequent studies examining mutations in IM. Similar mutations in IM to those frequently observed in posterior UM have been identified in GNAQ, GNA11, BAP1, SF3B1 and EIF1AX in addition to less frequent mutations in NRAS, BRAF, PTEN, cKIT and TP53. More research needs to be undertaken in larger scale studies to establish the mutational signature of IM and whether they share a similar clinical outcome to posterior UM.

In **Chapter 3,** I performed an audit of 285 UM that were genotyped by MSA. The majority of samples genotyped by this method are usually small DNA-yielding FNAB specimens, some of which have been irradiated prior to sampling. I was able to demonstrate that MSA is a molecular technique, which can accurately determine chromosome 3 status in small UM

biopsy samples with low DNA concentrations. When I compared the genotyping success rate of treatment naïve and irradiated UM samples, I found no demonstrable differences in the quality or clarity of the genotypes generated. Thus I showed that MSA can be used to reliably establish chromosome 3 status in post radiotherapy samples treated with either proton beam and ruthenium plaque. All cases followed the predicted clinical course irrespective of irradiation status. To establish the effects of surgical intervention and iatrogenic dissemination, I examined metastasis-free survival in samples taken before and after administration of RXT and found no significant difference in survival between the two cohorts. Our findings indicate that there is no increased metastatic risk when biopsies are taken before administration of radiotherapy. This study identified loss of 3q as an indicator of poor prognosis, which made this cohort of samples similar to M3 in terms of survival. In this study only a small group was identified. A study on the long-term significance of partial loss of chromosome 3, both 3p and 3q, on survival needs to be undertaken to fully understand the molecular behaviour of this UM subgroup and overall survival. Additionally, the cohort of UM with an AI genotype behaved the most similar to D3 in terms of survival. Similarly, longer follow-up is required to fully appreciate the clinical significance of this subgroup.

Nuclear BAP1 protein expression is easily examined by IHC: in **Chapter 4,** I sought to examine the prognostic potential of BAP1 IHC in a cohort of 165 UM enucleation specimens; the largest study to date. By performing multivariate analysis of clinical, histopathological and genetic factors, I was able to demonstrate that nuclear BAP1 negativity is a significant independent prognostic parameter associated with metastatic risk and thus reduced survival. In multivariate analysis loss of BAP1 protein expression was a more significant risk factor than loss of chromosome 3. I was also able to identify two

subgroups within M3 UM: either nBAP1 positive or negative, with distinct and independent survival profiles. Strikingly, nBAP1+ M3 UM were associated with prolonged survival compared to nBAP1- M3 UM. This subgroup of UM patients' need to be followed up closely to examine continued disease-free survival, and to determine whether the patients will eventually follow the same clinical course as M3 nBAP1- UM. This research has highlighted the utility of using BAP1 IHC as a surrogate marker for prognostication, especially in hospitals where genetic testing is not embedded into clinical management of UM patients. As a result of this study, BAP1 IHC is now part of the routine workup of all UM histological specimens sent to the Pathology Dept. in Liverpool, and assists in determining the appropriate surveillance program for patients. As the BAP1 data accrue, a larger scale audit is necessary to assess the impact of incorporating this as an additional covariate in LUMPO III, the prognostication model currently used to estimate all-cause mortality for UM patients at LOOC and around the world.

In **Chapter 5,** I assessed the feasibility of designing and implementing a targeted NGS panel examining mutations in *GNAQ*, *GNA11*, *BAP1*, *SF3B1*, *EIF1AX*, *CYSTLR2*, *PLCB4*, *TTC28*, *KTN1*, *TP53BP1*, and *CSMD1* in addition to copy number changes in chromosomes 1, 3, 6 and 8. I designed, compared and evaluated two different library preparation methodologies and validated their efficacy using samples where mutation data and copy number data was available, demonstrating the superiority of hybrid capture. I also demonstrated that it is possible to analyse copy number and single nucleotide variants in both fresh and formalin fixed tissue. I was able to establish that mutations in *GNAQ*, *GNA11* and *CYSLTR2* occurred in the mutually exclusive fashion described in the literature and were not associated with increased metastatic risk, supporting the evidence in the literature that these are initiating mutations. Additionally, I identified a mutation in *PLCB4* in this study that did not fall within

the hotspot on exon 20 in a sample with a *GNAQ* mutation; not previously described in UM. I also observed several other novel mutations in *TTC28* (22q12.1), *CSMD1* (8p23.2), *KTN1* (14q22.3) *and TP53BP1* (15q15.3) at a low frequency. To fully understand their role in tumour progression more functional studies focussed on the significance of these need to be undertaken. Mutations in *BAP1* were found to be the most important prognostic factor in terms of survival, consistent with the findings in **Chapter 4**. In contrast to the findings of others, in this study mutations in *SF3B1* were not associated with an increase in metastatic risk. However, the follow-up period for these patients was relatively short; therefore, the risk that *SF3B1* mutations poses for these patients cannot be fully appreciated. This cohort of patients' needs to be followed-up regularly to comprehend the long-term risk that mutations in *SF3B1* pose. Mutations in *EIF1AX* were associated with improved disease-free survival despite regression analysis associating *EIF1AX* with an increase in metastatic risk; however this was due to a relatively small follow-up. Consistent with other studies, copy number analysis showed monosomy 3, 6p gain, loss of 8p and 8q gains to be associated with a worse outcome. However, loss of 6q was not found to be associated with a poor survival contradicting the results of others. This study identified novel concomitant losses of 1p and gains of 1q, with gain of 1q being identified by cox-regression as a significant hazard contributing to the increased incidence of metastatic death. A larger cohort of UM samples with a longer follow up is now needed to further validate the panel for clinical use.

Constitutive activation of Gαq signaling by mutations in G-coupled protein receptors *GNAQ* or *GNA11* occur in over 80% of UM and activate MAPK signalling. In **Chapter 6**, in collaboration with the University of California San Francisco, I worked with Dr. Boris Bastian and Dr. Xu Chen to investigate a potential target *RasGRP3,* which was identified as significantly and selectively overexpressed in response to *GNAQ/11* mutations. Conjunctival

melanoma (ConM) and UM cell lines were used to create cell lysates for the examination of RasGRP3 protein expression by western blotting. I found that *BRAF* V600E mutant and wild-type ConM did not express RasGRP3 whereas *GNAQ/11* mutant UM cell lines did. I also performed a series of immunohistochemistry (IHC) experiments to examine the expression of RasGRP3 in UM and ConM cell lines in addition to a tissue microarray of primary UM tumour tissue, which also confirmed overexpression of this molecule in UM. This demonstrates that activation of the MAPK pathway occurs through a different mechanism to cutaneous melanoma. This opens up the potential of using RasGRP3 as a therapeutic target for UM patients requiring initial testing in in vitro and in vivo models of the disease.

In conclusion, our understanding of the factors influencing metastatic risk in UM has been significantly expanded from analysing only copy number alterations in chromosomes 3 and 8q. I and others have clearly demonstrated the clinical need for integrating somatic copy number variations and gene mutation status when determining the prognosis for UM patients. Prediction of disease risk or treatment response is one of the pillars of personalised medicine. Prognostication is an important but often underused tool in clinical practice. It impacts highly medical decision-making in daily clinical practice. This is particularly important for patients with advanced terminal illness' such as cancer, as prognostication aids in discussions about advanced care planning.

Appendix 1. Illumina Sequence Quality Data

Sample ID	Total reads	reads mapped	reads mapped %	After UMI removed	Reads mapped % after UMI removed	Number of bases with coverage more than 0 (%)	Mean Depth of Coverage for the bases with coverage more than 0
1	2,478,326	2,248,499	90.73%	286,408	11.56%	124,149 (96.28%)	374.21x
2	1,269,340	1,142,922	90.04%	218,890	17.24%	123,845 (96.05%)	292.49x
3	924,312	849,156	91.87%	95,768	10.36%	123,033 (95.42%)	129.94x
4	3,265,808	3,096,256	94.81%	246,311	7.54%	124,174 (96.30%)	331.42x
5	1,286,042	1,183,523	92.03%	230,935	17.96%	124,023 (96.19%)	311.93x
6	6,142,882	5,969,994	97.19%	227,976	3.71%	123,679 (95.92%)	309.14x
7	2,163,454	1,925,847	89.02%	278,625	12.88%	124,101 (96.25%)	367.22x
8	2,402,312	2,134,430	88.85%	807,969	33.63%	123,303 (95.63%)	319.14x
9	2,533,624	2,374,497	93.72%	614,043	24.24%	124,264 (96.37%)	352.92x
10	3,720,226	3,627,122	97.50%	274,837	7.39%	124,266 (96.37%)	375.93x
11	6,791,340	6,664,085	98.13%	238,491	3.51%	123,663 (95.91%)	320.14x
12	3,445,808	3,186,811	92.48%	210,132	6.10%	123,825 (96.03%)	277.22x
13	2,962,808	2,843,195	95.96%	228,020	7.70%	124,090 (96.24%)	309.51x
14	2,420	1,768	73.06%	1,718	70.99%	63,962 (49.61%)	4.70x
15	3,222,334	3,077,388	95.50%	327,489	10.16%	124,139 (96.28%)	450.69x
Mean	**2,840,736**	**2,688,366**	**92.06%**	**285,841**	**16.33%**	**119,901 (92.99%)**	**302x**

Appendix 2. Agilent Sequence Quality Data

Sample ID	Total reads	reads mapped	reads mapped %	After duplicates removed	Reads mapped % after duplicates removed	Number of bases with coverage more than 0 (%)	Mean Depth of Coverage for the bases with coverage more than 0
1	2,376,700	2,335,881	98.28%	1,784,958	75.10%	471,242 (99.99%)	462.43x
2	2,545,582	2,493,908	97.97%	1,912,437	75.13%	471,284 (100.00%)	479.19x
3	2,308,124	2,246,406	97.33%	1,479,937	64.12%	471,284 (100.00%)	409.62x
4	2,947,696	2,880,098	97.71%	2,149,398	72.92%	471,242 (99.99%)	547.34x
5	2,508,522	2,458,067	97.99%	1,895,731	75.57%	471,284 (100.00%)	483.09x
6	2,996,436	2,914,272	97.26%	2,402,807	80.19%	471,284 (100.00%)	453.31x
7	2,420,862	2,367,918	97.81%	1,834,341	75.77%	471,284 (100.00%)	447.92x
8	2,428,668	2,368,412	97.52%	1,879,672	77.40%	471,242 (99.99%)	437.77x
9	2,588,586	2,528,706	97.69%	1,952,734	75.44%	471,284 (100.00%)	464.82x
10	2,862,900	2,802,999	97.91%	2,061,664	72.01%	471,284 (100.00%)	540.84x
11	2,840,288	2,772,997	97.63%	1,982,899	69.81%	471,284 (100.00%)	531.48x
12	3,166,404	3,082,413	97.35%	2,389,347	75.46%	471,242 (99.99%)	491.03x
13	3,889,588	3,804,658	97.82%	2,869,632	73.78%	471,284 (100.00%)	725.36x
14	2,886,854	2,798,417	96.94%	2,217,223	76.80%	471,284 (100.00%)	426.24x
15	2,828,828	2,771,046	97.96%	2,151,815	76.07%	471,284 (100.00%)	558.25x
Mean	**2,773,069**	**2,708,413**	**97.68%**	**2,064,306**	**74.37%**	**471,273 (99.99%)**	**497.25x**

Appendix 3.

Br J Ophthalmol. 2016 Jul;100(7):1012-1016. doi: 10.1136/bjophthalmol-2015-308301. Epub 2016 Apr 20.

Genetic findings in treatment-naïve and proton-beam-radiated iris melanomas.

Krishna Y[1], Kalirai H[2], Thornton S[2], Damato BE[1,3], Heimann H[1], Coupland SE[2].

Author information

PMID: 27098748

Appendix 4.

Cancer Cell. 2017 May 8;31(5):685-696.e6. doi: 10.1016/j.ccell.2017.04.002.

RasGRP3 Mediates MAPK Pathway Activation in GNAQ Mutant Uveal Melanoma.

Chen X[1], Wu Q[2], Depeille P[3], Chen P[2], Thornton S[4], Kalirai H[4], Coupland SE[4], Roose JP[3], Bastian BC[5].

PMID: 28486107

Appendix 5.

The Journal of Pathology: Clinical Research
J Path: Clin Res 2017
Published online in Wiley Online Library (wileyonlinelibrary.com). DOI: 10.1002/cjp2.86

ORIGINAL ARTICLE

Patterns of BAP1 protein expression provide insights into prognostic significance and the biology of uveal melanoma

Neil Farquhar[1†], Sophie Thornton[1†], Sarah E Coupland[1,2*], Judy M Coulson[3], Joseph J Sacco[1,4], Yamini Krishna[2], Heinrich Heimann[1,5], Azzam Taktak[1,6], Colleen M Cebulla[7], Mohamed H Abdel-Rahman[7,8] and Helen Kalirai[1‡]

[1] *Liverpool Ocular Oncology Research Group, Department of Molecular and Clinical Cancer Medicine, Institute of Translational Medicine, University of Liverpool, Liverpool, UK*
[2] *Department of Cellular Pathology, Royal Liverpool University Hospital, Liverpool, UK*
[3] *Department of Cellular and Molecular Physiology, Institute of Translational Medicine, University of Liverpool, Liverpool, UK*
[4] *Department of Medical Oncology, Clatterbridge Cancer Centre, Clatterbridge, UK*
[5] *Liverpool Ocular Oncology Centre, Royal Liverpool University Hospital, Liverpool, UK*
[6] *Department of Medical Physics & Clinical Engineering, Royal Liverpool University Hospital, Liverpool, UK*
[7] *Department of Ophthalmology and Visual Science, Havener Eye Institute, The Ohio State University, Columbus, OH, USA*
[8] *Division of Human Genetics, Department of Internal Medicine, The Ohio State University, Columbus, OH, USA*

**Correspondence to: Sarah E Coupland, Department of Molecular and Clinical Cancer Medicine, 3rd Floor William Henry Duncan Building, 6 West Derby Street, Liverpool L7 8TX, UK. E-mail: s.e.coupland@liverpool.ac.uk*

[†] *Co-first authors*

[‡] *Senior author*

Abstract

Uveal melanoma (UM) is a rare aggressive intraocular tumour with a propensity for liver metastases, occurring in ~50% of patients. The tumour suppressor *BAP1* is considered to be key in UM progression. Herein, we present the largest study to date investigating cellular expression patterns of BAP1 protein in 165 UMs, correlating these patterns to prognosis. Full clinical, histological, genetic, and follow-up data were available for all patients. *BAP1* gene sequencing was performed on a subset of 26 cases. An independent cohort of 14 UMs was examined for comparison. Loss of nuclear BAP1 (nBAP1) protein expression was observed in 54% (88/165) UMs. nBAP1 expression proved to be a significant independent prognostic parameter: it identified two subgroups within monosomy 3 (M3) UM, which are known to have a high risk of metastasis. Strikingly, nBAP1-positiveM3 UMs were associated with prolonged survival compared to nBAP1-negative M3 UMs (Log rank, $p = 0.014$). nBAP1 protein loss did not correlate with a *BAP1* mutation in 23% (6/26) of the UMs analysed. Cytoplasmic BAP1 protein (cBAP1) expression was also observed in UM: although appearing 'predominantly diffuse' in most nBAP1-negative UM, a distinct 'focal perinuclear' expression pattern – localized immediately adjacent to the cis Golgi – was seen in 31% (18/59). These tumours tended to carry loss-of-function *BAP1* mutations. Our study demonstrates loss of nBAP1 expression to be the strongest prognostic marker in UM, confirming its importance in UM progression. Our data suggest that non-genetic mechanisms account for nBAP1 loss in a small number of UMs. In addition, we describe a subset of nBAP1-negative UM, in which BAP1 is sequestered in perinuclear bodies, most likely within Golgi, warranting further mechanistic investigation.

Keywords: BAP1; uveal melanoma; prognosis; mutation; immunohistochemistry; cytoplasm; Golgi

Received 14 August 2017; Revised 28 September 2017; Accepted 12 October 2017

No conflicts of interest were declared.

Introduction

The incidence of uveal melanoma (UM) varies between 3 and 8 per million per year in Caucasians, making it the most common primary intraocular malignancy in adults [1,2]. Whilst primary tumours are successfully treated using either surgery and/or radiotherapy [3], up to 50% of patients die from metastatic disease, typically occurring in the liver, for which there is currently no effective systemic therapy

[4,5]. Stratifying UM patients as at either high or low risk of metastatic spread is critical to ensure patients are managed accordingly: low metastatic risk UM patients can be reassured that they are very unlikely to develop metastases, whilst high metastatic risk UM patients can undergo more intensive liver screening, with the potential of undergoing liver resection surgery at the earliest onset of relapse, and/or enrolment in clinical trials [6]. Prognostication involves the integration of clinical, histological, and genetic features of the tumour, in order to obtain a refined predicted risk [6,7].

UM is characterized by distinct gross chromosomal abnormalities that are associated with patient outcome, the most common being monosomy 3 (M3), which corresponds with a significantly worse prognosis [8–12]. M3 is frequently accompanied by polysomy 8q, and increasing copies of 8q significantly correlate with reduced survival, in a dose-dependent fashion [8,10,13,14]. Further abnormalities described in UM include loss of 1p, which is associated with poor prognosis in the context of M3 [15], and gains on 6p, which, in the absence of additional chromosomal abnormalities, correspond with a good prognosis [16,17]. More recently, mutations occurring in UM have been identified in several genes, including *GNAQ*, *GNA11*, *BAP1*, *SF3B1*, *EIF1AX*, *PLCB4*, and *CYSLTR2* [11,18–22]. In particular, inactivating *BAP1* mutations are associated with a poor outcome, being present in ~84% of all UMs that went on to produce metastases [19,23,24]. *BAP1* mutations similarly correspond with a significantly worse prognosis in renal clear cell carcinoma [25] and cholangiocarcinoma [26], whilst in mesothelioma *BAP1* inactivation is associated with a good prognosis [27]. Families with members carrying germline mutations in *BAP1* have also been described, with individuals most often affected by mesothelioma, melanomas including UM, and renal cell carcinoma [28,29].

BRCA1-associated protein 1 (BAP1), encoded by *BAP1* on chromosome 3p21.1, is a nuclear-localized deubiquitylase (DUB) belonging to the ubiquitin carboxy-terminal hydrolase family of DUBs [19,30]. The 729-amino acid BAP1 protein includes an N-terminal catalytic domain, a bipartite C-terminal nuclear localisation signal (NLS), and binding domains for BRCA1 (Breast Cancer 1), BARD1 (BRCA1-associated RING domain protein 1), and HCF1 (Host cell factor 1), among others [30–32]. BAP1 has multiple functions, including involvement in DNA damage responses [33–35], transcriptional activation [35], chromatin remodelling [36], and cell cycle regulation [33,37].

Functionally, *BAP1* nonsense or frameshift mutations lead to truncated BAP1 protein with loss of nuclear localisation and/or reduced protein or mRNA stability [23]. This has led to several recent studies assessing the prevalence of nuclear BAP1 protein expression (nBAP1) in UM, and correlating this with clinical outcome [23,38,39]. Koopmans *et al* [39] and Kalirai *et al* [38] observed loss of nBAP1 protein expression in 43% and 51% of all UM, respectively, which was significantly associated with increased metastatic risk, along with other clinical features linked to poor prognosis. In the latter study, we also noted the presence of differing cytoplasmic staining patterns of BAP1 protein (cBAP1) using immunohistochemistry (IHC). This has also been observed by groups examining BAP1 IHC expression in other cancers [40–42], and in atypical Spitz tumours [43]. Although the significance of cBAP1 remains unclear, shuttling of BAP1 between the cytoplasm and nucleus has been previously described [44]. Indeed, in cell lines derived from mesothelioma patients, mutant *BAP1* was associated with cytoplasmic sequestration of the protein due to loss of the NLS [45].

Herein, we report the largest study to date of BAP1 protein expression in UM and provide a comprehensive analysis of nBAP1 and cBAP1, correlating these findings with clinical, genetic, and histopathological tumour characteristics, as well as with outcome.

Materials and methods

Ethics

This study conformed to the principles of the Declaration of Helsinki and Good Clinical Practice guidelines. Approval for the study was obtained from the Health Research Authority (NRES REC ref 16/SW/0112), and all patients provided informed consent.

Validation studies were carried out on an independent set of samples obtained from The Ohio State University (OSU) and collected according to a separate IRB (OSU2006C0045).

Sample collection

For samples collected in Liverpool, 4 µm sections were cut from formalin-fixed paraffin-embedded (FFPE) material obtained from 145 UM patients who were treated by enucleation or local resection at the Liverpool Ocular Oncology Centre (LOOC), Royal Liverpool University Hospital NHS Trust between January 2013 and December 2015. For a further 20 patients, BAP1 IHC had already been undertaken as

part of their routine prognostication, and nBAP1 expression data were available from the Ocular Oncology Biobank.

Fourteen samples from OSU were provided as 4 µm sections cut from FFPE blocks.

Immunohistochemistry

The IHC for BAP1was performed as previously described [38] using the Dako PT Link and the Dako EnVision Flex kit on the Autostainer Plus according to the manufacturer's standard instructions (Dako, Agilent Technologies LDA UK Limited, Stockport, UK). Briefly, a mouse anti-human BAP1 antibody (0.5 $\mu g\ ml^{-1}$; C-4, Santa Cruz, Insight Biotechnology Ltd, Middlesex, UK) and a rabbit anti-human GM130 antibody (0.236 $\mu g\ ml^{-1}$; EP892Y, Abcam, Cambridgeshire, UK; a marker for the Golgi apparatus) were used. Bound antibody was visualized with either EnVision™ FLEX 3,3′-diaminobenzidine (DAB+) (Dako) or aminoethylcarbazole (AEC; for highly pigmented tumours) (Vector Labs UK, Peterborough, UK). All sections were counterstained with Mayer's haematoxylin (VWR International Ltd, Lutterworth, UK), blued with Scott's tap water (Leica Microsystems Ltd, Milton Keynes, UK) and mounted with either Aquatex™ (VWR) or DPX mountant for AEC or DAB+ sections, respectively. Human pancreas tissue was used as a positive control for both BAP1 and GM130. Mouse IgG1 was used as a negative control for BAP1 in tissue sections.

Scoring

The IHC stained slides were scored by four independent investigators (SEC, HK, NF, ST) using a light microscope (Nikon Eclipse E600). A binary score was used for nBAP1expression; with cases being defined as positive when staining was present in tumour cell nuclei, and negative in its absence. cBAP1 was also defined as 'positive' or 'negative', with the subcellular localisation additionally being recorded as either 'predominantly diffuse', or 'predominantly focal perinuclear'.

DNA extraction and quantification

All methods for DNA extraction from FFPE and frozen UM samples and their quantification have been previously described elsewhere [46,47].

Chromosomal copy number analysis

The Multiplex Ligation Dependent Probe Amplification (MLPA) and microsatellite (MSA) procedures for the assessment of chromosome 3 copy number alterations were performed as previously described [8,48,49]. MLPA was performed in all cases yielding > 100 ng DNA whilst MSA was undertaken for samples with lower DNA yield. For samples obtained from OSU, chromosome 3 status was assessed by microsatellite-based genotyping [46].

Mutation analysis

We hypothesized that the phenomenon of 'focal perinuclear' cBAP1 may be due to distinct *BAP1* mutations resulting in mis-localisation. To study this, we sequenced all *BAP1* exons in 9 UM cases that were nBAP1 positive as well as 17 nBAP1 negative UM (7 cBAP1 diffuse, 9 cBAP1 focal perinuclear, and 1 cBAP1 negative). These cases were chosen because they demonstrated a clear immunophenotype for nBAP1 and also provided good quality DNA. Targeted sequencing of *BAP1* in these cases was performed by the Rotterdam Ocular Melanoma Study group, using the Ion Torrent Personal Genome Machine or by direct Sanger sequencing at OSU [50]. SNPs were called using Torrent Suite Software V4.4.3 (Thermofisher Scientific Ltd, Hemel Hempstead, UK) and variants were identified and annotated using SnpEff version 3.2a.

A second cohort of 14 UM samples had previously undergone direct sequencing for *BAP1* alterations at OSU. Results were read by aligning with the reference sequence provided by Genbank accession number NM_004656.2, utilizing the Sequencher software (Version 4.8, Gene Codes Corp, Ann Arbor, MI, USA).

Statistical analysis

Multivariate analysis of risk factors associated with development of metastatic disease was undertaken using the Cox proportional hazards model for all covariates with $p \leq 0.10$ by univariate analysis. Survival time (months) was calculated from the date of first diagnosis until death, or study closure on 28 February 2017. All analyses were carried out using SPSS Statistics v.24 (IBM).

Results

Patient demographics and tumour sample details

Initial analyses relate to 165 UM patients treated with surgical excision at the LOOC between January 2013 and December 2015 (supplementary material, Table S1); 154 enucleation, 9 local resection and 2

endoresections. In 29 cases, the surgical excision analysed was not the primary treatment, but instead was performed when tumour recurrence or local complications had followed first treatment. The median time from first presentation to surgical excision for these cases was 33.5 months (range 1–570).

Of the 165 patients, 96 were males and 69 females, with a median age of 63 years at primary management (range, 20–88 years) and a median follow-up of 31.3 months (range, 5.7–348.5 months). At the time of study closure (28 February 2017), 133/165 (81%) UM patients were alive; 25/165 (15%) patients had died from metastatic disease, and 7/165 (4%) had died from other causes. The median largest basal diameter (LBD) was 14.4 mm (range, 3.3–23.6 mm), with a median tumour height of 8.3 mm (range, 0.1–18.5 mm). Epithelioid cells were present in 104/165 (63%) UM, 61/165 (37%) tumours involved the ciliary body, and 20/165 (12%) had extraocular extension. Further histomorphological characteristics of the tumours are summarized in supplementary material, Table S1.

As determined by either MLPA (153 cases) or MSA (12 cases), 103/165 (62%) UM were classified as M3, 48/165 (29%) UM as disomy 3 (D3), and one UM(1%) was isodisomy 3; in all subsequent statistical analyses, this was classified with the M3 cases (supplementary material, Table S2). Thirteen UM (8%) could not be classified as either M3 or D3 due to poor quality DNA.

Nuclear BAP1 protein localisation was observed in 77/165 (45.5%) UM, and absent in 88/165 (54.5%) (Figure 1 and supplementary material, Tables S1 and S2). There was no significant heterogeneity of nBAP1 protein expression amongst the tumour cells, such that the cases were either clearly nBAP1 positive or negative. Glial cells within the optic nerve as well as within the plexiform cells of the neurological retina were used as intrinsic positive controls for nBAP1 expression (Figure 1A). Pancreas sections served as external controls (Figure 1B). Non-neoplastic uveal melanocytes were positive for nBAP1 expression (Figure 1C). No positive staining was observed in sections incubated with mouse IgG1 instead of the BAP1 antibody.

As expected, the majority of M3 (84/104, 81%) were nBAP1 negative; however, 20/104 (19%) demonstrated nBAP1positivity (Figure 2A). Of the 48 D3 UM, the majority (46/48, 96%) were nBAP1 positive. Two D3 UM were nBAP1 negative and were subsequently re-tested by MSA to rule out isodisomy 3, which is not detectable by MLPA; both had a D3 classification by MSA. Of interest, 90 UM demonstrated 8q gains with 61/90 (68%) being BAP1 negative (supplementary material, Table S2). Furthermore, of the 25 UM patients who died from metastatic UM, 22 (88%) had nBAP1 negative primary tumours (supplementary material, Table S1). Of the three nBAP1 positive cases in this group, the chromosome 3 status was M3 in one, D3 in one, and unclassifiable in the remaining case.

Survival

Kaplan-Meier survival curves and tables were examined for all primary UMs stratified according to nBAP1 protein expression or chromosome 3 status. Both UMs negative for nBAP1 (Log Rank, $p < 0.001$) and M3 UMs (Log rank, $p = 0.001$) were significantly associated with a reduced survival time (Figure 1D,E). The cases were further subdivided according to their chromosome 3 status (Figure 2A–C). Strikingly, M3/nBAP1 positive UM had a significantly better prognosis than M3/nBAP1 negative tumours (Log rank, $p = 0.014$), which was in fact similar to that of patients with D3/nBAP1 positive UM (Figure 2B).

Univariate and multivariate analysis

Univariate analysis identified the following factors as significantly associated with survival time (supplementary material, Table S3): nBAP1 protein expression, $p \leq 0.001$ (HR 0.173; 95% CI 0.067–0.450); age at primary management, $p = 0.005$ (HR 1.046; 95% CI 1.014–1.080); presence of closed connective loops, $p = 0.003$ (HR 3.596; 95% CI 1.541–8.389); mitotic count per 40 high power field, $p = 0.016$ (HR 1.029; 95% CI 1.005–1.054); epithelioid cell morphology, $p = 0.014$ (HR 3.059; 95% CI 1.257–7.443); tumour height, $p = 0.002$ (HR 1.169; 95% CI 1.058–1.292); LBD, $p = 0.006$ (HR 1.142; 95% CI 1.039–1.255); and chromosome 3 loss, $p = 0.036$ (HR 0.482; 95% CI 0.243–0.955). Multivariate analysis demonstrated only nBAP1 protein expression as an independent factor significantly associated with survival, $p = 0.002$ (HR 0.211; 95% CI 0.079–0.562) in this cohort (Table 1).

Cytoplasmic BAP1 protein expression

We next examined the 145 UM stained by the Liverpool Ocular Oncology Research Group for cytoplasmic expression of BAP1. Eighteen of these were excluded from the analysis due to high levels of pigmentation, which made the cBAP1 localisation difficult to distinguish, so 127 UM were ultimately included in the analysis. cBAP1 staining was not observed in the glial cells of the optic nerve or the plexiform cells of the neurological retina, which

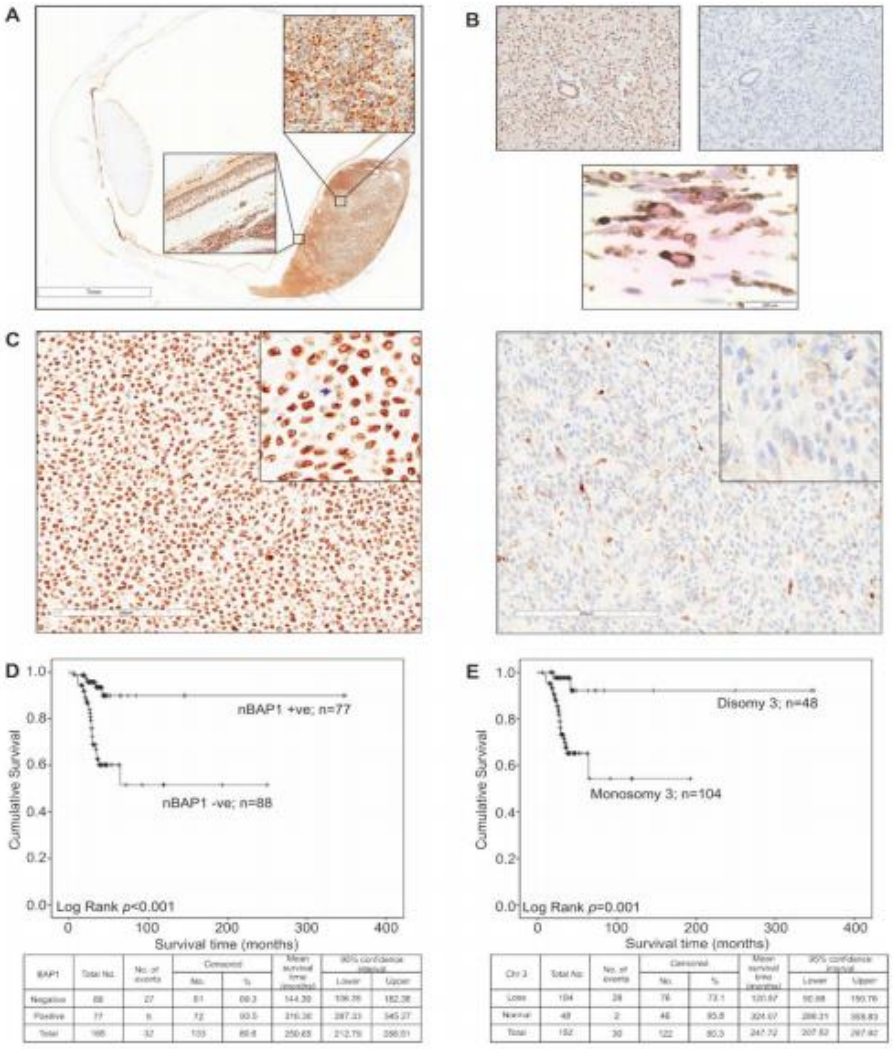

Figure 1. Prognostic value of nuclear BAP1 protein expression. (A–C) Representative images of nuclear BAP1 protein (nBAP1) expression in primary UM (x10 magnification); insets show nBAP1 at x40 magnification. (A) nBAP1 negative tumour with focal perinuclear cBAP1. Intrinsic nuclear positivity is present in the adjacent neural retinal tissue (bottom inset). (B) Positive (left) and negative (right) nBAP1 staining in pancreas control sections. (C) nBAP1 staining in non-neoplastic uveal melanocytes. (D) nBAP1 positive UM (left) and a nBAP1 negative UM (right). (E, F) Kaplan-Meier survival curves and tables for primary UM in the Liverpool cohort stratified according to: (E) nBAP1 protein expression ($n = 165$; Log Rank, $p < 0.001$) (nBAP1 protein expression was scored as positive or negative); or (F) chromosome 3 status ($n = 152$; Log Rank, $p = 0.001$), where only cases with a discernible normal or loss of chromosome 3 were included. Number of events indicates the number of deaths due to metastatic melanoma. Log-rank tests were used to compare survival across groups. BAP1 positivity was detected using a brown chromogen in (A), (B), and (D) and a red chromogen in (C).

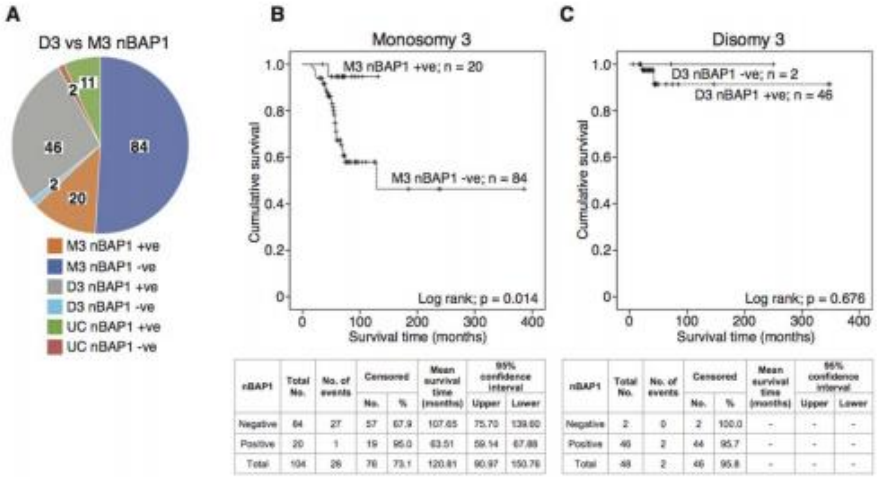

nBAP1	Total No.	No. of events	Censored		Mean survival time (months)	95% confidence interval	
			No.	%		Upper	Lower
Negative	84	27	57	67.9	107.65	75.70	139.60
Positive	20	1	19	95.0	63.51	59.14	67.88
Total	104	28	76	73.1	120.81	90.97	150.76

nBAP1	Total No.	No. of events	Censored		Mean survival time (months)	95% confidence interval	
			No.	%		Upper	Lower
Negative	2	0	2	100.0	-	-	-
Positive	46	2	44	95.7	-	-	-
Total	48	2	46	95.8	-	-	-

Figure 2. nBAP1 status contributes additional prognostic information in M3-UM patients. (A) Pie chart summarizing the breakdown of nBAP1 staining and chromosome 3 status in the Liverpool cohort of patients, $n = 165$. (B, C) Kaplan-Meier survival curves and tables estimating disease-free survival in UM patients stratified by: (B) nBAP1+ve/–ve status in monosomy 3 (M3) patients, $n = 104$ and (C) nBAP1+ve/–ve status in disomy 3 (D3) patients, $n = 48$. Number of events indicates the number of deaths due to metastatic melanoma. Log-rank tests were used to compare survival across groups.

served as intrinsic positive controls, nor was it detected in mouse IgG1 incubated negative control sections. cBAP1 localisation was recorded as 'predominantly diffuse', 'predominantly focal perinuclear', or negative. Of the127 UM examined, 68 (53.5%) were nBAP1 positive, whilst 59 (46.5%) were nBAP1 negative (Figure 3). nBAP1 positive UM demonstrated 'predominantly diffuse' cytoplasmic staining in 53/68 (77.9%) cases examined; the remaining 15/68 (22.1%) showed no detectable cBAP1 expression, with none showing the focal perinuclear phenotype.

Of particular interest were the nBAP1 negative UMs that exhibited a distinct 'focal perinuclear' cBAP1 localisation in 18/59 (31%) cases (Figure 3A,B). 'Predominantly diffuse' cBAP1 was noted in 36/59 (61%) cases and there was no detectable cBAP1 in 5/59 (8%). Overall, these results suggest that complete loss of BAP1protein expression is uncommon in UM.

Table 1. Multivariate analysis of risk factors associated with metastasis in uveal melanoma

Variable	Significance	Hazard ratio (HR)	95% CI for HR	
			Lower	Upper
nBAP1	0.006	0.212	0.070	0.645
AgePM	0.071	1.030	0.997	1.064
Chr3	0.974	1.011	0.540	1.892

AgePM, age at primary management; Chr3, Chromosome 3; nBAP1, nuclear BAP1; CI, confidence interval.

This 'focal perinuclear' cBAP1 phenotype did not significantly affect overall survival relative to predominantly diffuse or negative cBAP1 in the nBAP1 negative UM (Log rank, $p = 0.925$; Figure 3C), nor did it correlate significantly with other clinical parameters or gross chromosomal abnormalities.

To take into account possible artefacts created by fixation and processing, we further examined our cBAP1 findings using an external independent cohort of UM ($n = 14$) with available *BAP1* mutational status from the pathology archives of OSU. In keeping with the frequency of nBAP1 loss by IHC in the Liverpool cohort, 7/16 (44%) UM were nBAP1 positive and 9/16 (56%) were nBAP1 negative. All nBAP1 positive UM in this cohort had 'predominantly diffuse' cBAP1. nBAP1 negative UM showed 'focal perinuclear' cBAP1 localisation in 3/9 (33%) cases with6/9 (66%) showing 'predominantly diffuse' cBAP1 staining, again consistent with our findings above.

Golgi localisation of cytoplasmic BAP1

Our results showing "focal perinuclear" cBAP1 protein accumulation in nBAP1 negative (but not nBAP1

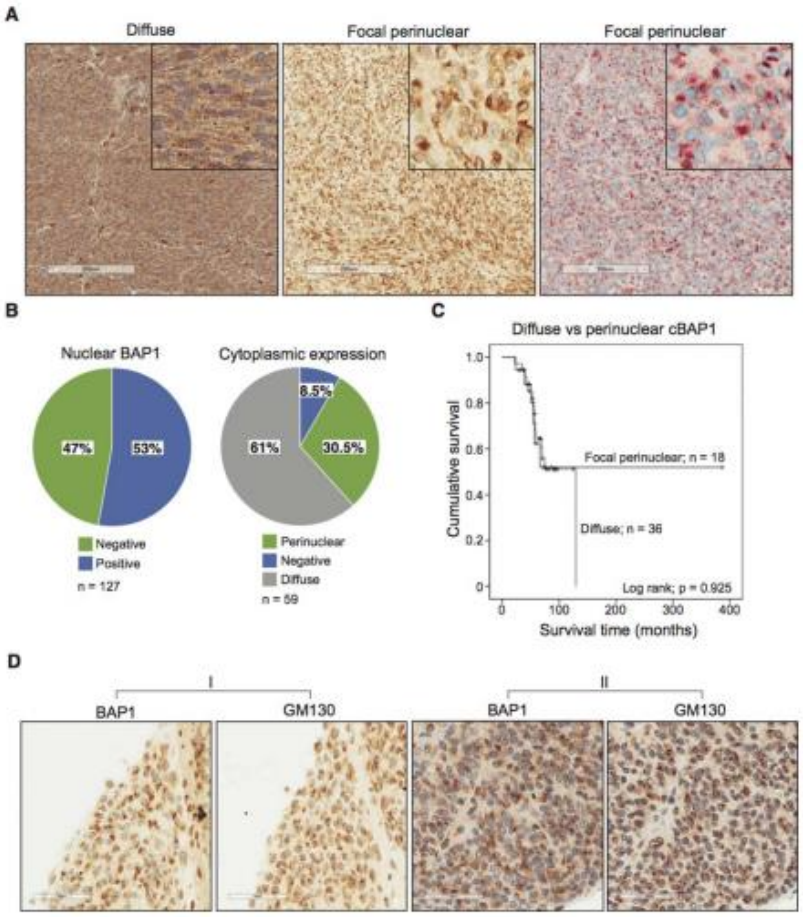

Figure 3. Cytoplasmic BAP1 exhibits differential localisation in UM. (A) Images showing either diffuse (left; DAB) or focal perinuclear (centre; DAB and right; AEC) localisation of cytoplasmic BAP1 (cBAP1) in three nBAP1 negative UM (main image and insets are at ×10 and ×40 magnification, respectively; scale bars 200 μm). (B) Pie charts summarizing the breakdown of nBAP1 expression in the 127 UMs studied (left) and cBAP1 expression in the 59 nBAP1 negative cases (right). (C) Kaplan–Meier survival curve for 54 nBAP1 negative UM patients stratified by focal perinuclear and diffuse cBAP1 staining patterns. The difference in survival was not significant (Log rank; $p = 0.925$). (D) Images showing similar localisation of focal perinuclear cBAP1 with the cis Golgi marker GM130 in 3 μm serial sections of two UM cases (I and II) (scale bars 60 μm).

positive) UM suggests that this reflects aberrant BAP1 processing and/or trafficking. We noted that the perinuclear distribution was similar to the location of the Golgi apparatus: to assess whether the cBAP1 may indeed be accumulating in the Golgi apparatus, adjacent serial UM sections were stained for BAP1 and the cis Golgi marker, GM130. Interestingly, the GM130 and cBAP1 staining profiles were very similar, indicating that BAP1 is localized near, or possibly within, the cis Golgi in these cells (Figure 3D).

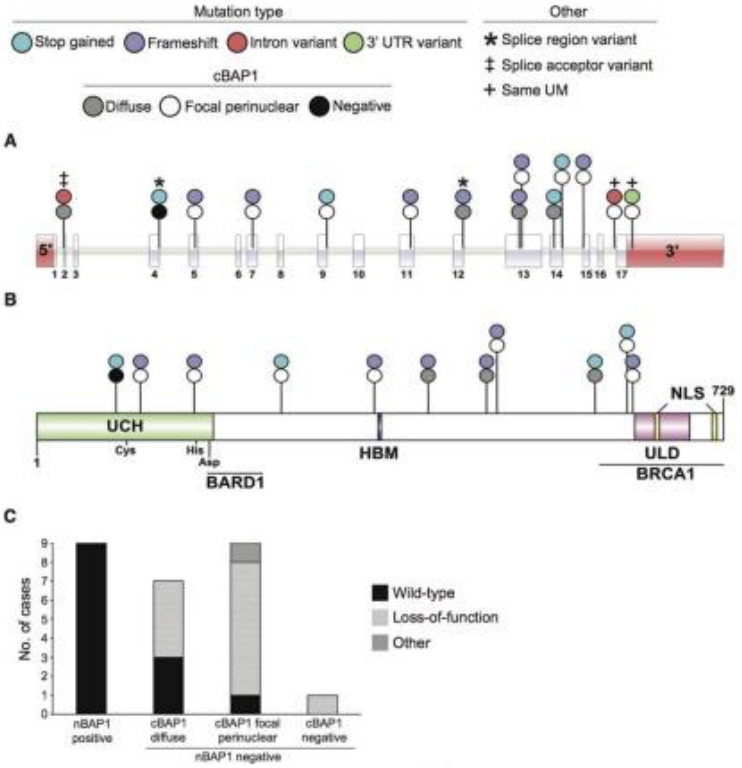

Figure 4. UMs with focal perinuclear cBAP1 tend to harbour loss-of-function *BAP1* mutations. (A) Schematic showing the location of mutations within the *BAP1* gene. 5′ and 3′ UTRs are depicted in red. One UM had two mutations flanking exon 17 (+); (B) location of the mutations shown in (A) mapped to the BAP1 protein (UCH, ubiquitin carboxy-terminal hydrolase domain; BARD1, BARD1-binding domain; HBM, HCF1-binding domain; BRCA1, BRCA1-binding domain; ULD, UCH-37-like domain; NLS, nuclear localisation signal. The location of cysteine, histidine, and aspartic acid residues of the catalytic triad are shown in the catalytic domain. (C) Histogram showing the distribution of mutation types for the nBAP1 positive, nBAP1 negative (cBAP1 diffuse), nBAP1 negative (cBAP1 focal perinuclear), and nBAP1 negative (cBAP1 negative) UMs.

BAP1 mutation analysis

As expected, all 9 nBAP1 positive UM had wild-type *BAP1*. Of the 17 nBAP1 negative cases examined, 3/7 cBAP1 diffuse UM were wild-type for *BAP1* and 1/7 harboured a splice acceptor mutation prior to exon 2, causing loss-of-function, while 3/7 had truncating, loss-of-function *BAP1* mutations (Figure 4 and supplementary material, Table S4). In contrast, 7/9 cBAP1 'focal perinuclear' UM harboured loss-of-function *BAP1* mutations. In one case, exon 17 was flanked by an intron variant and a 3′ UTR variant, the pathogenic significance of which is unclear. The remaining case was wild-type for *BAP1*. In the independent OSU cohort, 6/9 nBAP1 negative UM harboured a *BAP1* mutation, and 1/9 had a benign variant rs149499021. In the nBAP1 positive UM, 4/5 showed no mutation with only one case having the benign variant rs149499021 [40]. Of the three cases showing 'focal perinuclear' cBAP1, two had INDELs and one had a benign variant (supplementary material, Table S5).

Overall, we identified 6/25 (24%) cases in both cohorts analysed that were nBAP1 negative but did not harbour a *BAP1* mutation.

Discussion

This is the largest study to date examining BAP1 protein expression in UM by IHC. Where feasible, we have also correlated the nuclear and cytoplasmic staining patterns of BAP1with clinical features, including outcome, as well as with BAP1 sequencing data. In this study, we have demonstrated that nBAP1 protein expression is lost in 54% of UM, and that nBAP1 is a significant independent prognostic indicator, which identifies a subset of M3 UM with nBAP1 expression that have prolonged survival as compared with M3 UM that have lost nBAP1 expression. We provide evidence to suggest that the subcellular localisation of cBAP1 in nBAP1-negative UM is associated with the presence of *BAP1* mutations. That is, UM with 'focal perinuclear' cBAP1 tended to carry loss-of-function *BAP1* mutations compared to UM with diffuse cytoplasmic BAP1.

Nuclear BAP1 findings

BAP1 IHC is currently routinely performed only on surgically resected specimens in our centre. In the current study, this included tumours resected because of size, location, recurrence, secondary complications, and patient preference. Whilst we recognize that there may be a potential bias as compared with an analysis of all UM, the frequency of nBAP1 negativity in this study (54%) is consistent with that reported in the literature (43–58%) [23,38,39]. Similar to these other reports, we demonstrated a correlation between loss of nBAP1 expression and poor prognostic parameters known to be associated with 'high risk' UM – i.e. increasing age at primary management; ciliary body involvement; increasing tumour LBD; large tumour height; epithelioid cell morphology; PAS-positive connective tissue loops; and loss of chromosome 3 [6].

Previous studies have indicated that there is a strong association between the absence of nBAP1 protein expression and mutations in *BAP1* [23,39]. For example, Van de Nes *et al* demonstrated in a cohort of 66 UM that 33/37 (89%) M3 UM had a *BAP1* mutation together with an absence of nBAP1 protein expression [23]. A similar proportion was reported by Koopmans *et al* in their study of 74 UM, with 88% of the M3 UM harbouring a *BAP1* mutation together with loss of nuclear protein expression [39]. In our current study of 26 nBAP1 negative UM, 20 (77%) harboured mutations in *BAP1*, which is similar to the previous reports detailed above.

Of particular interest in our current study was the identification of a subset of M3 UM (20/104; 19%) that showed nBAP1 positivity, correlating with a significantly increased survival time as compared with the M3/nBAP1-negative UM ($p = 0.014$) (Figure 2B). Whilst the follow-up is relatively short for these 20 individuals, the data support our previous description of a patient with nBAP1 positive liver metastases who was still alive after more than 10 years post enucleation [51]. More recently, BAP1 IHC performed at our centre showed nBAP1 positivity in metastatic UM cells within the liver of a patient who is alive 37 years after diagnosis of the primary UM. This suggests that two distinct subgroups exist within UM with loss of chromosome 3: those M3 UM with a loss of *BAP1* function, and those M3 UM with a retained functional copy of *BAP1*. Indeed, three M3/nBAP1 positive cases were analysed for *BAP1* mutations and found to be wild type. These data were also reflected in the multivariate analysis where nBAP1 was found to be the only independent variable significantly associated with increased risk of developing metastatic disease. Overall, our data strongly suggest that bi-allelic inactivation of *BAP1* is required to influence prognosis; on this basis, we would predict that the loss of other genes on chromosome 3 may have little or no additional effect on prognosis in this group.

In a small number of cases, however, BAP1 loss is clearly not the metastatic driver. For example, 3/26 (12%) UM patients in our study who developed metastatic disease were found to have nBAP1 positive primary tumours. Two of these patients also had unfavourable clinical and histological characteristics, which would have placed them in the 'high risk' category for developing metastatic disease, irrespective of the tumour's nBAP1 status. These other factors included epithelioid cell morphology, high mitotic count, large tumour size, 8q gain, ciliary body involvement, and extraocular growth [3].The remaining case, however, is unusual in that it was D3 with clinical and histological features of a low metastatic risk tumour. Previous studies have suggested that D3 UM with a mutation in splicing Factor 3B Subunit 1A (*SF3B1*) have an increased risk of developing metastases [52]. Further studies are necessary to determine whether such a mutation is present in this particular case.

Other unusual cases in our patient cohort included three nBAP1 negative UM with no corresponding loss of chromosome 3. Chromosome 3 copy number for all three cases was re-examined by MSA, which is able to detect isodisomy, i.e. loss of heterozygosity due to acquisition of both copies of the chromosome from the same parent. Only one of the three cases showed isodisomy 3 by MSA. The remaining two

cases were tested for *BAP1* mutations, but were found to be wild type, suggesting alternative mechanisms of nBAP1 loss.

Cytoplasmic *BAP1* expression findings

Our study is the first to characterize cBAP1 in UM by IHC, and the first to investigate the link between cBAP1 genotype and phenotype. Our observation of 'focal perinuclear' cBAP1 localisation is consistent with a study by Gammon *et al* [43], who observed 'clumped perinuclear' cBAP1 in 53% of nBAP1 negative sporadic epithelioid Spitz tumours. They further hypothesized that 'focal perinuclear' cBAP1 may be trapped in the Golgi zone, which our experimental findings using the cis Golgi marker, GM130, would support. It should also be mentioned that mouse acites Golgi reactive (MAG) antibodies have been described in some monoclonal antibody preparations, resulting in non-specific cross reactivity with blood group A1 antigens present in patient tissues [53–55]. It is unlikely, given the prevalence of blood group A1 in the population (~35% individuals), however, that MAG antibodies are responsible for the small percentage of cases (11%) with 'focal perinuclear' positivity observed in our study. Moreover, a recent study by Bononi *et al* also described cBAP1 localisation to the endoplasmic reticulum where it regulates Ca^{2+} release to promote apoptosis [56]. In fibroblasts and mesothelial cells derived from individuals with a heterozygous germline $BAP1^{+/-}$ mutation, they demonstrated a reduced Ca^{2+} flux that reduced the ability of $BAP1^{+/-}$ mutant cells to undergo apoptosis following DNA damage. Taken together, these results suggest that there is indeed a functional role of cBAP1 in particular cancer types requiring further study.

The preponderance of UM with 'focal perinuclear' cBAP1 that harbour truncating mutations is of interest as one might assume that mutations causing premature stop codons would trigger nonsense-mediated decay of the aberrant transcript, so that incorrect protein is not produced. One possibility, however, is that the UM cells bypass the premature stop codon by using alternative splice sites [57] and/or read-through translation [58] to generate misfolded proteins that are not able to exit the Golgi following processing. Consistent with this, Jensen *et al*, who first described BAP1, identified a number of putative N-linked BAP1 glycosylation sites, suggesting that BAP1 may traverse the Golgi during maturation [30]. Bhattacharya and colleagues [59] suggested an alternative mechanism for the observation of 'focal perinuclear' cBAP1 in the form of cBAP1 aggregates promoted by *BAP1* mutations, which expose hydrophobic regions of the protein, leading to beta amyloid aggregation. However, their study proposed that specific mis-sense mutations in the catalytic domain were responsible for the observed aggregation, whereas our sequencing results suggest that sporadic truncating mutations throughout *BAP1* can induce the 'focal perinuclear' phenotype. Further studies of the molecular biology of the focal perinuclear phenotype will be warranted.

Our results identifying six nBAP1 negative UM with wild-type *BAP1* is consistent with reports by van de Nes *et al* [23] and Royer-Bertrand *et al* [12], in which five and three cases, respectively, with this phenotype/genotype were described. It is tempting to speculate that a post-translational mechanism, perhaps in the form of UBE2O upregulation, could be responsible for the aberrant cytoplasmic localisation of BAP1 in these cases. The putative E2/E3 hybrid ubiquitin ligase, UBE2O, has been reported to mediate cytoplasmic translocation of BAP1 by multimonoubiquitylation of the NLS. Auto-deubiquitylation by BAP1 antagonizes the activity of UBE2O, promoting its nuclear retention [44].

Finally, whilst our study found no link between cBAP1 expression and overall survival (Log rank; $p = 0.33$), it is of interest that Zhang *et al* [60] found that high expression of cBAP1 in gliomas was significantly associated with worse overall survival compared to low cBAP1 expression, although there was no mention of any specific localisation of the cBAP1 in this study. A larger cohort of UM with a longer follow-up period is required to ascertain whether a dose-dependent effect of cBAP1 is of clinical relevance.

In summary, we have demonstrated the importance of nBAP1 protein expression as an independent marker of prognosis in patients with UM and that identifies a subpopulation of M3 tumours with favourable survival times compared to their nBAP1-negative counterparts. We also report that exclusion of BAP1 protein from the nucleus is most commonly associated with retention of cBAP1. The molecular mechanisms underpinning 'focal perinuclear' cBAP1 remain unknown, and warrant further study.

Acknowledgements

We thank Mr Simon Biddolph of the NHS Cellular Pathology Department of the Royal Liverpool University Hospital for his meticulous preparation of the FFPE UM sections. We thank also Drs Annelies de Klein and Kyra Smit of the Rotterdam Ocular Melanoma Study Group for their expert sequencing of our UM samples,

as well as Dr Xuan Liu of the Centre for Genomics Research, University of Liverpool, for his generous help with identifying and annotating SNP variants. In addition, we express our gratitude to Dr Michael Marcus, Institute of Translational Medicine, University of Liverpool, for providing his expertise and statistical support.

Finally, we would like to acknowledge funding from Fight for Sight UK (1497/98) and from the Eye Tumour Research Fund, RLBUHT, who are funding the PhD studentships of Neil Farquhar and Sophie Thornton, respectively. Colleen Cebulla is supported by NEI Award Number K08EY022672. The content is solely the responsibility of the authors and does not necessarily represent the official views of the funding institutions. Additional funds were provided by the Ohio Lions Eye Research Foundation and the Patti Blow Fund.

Author contributions statement

NF, ST, SEC, JC, JJS, HK: design of study; NF, ST, YK, CC, MHAR: undertaking the IHC experiments; HH, CC, MHAR: patient care/contribution of patient samples; NF, ST, SEC, HK: evaluation of IHC; ST: undertaking of MLPA/MSA; NF, MHAR: evaluation of sequencing results; AT, NF, ST, HK: evaluation of laboratory data with clinical data and outcomes; All authors: Interpretation of results; All authors: manuscript writing; All authors: critical review of the manuscript.

References

1. Virgili G, Gatta G, Ciccolallo L, *et al*. Incidence of uveal melanoma in Europe. *Ophthalmology* 2007; **114:** 2309–2315.
2. Yonekawa Y, Kim IK, Damato B. Epidemiology and management of uveal melanoma. *Hematol Oncol Clin North Am* 2012; **26:** 1169–1184.
3. Damato B. Progress in the management of patients with uveal melanoma. The 2012 Ashton Lecture. *Eye (Lond)* 2012; **26:** 1157–1172.
4. Carvajal RD, Schwartz GK, Tezel T, *et al*. Metastatic disease from uveal melanoma: treatment options and future prospects. *Br J Ophthalmol* 2017; **101:** 38–44.
5. Woodman SE. Metastatic uveal melanoma: biology and emerging treatments. *Cancer J* 2012; **18:** 148–152.
6. Damato B, Eleuteri A, Taktak AFG, Coupland SE. Estimating prognosis for survival after treatment of choroidal melanoma. *Prog Retin Eye Res* 2011; **30:** 285–295.
7. DeParis SW, Taktak A, Eleuteri A, *et al*. External validation of the Liverpool uveal melanoma prognosticator online. *Invest Ophthalmol Vis Sci* 2016; **57:** 6116–6122.
8. Caines R, Eleuteri A, Kalirai H, *et al*. Cluster analysis of multiplex ligation-dependent probe amplification data in choroidal melanoma. *Mol Vis* 2015; **21:** 1–11.
9. Damato B, Duke C, Coupland SE, *et al*. Cytogenetics of uveal melanoma: a 7-year clinical experience. *Ophthalmology* 2007; **114:** 1925–1931.
10. Prescher G, Bornfeld N, Hirche H, *et al*. Prognostic implications of monosomy 3 in uveal melanoma. *Lancet* 1996; **347:** 1222–1225.
11. Robertson AG, Shih J, Yau C, *et al*. Integrative analysis identifies four molecular and clinical subsets in uveal melanoma. *Cancer Cell* 2017; **32:** 204–220.
12. Royer-Bertrand B, Torsello M, Rimoldi D, *et al*. Comprehensive genetic landscape of uveal melanoma by whole-genome sequencing. *Am J Hum Genet* 2016; **99:** 1190–1198.
13. Horsman DE, Sroka H, Rootman J, *et al*. Monosomy 3 and isochromosome 8q in a uveal melanoma. *Cancer Genet Cytogenet* 1990; **45:** 249–253.
14. Sisley K, Cottam DW, Rennie IG, *et al*. Non-random abnormalities of chromosomes 3, 6, and 8 associated with posterior uveal melanoma. *Genes, Chromosomes Cancer* 1992; **5:** 197–200.
15. Kilic E, Naus NC, van Gils W, *et al*. Concurrent loss of chromosome arm 1p and chromosome 3 predicts a decreased disease-free survival in uveal melanoma patients. *Invest Ophthalmol Vis Sci* 2005; **46:** 2253–2257.
16. Damato B, Dopierala J, Klaasen A, *et al*. Multiplex ligation-dependent probe amplification of uveal melanoma: correlation with metastatic death. *Invest Ophthalmol Vis Sci* 2009; **50:** 3048–3055.
17. Häusler T, Stang A, Anastassiou G, *et al*. Loss of heterozygosity of 1p in uveal melanomas with monosomy 3. *Int J Cancer* 2005; **116:** 909–913.
18. Dono M, Angelini G, Cecconi M, *et al*. Mutation frequencies of GNAQ, GNA11, BAP1, SF3B1, EIF1AX and TERT in uveal melanoma: detection of an activating mutation in the TERT gene promoter in a single case of uveal melanoma. *Br J Cancer* 2014; **110:** 1058–1065.
19. Harbour JW, Onken MD, Roberson EDO, *et al*. Frequent mutation of BAP1 in metastasizing uveal melanomas. *Science* 2010; **330:** 1410–1413.
20. Martin M, Maßhöfer L, Temming P, *et al*. Exome sequencing identifies recurrent somatic mutations in EIF1AX and SF3B1 in uveal melanoma with disomy 3. *Nat Genet* 2013; **45:** 933–936.
21. Van Raamsdonk CD, Bezrookove V, Green G, *et al*. Frequent somatic mutations of GNAQ in uveal melanoma and blue naevi. *Nature* 2009; **457:** 599–602.
22. Van Raamsdonk CD, Griewank KG, Crosby MB, *et al*. Mutations in GNA11 in uveal melanoma. *N Engl J Med* 2010; **363:** 2191–2199.
23. van de Nes JAP, Nelles J, Kreis S, *et al*. Comparing the prognostic value of BAP1 mutation pattern, chromosome 3 status, and BAP1 immunohistochemistry in uveal melanoma. *Am J Surg Pathol* 2016; **40:** 796–805.
24. van Essen TH, van Pelt SI, Versluis M, *et al*. Prognostic parameters in uveal melanoma and their association with BAP1 expression. *Br J Ophthalmol* 2014; **98:** 1738–1743.
25. Cancer Genome Atlas Research Network. Comprehensive molecular characterization of clear cell renal cell carcinoma. *Nature* 2013; **499:** 43–49.

26. Al-Shamsi HO, Anand D, Shroff RT, *et al*. BRCA-associated protein 1 mutant cholangiocarcinoma: an aggressive disease subtype. *J Gastrointest Oncol* 2016; **7:** 556–561.
27. Righi L, Duregon E, Vatrano S, *et al*. BRCA1-associated protein 1 (BAP1) immunohistochemical expression as a diagnostic tool in malignant pleural mesothelioma classification: a large retrospective study. *J Thorac Oncol* 2016; **11:** 2006–2017.
28. Rai K, Pilarski R, Boru G, *et al*. Germline BAP1 alterations in familial uveal melanoma. *Genes Chromosomes Cancer* 2017; **56:** 168–174.
29. Rai K, Pilarski R, Cebulla CM, *et al*. Comprehensive review of BAP1 tumor predisposition syndrome with report of two new cases. *Clin Genet* 2016; **89:** 285–294.
30. Jensen DE, Proctor M, Marquis ST, *et al*. BAP1: a novel ubiquitin hydrolase which binds to the BRCA1 RING finger and enhances BRCA1-mediated cell growth suppression. *Oncogene* 1998; **16:** 1097–1112.
31. Misaghi S, Ottosen S, Izrael-Tomasevic A, *et al*. Association of C-terminal ubiquitin hydrolase BRCA1-associated protein 1 with cell cycle regulator host cell factor 1. *Mol Cell Biol* 2009; **29:** 2181–2192.
32. Nishikawa H, Wu W, Koike A, *et al*. BRCA1-associated protein 1 interferes with BRCA1/BARD1 RING heterodimer activity. *Cancer Res* 2009; **69:** 111–119.
33. Eletr ZM, Wilkinson KD. An emerging model for BAP1's role in regulating cell cycle progression. *Cell Biochem Biophys* 2011; **60:** 3–11.
34. Ismail IH, Davidson R, Gagne J-P, *et al*. Germline mutations in BAP1 impair its function in DNA double-strand break repair. *Cancer Res* 2014; **74:** 4282–4294.
35. Yu H, Mashtalir N, Daou S, *et al*. The ubiquitin carboxyl hydrolase BAP1 forms a ternary complex with YY1 and HCF-1 and is a critical regulator of gene expression. *Mol Cell Biol* 2010; **30:** 5071–5085.
36. Sahtoe DD, van Dijk WJ, Ekkebus R, *et al*. BAP1/ASXL1 recruitment and activation for H2A deubiquitination. *Nat Commun* 2016; **7:** 10292.
37. Machida YJ, Machida Y, Vashisht AA, *et al*. The deubiquitinating enzyme BAP1 regulates cell growth via interaction with HCF-1. *J Biol Chem* 2009; **284:** 34179–34188.
38. Kalirai H, Dodson A, Faqir S, *et al*. Lack of BAP1 protein expression in uveal melanoma is associated with increased metastatic risk and has utility in routine prognostic testing. *Br J Cancer* 2014; **111:** 1373–1380.
39. Koopmans AE, Verdijk RM, Brouwer RWW, *et al*. Clinical significance of immunohistochemistry for detection of BAP1 mutations in uveal melanoma. *Mod Pathol* 2014; **27:** 1321–1330.
40. Pilarski R, Cebulla CM, Massengill JB, *et al*. Expanding the clinical phenotype of hereditary BAP1 cancer predisposition syndrome, reporting three new cases. *Genes Chromosomes Cancer* 2014; **53:** 177–182.
41. Piris A, Mihm MC Jr, Hoang MP. BAP1 and BRAFV600E expression in benign and malignant melanocytic proliferations. *Hum Pathol* 2015; **46:** 239–245.
42. Testa JR, Cheung M, Pei J, *et al*. Germline BAP1 mutations predispose to malignant mesothelioma. *Nat Genet* 2011; **43:** 1022–1025.
43. Gammon B, Traczyk TN, Gerami P. Clumped perinuclear BAP1 expression is a frequent finding in sporadic epithelioid Spitz tumors. *J Cutan Pathol* 2013; **40:** 538–542.
44. Mashtalir N, Daou S, Barbour H, *et al*. Autodeubiquitination protects the tumor suppressor BAP1 from cytoplasmic sequestration mediated by the atypical ubiquitin ligase UBE2O. *Mol Cell* 2014; **54:** 392–406.
45. Hakiri S, Osada H, Ishiguro F, *et al*. Functional differences between wild-type and mutant-type BRCA1-associated protein 1 tumor suppressor against malignant mesothelioma cells. *Cancer Sci* 2015; **106:** 990–999.
46. Abdel-Rahman MH, Cebulla CM, Verma V, *et al*. Monosomy 3 status of uveal melanoma metastases is associated with rapidly progressive tumors and short survival. *Exp Eye Res* 2012; **100:** 26–31.
47. Lake SL, Kalirai H, Dopierala J, *et al*. Comparison of formalin-fixed and snap-frozen samples analyzed by multiplex ligation-dependent probe amplification for prognostic testing in uveal melanoma. *Invest Ophthalmol Vis Sci* 2012; **53:** 2647–2652.
48. Dopierala J, Damato BE, Lake SL, *et al*. Genetic heterogeneity in uveal melanoma assessed by multiplex ligation-dependent probe amplification. *Invest Ophthalmol Vis Sci* 2010; **51:** 4898–4905.
49. Tschentscher F, Prescher G, Horsman DE, *et al*. Partial deletions of the long and short arm of chromosome 3 point to two tumor suppressor genes in uveal melanoma. *Cancer Res* 2001; **61:** 3439–3442.
50. Abdel-Rahman MH, Pilarski R, Cebulla CM, *et al*. Germline BAP1 mutation predisposes to uveal melanoma, lung adenocarcinoma, meningioma, and other cancers. *J Med Genet* 2011; **48:** 856–859.
51. McCarthy C, Kalirai H, Lake SL, *et al*. Insights into genetic alterations of liver metastases from uveal melanoma. *Pigment Cell Melanoma Res* 2016; **29:** 60–67.
52. Yavuzyigitoglu S, Koopmans AE, Verdijk RM, *et al*. Uveal melanomas with SF3B1 mutations: a distinct subclass associated with late-onset metastases. *Ophthalmology* 2016; **123:** 1118–1128.
53. Finstad CL, Yin BW, Gordon CM, *et al*. Some monoclonal antibody reagents (C219 and JSB-1) to P-glycoprotein contain antibodies to blood group A carbohydrate determinants: a problem of quality control for immunohistochemical analysis. *J Histochem Cytochem* 1991; **39:** 1603–1610.
54. Kliman HJ, Feinberg RF, Schwartz LB, *et al*. A mucin-like glycoprotein identified by MAG (mouse ascites Golgi) antibodies. Menstrual cycle-dependent localization in human endometrium. *Am J Pathol* 1995; **146:** 166–181.
55. Ouwendijk WJD, Flowerdew SE, Wick D, *et al*. Immunohistochemical detection of intra-neuronal VZV proteins in snap-frozen human ganglia is confounded by antibodies directed against blood group A1-associated antigens. *J Neurovirol* 2012; **18:** 172–180.
56. Bononi A, Giorgi C, Patergnani S, *et al*. BAP1 regulates IP3R3-mediated Ca2+ flux to mitochondria suppressing cell transformation. *Nature* 2017; **546:** 549–553.
57. Dvinge H, Kim E, Abdel-Wahab O, *et al*. RNA splicing factors as oncoproteins and tumour suppressors. *Nat Rev Cancer* 2016; **16:** 413–430.

58. Schueren F, Thoms S, Brosius J. Functional translational readthrough: a systems biology perspective. *PLoS Genet* 2016; **12:** e1006196.
59. Bhattacharya S, Hanpude P, Maiti TK. Cancer associated missense mutations in BAP1 catalytic domain induce amyloidogenic aggregation: a new insight in enzymatic inactivation. *Sci Rep* 2016; **5:** 18462.
60. Zhang X-K, Xi S-Y, Sai KE, *et al*. Cytoplasmic expression of BAP1 as an independent prognostic biomarker for patients with gliomas. *Int J Clin Exp Pathol* 2015; **8:** 5035–5043.

SUPPLEMENTARY MATERIAL ONLINE

Table S1. Association between nBAP1 status and clinical and pathological risk factors in the Liverpool uveal melanoma cohort

Table S2. Association between nBAP1 status and genetic factors in the Liverpool uveal melanoma cohort

Table S3. Univariate analysis of risk factors associated with metastatic disease in uveal melanoma

Table S4. Mutation results from the Liverpool Ocular Oncology Centre cohort

Table S5. Mutation results from the Ohio cohort

Appendix 6

Mod Pathol. 2018 May;31(5):763-771. doi: 10.1038/modpathol.2017.187. Epub 2018 Jan 12.

Combined mutation and copy-number variation detection by targeted next-generation sequencing in uveal melanoma.

Smit KN[1,2], van Poppelen NM[1,2], Vaarwater J[1], Verdijk R[3], van Marion R[3], Kalirai H[4], Coupland SE[4], Thornton S[4], Farquhar N[4], Dubbink HJ[3], Paridaens D[5], de Klein A[2], Kiliç E[1].

PMID: 29327717

Appendix 7

	A	B	C	D	E	F	G	H	I	J	K	L	M
1			Pancreas Normal Control		Testis Normal Control	Colon Normal Control		PUMS114.14 G_{11} mt	PUMS145.14 G_{11} mt	PUMS082.14 G_q mt	Conj Mel BRAF mt G_q/ G_{11}wt	PUMS006.15 G_q mt	PUMS066.14 G_q mt
2	PUMS111.14 G_q mt	PUMS154.14 wt	PUMS044.14 G_q mt	PUMS035.15 G_q mt	PUMS183.14 G_q mt	PUMS181.14 G_{11} mt	PUMS009.15 G_{11} mt	PUMS144.14 G_{11} mt	PUMS056.14 G_{11} mt	PUMS090.14 G_q mt	PUMS075.14 G_{11} mt	PUMS106.14 G_{11} mt	
3		PUMS114.14 G_{11} mt	PUMS145.14 G_{11} mt	PUMS082.14 G_q mt	Conj Mel BRAF mt G_q/ G_{11}wt	PUMS006.15 G_q mt	PUMS066.14 G_q mt	PUMS111.14 G_q mt	PUMS154.14 wt	PUMS044.14 G_q mt	PUMS035.15 G_q mt	PUMS183.14 G_q mt	
4	PUMS181.14 G_{11} mt	PUMS009.15 G_{11} mt	PUMS144.14 G_{11} mt	PUMS056.14 G_{11} mt	PUMS090.14 G_q mt	PUMS075.14 G_{11} mt	PUMS106.14 G_{11} mt	PUMS114.14 G_{11} mt	PUMS145.14 G_{11} mt	PUMS082.14 G_q mt	Conj Mel BRAF mt G_q/ G_{11}wt	PUMS006.15 G_q mt	PUMS066.14 G_q mt
5		PUMS111.14 G_q mt	PUMS154.14 wt	PUMS044.14 G_q mt	PUMS035.15 G_q mt	PUMS183.14 G_q mt	PUMS181.14 G_{11} mt	PUMS009.15 G_{11} mt		Gallbladder Normal Control			
6	PUMS144.14 G_{11} mt	PUMS056.14 G_{11} mt	PUMS090.14 G_q mt	PUMS075.14 G_{11} mt	PUMS106.14 G_{11} mt		Gallbladder Normal Control		Pancreas Normal Control		Testis Normal Control	Colon Normal Control	

REFERENCES

1. Coupland SE, Lake SL, Zeschnigk M, Damato BE. Molecular pathology of uveal melanoma. Eye. 2013;27(2):230-42.
2. Hu DN, McCormick SA, Schneider S, Finger PT, Yu GP. Population-based incidence of uveal melanoma in various races and ethnic groups. American Journal of Ophthalmology. 2005;140(4):612.e1-.e8.
3. Carbone M, Baumann F, Napolitano A, Lum CA, Flores EG, Gaudino G, et al. BAP1 cancer syndrome: malignant mesothelioma, uveal and cutaneous melanoma, and MBAITs. Journal of Translational Medicine. 2012;10(1).
4. Van Hees CLM, De Boer A, Jager MJ, Bleeker JC, Kakebeeke HM, Crijns MB, et al. Are atypical nevi a risk factor for uveal melanoma? A case-control study. Journal of Investigative Dermatology. 1994;103(2):202-5.
5. Abdel-Rahman MH, Pilarski R, Cebulla CM, Massengill JB, Christopher BN, Boru G, et al. Germline BAP1 mutation predisposes to uveal melanoma, lung adenocarcinoma, meningioma, and other cancers. Journal Of Medical Genetics. 2011;48(12):856-9.
6. Rietschel P, Panageas KS, Hanlon C, Patel A, Abramson DH, Chapman PB. Variates of survival in metastatic uveal melanoma. Journal of Clinical Oncology. 2005;23(31):8076-80.
7. Damato BE, Coupland SE. Ocular melanoma. Saudi Journal of Ophthalmology. 2012;26(2):137-44.
8. Damato EM, Damato BE. Detection and time to treatment of uveal melanoma in the United Kingdom: an evaluation of 2,384 patients. Ophthalmology. 2012;119(8):1582-9.
9. Damato EM, Damato BE. Original article: Detection and Time to Treatment of Uveal Melanoma in the United Kingdom: An Evaluation of 2384 Patients. Ophthalmology. 2012;119:1582-9.
10. Damato B. Does ocular treatment of uveal melanoma influence survival? British Journal of Cancer. 2010;103(3):285-90.
11. Shields CL, Shields JA, Kiratli H, De Potter P, Cater JR. Risk factors for growth and metastasis of small choroidal melanocytic lesions. Ophthalmology. 1995;102(9):1351-61.
12. Shields CL, Furuta M, Berman EL, Zahler JD, Hoberman DM, Dinh DH, et al. Choroidal nevus transformation into melanoma: Analysis of 2514 consecutive cases. Archives of Ophthalmology. 2009;127(8):981-7.
13. Damato B. Developments in the management of uveal melanoma. Clinical and Experimental Ophthalmology. 2004;32(6):639-47.
14. Lommatzsch PK. Results after beta-irradiation (106Ru/106Rh) of choroidal melanomas: 20 years' experience. British Journal of Ophthalmology. 1986;70(11):844.
15. Bergman L, Nilsson B, Lundell G, Lundell M, Seregard S. Original article: Ruthenium Brachytherapy for Uveal Melanoma, 1979–2003. Survival and Functional Outcomes in the Swedish Population. Ophthalmology. 2005;112:834-40.
16. Shields CL, Shields JA, Cater J, Gündüz K, Miyamoto C, Micaily B, et al. Plaque radiotherapy for uveal melanoma: Long-term visual outcome in 1106 consecutive patients. Archives of Ophthalmology. 2000;118(9):1219-28.

17. Dienerwest M, Hawkins BS, Fine SL, Earle JD, Straatsma BR, Mowery RL. DESIGN AND METHODS OF A CLINICAL-TRIAL FOR A RARE CONDITION - THE COLLABORATIVE OCULAR MELANOMA STUDY - COMS REPORT NO 3.
18. Damato B, Patel I, Campbell IR, Mayles HM, Errington RD. Local tumor control after 106Ru brachytherapy of choroidal melanoma. International Journal Of Radiation Oncology, Biology, Physics. 2005;63(2):385-91.
19. Bianciotto C, Shields CL, Pirondini C, Mashayekhi A, Furuta M, Shields JA. Proliferative Radiation Retinopathy after Plaque Radiotherapy for Uveal Melanoma. Ophthalmology. 2010;117(5):1005-12.
20. Bianciotto C, Shields CL, Mashayekhi A, Furuta M, Shields JA, Pirondini C. Vitreous hemorrhage after plaque radiotherapy for uveal melanoma. Retina. 2012;32(6):1156-64.
21. Finger PT, Chin KJ, Patel NS, Yu GP. Risk factors for cataract after palladium-103 ophthalmic plaque radiation therapy. International Journal of Radiation Oncology Biology Physics. 2011;80(3):800-6.
22. Gündüz K, Shields CL, Shields JA, Cater J, Freire JE, Brady LW. Plaque radiotherapy of uveal melanoma with predominant ciliary body involvement. Archives of Ophthalmology. 1999;117(2):170-7.
23. Finger PT, Chin KJ. Intravitreous ranibizumab (lucentis) for radiation maculopathy. Archives of Ophthalmology. 2010;128(2):249-52.
24. Summanen P, Immonen I, Kivelä T, Tommila P, Heikkonen J, Tarkkanen A. Radiation related complications after ruthenium plaque radiotherapy of uveal melanoma. The British Journal Of Ophthalmology. 1996;80(8):732-9.
25. Schlienger P, Habrand JL, Schwartz L, Desjardins L, d'Hermies F, Frau E, et al. Initial results with one-year minimum follow-up of the first 146 patients with a uveal melanoma treated with protons at CPO (Orsay). Bulletin du cancer Radiotherapie : journal de la Societe francaise du cancer : organe de la societe francaise de radiotherapie oncologique. 1996;83 Suppl:212s-4s.
26. Lumbroso L, Levy C, Plancher C, Frau E, D'Hermies F, Schlienger P, et al. [Results of proton beam irradiation for treatment of choroidal melanoma]. Journal francais d'ophtalmologie. 2002;25(3):290-7.
27. Macdonald ECA, Cauchi P, Kemp EG. Proton beam therapy for the treatment of uveal melanoma in Scotland.
28. Seddon JM, Gragoudas ES, Egan KM, Glynn RJ, Munzenrider JE, Austin-Seymour M, et al. Uveal melanomas near the optic disc or fovea. Visual results after proton beam irradiation. Ophthalmology. 1987;94(4):354-61.
29. Gragoudas ES, Lane AM, Regan S, Li W, Judge HE, Seddon JM, et al. A randomized controlled trial of varying radiation doses in the treatment of choroidal melanoma. Archives of Ophthalmology. 2000;118(6):773-8.
30. Damato B, Heimann H, Kacperek A, Errington D. Proton beam radiotherapy of uveal melanoma. Saudi Journal of Ophthalmology. 2013;27(3):151-7.
31. Egger E, Zografos L, Schalenbourg A, Beati D, Bhringer T, Chamot L, et al. Clinical investigation: eye: Eye retention after proton beam radiotherapy for uveal melanoma. International Journal of Radiation Oncology, Biology, Physics. 2003;55:867-80.
32. Dendale R, Mazal A, Mammar H, Schlienger P, Lumbroso-Le Rouic L, Levy C, et al. Proton beam radiotherapy for uveal melanoma: Results of Curie Institut-Orsay Proton Therapy Center (ICPO). International Journal of Radiation Oncology Biology Physics. 2006;65(3):780-7.

33. Guyer DR, Mukai S, Egan KM, Seddon JM, Walsh SM, Gragoudas ES. Radiation maculopathy after proton beam irradiation for choroidal melanoma. Ophthalmology. 1992;99(8):1278-85.
34. Kim IK, Lane AM, Egan KM, Munzenrider J, Gragoudas ES. Natural history of radiation papillopathy after proton beam irradiation of parapapillary melanoma. Ophthalmology. 2010;117(8):1617-22.
35. Mishra KK, Daftari IK, Weinberg V, Cole T, Quivey JM, Castro JR, et al. Risk factors for neovascular glaucoma after proton beam therapy of uveal melanoma: a detailed analysis of tumor and dose-volume parameters. Int J Radiat Oncol Biol Phys. 2013;87(2):330-6.
36. Damato B, Kacperek A, Chopra M, Sheen MA, Campbell IR, Errington RD. Proton beam radiotherapy of iris melanoma. Int J Radiat Oncol Biol Phys. 2005;63(1):109-15.
37. Gailloud C, Zografos L, Uffer S, Egger E. [Uveal melanomas and vitreous hemorrhage. Diagnosis and treatment]. Klinische Monatsblatter fur Augenheilkunde. 1991;198(5):365-70.
38. Lumbroso L, Desjardins L, Levy C, Plancher C, Asselain B, Frau E, et al. Intraocular inflammation after proton beam irradiation for uveal melanoma. British Journal of Ophthalmology. 2001;85(11):1305-8.
39. Konstantinidis L, Roberts D, Errington RD, Kacperek A, Heimann H, Damato B. Transpalpebral proton beam radiotherapy of choroidal melanoma. Br J Ophthalmol. 2015;99(2):232-5.
40. Foulds WS. The local excision of choroidal melanomata. Transactions of the ophthalmological societies of the United Kingdom. 1973;93(0):343-6.
41. Foulds W. Techniques for the Local Excision of Choroidal Melanomas. In: Deutman AF, editor. New Developments in Ophthalmology Nijmegen 16–18 October 1975. Documenta Ophthalmologica Proceedings Series. 7: Springer Netherlands; 1976. p. 237-40.
42. Damato B. Adjunctive Plaque Radiotherapy after Local Resection of Uveal Melanoma. In: Meyer JL, Vaeth JM, editors. Frontiers of Radiation Therapy and Oncology. Radiotherapy of Ocular Disease: Karger; 1997. p. p 123 - 32.
43. Damato B, Foulds WS. Indications for trans-scleral local resection of uveal melanoma. The British Journal Of Ophthalmology. 1996;80(11):1029-30.
44. Konstantinidis L, Groenewald C, Coupland SE, Damato B. Trans-scleral local resection of toxic choroidal melanoma after proton beam radiotherapy. British Journal of Ophthalmology. 2014;98(6):775-9.
45. Foulds WS, Damato BE, Burton RL. Local resection versus enucleation in the management of choroidal melanoma. Eye (London, England). 1987;1 (Pt 6):676-9.
46. Damato BE, Foulds WS, Paul J. Risk factors for metastatic uveal melanoma after trans-scleral local resection. British Journal of Ophthalmology. 1996;80(2):109-16.
47. Bechrakis NE, Bornfeld N, Zoller I, Foerster MH. Iodine 125 plaque brachytherapy versus transscleral tumor resection in the treatment of large uveal melanomas. Ophthalmology. 2002;109(10):1855-61.
48. Puusaari I, Damato B, Kivela T. Transscleral local resection versus iodine brachytherapy for uveal melanomas that are large because of tumour height. Graefe's archive for clinical and experimental ophthalmology = Albrecht von Graefes Archiv fur klinische und experimentelle Ophthalmologie. 2007;245(4):522-33.
49. Damato BE, Paul J, Foulds WS. Risk factors for residual and recurrent uveal melanoma after trans-scleral local resection. Br J Ophthalmol. 1996;80(2):102-8.

50. Damato B, Groenewald CP, McGalliard JN, Wong D. Rhegmatogenous retinal detachment after transscleral local resection of choroidal melanoma. Ophthalmology. 2002;109(11):2137-43.
51. Damato B, Groenewald C, McGalliard J, Wong D. Endoresection of choroidal melanoma. Br J Ophthalmol. 1998;82(3):213-8.
52. Peyman GA, Juarez CP, Diamond JG, Raichand M. Ten years experience with eye wall resection for uveal malignant melanomas. Ophthalmology. 1984;91(12):1720-5.
53. Peyman GA, Charles H. Internal eye wall resection in the management of uveal melanoma. Canadian journal of ophthalmology Journal canadien d'ophtalmologie. 1988;23(5):218-23.
54. Garcia-Arumi J, Sararols L, Martinez V, Corcostegui B. Vitreoretinal surgery and endoresection in high posterior choroidal melanomas. Retina. 2001;21(5):445-52.
55. McCannel TA. Post-brachytherapy tumor endoresection for treatment of toxic maculopathy in choroidal melanoma. Eye (London, England). 2013;27(8):984-8.
56. Konstantinidis L, Groenewald C, Coupland SE, Damato B. Long-term outcome of primary endoresection of choroidal melanoma. Br J Ophthalmol. 2014;98(1):82-5.
57. Karkhaneh R, Chams H, Amoli FA, Riazi-Esfahani M, Ahmadabadi MN, Mansouri MR, et al. Long-term surgical outcome of posterior choroidal melanoma treated by endoresection. Retina. 2007;27(7):908-14.
58. Joussen AM, Wong D. Egress of large quantities of heavy liquids from exposed choroid: a route for possible tumor dissemination via vortex veins in endoresection of choroidal melanoma. Graefe's archive for clinical and experimental ophthalmology = Albrecht von Graefes Archiv fur klinische und experimentelle Ophthalmologie. 2015;253(2):177-8.
59. Garcia-Arumi J, Zapata MA, Balaguer O, Fonollosa A, Boixadera A, Martinez-Castillo V. Endoresection in high posterior choroidal melanomas: long-term outcome. Br J Ophthalmol. 2008;92(8):1040-5.
60. Shields JA, Shields CL, Donoso LA. Management of posterior uveal melanoma. Survey of ophthalmology. 1991;36(3):161-95.
61. De Potter P, Shields CL, Shields JA. New treatment modalities for uveal melanoma. Current opinion in ophthalmology. 1996;7(3):27-32.
62. Wright PK, Damato BE. Auditing outcomes after treatment of Scottish patients with uveal melanoma in Liverpool. Journal of the Royal College of Surgeons of Edinburgh. 1999;44(4):260-4.
63. Shields CL, Shields JA, Karlsson U, Markoe AM, Brady LW. Reasons for enucleation after plaque radiotherapy for posterior uveal melanoma. Clinical findings. Ophthalmology. 1989;96(6):919-23; discussion 24.
64. Zimmerman LE, McLean IW, Foster WD. Does enucleation of the eye containing a malignant melanoma prevent or accelerate the dissemination of tumour cells? British Journal of Ophthalmology. 1978;62(6):420-5.
65. Manschot WA, Van Strik R. Is irradiation a justifiable treatment of choroidal melanoma? Analysis of published results. British Journal of Ophthalmology. 1987;71(5):348-52.
66. Earle JD. Results from the Collaborative Ocular Melanoma Study (COMS) of enucleation versus preoperative radiation therapy in the management of large ocular melanomas. Int J Radiat Oncol Biol Phys. 1999;43(5):1168-9.
67. Jakobiec FA, Coleman DJ, Chattock A, Smith M. Ultrasonically guided needle biopsy and cytologic diagnosis of solid intraocular tumors. Ophthalmology. 1979;86(9):1662-81.

68. Naus NC, Verhoeven AC, van Drunen E, Slater R, Mooy CM, Paridaens DA, et al. Detection of genetic prognostic markers in uveal melanoma biopsies using fluorescence in situ hybridization. Clinical cancer research : an official journal of the American Association for Cancer Research. 2002;8(2):534-9.
69. Midena E, Bonaldi L, Parrozzani R, Radin PP, Boccassini B, Vujosevic S. In vivo monosomy 3 detection of posterior uveal melanoma: 3-year follow-up. Graefe's archive for clinical and experimental ophthalmology = Albrecht von Graefes Archiv fur klinische und experimentelle Ophthalmologie. 2008;246(4):609-14.
70. Shields CL, Ganguly A, Bianciotto CG, Turaka K, Tavallali A, Shields JA. Prognosis of uveal melanoma in 500 cases using genetic testing of fine-needle aspiration biopsy specimens. Ophthalmology. 2011;118(2):396-401.
71. McCannel TA, Chang MY, Burgess BL. Multi-year follow-up of fine-needle aspiration biopsy in choroidal melanoma. Ophthalmology. 2012;119(3):606-10.
72. Angi M, Kalirai H, Taktak A, Hussain R, Groenewald C, Damato BE, et al. Prognostic biopsy of choroidal melanoma: an optimised surgical and laboratory approach. Br J Ophthalmol. 2017;101(8):1143-6.
73. Kujala E, Kivelä T, Mäkitie T. Very Long-Term Prognosis of Patients with Malignant Uveal Melanoma. Investigative Ophthalmology and Visual Science. 2003;44(11):4651-9.
74. Dithmar S, Diaz CE, Grossniklaus HE. Intraocular melanoma spread to regional lymph nodes: report of two cases. Retina (Philadelphia, Pa). 2000;20(1):76-9.
75. Kath R, Hayungs J, Bornfeld N, Sauerwein W, Hoffken K, Seeber S. Prognosis and treatment of disseminated uveal melanoma. Cancer. 1993;72(7):2219-23.
76. Damato B, Dopierala JA, Coupland SE. Genotypic profiling of 452 choroidal melanomas with multiplex ligation-dependent probe amplification. Clinical Cancer Research. 2010;16(24):6083-92.
77. Diener-West M, Reynolds SM, Agugliaro DJ, Caldwell R, Cumming K, Earle JD, et al. Development of metastatic disease after enrollment in the COMS trials for treatment of choroidal melanoma: Collaborative Ocular Melanoma Study Group Report No. 26. Archives of ophthalmology (Chicago, Ill : 1960). 2005;123(12):1639-43.
78. Gragoudas ES, Egan KM, Seddon JM, Glynn RJ, Walsh SM, Finn SM, et al. Survival of patients with metastases from uveal melanoma. Ophthalmology. 1991;98(3):383-9; discussion 90.
79. Rivoire M, Kodjikian L, Baldo S, Kaemmerlen P, Négrier S, Grange J-D. Treatment of Liver Metastases From Uveal Melanoma. Ann Surg Oncol. 2005;12(6):422-8.
80. Kodjikian L, Grange J-D, Baldo S, Baillif S, Garweg J, Rivoire M. Prognostic factors of liver metastases from uveal melanoma. Graefe's Archive for Clinical and Experimental Ophthalmology. 2005;243(10):985-93.
81. Mariani P, Piperno-Neumann S, Servois V, Berry MG, Dorval T, Plancher C, et al. Surgical management of liver metastases from uveal melanoma: 16 years' experience at the Institut Curie. European Journal of Surgical Oncology (EJSO). 2009;35(11):1192-7.
82. Gomez D, Wetherill C, Cheong J, Jones L, Marshall E, Damato B, et al. The Liverpool uveal melanoma liver metastases pathway: outcome following liver resection. Journal Of Surgical Oncology. 2014;109(6):542-7.
83. Ben-Shabat I, Hansson C, Sternby Eilard M, Cahlin C, Rizell M, Lindner P, et al. Isolated hepatic perfusion as a treatment for liver metastases of uveal melanoma. Journal of visualized experiments : JoVE. 2015(95):52490.

84. Bedikian AY, Legha SS, Mavligit G, Carrasco CH, Khorana S, Plager C, et al. Treatment of uveal melanoma metastatic to the liver. A review of the M. D. Anderson cancer center experience and prognostic factors. Cancer. 1995;76(9):1665-70.
85. Yamamoto A, Chervoneva I, Sullivan KL, Eschelman DJ, Gonsalves CF, Mastrangelo MJ, et al. High-dose immunoembolization: survival benefit in patients with hepatic metastases from uveal melanoma. Radiology. 2009;252(1):290-8.
86. Farolfi A, Ridolfi L, Guidoboni M, Milandri C, Calzolari F, Scarpi E, et al. Liver metastases from melanoma: hepatic intra-arterial chemotherapy. A retrospective study. Journal of chemotherapy (Florence, Italy). 2011;23(5):300-5.
87. Eskelin S, Pyrhonen S, Hahka-Kemppinen M, Tuomaala S, Kivela T. A prognostic model and staging for metastatic uveal melanoma. Cancer. 2003;97(2):465-75.
88. Pons F, Plana M, Caminal JM, Pera J, Fernandes I, Perez J, et al. Metastatic uveal melanoma: is there a role for conventional chemotherapy? - A single center study based on 58 patients. Melanoma Res. 2011;21(3):217-22.
89. Moser JC, Pulido JS, Dronca RS, McWilliams RR, Markovic SN, Mansfield AS. The Mayo Clinic experience with the use of kinase inhibitors, ipilimumab, bevacizumab, and local therapies in the treatment of metastatic uveal melanoma. Melanoma Res. 2015;25(1):59-63.
90. Prescher G, Bornfeld N, Becher R. Nonrandom chromosomal abnormalities in primary uveal melanoma. Journal of the National Cancer Institute. 1990;82(22):1765-9.
91. Prescher G, Bornfeld N. Prognostic implications of monosomy 3 in uveal melanoma. Lancet. 1996;347(9010):1222.
92. Sisley K, Rennie IG, Parsons MA, Jacques R, Hammond DW, Bell SM, et al. Abnormalities of chromosomes 3 and 8 in posterior uveal melanoma correlate with prognosis. Genes, chromosomes & cancer. 1997;19(1):22-8.
93. White VA, Chambers JD, Courtright PD, Chang WY, Horsman DE. Correlation of cytogenetic abnormalities with the outcome of patients with uveal melanoma. Cancer. 1998;83(2):354-9.
94. Kilic E, van Gils W, Lodder E, Beverloo HB, van Til ME, Mooy CM, et al. Clinical and cytogenetic analyses in uveal melanoma. Investigative ophthalmology & visual science. 2006;47(9):3703-7.
95. Horsman DE, Rootman J, White VA, Sroka H. Monosomy 3 and isochromosome 8q in a uveal melanoma. Cancer Genetics and Cytogenetics. 1990;45(2):249-53.
96. Sisley K, Rennie IG, Cottom D, Potter AM, Potter CW, Rees RC. Abstract: Cytogenetic findings on six posterior uveal melanomas. Involvement of chromosomes. 3, 6 and 8. Cancer Genetics and Cytogenetics. 1991;52:215.
97. Speicher MR, Prescher G, du Manoir S, Jauch A, Horsthemke B, Bornfeld N, et al. Chromosomal gains and losses in uveal melanomas detected by comparative genomic hybridization. Cancer research. 1994;54(14):3817-23.
98. Parrella P, Caballero OL, Sidransky D, Merbs SL. Detection of c-myc amplification in uveal melanoma by fluorescent in situ hybridization. Investigative ophthalmology & visual science. 2001;42(8):1679-84.
99. van Gils W, Kilic E, Bruggenwirth HT, Vaarwater J, Verbiest MM, Beverloo B, et al. Regional deletion and amplification on chromosome 6 in a uveal melanoma case without abnormalities on chromosomes 1p, 3 and 8. Melanoma Res. 2008;18(1):10-5.
100. Griffin CA, Long PP, Schachat AP. Trisomy 6p in an ocular melanoma. Cancer Genet Cytogenet. 1988;32(1):129-32.

101. Rey JA, Bello MJ, de Campos J, Ramos MC, Benítez J. Cytogenetic findings in a human malignant melanoma metastatic to the brain. Cancer Genetics and Cytogenetics. 1985;16(2):179-83.
102. Aalto Y, Eriksson L, Seregard S, Larsson O, Knuutila S. Concomitant loss of chromosome 3 and whole arm losses and gains of chromosome 1, 6, or 8 in metastasizing primary uveal melanoma. Investigative ophthalmology & visual science. 2001;42(2):313-7.
103. Lake SL, Kalirai H, Dodson AR, Lloyd BH, Coupland SE, Damato BE, et al. Single nucleotide polymorphism array analysis of uveal melanomas reveals that amplification of CNKSR3 is correlated with improved patient survival. American Journal of Pathology. 2013;182(3):678-87.
104. Fountain JW, Bale SJ, Housman DE, Dracopoli NC. Genetics of melanoma. Cancer surveys. 1990;9(4):645-71.
105. Zhang J, Glatfelter AA, Taetle R, Trent JM. Frequent Alterations of Evolutionarily Conserved Regions of Chromosome 1 in Human Malignant Melanoma. Cancer Genetics and Cytogenetics. 1999;111(2):119-23.
106. Smedley D, Sidhar S, Birdsall S, Bennett D, Herlyn M, Cooper C, et al. Characterization of chromosome 1 abnormalities in malignant melanomas. Genes, chromosomes & cancer. 2000;28(1):121-5.
107. Prescher G, Bornfeld N, Friedrichs W, Seeber S, Becher R. Cytogenetics of twelve cases of uveal melanoma and patterns of nonrandom anomalies and isochromosome formation. Cancer Genetics and Cytogenetics. 1995;80(1):40-6.
108. Kilic E, Naus NC, van Gils W, Klaver CC, van Til ME, Verbiest MM, et al. Concurrent loss of chromosome arm 1p and chromosome 3 predicts a decreased disease-free survival in uveal melanoma patients. Investigative ophthalmology & visual science. 2005;46(7):2253-7.
109. Van Raamsdonk CD, Griewank KG, Crosby MB, Garrido MC, Vemula S, Wiesner T, et al. Mutations in GNA11 in uveal melanoma. The New England Journal Of Medicine. 2010;363(23):2191-9.
110. Dono M, Angelini G, Cecconi M, Amaro A, Esposito AI, Mirisola V, et al. Mutation frequencies of GNAQ, GNA11, BAP1, SF3B1, EIF1AX and TERT in uveal melanoma: detection of an activating mutation in the TERT gene promoter in a single case of uveal melanoma. British Journal of Cancer. 2014;110(4):1058-65.
111. Onken MD, Worley LA, Long MD, Duan SH, Council ML, Bowcock AM, et al. Oncogenic Mutations in GNAQ Occur Early in Uveal Melanoma.
112. Shoushtari AN, Carvajal RD. GNAQ and GNA11 mutations in uveal melanoma. Melanoma Research. 2014.
113. Koopmans AE, Vaarwater J, Paridaens D, Naus NC, Kilic E, de Klein A. Patient survival in uveal melanoma is not affected by oncogenic mutations in GNAQ and GNA11. Br J Cancer. 2013;109(2):493-6.
114. Pópulo H, Vinagre J, Lopes JM, Soares P. Analysis of GNAQ mutations, proliferation and MAPK pathway activation in uveal melanomas. British Journal of Ophthalmology. 2011;95(5):715-9.
115. Chen X, Wu Q, Tan L, Porter D, Jager MJ, Emery C, et al. Combined PKC and MEK inhibition in uveal melanoma with GNAQ and GNA11 mutations. Oncogene. 2014;33(39):4724-34.
116. Tsianakas A, Getova V, Metze D, Luger T, Schiller M, Sunderkötter C, et al. Skin metastases in metastatic uveal melanoma: GNAQ / GNA11 mutational analysis as a valuable tool. British Journal of Dermatology. 2013;169(1):160-3.

117. Bohm MRR, Tsianakas A, Merte RL, Schiller M, Spieker T, Ropke A, et al. Mutational Analysis of GNAQ and GNA11 to Aid Therapy Management of a Choroidal Melanoma Metastatic to the Contralateral Orbit.
118. Jeromin S, Weissmann S, Haferlach C, Dicker F, Bayer K, Grossmann V, et al. SF3B1 mutations correlated to cytogenetics and mutations in NOTCH1, FBXW7, MYD88, XPO1 and TP53 in 1160 untreated CLL patients. Leukemia. 2014;28(1):108-17.
119. Martin M, Maßhöfer L, Temming P, Rahmann S, Metz C, Bornfeld N, et al. Exome sequencing identifies recurrent somatic mutations in EIF1AX and SF3B1 in uveal melanoma with disomy 3. Nature Genetics. 2013;45(8):933-6.
120. Harbour JW, Onken MD, Worley LA, Roberson EDO, Anbunathan H, Bowcock AM. Recurrent mutations at codon 625 of the splicing factor SF3B1 in uveal melanoma. Nature Genetics. 2013;45(2):133-5.
121. Sundaramoorthy S, Vázquez-Novelle MD, Lekomtsev S, Petronczki M, Howell M. Functional genomics identifies a requirement of pre-mRNA splicing factors for sister chromatid cohesion. EMBO Journal. 2014;33(22):2623-42.
122. Furney SJ, Marais R, Pedersen M, Turajlic S, Gentien D, Rapinat A, et al. SF3B1 mutations are associated with alternative splicing in uveal melanoma. Cancer Discovery. 2013;3(10):1122-9.
123. Koopmans AE. Prognostic Implications of Acquired Genetic Changes in Uveal Melanoma [PhD]. Erasmus MC: Erasmus University Rotterdam; 2014.
124. Ewens KG, Richards-Yutz J, Purrazzella J, Ganguly A, Kanetsky PA, Shields CL, et al. Chromosome 3 status combined with BAP1 and EIF1AX mutation profiles are associated with metastasis in uveal melanoma. Investigative Ophthalmology and Visual Science. 2014;55(8):5160-7.
125. Kilic E, Koopmans AE, Yavuzyigitoglu S, Vaarwater J, Van Ijcken WFJ, Paridaens D, et al. SF3B1 and EIF1AX mutations in uveal melanoma: a protective factor, or not? Acta ophthalmologica. 2014;92:0-.
126. Murali R, Wiesner T, Scolyer RA. Tumours associated with BAP1 mutations.
127. Nishikawa H, Wu W, Koike A, Kojima R, Gomi H, Fukuda M, et al. BRCA1-associated protein 1 interferes with BRCA1/BARD1 RING heterodimer activity. Cancer research. 2009;69(1):111-9.
128. Jensen DE, Proctor M, Marquis ST, Gardner HP, Ha SI, Chodosh LA, et al. BAP1: a novel ubiquitin hydrolase which binds to the BRCA1 RING finger and enhances BRCA1-mediated cell growth suppression. Oncogene. 1998;16(9):1097-112.
129. Harbour JW, Onken MD, Worley LA, Matatall KA, Roberson EDO, Duan S, et al. Frequent mutation of BAP1 in metastasizing uveal melanomas. Science. 2010;330(6009):1410-3.
130. Koopmans AE, van den Berg MMP, Vaarwater J, Nellist M, de Klein A, Verdijk RM, et al. Clinical significance of immunohistochemistry for detection of BAP1 mutations in uveal melanoma. Modern Pathology. 2014.
131. Kalirai H, Dodson A, Faqir S, Damato BE, Coupland SE. Lack of BAP1 protein expression in uveal melanoma is associated with increased metastatic risk and has utility in routine prognostic testing. British Journal Of Cancer. 2014.
132. Moore AR, Ceraudo E, Sher JJ, Guan Y, Shoushtari AN, Chang MT, et al. Recurrent activating mutations of G-protein-coupled receptor CYSLTR2 in uveal melanoma. Nat Genet. 2016;48(6):675-80.

133. Johansson P, Aoude LG, Wadt K, Glasson WJ, Warrier SK, Hewitt AW, et al. Deep sequencing of uveal melanoma identifies a recurrent mutation in PLCB4. Oncotarget. 2016;7(4):4624-31.
134. Royer-Bertrand B, Torsello M, Rimoldi D, El Zaoui I, Cisarova K, Pescini-Gobert R, et al. Comprehensive Genetic Landscape of Uveal Melanoma by Whole-Genome Sequencing. American journal of human genetics. 2016;99(5):1190-8.
135. Robertson AG, Shih J, Yau C, Gibb EA, Oba J, Mungall KL, et al. Integrative Analysis Identifies Four Molecular and Clinical Subsets in Uveal Melanoma. Cancer Cell. 2017;32(2):204-20.e15.
136. Field MG, Durante MA, Anbunathan H, Cai LZ, Decatur CL, Bowcock AM, et al. Punctuated evolution of canonical genomic aberrations in uveal melanoma. Nature communications. 2018;9(1):116.
137. Komeno Y, Huang YJ, Qiu J, Lin L, Xu Y, Zhou Y, et al. SRSF2 Is Essential for Hematopoiesis, and Its Myelodysplastic Syndrome-Related Mutations Dysregulate Alternative Pre-mRNA Splicing. Molecular and cellular biology. 2015;35(17):3071-82.
138. Luscan A, Just PA, Briand A, Burin des Roziers C, Goussard P, Nitschke P, et al. Uveal melanoma hepatic metastases mutation spectrum analysis using targeted next-generation sequencing of 400 cancer genes. Br J Ophthalmol. 2015;99(4):437-9.
139. Coupland SE, Campbell I, Damato B. Routes of extraocular extension of uveal melanoma: risk factors and influence on survival probability. Ophthalmology. 2008;115(10):1778-85.
140. Isager P, Ehlers N, Overgaard J. Prognostic factors for survival after enucleation for choroidal and ciliary body melanomas. Acta ophthalmologica Scandinavica. 2004;82(5):517-25.
141. Damato B, Coupland SE. A reappraisal of the significance of largest basal diameter of posterior uveal melanoma. Eye (London, England). 2009;23(12):2152-60; quiz 61-2.
142. Eagle RC, Jr. The pathology of ocular cancer. Eye (London, England). 2013;27(2):128-36.
143. McLean IW, Ainbinder DJ, Gamel JW, McCurdy JB. Choroidal-ciliary body melanoma. A multivariate survival analysis of tumor location. Ophthalmology. 1995;102(7):1060-4.
144. Starr HJ, Zimmerman LE. EXTRASCLERAL EXTENSION AND ORBITAL RECURRENCE OF MALIGNANT MELANOMAS OF THE CHOROID AND CILIARY BODY. International ophthalmology clinics. 1962;2(2):369.
145. Affeldt JC, Minckler DS, Azen SP, Yeh L. Prognosis in uveal melanoma with extrascleral extension. Archives of ophthalmology (Chicago, Ill : 1960). 1980;98(11):1975-9.
146. Shammas HF, Blodi FC. Orbital extension of Choroidal and ciliary body melanomas. Archives of ophthalmology (Chicago, Ill : 1960). 1977;95(11):2002-5.
147. Damato BE, Coupland SE. Differences in uveal melanomas between men and women from the British Isles. Eye. 2012;26(2):292-9.
148. Virgili G, Gatta G, Ciccolallo L, Capocaccia R, Biggeri A, Crocetti E, et al. Survival in patients with uveal melanoma in Europe. Archives of ophthalmology (Chicago, Ill : 1960). 2008;126(10):1413-8.
149. Burr JM, Mitry E, Rachet B, Coleman MP. Survival from uveal melanoma in England and Wales 1986 to 2001. Ophthalmic epidemiology. 2007;14(1):3-8.
150. Rietschel P, Panageas KS, Hanlon C, Patel A, Abramson DH, Chapman PB. Variates of survival in metastatic uveal melanoma. Journal of clinical oncology : official journal of the American Society of Clinical Oncology. 2005;23(31):8076-80.

151. Callendar G. Malignant melanotic tumors of the eye: a study of histologic types in 111 cases. Trans Am Acad Ophthalmol Otolaryngol. 1931;36:131-42.
152. McLean IW, Foster WD, Zimmerman LE, Gamel JW. Modifications of Callender's classification of uveal melanoma at the Armed Forces Institute of Pathology. Am J Ophthalmol. 1983;96(4):502-9.
153. Kivelä T. Uveal Malignant Melanoma: Histopathalogic Features. In: A.D. S, Damato B, Pe'er J, Murphree AL, Perry JD, editors. Essentials of Ophthalmic Oncology: SLACK Incorporated; 2009. p. 89-91.
154. McLean MJ, Foster WD, Zimmerman LE. Prognostic factors in small malignant melanomas of choroid and ciliary body. Archives of ophthalmology (Chicago, Ill : 1960). 1977;95(1):48-58.
155. van Diest PJ, Baak JP, Matze-Cok P, Wisse-Brekelmans EC, van Galen CM, Kurver PH, et al. Reproducibility of mitosis counting in 2,469 breast cancer specimens: results from the Multicenter Morphometric Mammary Carcinoma Project. Human pathology. 1992;23(6):603-7.
156. Angi M, Damato B, Kalirai H, Dodson A, Taktak A, Coupland SE. Immunohistochemical assessment of mitotic count in uveal melanoma. Acta ophthalmologica. 2011;89(2):e155-60.
157. Scholzen T, Gerdes J. The Ki-67 protein: from the known and the unknown. Journal of cellular physiology. 2000;182(3):311-22.
158. Coupland S, Hiscott P, Smith P, Damato B. Revisiting the value of assessing the mitotic rate of choroidal melanomas. Melanoma research. 2006;16(supplement):S49-S50.
159. Folberg R, Pe'er J, Gruman LM, Woolson RF, Jeng G, Montague PR, et al. The morphologic characteristics of tumor blood vessels as a marker of tumor progression in primary human uveal melanoma: a matched case-control study. Human pathology. 1992;23(11):1298-305.
160. Folberg R, Rummelt V, Parys-Van Ginderdeuren R, Hwang T, Woolson RF, Pe'er J, et al. The prognostic value of tumor blood vessel morphology in primary uveal melanoma. Ophthalmology. 1993;100(9):1389-98.
161. Folberg R, Mehaffey M, Gardner LM, Meyer M, Rummelt V, Pe'er J. The microcirculation of choroidal and ciliary body melanomas. Eye (London, England). 1997;11 (Pt 2):227-38.
162. Makitie T, Summanen P, Tarkkanen A, Kivela T. Microvascular loops and networks as prognostic indicators in choroidal and ciliary body melanomas. J Natl Cancer Inst. 1999;91(4):359-67.
163. Maniotis AJ, Folberg R, Hess A, Seftor EA, Gardner LM, Pe'er J, et al. Vascular channel formation by human melanoma cells in vivo and in vitro: vasculogenic mimicry. Am J Pathol. 1999;155(3):739-52.
164. Folberg R, Hendrix MJC, Maniotis AJ. Vasculogenic Mimicry and Tumor Angiogenesis. The American Journal of Pathology. 2000;156(2):361-81.
165. Mantovani A, Allavena P, Sica A, Balkwill F. Cancer-related inflammation. Nature. 2008;454(7203):436-44.
166. Lang JR, Davidorf FH, Baba N. The prognostic significance of lymphocytic infiltration in malignant melanoma of the choroid. Cancer. 1977;40(5):2388-94.
167. Durie FH, Campbell AM, Lee WR, Damato BE. Analysis of lymphocytic infiltration in uveal melanoma. Investigative ophthalmology & visual science. 1990;31(10):2106-10.
168. Yu P, Fu YX. Tumor-infiltrating T lymphocytes: friends or foes? Laboratory investigation; a journal of technical methods and pathology. 2006;86(3):231-45.

169. de la Cruz PO, Jr., Specht CS, McLean IW. Lymphocytic infiltration in uveal malignant melanoma. Cancer. 1990;65(1):112-5.
170. Whelchel JC, Farah SE, McLean IW, Burnier MN. Immunohistochemistry of infiltrating lymphocytes in uveal malignant melanoma. Investigative ophthalmology & visual science. 1993;34(8):2603-6.
171. Bronkhorst IH, Vu TH, Jordanova ES, Luyten GP, Burg SH, Jager MJ. Different subsets of tumor-infiltrating lymphocytes correlate with macrophage influx and monosomy 3 in uveal melanoma. Investigative ophthalmology & visual science. 2012;53(9):5370-8.
172. Allavena P, Sica A, Solinas G, Porta C, Mantovani A. The inflammatory micro-environment in tumor progression: the role of tumor-associated macrophages. Critical reviews in oncology/hematology. 2008;66(1):1-9.
173. Makitie T, Summanen P, Tarkkanen A, Kivela T. Tumor-infiltrating macrophages (CD68(+) cells) and prognosis in malignant uveal melanoma. Investigative ophthalmology & visual science. 2001;42(7):1414-21.
174. Bronkhorst IH, Jager MJ. Uveal melanoma: the inflammatory microenvironment. Journal of innate immunity. 2012;4(5-6):454-62.
175. Serakinci N, Kolvraa S. Molecular Cytogenetic Applications in Diagnostics and Research: An Overview. In: Liehr T, editor. Fluorescence In Situ Hybridization (FISH) - Application Guide: Springer; 2009. p. 3 - 23.
176. Julien C, Bazin A, Guyot B, Forestier F, Daffos F. Rapid prenatal diagnosis of Down's syndrome with in-situ hybridisation of fluorescent DNA probes. Lancet. 1986;2(8511):863-4.
177. Ried T, Lengauer C, Cremer T, Wiegant J, Raap AK, van der Ploeg M, et al. Specific metaphase and interphase detection of the breakpoint region in 8q24 of Burkitt lymphoma cells by triple-color fluorescence in situ hybridization. Genes, chromosomes & cancer. 1992;4(1):69-74.
178. McNamara M, Felix C, Davison EV, Fenton M, Kennedy SM. Assessment of chromosome 3 copy number in ocular melanoma using fluorescence in situ hybridization. Cancer Genet Cytogenet. 1997;98(1):4-8.
179. Tschentscher F, Prescher G, Horsman DE, White VA, Rieder H, Anastassiou G, et al. Partial deletions of the long and short arm of chromosome 3 point to two tumor suppressor genes in uveal melanoma. Cancer research. 2001;61(8):3439-42.
180. White VA, McNeil BK, Thiberville L, Horsman DE. Acquired homozygosity (isodisomy) of chromosome 3 during clonal evolution of a uveal melanoma: association with morphologic heterogeneity. Genes, chromosomes & cancer. 1996;15(2):138-43.
181. Young TA, Burgess BL, Rao NP, Gorin MB, Straatsma BR. High-density genome array is superior to fluorescence in-situ hybridization analysis of monosomy 3 in choroidal melanoma fine needle aspiration biopsy. Molecular vision. 2007;13:2328-33.
182. van Dijk MC, Rombout PD, Boots-Sprenger SH, Straatman H, Bernsen MR, Ruiter DJ, et al. Multiplex ligation-dependent probe amplification for the detection of chromosomal gains and losses in formalin-fixed tissue. Diagnostic molecular pathology : the American journal of surgical pathology, part B. 2005;14(1):9-16.
183. Damato EM, Damato B, Sibbring JS, Coupland SE. Ciliary body melanoma with partial deletion of chromosome 3 detected with multiplex ligation-dependent probe amplification. Graefe's archive for clinical and experimental ophthalmology = Albrecht von Graefes Archiv fur klinische und experimentelle Ophthalmologie. 2008;246(11):1637-40.
184. Damato B, Dopierala J, Klaasen A, van Dijk M, Sibbring J, Coupland SE. Multiplex ligation-dependent probe amplification of uveal melanoma: correlation with metastatic death. Investigative ophthalmology & visual science. 2009;50(7):3048-55.

185. Caines R, Eleuteri A, Kalirai H, Fisher AC, Heimann H, Damato BE, et al. Cluster analysis of multiplex ligation-dependent probe amplification data in choroidal melanoma. Molecular vision. 2015;21:1-11.
186. Lake SL, Kalirai H, Dopierala J, Damato BE, Coupland SE. Comparison of formalin-fixed and snap-frozen samples analyzed by multiplex ligation-dependent probe amplification for prognostic testing in uveal melanoma. Investigative ophthalmology & visual science. 2012;53(6):2647-52.
187. Dopierala J, Lake SL, Coupland SE, Damato BE, Taktak AFG. Genetic heterogeneity in uveal melanoma assessed by multiplex ligation-dependent probe amplification. Investigative Ophthalmology and Visual Science. 2010;51(10):4898-905.
188. Mann K, Donaghue C, Fox SP, Docherty Z, Ogilvie CM. Strategies for the rapid prenatal diagnosis of chromosome aneuploidy. Eur J Hum Genet. 2004;12(11):907-15.
189. Zeschnigk M, Lohmann DR. Prognostic Testing in Uveal Melanoma. Cancer Genomics. 2013:79.
190. Thomas S, Putter C, Weber S, Bornfeld N, Lohmann DR, Zeschnigk M. Prognostic significance of chromosome 3 alterations determined by microsatellite analysis in uveal melanoma: a long-term follow-up study. Br J Cancer. 2012;106(6):1171-6.
191. Tschentscher F, Husing J, Holter T, Kruse E, Dresen IG, Jockel KH, et al. Tumor classification based on gene expression profiling shows that uveal melanomas with and without monosomy 3 represent two distinct entities. Cancer research. 2003;63(10):2578-84.
192. Harbour JW. Molecular Prognostic Testing and Individualized Patient Care in Uveal Melanoma. American Journal of Ophthalmology. 2009;148(6):823-9.e1.
193. Landreville S, Agapova OA, Harbour JW. Emerging insights into the molecular pathogenesis of uveal melanoma. Future oncology (London, England). 2008;4(5):629-36.
194. Field MG, Decatur CL, Kurtenbach S, Gezgin G, van der Velden PA, Jager MJ, et al. PRAME as an Independent Biomarker for Metastasis in Uveal Melanoma. Clinical cancer research : an official journal of the American Association for Cancer Research. 2016;22(5):1234-42.
195. Field MG, Durante MA, Decatur CL, Tarlan B, Oelschlager KM, Stone JF, et al. Epigenetic reprogramming and aberrant expression of PRAME are associated with increased metastatic risk in Class 1 and Class 2 uveal melanomas. Oncotarget. 2016;7(37):59209-19.
196. Seider MI, Stewart PJ, Mishra KK, Damato BE. Uveal melanoma gene expression profile test result provided for uveal metastasis. Ophthalmic Surg Lasers Imaging Retina. 2014;45(5):441-2.
197. Damato B, Eleuteri A, Taktak AFG, Coupland SE. Estimating prognosis for survival after treatment of choroidal melanoma. PROGRESS IN RETINAL AND EYE RESEARCH. 2011;30(5):285-95.
198. Smit KN, van Poppelen NM, Vaarwater J, Verdijk R, van Marion R, Kalirai H, et al. Combined mutation and copy-number variation detection by targeted next-generation sequencing in uveal melanoma. Modern pathology : an official journal of the United States and Canadian Academy of Pathology, Inc. 2018;31(5):763-71.
199. Sisley K, Brand C, Parsons MA, Maltby E, Rees RC, Rennie IG. Cytogenetics of iris melanomas: disparity with other uveal tract melanomas. Cancer Genet Cytogenet. 1998;101(2):128-33.

200. Grossniklaus HE, Oakman JH, Cohen C, Calhoun FP, Jr., DeRose PB, Drews-Botsch C. Histopathology, morphometry, and nuclear DNA content of iris melanocytic lesions. Investigative ophthalmology & visual science. 1995;36(3):745-50.
201. Khan S, Finger PT, Yu GP, Razzaq L, Jager MJ, de Keizer RJ, et al. Clinical and pathologic characteristics of biopsy-proven iris melanoma: a multicenter international study. Archives of ophthalmology (Chicago, Ill : 1960). 2012;130(1):57-64.
202. Shields CL, Furuta M, Thangappan A, Nagori S, Mashayekhi A, Lally DR, et al. Metastasis of uveal melanoma millimeter-by-millimeter in 8033 consecutive eyes. Archives of Ophthalmology. 2009;127(8):989-98.
203. Shields CL, Shields JA, Materin M, Gershenbaum E, Singh AD, Smith A. Iris melanoma: risk factors for metastasis in 169 consecutive patients. Ophthalmology. 2001;108(1):172-8.
204. Krishna Y, Kalirai H, Thornton S, Damato BE, Heimann H, Coupland SE. Genetic findings in treatment-naive and proton-beam-radiated iris melanomas. Br J Ophthalmol. 2016.
205. White VA, Horsman DE, Rootman J. Cytogenetic characterization of an iris melanoma. Cancer Genet Cytogenet. 1995;82(1):85-7.
206. Mensink HW, Vaarwater J, de Keizer RJ, de Wolff-Rouendaal D, Mooy CM, de Klein A, et al. Chromosomal aberrations in iris melanomas. Br J Ophthalmol. 2011;95(3):424-8.
207. Shields CL, Ramasubramanian A, Ganguly A, Mohan D, Shields JA. Cytogenetic testing of iris melanoma using fine needle aspiration biopsy in 17 patients. Retina. 2011;31(3):574-80.
208. Scholz SL, Moller I, Reis H, Susskind D, van de Nes JAP, Leonardelli S, et al. Frequent GNAQ, GNA11, and EIF1AX Mutations in Iris Melanoma. Investigative ophthalmology & visual science. 2017;58(9):3464-70.
209. van Poppelen NM, Vaarwater J, Mudhar HS, Sisley K, Rennie IG, Rundle P, et al. Genetic Background of Iris Melanomas and Iris Melanocytic Tumors of Uncertain Malignant Potential. Ophthalmology. 2018;125(6):904-12.
210. Gerken S, Whisenant E, Varkony T, Todd S, Gemmill R, Jones C, et al. Physical and genetic mapping of human chromosome 3 loci containing microsatellite repeats. Chromosome research : an international journal on the molecular, supramolecular and evolutionary aspects of chromosome biology. 1994;2(6):423-7.
211. Tschentscher F, Prescher G, Zeschnigk M, Horsthemke B, Lohmann DR. Identification of chromosomes 3, 6, and 8 aberrations in uveal melanoma by microsatellite analysis in comparison to comparative genomic hybridization. Cancer Genet Cytogenet. 2000;122(1):13-7.
212. Shields CL, Ganguly A, Materin MA, Teixeira L, Mashayekhi A, Swanson LA, et al. CHROMOSOME 3 ANALYSIS OF UVEAL MELANOMA USING FINE-NEEDLE ASPIRATION BIOPSY AT THE TIME OF PLAQUE RADIOTHERAPY IN 140 CONSECUTIVE CASES. Transactions of the American Ophthalmological Society. 2007;105:43-53.
213. Jensen OA, Andersen SR. Late complications of biopsy in intraocular tumors. Acta Ophthalmol (Copenh). 1959;37:568-75.
214. Abi-Ayad N, Grange JD, Salle M, Kodjikian L. Transretinal uveal melanoma biopsy with 25-gauge vitrectomy system. Acta ophthalmologica. 2013;91(3):279-81.
215. Singh AD, Medina CA, Singh N, Aronow ME, Biscotti CV, Triozzi PL. Fine-needle aspiration biopsy of uveal melanoma: outcomes and complications. Br J Ophthalmol. 2016;100(4):456-62.

216. Caminal JM, Sanz S, Carreras M, Catala I, Arruga J, Roca G. Epibulbar seeding at the site of a transvitreal fine-needle aspiration biopsy. Archives of ophthalmology (Chicago, Ill : 1960). 2006;124(4):587-9.
217. Schefler AC, Gologorsky D, Marr BP, Shields CL, Zeolite I, Abramson DH. Extraocular extension of uveal melanoma after fine-needle aspiration, vitrectomy, and open biopsy. JAMA Ophthalmol. 2013;131(9):1220-4.
218. Glasgow BJ, Brown HH, Zargoza AM, Foos RY. Quantitation of tumor seeding from fine needle aspiration of ocular melanomas. Am J Ophthalmol. 1988;105(5):538-46.
219. Abdel-Rahman MH, Christopher BN, Faramawi MF, Said-Ahmed K, Cole C, McFaddin A, et al. Frequency, molecular pathology and potential clinical significance of partial chromosome 3 aberrations in uveal melanoma. Modern pathology : an official journal of the United States and Canadian Academy of Pathology, Inc. 2011;24(7):10.1038/modpathol.2011.51.
220. Mensink HW, Vaarwater J, Kilic E, Naus NC, Mooy N, Luyten G, et al. Chromosome 3 intratumor heterogeneity in uveal melanoma. Investigative ophthalmology & visual science. 2009;50(2):500-4.
221. Coupland SE, Kalirai H, Ho V, Thornton S, Damato BE, Heimann H. Concordant chromosome 3 results in paired choroidal melanoma biopsies and subsequent tumour resection specimens. Br J Ophthalmol. 2015;99(10):1444-50.
222. Hussain RN, Kalirai H, Groenewald C, Kacperek A, Errington RD, Coupland SE, et al. Prognostic Biopsy of Choroidal Melanoma after Proton Beam Radiation Therapy. Ophthalmology. 2016;123(10):2264-5.
223. Wackernagel W, Tarmann L, Mayer C, Langmann G, Wedrich A. Genetic analysis of uveal melanoma by array comparative genomic hybridization before and after radiotherapy. Spektrum der Augenheilkunde. 2013;27(6):286-91.
224. Dogrusoz M, Kroes WG, van Duinen SG, Creutzberg CL, Versluis M, Bleeker JC, et al. Radiation Treatment Affects Chromosome Testing in Uveal Melanoma. Investigative ophthalmology & visual science. 2015;56(10):5956-64.
225. Mashayekhi A, Lim RP, Shields CL, Eagle RC, Jr., Shields JA. EXTRAOCULAR EXTENSION OF CILIOCHOROIDAL MELANOMA AFTER TRANSSCLERAL FINE-NEEDLE ASPIRATION BIOPSY. Retinal cases & brief reports. 2016;10(3):289-92.
226. Bagger M, Smidt-Nielsen I, Andersen MK, Jensen PK, Heegaard S, Andersen KK, et al. Long-Term Metastatic Risk after Biopsy of Posterior Uveal Melanoma. Ophthalmology. 2018.
227. Komander D, Rape M. The ubiquitin code. Annual review of biochemistry. 2012;81:203-29.
228. Komander D, Clague MJ, Urbe S. Breaking the chains: structure and function of the deubiquitinases. Nature reviews Molecular cell biology. 2009;10(8):550-63.
229. Wang A, Papneja A, Hyrcza M, Al-Habeeb A, Ghazarian D. Gene of the month: BAP1. J Clin Pathol. 2016;69(9):750-3.
230. Misaghi S, Ottosen S, Izrael-Tomasevic A, Arnott D, Lamkanfi M, Lee J, et al. Association of C-terminal ubiquitin hydrolase BRCA1-associated protein 1 with cell cycle regulator host cell factor 1. Molecular and cellular biology. 2009;29(8):2181-92.
231. Machida YJ, Machida Y, Vashisht AA, Wohlschlegel JA, Dutta A. The deubiquitinating enzyme BAP1 regulates cell growth via interaction with HCF-1. The Journal of biological chemistry. 2009;284(49):34179-88.

232. Baer R, Ludwig T. The BRCA1/BARD1 heterodimer, a tumor suppressor complex with ubiquitin E3 ligase activity. Current opinion in genetics & development. 2002;12(1):86-91.
233. Yu H, Mashtalir N, Daou S, Hammond-Martel I, Ross J, Sui G, et al. The ubiquitin carboxyl hydrolase BAP1 forms a ternary complex with YY1 and HCF-1 and is a critical regulator of gene expression. Molecular and cellular biology. 2010;30(21):5071-85.
234. Bott M, Brevet M, Taylor BS, Shimizu S, Ito T, Wang L, et al. The nuclear deubiquitinase BAP1 is commonly inactivated by somatic mutations and 3p21.1 losses in malignant pleural mesothelioma. Nat Genet. 2011;43(7):668-72.
235. Pena-Llopis S, Vega-Rubin-de-Celis S, Liao A, Leng N, Pavia-Jimenez A, Wang S, et al. BAP1 loss defines a new class of renal cell carcinoma. Nat Genet. 2012;44(7):751-9.
236. Njauw CN, Kim I, Piris A, Gabree M, Taylor M, Lane AM, et al. Germline BAP1 inactivation is preferentially associated with metastatic ocular melanoma and cutaneous-ocular melanoma families. PloS one. 2012;7(4):e35295.
237. Testa JR, Cheung M, Pei J, Below JE, Tan Y, Sementino E, et al. Germline BAP1 mutations predispose to malignant mesothelioma. Nat Genet. 2011;43(10):1022-5.
238. Wiesner T, Obenauf AC, Murali R, Fried I, Griewank KG, Ulz P, et al. Germline mutations in BAP1 predispose to melanocytic tumors. Nat Genet. 2011;43(10):1018-21.
239. Shah AA, Bourne TD, Murali R. BAP1 protein loss by immunohistochemistry: a potentially useful tool for prognostic prediction in patients with uveal melanoma. Pathology. 2013;45(7):651-6.
240. Farquhar N, Thornton S, Coupland SE, Coulson JM, Sacco JJ, Krishna Y, et al. Patterns of BAP1 protein expression provide insights into prognostic significance and the biology of uveal melanoma. The journal of pathology Clinical research. 2018;4(1):26-38.
241. van de Nes JA, Nelles J, Kreis S, Metz CH, Hager T, Lohmann DR, et al. Comparing the Prognostic Value of BAP1 Mutation Pattern, Chromosome 3 Status, and BAP1 Immunohistochemistry in Uveal Melanoma. The American journal of surgical pathology. 2016;40(6):796-805.
242. Yavuzyigitoglu S, Koopmans AE, Verdijk RM, Vaarwater J, Eussen B, van Bodegom A, et al. Uveal Melanomas with SF3B1 Mutations: A Distinct Subclass Associated with Late-Onset Metastases. Ophthalmology. 2016;123(5):1118-28.
243. Reiman A, Kikuchi H, Scocchia D, Smith P, Tsang YW, Snead D, et al. Validation of an NGS mutation detection panel for melanoma. BMC cancer. 2017;17(1):150.
244. Hung SS, Meissner B, Chavez EA, Ben-Neriah S, Ennishi D, Jones MR, et al. Assessment of Capture and Amplicon-Based Approaches for the Development of a Targeted Next-Generation Sequencing Pipeline to Personalize Lymphoma Management. The Journal of molecular diagnostics : JMD. 2018;20(2):203-14.
245. Samorodnitsky E, Jewell BM, Hagopian R, Miya J, Wing MR, Lyon E, et al. Evaluation of Hybridization Capture Versus Amplicon-Based Methods for Whole-Exome Sequencing. Human mutation. 2015;36(9):903-14.
246. Mamedov TG, Pienaar E, Whitney SE, TerMaat JR, Carvill G, Goliath R, et al. A fundamental study of the PCR amplification of GC-rich DNA templates. Computational biology and chemistry. 2008;32(6):452-7.
247. Bustin SA, Nolan T. Pitfalls of quantitative real-time reverse-transcription polymerase chain reaction. Journal of biomolecular techniques : JBT. 2004;15(3):155-66.
248. McCall CM, Mosier S, Thiess M, Debeljak M, Pallavajjala A, Beierl K, et al. False positives in multiplex PCR-based next-generation sequencing have unique signatures. The Journal of molecular diagnostics : JMD. 2014;16(5):541-9.

249. Koopmans AE, Vaarwater J, Paridaens D, Naus NC, Kilic E, de Klein A. Patient survival in uveal melanoma is not affected by oncogenic mutations in GNAQ and GNA11. Br J Cancer. 2013;109(2):493-6.
250. Staby KM, Gravdal K, Mork SJ, Heegaard S, Vintermyr OK, Krohn J. Prognostic impact of chromosomal aberrations and GNAQ, GNA11 and BAP1 mutations in uveal melanoma. Acta ophthalmologica. 2018;96(1):31-8.
251. Steeb T, Wessely A, Ruzicka T, Heppt MV, Berking C. How to MEK the best of uveal melanoma: A systematic review on the efficacy and safety of MEK inhibitors in metastatic or unresectable uveal melanoma. European journal of cancer (Oxford, England : 1990). 2018;103:41-51.
252. Koopmans AE, Verdijk RM, Brouwer RW, van den Bosch TP, van den Berg MM, Vaarwater J, et al. Clinical significance of immunohistochemistry for detection of BAP1 mutations in uveal melanoma. Modern pathology : an official journal of the United States and Canadian Academy of Pathology, Inc. 2014;27(10):1321-30.
253. Chua V, Lapadula D, Randolph C, Benovic JL, Wedegaertner PB, Aplin AE. Dysregulated GPCR Signaling and Therapeutic Options in Uveal Melanoma. Molecular cancer research : MCR. 2017;15(5):501-6.
254. Izumiyama T, Minoshima S, Yoshida T, Shimizu N. A novel big protein TPRBK possessing 25 units of TPR motif is essential for the progress of mitosis and cytokinesis. Gene. 2012;511(2):202-17.
255. Pitkanen E, Cajuso T, Katainen R, Kaasinen E, Valimaki N, Palin K, et al. Frequent L1 retrotranspositions originating from TTC28 in colorectal cancer. Oncotarget. 2014;5(3):853-9.
256. Chen J, Castelvecchi GD, Li-Villarreal N, Raught B, Krezel AM, McNeill H, et al. Atypical Cadherin Dachsous1b Interacts with Ttc28 and Aurora B to Control Microtubule Dynamics in Embryonic Cleavages. Developmental cell. 2018;45(3):376-91.e5.
257. Tang MR, Wang YX, Guo S, Han SY, Wang D. CSMD1 exhibits antitumor activity in A375 melanoma cells through activation of the Smad pathway. Apoptosis : an international journal on programmed cell death. 2012;17(9):927-37.
258. Ma C, Quesnelle KM, Sparano A, Rao S, Park MS, Cohen MA, et al. Characterization CSMD1 in a large set of primary lung, head and neck, breast and skin cancer tissues. Cancer biology & therapy. 2009;8(10):907-16.
259. Futterer A, Kruppa G, Kramer B, Lemke H, Kronke M. Molecular cloning and characterization of human kinectin. Molecular biology of the cell. 1995;6(2):161-70.
260. Machleidt T, Geller P, Schwandner R, Scherer G, Kronke M. Caspase 7-induced cleavage of kinectin in apoptotic cells. FEBS letters. 1998;436(1):51-4.
261. Ong LL, Er CP, Ho A, Aung MT, Yu H. Kinectin anchors the translation elongation factor-1 delta to the endoplasmic reticulum. The Journal of biological chemistry. 2003;278(34):32115-23.
262. Salassidis K, Bruch J, Zitzelsberger H, Lengfelder E, Kellerer AM, Bauchinger M. Translocation t(10;14)(q11.2:q22.1) fusing the kinetin to the RET gene creates a novel rearranged form (PTC8) of the RET proto-oncogene in radiation-induced childhood papillary thyroid carcinoma. Cancer research. 2000;60(11):2786-9.
263. Ciampi R, Nikiforov YE. RET/PTC rearrangements and BRAF mutations in thyroid tumorigenesis. Endocrinology. 2007;148(3):936-41.
264. Minde DP, Anvarian Z, Rudiger SG, Maurice MM. Messing up disorder: how do missense mutations in the tumor suppressor protein APC lead to cancer? Mol Cancer. 2011;10:101.

265. Panier S, Boulton SJ. Double-strand break repair: 53BP1 comes into focus. Nature reviews Molecular cell biology. 2014;15(1):7-18.
266. Liang X, Vacher S, Boulai A, Bernard V, Baulande S, Bohec M, et al. Targeted next-generation sequencing identifies clinically relevant somatic mutations in a large cohort of inflammatory breast cancer. Breast cancer research : BCR. 2018;20(1):88.
267. Bi J, Huang A, Liu T, Zhang T, Ma H. Expression of DNA damage checkpoint 53BP1 is correlated with prognosis, cell proliferation and apoptosis in colorectal cancer. Int J Clin Exp Pathol. 2015;8(6):6070-82.
268. Damato B, Duke C, Douglas A, Howard P, Coupland SE, Smith PA, et al. Cytogenetics of Uveal Melanoma. A 7-Year Clinical Experience. Ophthalmology. 2007;114(10):1925-31.e1.
269. Kaliki S, Shields CL, Shields JA. Uveal melanoma: estimating prognosis. Indian J Ophthalmol. 2015;63(2):93-102.
270. Ewens KG, Kanetsky PA, Richards-Yutz J, Al-Dahmash S, De Luca MC, Bianciotto CG, et al. Genomic profile of 320 uveal melanoma cases: chromosome 8p-loss and metastatic outcome. Investigative ophthalmology & visual science. 2013;54(8):5721-9.
271. Shields CL, Say EAT, Hasanreisoglu M, Saktanasate J, Lawson BM, Landy JE, et al. Personalized Prognosis of Uveal Melanoma Based on Cytogenetic Profile in 1059 Patients over an 8-Year Period: The 2017 Harry S. Gradle Lecture. Ophthalmology. 2017;124(10):1523-31.
272. Cassoux N, Rodrigues MJ, Plancher C, Asselain B, Levy-Gabriel C, Lumbroso-Le Rouic L, et al. Genome-wide profiling is a clinically relevant and affordable prognostic test in posterior uveal melanoma. Br J Ophthalmol. 2014;98(6):769-74.
273. Hausler T, Stang A, Anastassiou G, Jockel KH, Mrzyk S, Horsthemke B, et al. Loss of heterozygosity of 1p in uveal melanomas with monosomy 3. International journal of cancer Journal international du cancer. 2005;116(6):909-13.
274. Kilic E, Bruggenwirth HT, Meier M, Naus NC, Beverloo HB, Meijerink JP, et al. Increased expression of p73Deltaex2 transcript in uveal melanoma with loss of chromosome 1p. Melanoma Res. 2008;18(3):208-13.
275. Coughlin JJ, Stang SL, Dower NA, Stone JC. RasGRP1 and RasGRP3 regulate B cell proliferation by facilitating B cell receptor-Ras signaling. J Immunol. 2005;175(11):7179-84.
276. Lorenzo PS, Kung JW, Bottorff DA, Garfield SH, Stone JC, Blumberg PM. Phorbol esters modulate the Ras exchange factor RasGRP3. Cancer research. 2001;61(3):943-9.
277. Stone JC. Regulation of Ras in lymphocytes: get a GRP. Biochem Soc Trans. 2006;34(Pt 5):858-61.
278. Teixeira C, Stang SL, Zheng Y, Beswick NS, Stone JC. Integration of DAG signaling systems mediated by PKC-dependent phosphorylation of RasGRP3. Blood. 2003;102(4):1414-20.
279. Yang D, Kedei N, Li L, Tao J, Velasquez JF, Michalowski AM, et al. RasGRP3 contributes to formation and maintenance of the prostate cancer phenotype. Cancer research. 2010;70(20):7905-17.
280. Yang D, Tao J, Li L, Kedei N, Toth ZE, Czap A, et al. RasGRP3, a Ras activator, contributes to signaling and the tumorigenic phenotype in human melanoma. Oncogene. 2011;30(45):4590-600.
281. Chen X, Wu Q, Depeille P, Roose JP, Bastian BC. Abstract 2138: RasGRP3 mediates MAPK pathway activation in GNAQ mutant uveal melanoma. Cancer research. 2015;75(15 Supplement):2138-.

282. De Waard-Siebinga I, Blom DJ, Griffioen M, Schrier PI, Hoogendoorn E, Beverstock G, et al. Establishment and characterization of an uveal-melanoma cell line. International journal of cancer Journal international du cancer. 1995;62(2):155-61.
283. White JS, Becker RL, McLean IW, Director-Myska AE, Nath J. Molecular cytogenetic evaluation of 10 uveal melanoma cell lines. Cancer Genet Cytogenet. 2006;168(1):11-21.
284. Nareyeck G, Wuestemeyer H, von der Haar D, Anastassiou G. Establishment of two cell lines derived from conjunctival melanomas. Experimental eye research. 2005;81(3):361-2.
285. Chen PW, Murray TG, Uno T, Salgaller ML, Reddy R, Ksander BR. Expression of MAGE genes in ocular melanoma during progression from primary to metastatic disease. Clinical & experimental metastasis. 1997;15(5):509-18.
286. Chen X, Wu Q, Depeille P, Chen P, Thornton S, Kalirai H, et al. RasGRP3 Mediates MAPK Pathway Activation in GNAQ Mutant Uveal Melanoma. Cancer Cell. 2017;31(5):685-96.e6.
287. Yu FX, Luo J, Mo JS, Liu G, Kim YC, Meng Z, et al. Mutant Gq/11 promote uveal melanoma tumorigenesis by activating YAP. Cancer Cell. 2014;25(6):822-30.
288. Feng X, Degese MS, Iglesias-Bartolome R, Vaque JP, Molinolo AA, Rodrigues M, et al. Hippo-independent activation of YAP by the GNAQ uveal melanoma oncogene through a trio-regulated rho GTPase signaling circuitry. Cancer Cell. 2014;25(6):831-45.
289. Field MG, Harbour JW. GNAQ/11 mutations in uveal melanoma: is YAP the key to targeted therapy? Cancer Cell. 2014;25(6):714-5.